AD NUMBER

AD815661

LIMITATION CHANGES

TO:

Approved for public release; distribution is unlimited.

FROM:

**Distribution authorized to U.S. Gov't. agencies and their contractors;
Administrative/Operational Use; APR 1967. Other requests shall be referred to Air Force Weapons Laboratory, Kirland AFB, New NM 87117. This document contains export-controlled technical data.**

AUTHORITY

AFWL per ltr , 30 Nov 1971

MULTIPLE THREAT CRATERING EXPERIMENT

Volume I. Successive Cratering in Hard Rock

Thomas E. O'Brien, Capt, USAF
John E. Seknicka, Lt, USAF
R. H. Carlson, Boeing Company
G. D. Jones, Boeing Company

TECHNICAL REPORT NO. AFWL-TR-67-8 Vol I
April 1967

AIR FORCE WEAPONS LABORATORY
Research and Technology Division
Air Force Systems Command
Kirtland Air Force Base
New Mexico

DISCLAIMER NOTICE

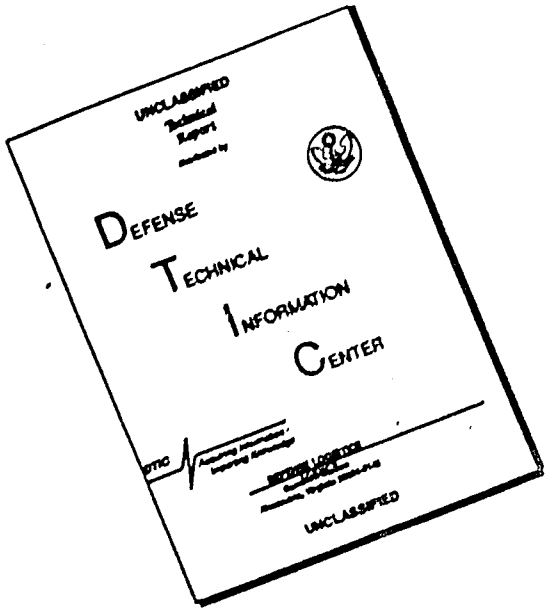

THIS DOCUMENT IS BEST QUALITY AVAILABLE. THE COPY FURNISHED TO DTIC CONTAINED A SIGNIFICANT NUMBER OF PAGES WHICH DO NOT REPRODUCE LEGIBLY.

AFWL-TR-67-8, Vol. I

Research and Technology Division
AIR FORCE WEAPONS LABORATORY
Air Force Systems Command
Kirtland Air Force Base
New Mexico

MULTIPLE THREAT CRATERING EXPERIMENT

Volume 1. Successive Cratering in Hard Rock

Thomas E. O'Brien, Capt, USAF
John E. Seknicka, Lt, USAF
R. H. Carlson, Boeing Company
G. D. Jones, Boeing Company

TECHNICAL REPORT NO. AFWL-TR-67-8

FOREWORD

This research was performed under Program Element 6.16.46.01.D, Project 5710, Subtask 13.144, and was funded by the Defense Atomic Support Agency (DASA). Portions of the report were prepared by the Boeing Company, Seattle, Washington, under Contract AF 29(601)-6787.

Inclusive dates of research were January 1965 through December 1965. The report was submitted 28 February 1967 by the AFWL Project Officer, Lt. Howard R. Pratt (WLDC).

The report is published in three volumes. The first volume contains the data and analysis of the cratering and ejecta portion of the experiment. The second volume contains the data and analysis of the active and passive measurements, primarily ground shock, of the experiment. The third volume is a statistical analysis of the distribution of missiles for the various events.

This program was under the general direction of Capt. Thomas E. O'Brien, USAF, assisted by 1Lt. John E. Seknicka, USAF. The instrumentation program was supervised by Capt. Gerald G. Leigh, USAF; seismic work was performed by Mr. Richard T. Zbur, AFWL, and technical assistance was provided by Capt. Harry E. Auld, USAF. Geologic description of the area and petrography of the rock was done by Charles U. Fulmer, Boeing Company. The cooperation of the personnel and use of the facilities at the US Army Yakima Firing Center, Yakima, Washington, is also acknowledged.

This report has been reviewed and is approved.

Howard R Pratt

HOWARD R. PRATT
Lt, USAF
Project Engineer

Robert H. Crawford, Lt Col

ALLEN F. DILL
CDR, CEC, USNR
Chief, Eivil Engineering Branch

George C. Darby, Jr.

GEORGE C. DARBY, JR.
Colonel, USAF
Chief, Development Division

ABSTRACT

A research program compares successive craters formed by high-explosive charges detonated in basalt along a common vertical axis with single explosions equivalent in yield to the sum of the successive bursts. Studies include craters and ejecta distribution; energy coupling of cratering explosions at and near the ground surface; charge shape effect on craters and related phenomena; and distribution, size, and weight of discrete ejecta missiles.

Results indicated that the excavated crater depth may be increased by a fourth half-buried successive shot. This increase is between zero and 25 percent, depending on the technique used. The data were not conclusive.

The apparent crater formed by a hemispherical surface charge exhibits a radius about 90 percent and depth about 85 percent of the dimensions formed by a corresponding spherical, half-buried charge. Excavated craters formed by hemispherical charges are likewise smaller.

Scaling relationships determined for apparent craters formed by half-buried spherical charges were $R_a = 1.30\ W^{0.27}$, $Da = 0.42\ W^{0.28}$; for apparent craters formed by hemispherical charges: $R_a = 0.48\ W^{0.37}$, $D_a = 0.06\ W^{0.47}$.

Fifty percent of material ejected from the 4000-pound and 16,000 pound half-buried charge craters were deposited between the crater edge and 1.9 and 1.2 crater radii, respectively.

(Distribution limitation statement No. 2)

This page intentionally left blank.

CONTENTS

ILLUSTRATIONS

ILLUSTRATIONS (cont'd)

ILLUSTRATIONS (cont'd)

ILLUSTRATIONS (cont'd)

ILLUSTRATIONS (cont'd)

TABLES

TABLES (cont'd)

NOMENCLATURE

Crater symbols used in this report are illustrated in Figure 1; this notation was taken from Reference 2. Crater nomenclature is as follows:

D_a	Maximum depth of apparent crater below preshot ground surface measured vertically from the preshot ground surface.
DOB	Normal depth of burst (measured vertically from the preshot ground surface).
HOB	Height of burst.
D_t	Maximum depth of true crater below preshot ground surface.
Ejecta	Material above and beyond the true crater, including fallback, ballistically ejected material, and dust.
Fallback	Material that falls back into the true crater.
H_{al}	Apparent crater lip crest height above preshot ground surface.
H_{tl}	True crater lip crest height above preshot ground surface.
H_{tlc}	True lip height at radial position of apparent lip crest.
R_a	Radius of apparent crater measured on the preshot ground surface.
h_{al}	Height of apparent crater lip at any radial distance from ground zero.
h_{tl}	Height of true crater lip at any radial distance from ground zero.
HE	High explosive (usually TNT).
M_a	Mass of material represented by the apparent crater.
M_e	Mass of ejecta.
M_f	Mass of fallback material and a portion of ruptured material.
M_i	Cumulative ejecta mass between crater edge and any distance of interest.
M_m	Crater mass that appears to be missing ($M_m = M'_t - M'_f$).

NOMENCLATURE (cont'd)

M'_t	Mass of material represented by the excavated crater.
M_u	Mass of material represented by the upthrust region.
M_β	Nonaccountable mass ($M_\beta = M_m - M_e - M_u$).
NE	Nuclear explosive.
R'_t	Radius of excavated crater measured on preshot ground surface.
R_z	Maximum distance that a missile is deposited from ground zero.
t	Ejecta thickness.
R_{al}	Radius of apparent lip crest to center.
R_{ds}	Outer radius of displaced surface.
R_t	Radius of true crater measured on the preshot ground surface.
SGZ	Surface ground zero or epicenter.
SUCCESSIVE CRATERING	Sequentially exploded charges along the same vertical axis or at a common aiming point, each on the bottom of a crater produced by a previous explosion with the exception of the first explosion. Also commonly called multiple cratering, sequential-charge-explosive-cratering, "nail-driving," repeated cratering.
V_a	Volume of apparent crater below preshot ground surface.
V_t	Volume of true crater below preshot ground surface.
ZP	Zero Point: effective center of explosive energy.

Additional symbols used in this report are defined below:

D	Radial distance from ground zero.
D_t	Depth of excavated crater below preshot ground surface.
V_e	Volume of ejecta material.
V'_f	Volume of fallback material and some ruptured material ($V'_f = V'_t - V_a$).
V_u	Volume of upthrust region.

NOMENCLATURE (cont'd)

V'_t	Volume of excavated crater below preshot ground surface.
W	Explosive energy release.
λ	Scaled dimension. (For example, scaled burst depth is the actual burst depth divided by the cube root of charge weight.)
ρ_1	Density of undisturbed material.
ρ_2	Density of fallback material.
ρ_3	Density of upthrusted material.
ρ_4	Density of ejecta material.
CEP	Circular error of probability.

This page intentionally left blank.

SECTION I

INTRODUCTION

1. Objectives

The primary objective of this study is to relate cratering, ejecta distribution, and ground shock from successive bursts detonated along the same axis to a single surface burst, equivalent in yield to the sum of the successive bursts.

Secondary objectives are the investigation of charge shape influence (spherical vs. hemispherical charges) and determination of the distribution, size, and nominal weight of discrete missiles originating in the crater zone.

2. Background

The detonation of a charge on or near the surface of the earth results in the formation of a crater and the disposition of ejected material on the ground surface surrounding the crater.

An aerial view of a typical surface crater in rock is shown in Figure 1. The size of the crater and the resulting amount and distribution of ejecta is dependent upon:

a. The effective yield of the charge.

b. The HOB/DOB.

c. The type and condition of the earth media involved.

The actual formation of the crater is caused by the media being pushed, thrown, or ejected and scoured out by forces resulting from the rapid expansion of the hot gas bubble and the accompanying blast wave. A more comprehensive discussion of the basic crater formation mechanisms is given in Reference 1.

A profile of a typical crater is shown in Figure 2. The symbols are defined under nomenclature. A more detailed list of crater dimensions and nomenclature can be found in Reference 2.

The height or depth of burst (HOB, DOB) is a critical parameter in determining crater dimensions and ejecta quantities. However, the realities of weapon delivery have focused military attention on near-surface bursts only. For that reason the following definitions apply regarding HOB and DOB:

Figure 1. Aerial View of Typical Surface Crater in Rock.

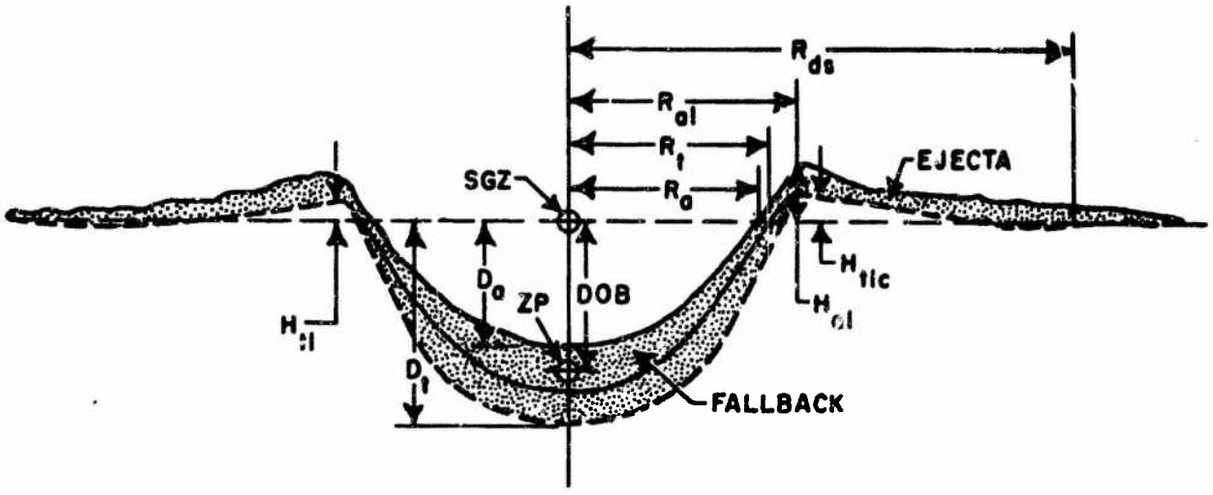

Figure 2. Profile of a Typical Crater.

a. A contact burst is one in which the center of gravity (c.g.) of the nuclear weapon is slightly above the ground surface at the time of detonation.

b. A coupled burst is one in which the center of gravity of the weapon is slightly below the ground surface at the time of detonation.

c. A true surface burst is one in which the center of gravity of the weapon coincides with the ground surface at the time of detonation.

Prediction methods presented in current publications such as Reference 1 are for a true surface-burst condition. Such an experimental condition has evolved as a standard although not generally specified as such. Predicted crater dimensions and ejecta distribution based on true surface-burst conditions will be too large for a contact burst and too small for a coupled burst.

For this experiment the contact burst was chosen as the closest approximation of the type of near-surface burst expected in a defensive situation.

The size of an explosively formed crater can be increased by detonating additional charges along a common vertical axis with each charge placed in the bottom of the crater formed by the preceding charge. The amount of apparent

crater enlargement and the resulting ejecta distribution decreases with successive charges because the distance through which material must be ejected to clear the crater zone increases and the relative amount of fallback material increases with each additional successive charge. This experiment investigates crater and ejecta distribution resulting from a series of four detonations along a common vertical axis versus a single explosion of yield equivalent to the sum of the series of four successive explosions.

Targets constructed at considerable depths beneath the surface in hard rock can be attacked by a specially designed weapon capable of penetrating the rock to some predetermined depth, by employing a nonpenetrating weapon of a yield sufficiently large to destroy the target when detonated on the rock surface, or by repetitively surface detonating stockpile weapons of limited yield along the same vertical axis, thus producing successively deeper and deeper craters. The multiple-shot technique for destroying hard targets may be feasible if the crater resulting from the multiple shots exhibits specific advantageous differences in its dimensions when compared to those of the crater produced by a single surface shot equivalent in yield to the sum of the multiple shots. The successive-cratering part of this program is designed specifically to obtain data that will aid in determining whether such advantageous differences in crater dimensions do exist.

Three rather cursory attempts have been made to study the successive-cratering problem experimentally. The first, conducted by Sandia Corporation, consisted of a series of three 64-pound spheres of TNT detonated in a fan delta alluvium (Reference 3). The second, conducted by the Boeing Company, consisted of two series of successive 64-pound TNT surface bursts along the same vertical axis, in a hard, dense argillite (Reference 4). The third experiment, conducted by the Waterways Experiment Station (WES), consisted of a series of five 4-pound TNT shots and series of five 21-pound TNT shots detonated in a sandy, clayey silt (Reference 5). Data resulting from these three experiments are summarized in Table 1.

The data of interest from the Sandia study (Reference 3) are the apparent crater dimensions resulting from each shot. The apparent crater depth for the second shot was 78 percent greater than the depth of the first and third shot increased the apparent crater depth an additional nine percent. The apparent crater depth increased 95 percent from first to third shots.

Table 1

SUMMARY OF RESULTS FROM PRIOR SUCCESSIVE-CRATERING EXPERIMENTS

Sandia Experiment (Reference 3)

	Shot 1	Shot 2	Shot 3
Apparent Crater Depth (ft)	1.8	3.2	3.5
% increase previous shot	—	78	9
% increase Shot 1	—	78	95
Apparent Crater Radius (ft)	3.7	5.5	5.7
% increase previous shot	—	49	4
% increase Shot 1	—	49	54
Apparent Crater Volume (ft^3)	31.1	116	142
% increase previous shot	—	273	22
% increase Shot 1	—	273	357

Boeing Experiment (Reference 4)

	Series 1			Series 2	
	Shot 1	Shot 2	Shot 3	Shot 1	Shot 2
Apparent Crater Depth (ft)	1.4	2.7	3.0	1.6	2.5
% increase previous shot	—	93	11	—	56
% increase Shot 1	—	93	114	—	56
Apparent Crater Radius (ft)	3.8	4.7	5.2	4.7	5.4
% increase previous shot	—	24	11	—	15
% increase Shot 1	—	24	37	—	15
Apparent Crater Volume (ft^3)	36.2	73.1	113.0	55.8	94.9
% increase previous shot	—	102	55	—	70
% increase Shot 1	—	102	212	—	70
Excavated Crater Depth (ft)	—	—	4.1	1.7	2.7
% increase previous shot	—	—	—	—	59
% increase Shot 1	—	—	—	—	59
Excavated Crater Radius (ft)	—	—	6.3	5.8	5.9
% increase previous shot	—	—	—	—	2
% increase Shot 1	—	—	—	—	2
Excavated Crater Volume (ft^3)	—	—	187.2	114.1	152.0
% increase previous shot	—	—	—	—	33
% increase Shot 1	—	—	—	—	33

Table 1 (cont'd)

SUMMARY OF RESULTS FROM PRIOR SUCCESSIVE-CRATERING EXPERIMENTS

WES Experiment — 4-lb Charges (Reference 5)

	Shot 1	Shot 2	Shot 3	Shot 4	Shot 5
Apparent Crater Depth (ft)	1.10	1.30	1.50	1.75	2.35
% increase previous shot	—	18.2	15.4	16.7	34.2
% increase Shot 1	—	18.2	36.4	59.1	114
Apparent Crater Radius (ft)	1.94	2.30	2.70	3.17	3.30
% increase previous shot	—	18.6	17.4	17.4	4.1
% increase Shot 1	—	18.6	39.2	63.4	70.1
True Crater Depth (ft)[a]	1.90	—	—	—	3.80
% increase previous shot	—	—	—	—	—
% increase Shot 1	—	—	—	—	100
True Crater Radius (ft)[a]	2.20	—	—	—	3.74
% increase previous shot	—	—	—	—	—
% increase Shot 1	—	—	—	—	70.0

WES Experiment — 21-lb Charges (Reference 5)

	Shot 1	Shot 2	Shot 3	Shot 4	Shot 5
Apparent Crater Depth (ft)	2.62	3.03	3.95	4.37	4.90
% increase previous shot	—	15.6	30.4	10.6	12.1
% increase Shot 1	—	15.6	50.7	66.8	87.0
Apparent Crater Radius (ft)	4.21	4.81	5.42	5.75	5.95
% increase previous shot	—	14.2	12.7	6.1	3.5
% increase Shot 1	—	14.2	28.7	36.6	41.3
True Crater Depth (ft)[a]	4.10	5.43	5.70	6.20	6.7
% increase previous shot	—	32.4	5.0	8.8	8.1
% increase Shot 1	—	32.4	39.0	51.2	63.4
True Crater Radius (ft)[a]	4.32	5.00	5.60	6.00	6.2
% increase previous shot	—	15.7	12.0	7.1	3.3
% increase Shot 1	—	15.7	29.6	38.9	43.5

[a]True crater dimensions probed

The first series in the Boeing experiment (Reference 4) used three spheres of TNT on the same aiming point, the first sphere being detonated with its center of gravity coincident with the ground surface, and successive shots with their centers of gravity coincident with the bottom of the apparent crater resulting from each preceding shot. The second series in the Boeing experiment used only two TNT spheres, the first being detonated at the ground surface, and the second at the bottom of the apparent crater caused by the first. Data collected from the Boeing study included apparent crater dimensions after all shots, and true crater dimensions after the last shot of the first series and after each shot of the second series. The results of the first series indicated that the apparent crater was deepened 93 percent by the second shot and 11 percent by the third shot. The excavated crater depth was increased by 59 percent by the second shot of the second series and an additional 34 percent by a third shot, one derived from the third shot from the first series and having an excavated crater depth of 4.1 feet.

The results of the WES study as reported in Reference 5 indicated that the increase in magnitude of both the true and apparent crater dimensions was significant after the fifth shot. The results from the 21-pound series indicated that with each succeeding shot crater depth appeared to increase at a decreasing rate. True crater dimensions were obtained in the WES study by a probing technique.

If true crater depth is taken as a reliable measure of damage to hard targets, the Boeing data indicate that the multiple-burst technique is a relatively efficient method of attack in a rock medium such as argillite. On the other hand, assuming a normal relationship (Ref. TM 23-200, Nov 1964) between true and apparent crater depths, the Sandia data indicate that this method of attack is relatively inefficient after the second burst for an alluvium medium.

A serious limitation on the usefulness of data from these prior successive-cratering studies is the small charge size. The Multiple Threat Cratering Experiment (MTCE) reported here has the advantage of using larger charges (4000 pounds) than used in prior similar experiments. This program also yielded data that permit the comparison of crater dimensions resulting from a single surface burst with those resulting from four successive charges equal in total energy release to the single surface charge.

The charge-geometry portion of this project permits, for the first time, comparison of crater data resulting from half-buried spherical and hemispherical charges. During recent years Canadian scientists working at the Suffield Experimental Station have conducted cratering experiments using hemispherical charges. The hemispherical charge is usually emplaced with its base plane on the ground surface and its center of gravity above the ground surface. United States scientists working at the Nevada Test Site and at other installations have conducted a multitude of cratering experiments using spherical charges emplaced with their centers of gravity coincident with the ground surface. Before the MTCE project, the only source of data on crater dimensions resulting from spheres and hemispheres of equal yield detonated in the same geologic medium was a Boeing-sponsored program conducted at the Tulalip Test Site (Reference 6). The program consisted of five 1-pound spheres and five 1-pound hemispheres detonated on the surface of a dry-sand medium. Resulting crater dimensions are given in Table 2. These data indicate that apparent radius and depth for craters formed by spherical charges were about 18 percent greater than similar apparent dimensions for craters formed by hemispherical charges. The apparent volumes for craters formed by spherical charges were about 33 percent greater than similar volumes for craters formed by hemispherical charges. As shown in Table 2, reproducibility of crater dimensions for craters resulting from the same burst conditions was remarkably good. The MTCE project was designed to provide information on the effect of charge shape on craters formed in a hard-rock medium. Additional charge-shape-equivalence data will be obtained by Canadian scientists at the Suffield Experimental Station in July and August of 1966 (Reference 7).

It has long been recognized that crater dimensions are strongly dependent on the position of detonation relative to the ground surface. Apparent crater radius, depth, and volume as a function of burst position in the near-ground-surface region in a soil medium is shown in Figure 3 (Reference 8). This illustration shows that, for a soil medium, crater radius will be increased by a factor of about 3, depth will be increased by a factor of about 4, and volume will be increased by a factor of about 6 when scaled burst depth is decreased from about 0.2 above the ground surface to a 0.2 below the ground surface (scaled burst depth is the actual burst depth divided by the cube root of the charge weight). The MTCE project was planned to provide similar data on crater dimensions versus burst position in the ground-surface region for a hard-rock

Table 2.

APPARENT SURFACE CRATER DIMENSIONS RESULTING FROM SPHERICAL AND HEMISPHERICAL CHARGES FIRED IN SAND.

Shot	Charge Shape	Radius, R_a	Depth, D_a	Volume, V_a
		(ft)	(ft)	(ft^3)
D2a	Sphere	1.60	0.30	1.02
D2b	Sphere	1.66	0.30	1.12
D2c	Sphere	1.83	0.34	1.42
D2d	Sphere	1.60	0.34	1.30
D2e	Sphere	1.64	0.32	1.24
Mean		$1.68^{+0.15}_{-0.08}$	$0.32^{+0.02}_{-0.02}$	$1.22^{+0.20}_{-0.20}$
H2b	Hemisphere	1.43	0.25	0.83
H2c	Hemisphere	1.45	0.31	1.02
H2d	Hemisphere	1.31	0.28	0.71
H2f	Hemisphere	1.54	0.28	1.22
H2g	Hemisphere	1.45	0.24	0.82
Mean		$1.44^{+0.10}_{-0.13}$	$0.27^{+0.04}_{-0.03}$	$0.92^{+0.30}_{-0.21}$

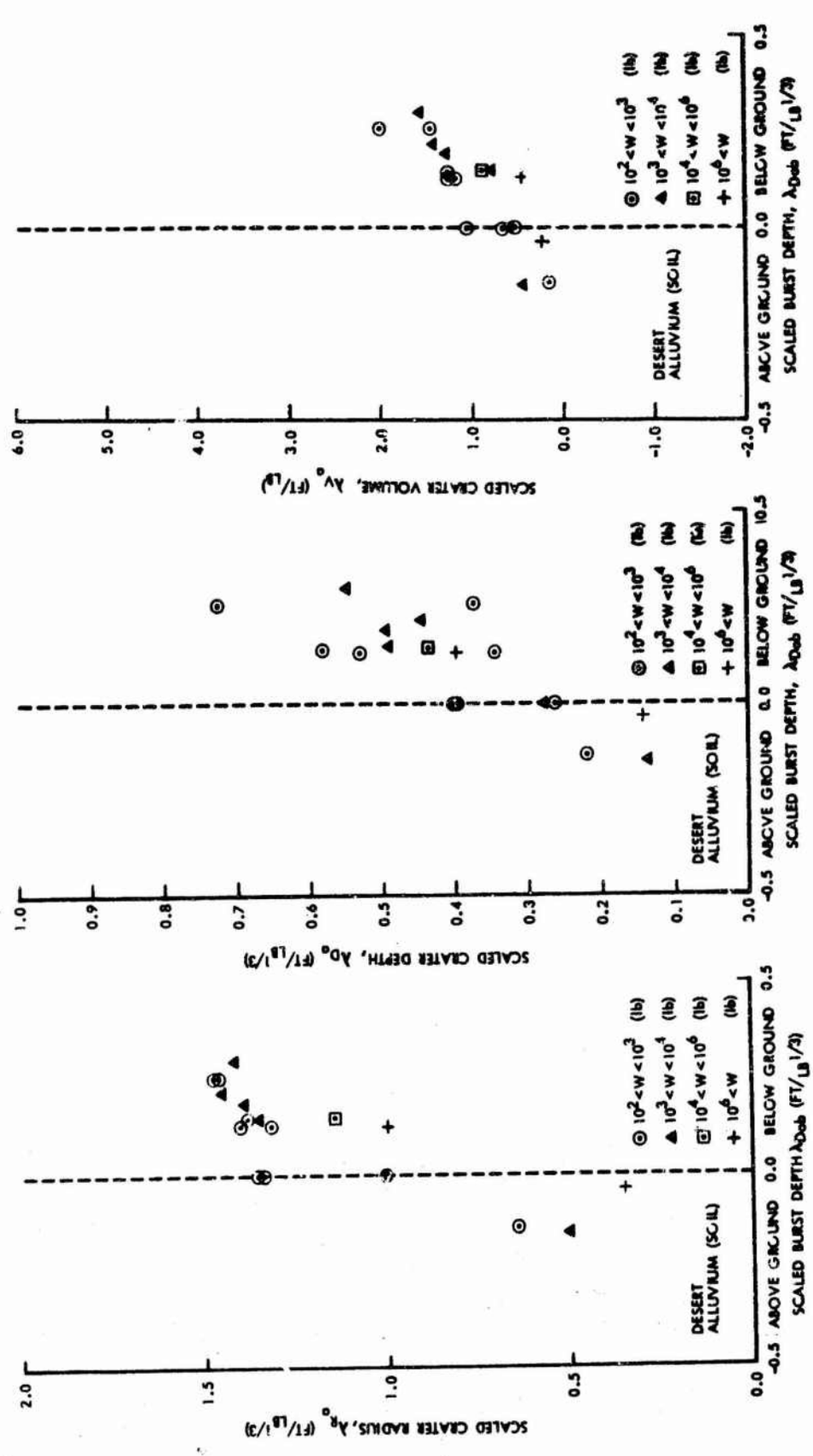

Figure 3. Crater Dimensions as a Function of Burst Position in the Near-Ground Surface Region in Soil (Data from Reference 8).

medium. Interest in this problem is directly related to weapon fuzing requirements and resulting data may be used to support design requirements for penetrating weapons.

From a military standpoint, there are certain surface components of existing defense systems that may be adversely affected by an accumulation of ejecta-debris cover resulting from cratering detonations. The ejecta distribution problem in soil and rock media has been examined recently in an Air Force Weapons Laboratory report; however, there are few ejecta data for surface craters in rock (Reference 1). The MTCE project was planned to provide additional needed data on ejecta distribution associated with surface craters in rock.

The boundary of the true crater is generally thought of as the extent of definite damage-causing mechanisms of crater formation. However, true crater measurements were not obtained on this experiment. Rather, the crater measured was the one which resulted when all loose and fractured material was removed from the apparent crater. The boundary of this crater is called the excavated crater boundary and its associated dimensions have been designated R'_t, D'_t, and V'_t for the excavated radius, excavated depth, and excavated volume, respectively. The excavated crater actually is larger than the conventional true crater. Figure 4 shows the apparent, true, and excavated crater boundaries for a typical crater in hard rock. In electing to document the excavated crater boundary, it was felt that this boundary would occur at that distance from the charge where the stress level would have fallen to a specific value dependent only on the strength of the native basalt and would therefore be consistent from crater to crater.

Discrete missiles originating in the crater zone may in themselves represent a damage-causing mechanism. Missiles, as used herein, refer to natural earth media, boulders or discrete ejecta masses which are ballistically ejected from the crater zone. The scant data previously obtained on such missiles indicate that the missile damage radius for certain types of surface components such as radomes, etc., may extend beyond the radius of damage from air blast and ground shock. In this experiment the distribution, size, and nominal weight of missiles were studied and correlated with yield and HOB/DOB for rock media.

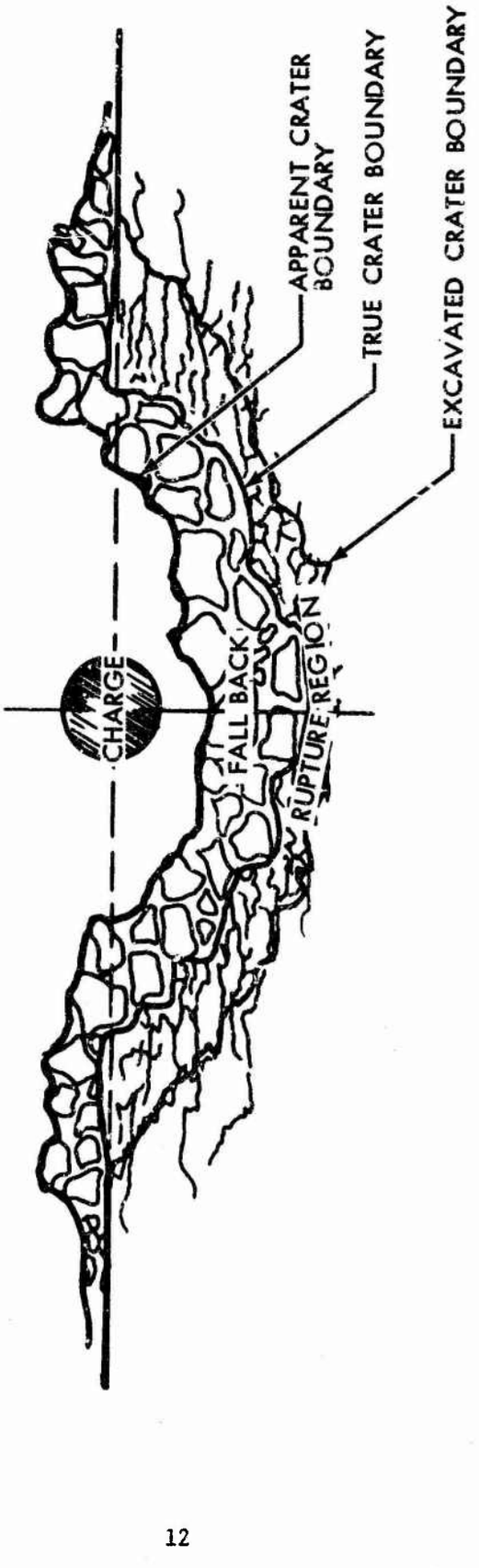

Figure 4. Identification of Boundaries Associated with a Surface Crater in Hard Rock.

3. Scope of Program

The MTCE project, consisting of twenty high explosive shots, was conducted during June and July of 1965. Table 3 summarizes the cratering events included in the overall program along with charge weight, shape, and burst position for each shot. Also given in Table 3 is the applicability of each shot to the primary objectives (that is, successive cratering, charge geometry, and energy coupling) and the measurements that were specifically made as part of the MTCE program.

All charges were made from 8-pound blocks of cast TNT (2 by 12 by 6.25 inches). Thus, the TNT density was about 92 pounds per cubic foot. Blocks were stacked to form the desired charge shape, spherical or hemispherical. Figure 5 shows the 8-pound cast TNT blocks. The 4000-pound spheres were approximately 2.2 feet in radius, and the 16,000-pound sphere was about 3.5 feet in radius. The 4000-pound hemisphere was about 2.8 feet in radius, and the 16,000-pound hemisphere was 4.4 feet in radius. The ST series charges were fired tangent to (that is, on) the rock or rubble surface. Figure 5 includes a photograph of the ST3a charge in position immediately prior to detonation. The S series charges were half buried. The placement hole for the S3a charge is shown in Figure 5. Charges in position immediately prior to detonation for S4 events are shown in Figure 6.

Several agencies participated in the MTCE project. The Naval Ordnance Test Station of China Lake, California, measured free-field overpressure in the vicinity of an earth berm on the H2 event. The U. S. Army Corps of Engineers Waterways Experiment Station (WES) was responsible for grouting the Air Force Weapons Laboratory (AFWL) instrumentation holes. WES also emplaced three microfracture columns for the LS event. A total of eight reed-gage canisters were installed on each of the S4a and LS events by TRW, Inc., to measure horizontal and vertical components of the ground shock near the ground surface. The AFWL ground shock program consisted of velocity, strain, and acceleration gages emplaced in instrumentation holes directly below ground zero in the LS, H2, and S4 events. In addition to the above government-sponsored programs and the crater and ejecta program reported here, the Boeing Company participated with a company-sponsored program designed to measure strong shock in the S3 and C2 events. The ground motion measurement program is presented in Volume II of this report, to be published at a later date.

Table 3

SHOT SUMMARY OF THE MTCE

Charges H1 and H2 were hemispheres; all others were spheres. Burst depth listed is the position of charge center of gravity relative to the rock surface.

Shot	Charge Weight, W (lb)	Burst Position: Actual Dob (ft)	Burst Position: Schematic	Type of Study: Successive Cratering	Type of Study: Charge Geometry	Type of Study: Energy Coupling	Measurements on Boeing Program: Apparent	Measurements on Boeing Program: Excavated	Measurements on Boeing Program: Upthrust	Measurements on Boeing Program: Ejecta
S1(C1)	4,000	0.0		x	x	x	x	x	x	x
S2a	4,000	0.0		x	x	x	x		x	x
S2b	4,000	3.9		x			x	x	x	x
S3a	4,000	0.0		x	x	x	x		x	x
S3b	4,000	3.7		x			x		x	x
S3c	4,000	4.4		x			x		x	x
S4a	4,000	0.0		x	x	x	x		x	x
S4b	4,000	3.1		x			x		x	x
S4c	4,000	4.6		x			x		x	x
S4d	4,000	5.5		x			x	x	x	x
LS	16,000	0.0		x	x		x	x	x	x
H2	16,000	-1.6			x		x	x	x	x
H1	4,000	-1.0			x		x	x	x	x
C2	4,000	2.2				x	x	x	x	x
ST1	4,000	-2.2		x	x	x	x	x		
ST2a	4,000	-2.2		x	x	x	x		x	x
ST2b	4,000	-0.8		x			x	x	x	x
ST3a(C3)	4,000	-2.2		x	x	x	x		x	x
ST3b	4,000	-1.3		x			x		x	x
ST3c	4,000	-0.5		x			x	x	x	x

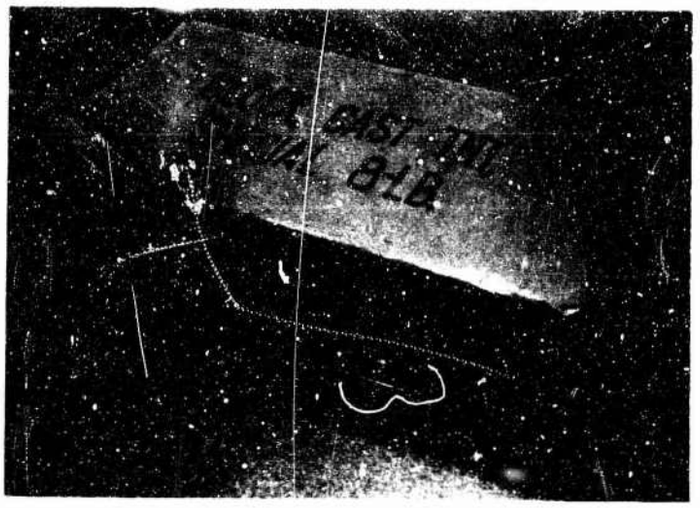

EIGHT POUND
CAST TNT BLOCK

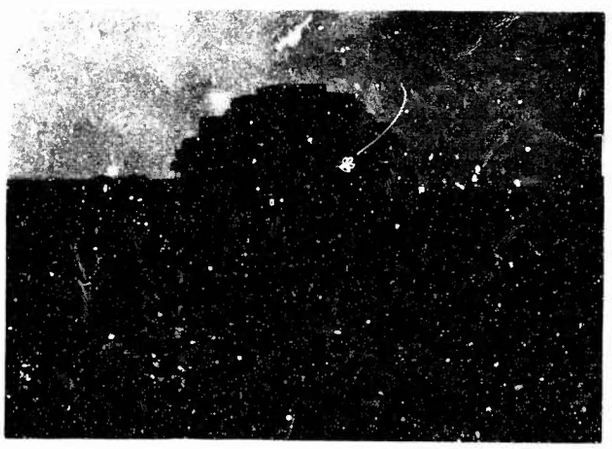

CHARGE
ST3a(C3)

CHARGE PLACEMENT
HOLE - S3a

Figure 5. Photographs Showing an 8-pound Cast TNT Block, Charge ST3a(C3) in Position and the Placement Hole for Charge S3a.

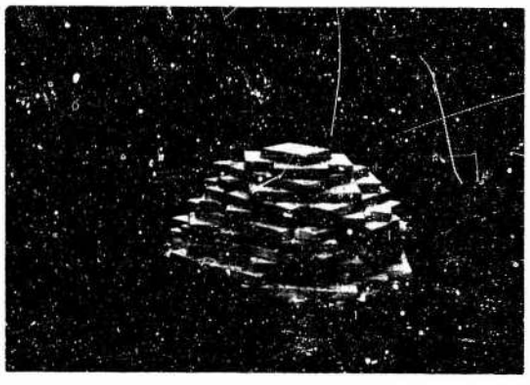

S4a

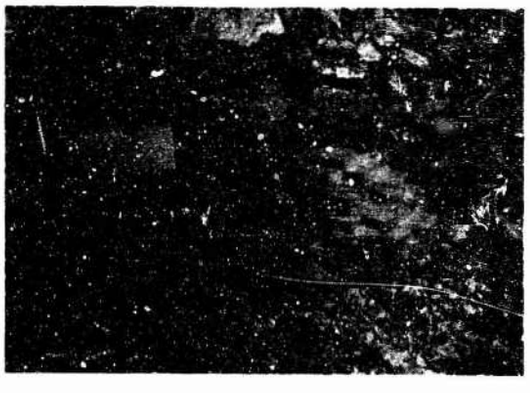

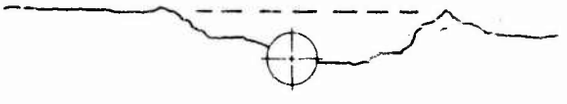

S4b

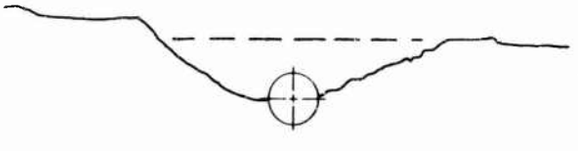

S4c

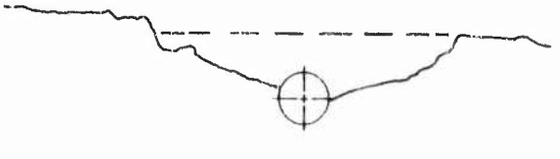

S4d

Figure 6. Charges in Position for Detonation for S4 Shot Series.

4. Location and Geology of Test Site

The MTCE project was conducted at the U. S. Army Yakima Firing Center located about 140 road miles southeast of Seattle, Washington, and 8 miles north of the city of Yakima, Washington. Approximate coordinates of the site are: Latitude 45°42'N, Longitude 120°20'W. A map of the site is shown in Figure 7. The topography of the test site, specific location of each shot, and exploratory bore-hole locations are shown in Figure 8.

The site is located on a rock slope that dips about 3.5 degrees to the north. A thin covering of valley alluvium, from 1 to 12 inches thick, remained on most of the surface after a blade had stripped the site of sparse vegetation and removed as much of the overlying alluvium as possible. Bare rock was exposed over about one third of the site. Figure 9 shows the rock surface near the H2 ground zero after overlying material had been carefully removed.

A seismic refraction survey of the site was conducted by the Air Force Weapons Laboratory (AFWL) in March 1965. The results of this exploratory survey revealed two refracting interfaces within 300 feet of the surface. These interfaces were located at depths of about 50 feet and 160 feet, forming boundaries between material of 11,100, 8,300, and 13,000 feet per second velocities from the rock surface downward. Results of AFWL tests of NX cores (cylindrical cores 2 inches in diameter) from the site are shown in Table 4. An average for the *in situ* densities measured in the upper 50 feet of basalt is 170 pounds per cubic foot. Mass calculations given in this report are based on this average *in situ* rock density. The rock compressive strength in the upper solid basalt region averaged about 18,500 pounds per square inch.

The western border of the site is a steep box canyon terminating to the north at about the location of the benchmark indicated in Figure 8. This benchmark elevation was taken arbitrarily to be 1,000 feet. The canyon, which opens into Selah Creek to the south, is occupied by an intermittent stream during spring runoff. The head of the canyon is composed of nearly vertical rock walls about 40 to 50 feet high.

Three rock formations represented in the test area are, from oldest to youngest, the Yakima basalt, the Ellensburg formation, and the Wenas basalt. The Ellensburg formation is of sedimentary origin and is composed of eight colored tuffaceous sandstone, claystone, and minor pebble conglomerate.

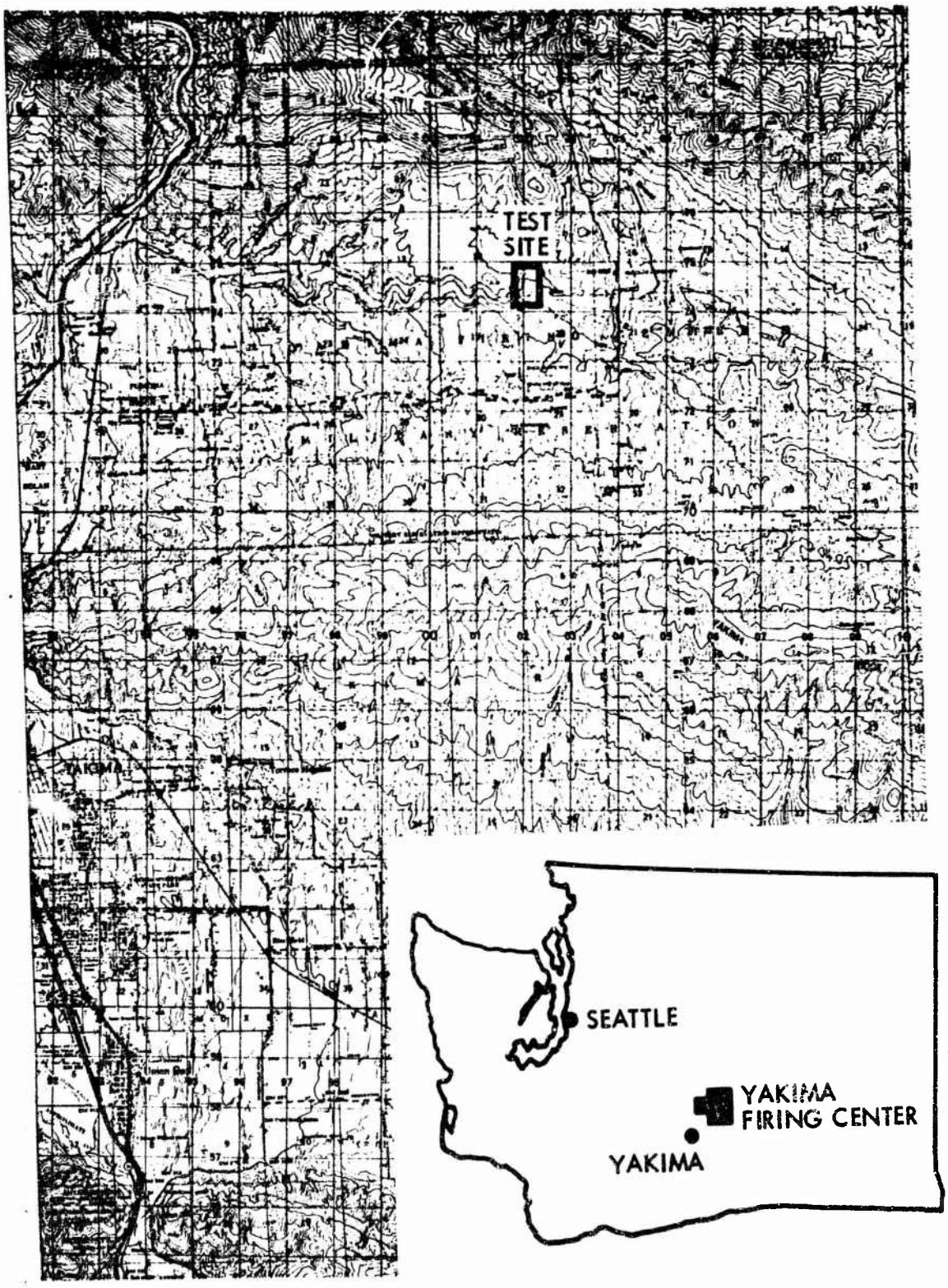

Figure 7. Location of Test Site.

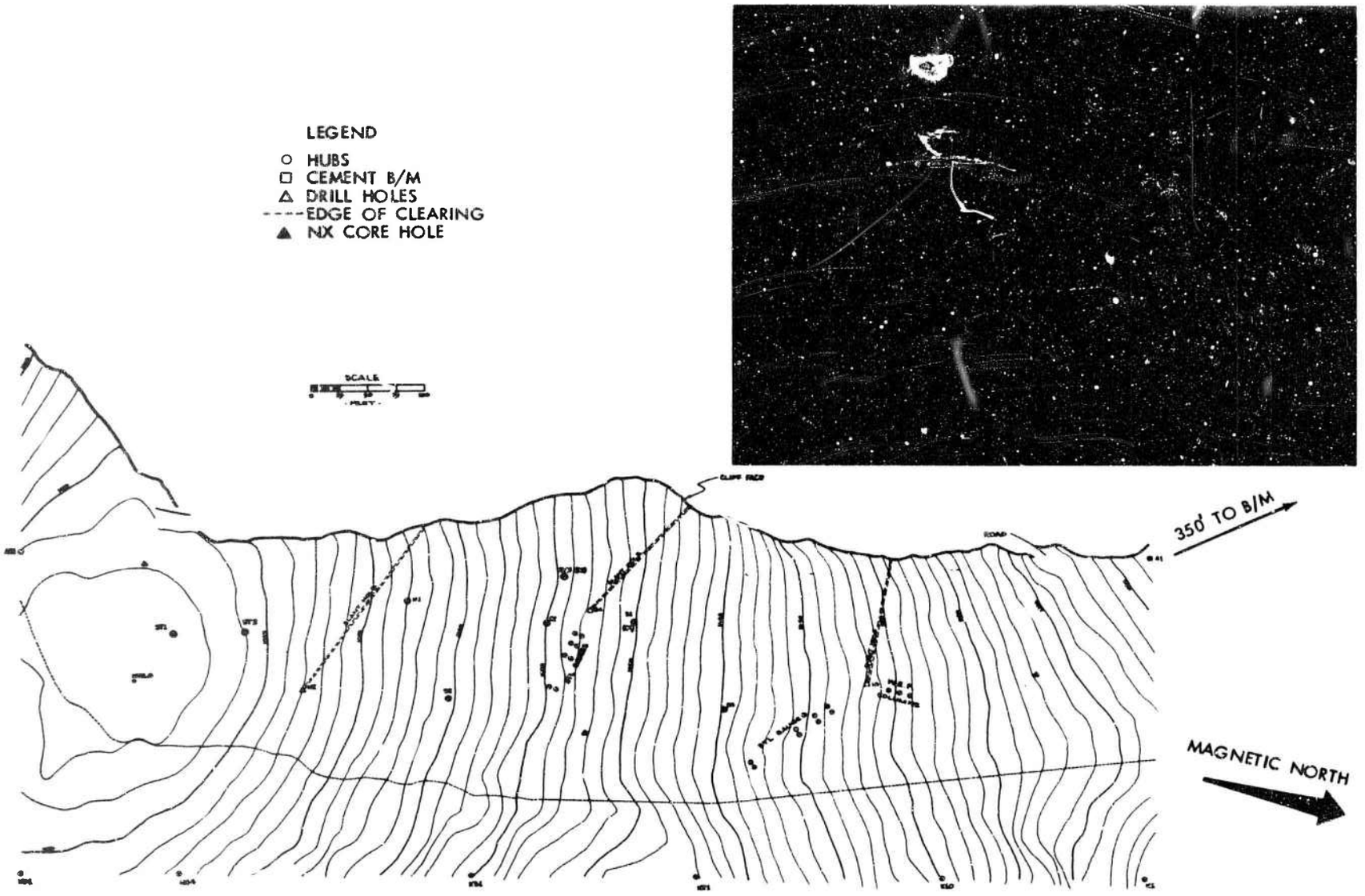

Figure 8. Test Site Topography and Shot Locations.

Figure 9. Bare Rock Surface Near Shot H2 Ground Zero.

Table 4

EXPLORATORY CORE HOLE RESULTS

	NX HOLE NO. 1 (South Hole)				NX HOLE NO. 2 (Middle Hole)				NX HOLE NO. 3 (North Hole)			
	Compressive Strength (psi)	Bulk Density (pcf)	Specific Gravity	Porosity (pct)	Compressive Strength (psi)	Bulk Density (pcf)	Specific Gravity	Porosity (pct)	Compressive Strength (psi)	Bulk Density (pcf)	Specific Gravity	Porosity (pct)
0												
Vesiculated Basalt	11,937	173	3.11	11	2,395				5,718	150	3.01	18.6
	4,790	173	3.03	8.4	4,910	158	2.93	14				
	23,054	173	2.93	5.2	8,084	183	2.99	12.7				
10					7,485	175	2.97	5.5				
					8,293	174	2.96	5.8				
									12,305	159	2.97	14.2
20					15,269				10,718	158	2.97	14.4
Solid Basalt												
30	34,000	178	2.91	2.3	25,150	175	3.03	7.4	26,048	182	2.96	12.2
					13,114	182	3.02	3.2				
40									27,096	160	2.96	14.1
Vesiculated Basalt Tuff	3,458	147	2.90	19	14,790	182	3.02	3.3				
		109	2.77	37	13,353	176	3.00	5.8				
					17,515	177	2.98	5.4				
50 Conglomerate & Breccia												
									Sandstone			
									Brown Clay			
Volcanic Ash												
60									918	122	2.88	32.4
									Volcanic Ash			
Breccia	630	108	2.84	34								
70												
Volcanic Ash									Sandstone	889	119	2.85	33.2
Brown Clay					Missing	823	114	2.66	31.1	Volcanic Ash	368	101	2.62	42.6
						1,003	111	2.70	33.9	Bottom of Hole				
Highly Fractured Basalt					Volcanic Ash	883	118	2.73	30.7	80				
80							77	2.66				
Volcanic Ash												
90 Deteriorated & Brownish-Gray Basalt	1,900	154	2.96	16						90		
					Vesiculated Basalt	2,560	152	2.97	18.1			
						4,551	159	2.93	13.2			
Bottom of Hole					Brown Shale	6,188	162	2.94	11.5			
100					100 Bottom of Hole					100		

The Yakima and Wenas basalts do not differ much in age or in general appearance. The most noticeable feature of the basalt is its columnar structure that characterizes the numerous flows constituting a combined thickness in excess of 10,000 feet. The upper portion of the basalt flows are often scoriaceous and glassy but become more dense and crystalline toward the interior of the flow.

The portion of the Yakima Firing Center on which the MTCE experiments were conducted is situated in a broad, synclinal valley that plunges to the northwest. This syncline is flanked on the north by Umtanum Ridge and on the south by Yakima Ridge. The subsurface structure of the test area is shown in Figure 10.

The cratering experiments were conducted on the weathered surface of one of the lower Wenas flows. This particular flow is approximately 50 feet thick. The relationship of the Wenas Basalt and the Ellensburg sedimentary interval at the test site is shown in Figure 11. The surface of the basalt is glassy, scoriaceous, and well exposed. The interior of this flow is hard, dense, microcrystalline, and generally unaltered.

Both the Yakima and Wenas are dark gray to black, dense usually fine-grained basalts. Locally interbedded with the basalt flows are minor sedimentary beds and weathered soil profiles. The weathered surface of the basalt flow is usually brownish gray in color and stained by iron oxide.

The general petrographic character of the test medium is shown in Figures 12 and 13. These photomicrographs display the fine, dense crystalline character, mineral composition, and texture of the subsurface unweathered basalt. These samples were obtained from drill cores.

The shock brecciated character of the test medium resulting from detonations is shown on the photomicrographs in Figure 14. Much of the microbrecciation appears to have taken place at the contacts of individual crystals. Most of the larger plagioclase crystals are fractured and bent. The glassy and fine grained matrix displays considerable microbrecciation.

These samples represent the most shocked breccia produced by detonations. The shock-compressed breccia also contain fragments of basalt that show only minor amounts of shock alteration.

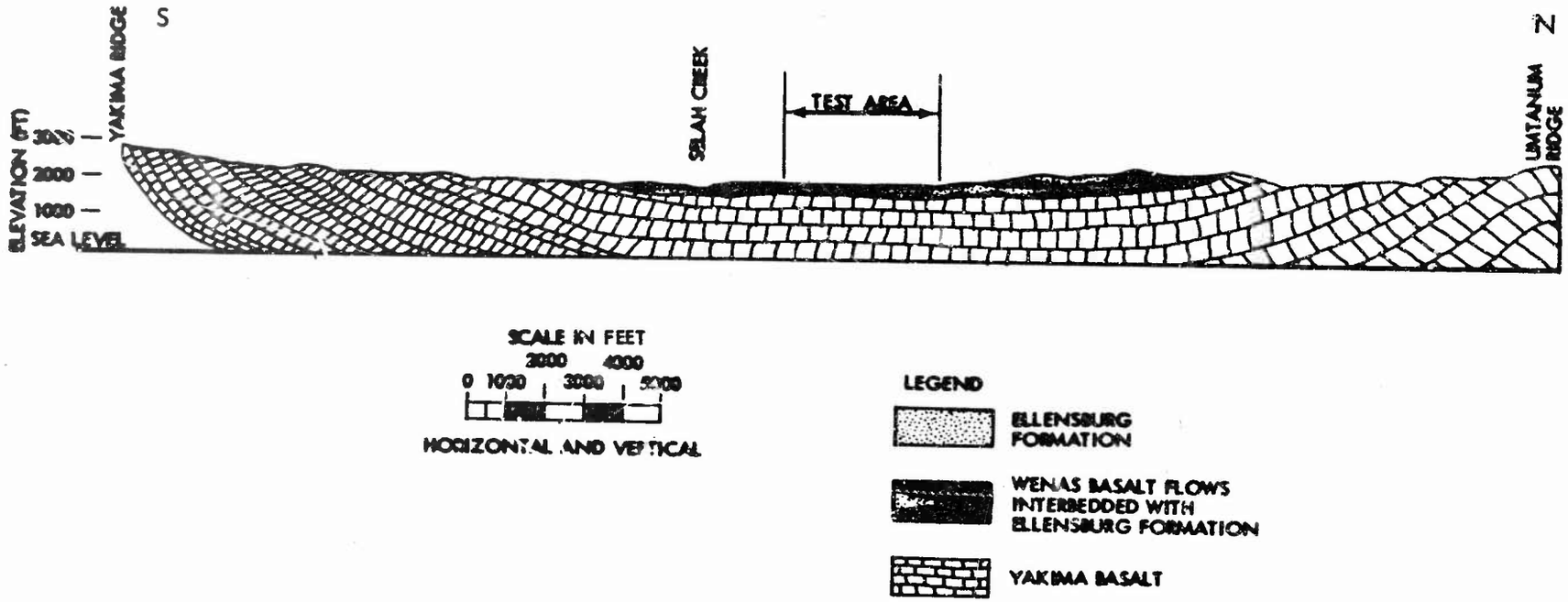

Figure 10. Subsurface Geologic Structure of the Test Site Area.

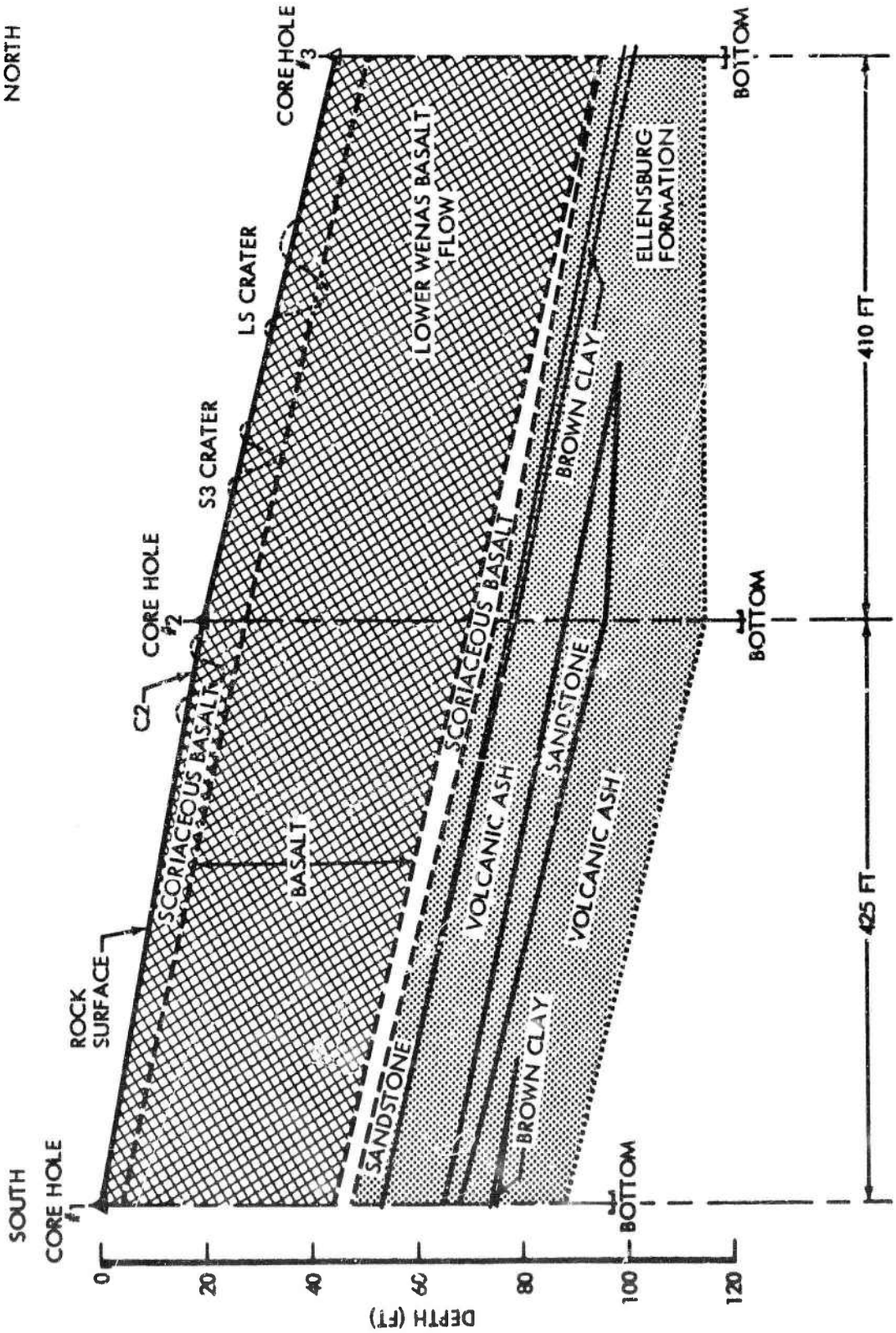

Figure 11. Structure of Test Site Based on Air Force Core Log.

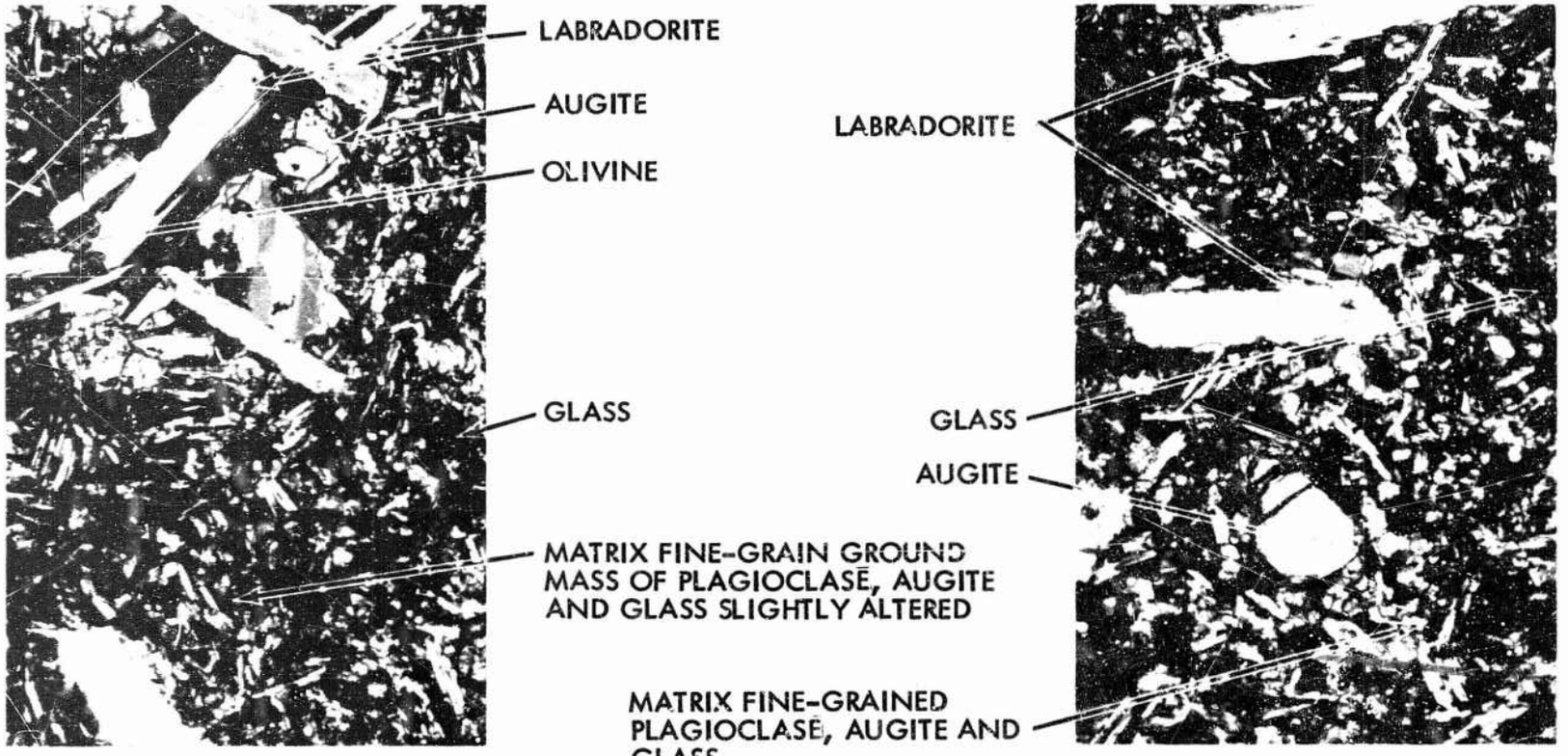

Figure 12. Photomicrographs of Unshocked Basalt Core (X-Nicols, 63X).

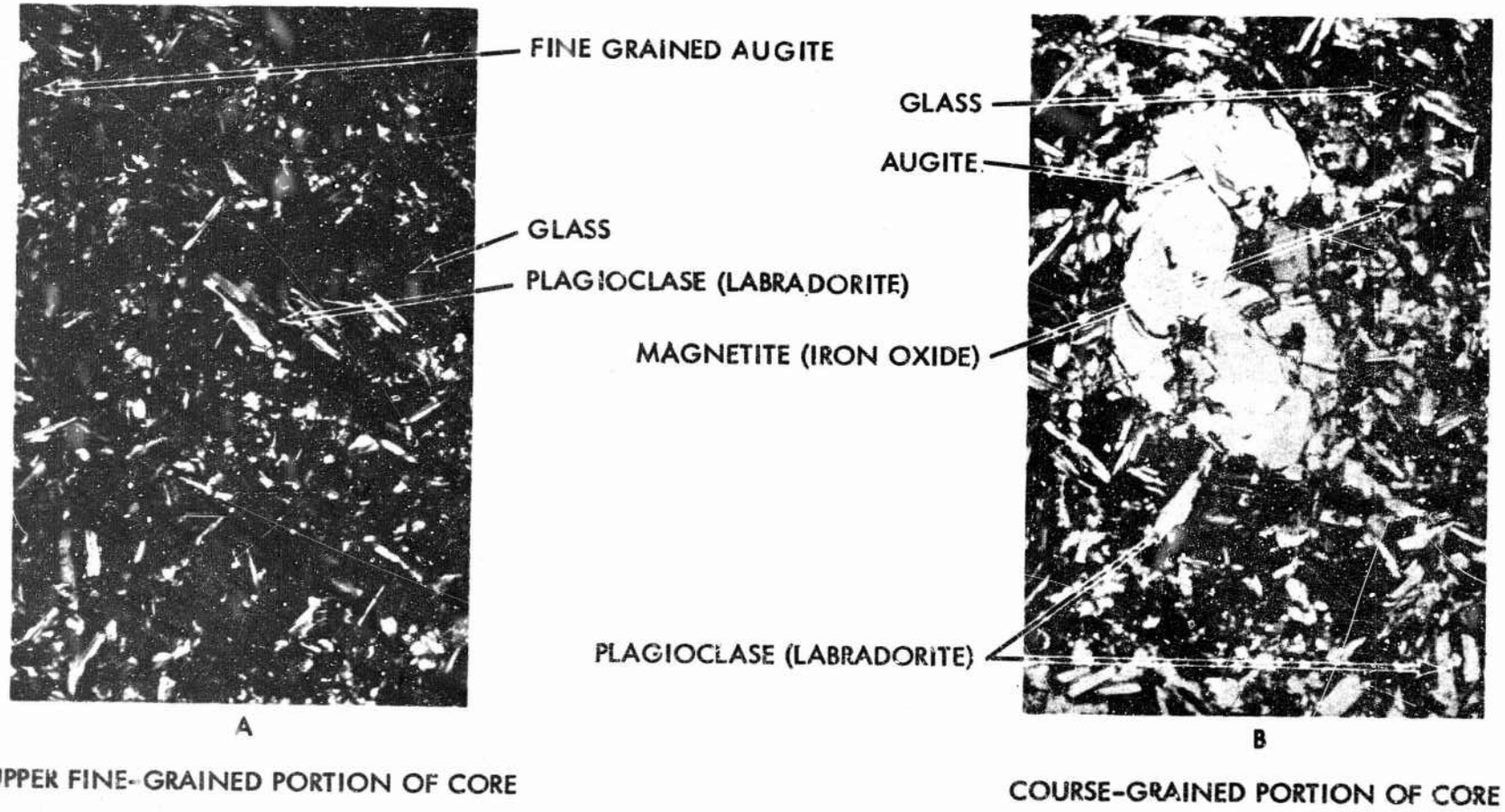

Figure 13. Photomicrographs of Unshocked Basalt Core (X-Nicols, 63X).

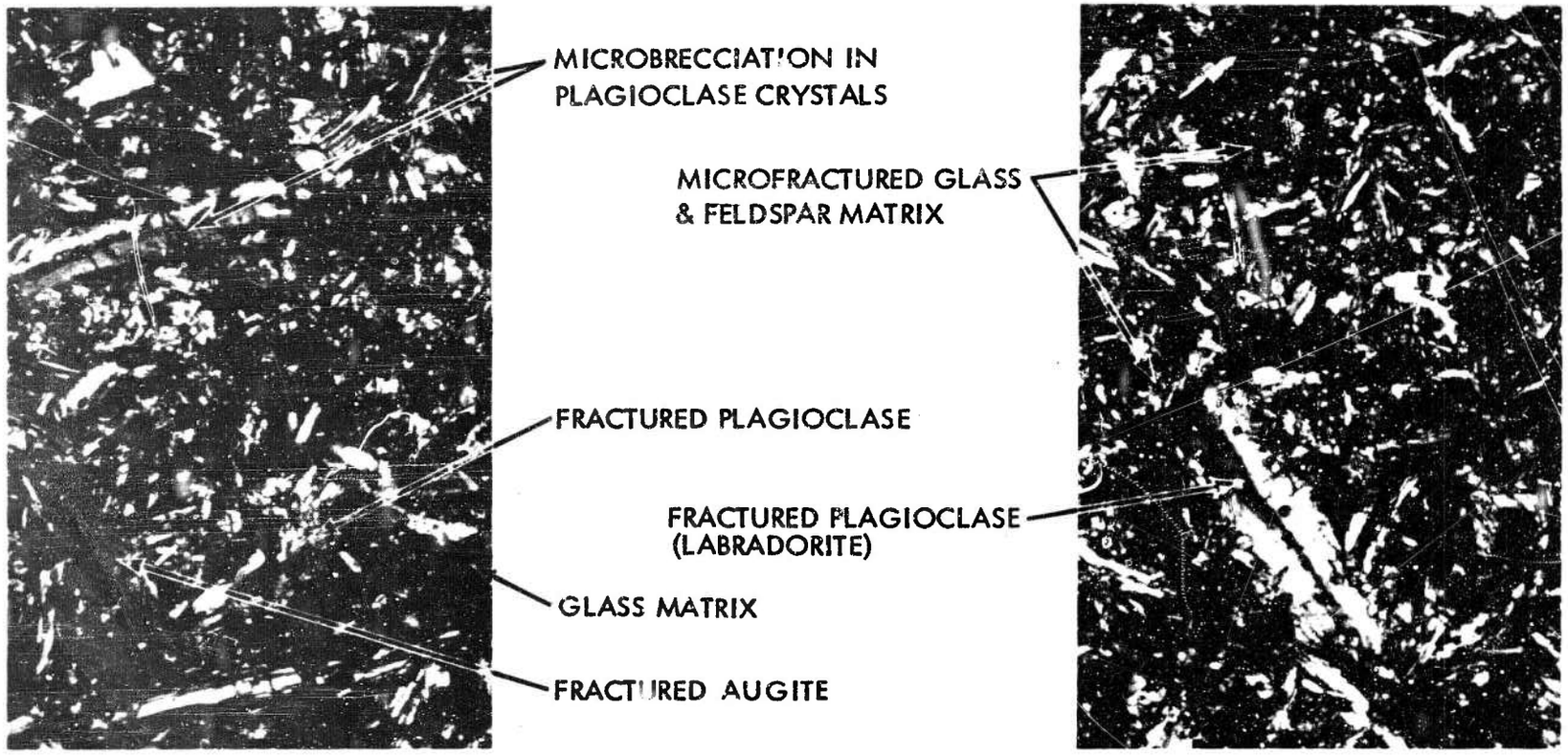

Figure 14. Photomicrographs of Shock Brecciated Basalt (X-Nicols, 63X).

SECTION II

EXPERIMENTAL PROCEDURE

1. Charge Placement

All shots in the MTCE series were formed by stacking the aforementioned 8-pound, 2 x 12 x 6 1/2 inch TNT blocks to represent the shape desired. Procedures to stack the blocks were perfected at AFWL prior to the field test program. Scaled wooden blocks were used to represent each layer of the TNT blocks. Templates were revolved around the model to insure the stack represented the desired shape as closely as possible. A model of the H2 shot model is shown in Figure 15. In the field, the half-buried and fully-buried spherical charges were grouted into holes. The surface tangent spheres were stacked using styrofoam for support around the lower half of the sphere. Figures 16 through 19 show a typical charge placement sequence for various charges.

2. Crater Measurements

a. The Apparent Crater.

Stereophotographs were taken to record the preshot topography of each ground zero area and to record that of the resulting crater and its lip region. An aerial stereo camera was mounted on a platform, which was elevated by a crane to a height of 60 feet above each crater. Both pre- and postshot photographs were taken from this height. Each photograph covered a ground area of about 80 by 80 feet. Figure 20 illustrates the field technique used to make aerial stereophotographs of each crater.

For ground elevation control, a minimum of eight points were established and surveyed in the vicinity of ground zero for each shot. Figure 21 shows a typical elevation control survey layout and illustrates the area photographed in relation to the largest and smallest crater. As illustrated in Figure 21, the photographic coverage and resulting topographic map of each crater covers approximately an 80- by 80-foot area. Thus, the area photographed had a radius equal to about two crater radii for the largest crater (LS) and ten crater radii for the smallest crater (ST1). All ground elevations were based on a control bench mark (see Figure 8) with an assumed elevation of 1000 feet.

Figure 15. Model of Large Hemisphere Shot (H-2).

Figure 16. Large Hemisphere Shot In-place (H-2).

Figure 17. Placement of Half-buried Sphere (LS).

Figure 18. Placement of Surface-tangent Sphere (ST1).

Figure 19. Placement of Fully-buried Sphere (C-2).

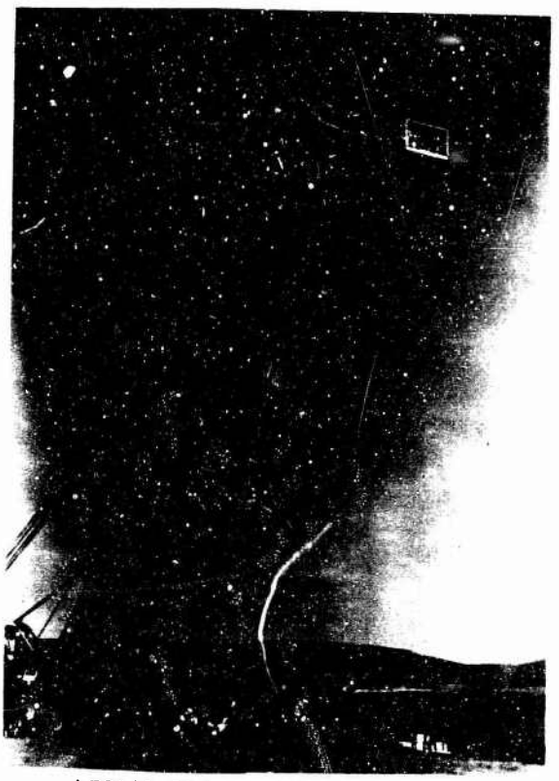

AERIAL PLATFORM AND CRANE

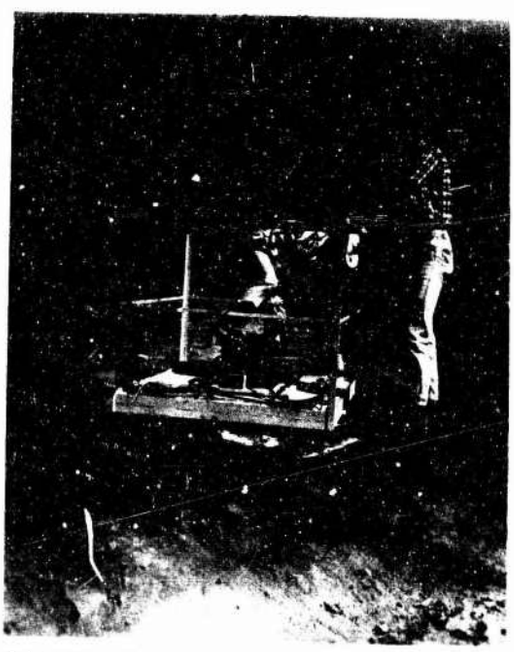

CAMERA IN POSITION ON PLAT. ORM

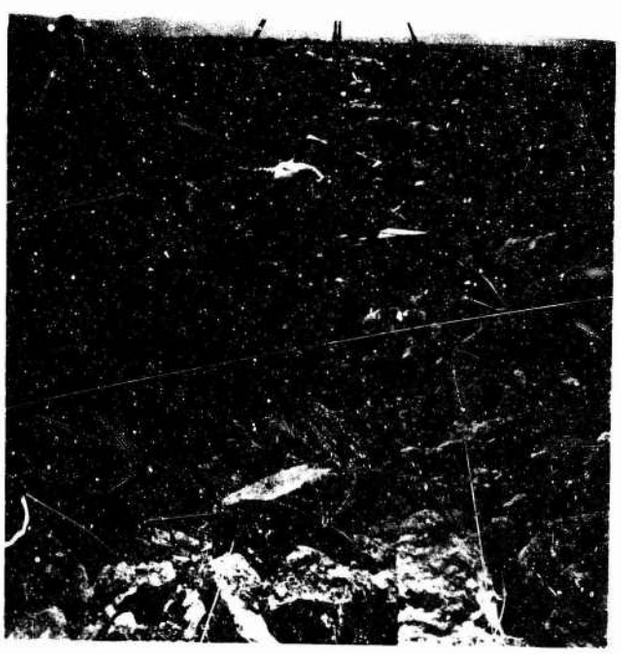

PLATFORM IN POSITION READY TO BE ELEVATED OVER CRATER

Figure 20. Field Technique for Taking Aerial Stereophotographs of Each Crater.

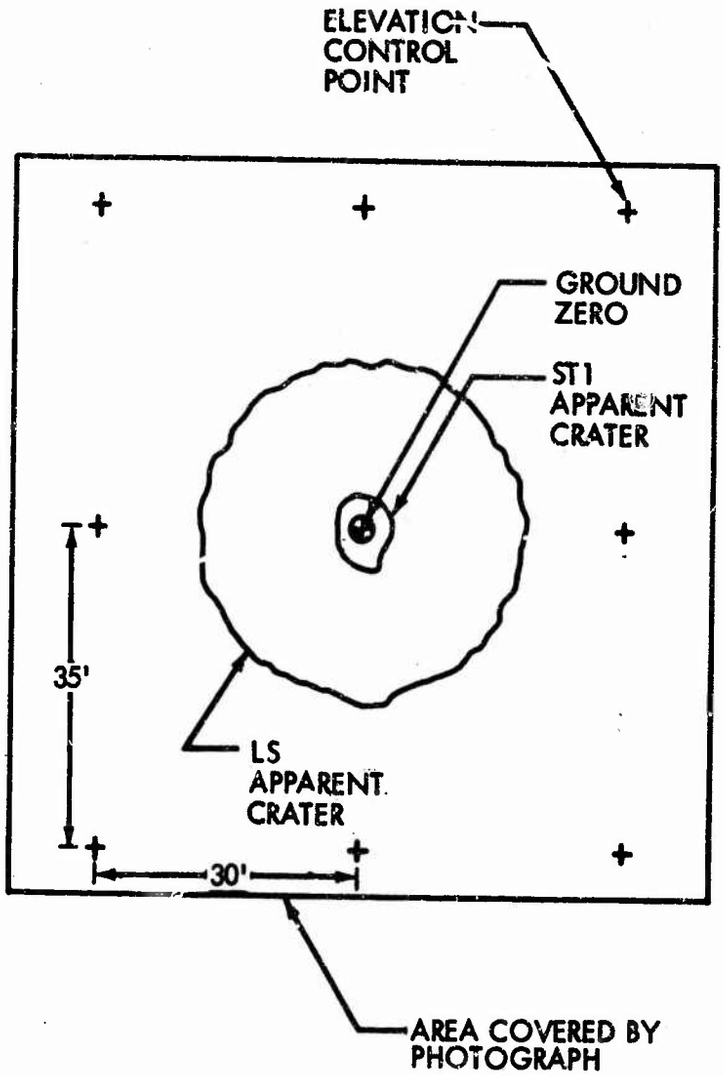

Figure 21. Elevation Control Survey Points and Area Covered by Each Aerial Photograph.

Apparent crater dimensions were obtained frc topographic maps prepared from aerial stereophotographs by American Aerial Surveys, Inc., Covina, California. Crater contour maps were prepared to a scale of 1 inch to 2 feet, with a contour interval of 0.2 foot, using conventional photogrammetric mapping techniques. Topographic maps and photographs of each crater are presented in Appendix II.

American Aerial Surveys, Inc., was also responsible for determining crater and ejecta volumes by photogrammetric cross sectioning of pre- and postshot topographic maps using the Kelsh DI System with an automatic digitizer and card punch. Data were reduced on a computer using a program that calculated volumes by the average-end-area method. This method consists of multiplying the average area of two profiles by the distance between them. Profiles used in this calculation were taken from pre- and postshot topographic maps.

b. The Excavated Crater

After the test series was completed, a backhoe was used to remove all fallback and loose fractured rock along 2 diameters in each apparent crater. Figure 22 shows the backhoe excavating material from the S2b crater and an excavated trench in that crater. Hand tools were used to remove fine material that could not be excavated by the backhoe. Conventional topographic surveys were run along these excavated crater floors. The crater region defined by these profiles is described in Section I.

3. Lip Measurements

a. Ejecta

Close-in apparent-lip thicknesses were determined from topographic maps of the preshot ground surface and the lip region of the resulting crater. Upthrust profiles along four radials were superimposed over corresponding plots of the orginal ground surface and the postshot apparent lip. The net differences between the apparent-lip profiles and the corresponding upthrust profile were then determined at selected distances from ground zero. The defined ejecta thicknesses were averaged at selected radial distances. To determine total ejecta mass and thickness as a function of radial distance from ground zero, ejecta data were combined with data derivable from the AFWL missile survey.

EXCAVATING CRATER S2b

EXCAVATED PROFILE OF CRATER S2b

Figure 22. Crater Excavation.

b. Upthrust Measurements

Control marks, used to measure permanent ground movement, were painted on the exposed basalt surface before each single shot and before each series of shots. These control points were located along 2 diameters adjacent to the edge of the anticipated crater and extended radially toward the aerial-survey corner control pins. Elevations were read on these marks before each shot. Immediately after taking postshot aerial photos, upthrust points were relocated and resurveyed to determine the change in elevation from preshot conditions. For series shots, the postshot elevations of marks used on a preceding shot were again used as preshot elevations for the next successive shot. On the H2 shot, a number of permanent pins were set into the basalt adjacent to the anticipated crater edge to permit close horizontal and vertical control. It was then possible to determine the vertical displacement and the permanent horizontal displacement of the rock surface. Pin locations on shot H2 and a photograph of a pin in position are shown in Figure 23.

4. Volumetric Density Measurements

Ejecta volumetric densities were determined on the LS and S2b shots. An area of ejecta in the lip region of these craters was selected and topographically surveyed. The ejecta was then removed and weighed, and each area was resurveyed. Computation of volumes were made from the pre- and post-excavation surveys. Figure 24 shows a photograph of each sampling region and the area covered relative to the crater. Survey profiles were made at 2-foot intervals in the NS direction on the LS crater, and at 2-foot intervals in the EW direction on the S2b crater. Thus, a total of 19 profiles were recorded for shot LS, and 13 profiles were recorded for shot S2b.

The bulk (volumetric) density for the two areas, computed by dividing the weight of the samples by the corresponding volumes computed from the profiles, was 141 pounds per cubic foot for the LS crater and 108 pounds per cubic foot for the S2b crater.

The erratic nature of the distribution of ejecta resulting from craters in rock and the limited upthrust data obtained from this experiment prohibit the determination of meaningful scaling relationships for ejecta thickness and upthrust.

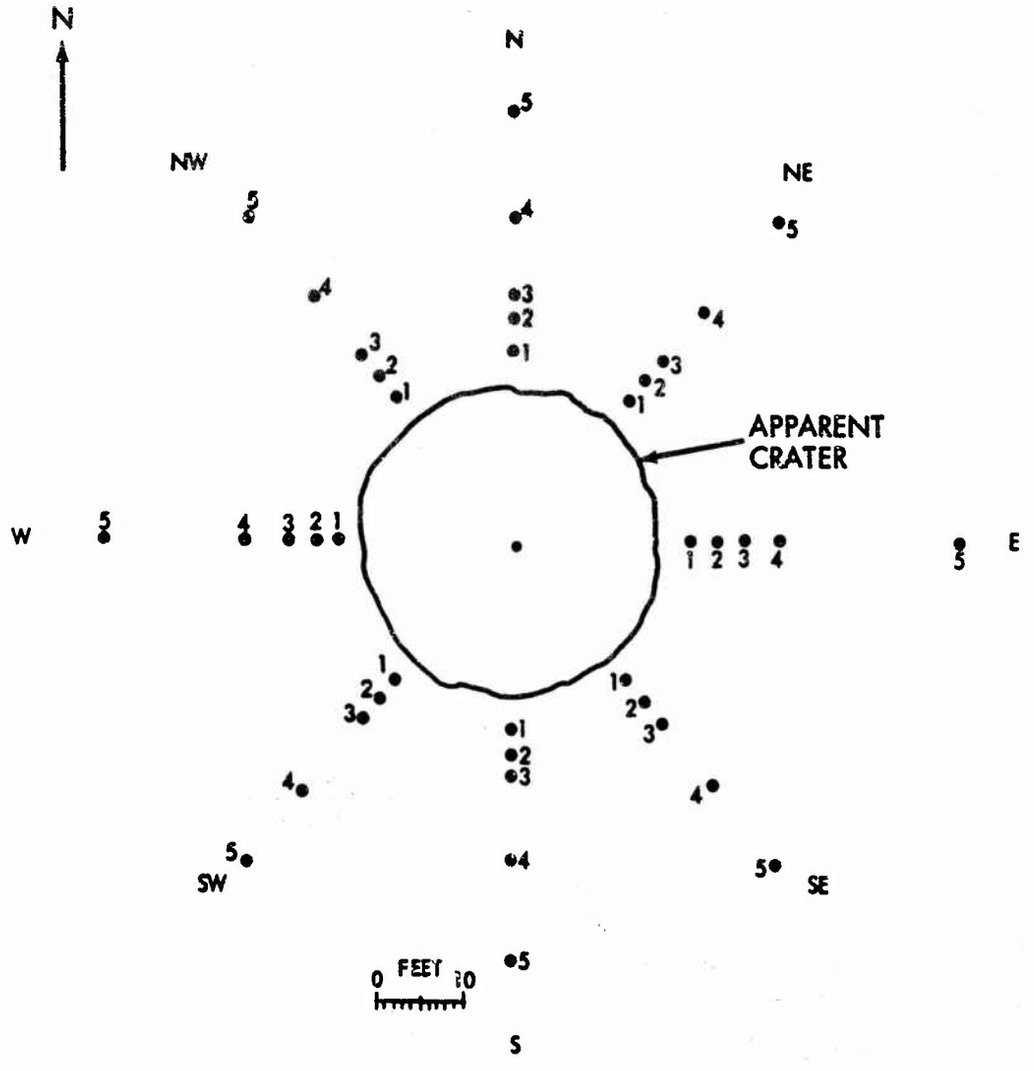

Figure 23. Layout of Upthrust Pins and Pin in Position for Recording Permanent Ground Displacement Adjacent to the H2 Crater.

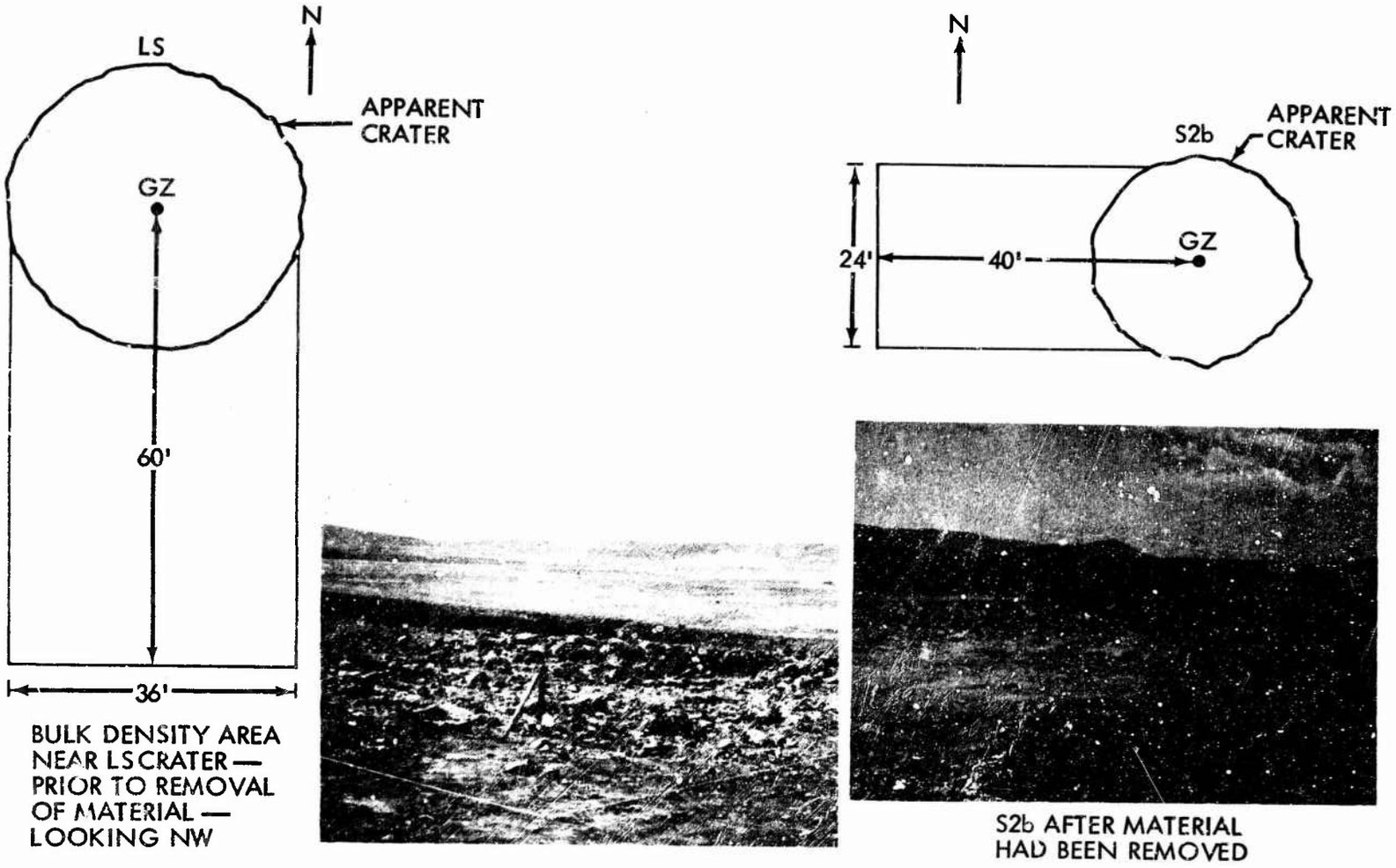

Figure 24. Ejecta Volumetric Density Areas.

Fifty percent of the ejected material was deposited between the crater edge and 1.7 crater radii for the H1 shot. This 50 percent distance was 2.0 crater radii for the H2 crater, 1.2 crater radii for the LS crater, and 1.9 crater radii for the S4a crater.

5. Missile Survey

A survey of discrete missiles was performed for various shots as listed in Table II.3, Appendix II. This survey was accomplished by plotting, weighing, and measuring individual rock missiles after each shot. The surveying of missile position was accomplished by a plane table and transit with an accuracy of $\pm$ 1 foot. After each survey the missiles were painted to avoid confusing them with missiles from later shots. The site was periodically cleared of debris to enhance the quality of the survey. A detailed statistical analysis of the distribution of missiles will be reported in Volume III of this report.

SECTION III

RESULTS

1. Craters

a. Dimensions and Volumes

A topographic map of each preshot site and a topographic map, profile, and aerial photograph for each MTCE crater is given in Appendix I.

Apparent and excavated crater dimensions and volumes are listed in Table 5. The apparent crater radius (R_a) represents an average of 16 radial readings made on the crater topographic map. The listed excavated crater radius (R_t') is an average of the four (in certain cases, three) excavated crater radii obtained from the radial profiles that were made for each crater. Each excavated crater volume (V_t') represents the sum of incremental volumes generated by revolving each excavated crater profile through its appropriate angle. Apparent crater volume (V_a) calculations were made by American Aerial Surveys, Inc., using the digitizing and computing technique described in Section II.

The apparent crater radius given in Table 5 is approximately equal to that radius calculated by assuming that the crater area at the original rock surface is circular. As an example, the average apparent crater radius for C2 is 13.96 feet using 16 radial measurements. (The radius of 14.0 in Table 5 is consistent with the 0.1 foot accuracy given for all tabulated data.) When the 32 radial measurements are averaged, the crater radius is 14.00 feet. When the area defined by connecting the 32 crater edge points along the 32 radials cited above, is measured and assumed to be circular, its radius is computed to be 13.77 feet. Thus, it is estimated that radius values given in Table 5 are within $\pm$ 3 percent of radius values that would be calculated by assuming the original ground surface crater area to be a circle.

Figure 25 shows two views of the four craters located in the central region of the test site. Air Force personnel recorded ground shock signals sensed by instruments in a hole below the S4 ground zero. Shock records were also made by utilizing the S4 instrumented hole for the C2, ST3a(C3), and S1(C1) events. The parenthetical designations of C3 and C1 associated with the ST3a and S1 shots, respectively, were originally selected because of the applicability

Table 5

CRATER DIMENSIONS AND VOLUMES

Shot	Apparent Crater				Excavated Crater		
	Radius, R_a[a]	Depth (GZ) D_a	Depth (Max) D_a	Volume V_a	Radius, R'_t	Depth (GZ) D'_t	Volume V'_t
	(ft)	(ft)	(ft)	(ft^3)	(ft)	(ft)	(ft^3)
S1(C1)	12.1	3.4	3.6	733	16.0[c]	5.3	2060
S2a	10.7	3.9	4.0	672	—	—	—
S2b	13.6	4.2	4.8	1812	19.4[b]	9.0	3096
S3a	11.4	4.0	4.0	853	—	—	—
S3b	12.3	4.8	6.0	1223	—	—	—
S3c	14.8	6.5	7.7	2411	24.2[b]	12.2	6233
S4a	10.4	3.1	4.0	605	—	—	—
S4b	12.2	5.5	5.8	1178	—	—	—
S4c	13.6	5.5	5.9	1577	—	—	—
S4d	14.8	8.0	8.4	2081	25.2[c]	11.7	6615
LS	18.7	5.4	5.6	3659	23.8[b]	9.1	7527
H2	17.1	5.0	5.4	2417	25.2[b]	7.5	5716
H1	10.2	1.9	3.0	536	17.3[b]	4.1	1608
C2	14.0	4.6	5.3	1500	25.8[c]	7.3	4189
ST1	3.7	1.0	1.3	37	5.4[b]	1.7	—
ST2a	6.8	1.4	1.9	139	—	—	—
ST2b	8.8	1.8	2.3	242	14.3[b]	4.4	946
ST3a(C3)	4.5	0.9	1.2	25	—	—	—
ST3b	9.2	1.7	2.4	324	—	—	—
ST3c	12.3	1.3	3.3	560	16.8[c]	4.9	1512

[a] Average of sixteen readings
[b] Average of four readings
[c] Average of three readings

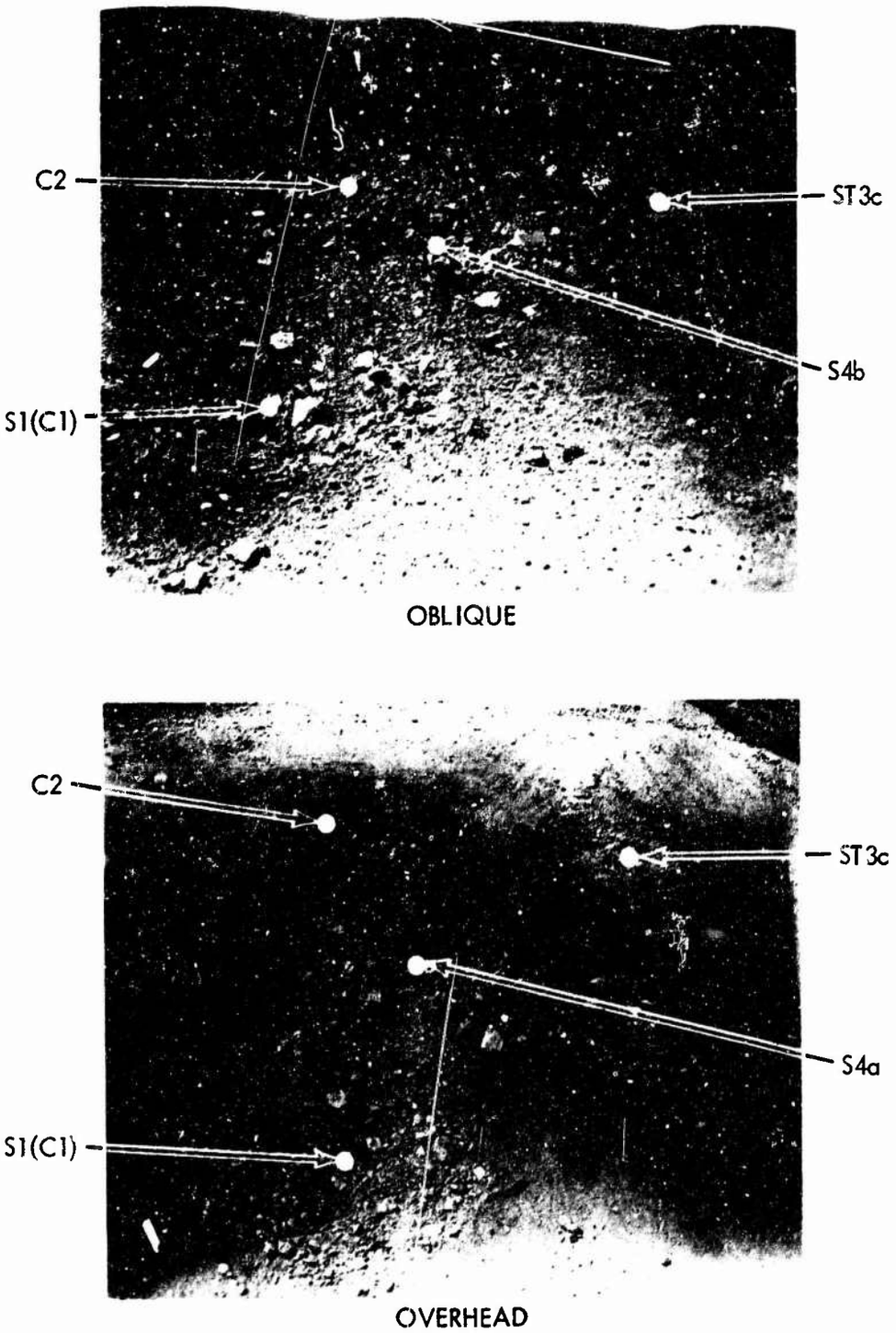

Figure 25. Craters Located Near Central Region of Test Site.

of these shots to the coupling objectives of the ground shock program. Several other shots apply to the coupling objectives when cratering effects are studied.

An aerial photograph of the S4C crater with contour lines superimposed is shown in Figure 26. This crater was formed by a series of four successive 4000-pound half-buried TNT spherical charges. A similar aerial photograph for the LS crater is shown in Figure 27. This crater was formed by a single 16,000-pound half-buried TNT spherical charge. The photographs shown in Figures 26 and 27 are the same scale. The C2 crater (4000-pound fully-buried sphere) is shown in Figure 28. Also shown in this figure are upthrusted rock blocks near the crater edge. Similar upthrusted blocks were observed on several other MTCE craters.

The blocky nature of the MTCE craters, particularly evident on the C2 crater, is a characteristic of high-explosive craters in rock media. BUCKBOARD craters, although formed from buried charges, were similar in appearance (Reference 9). This blocky appearance of rock craters is most evident when the size of the natural fragmentation pattern of the rock medium is large relative to the charge size, and when the resultant crater is small relative to the block size. When very large charges are detonated in rock (see for example the photograph of the DANNY BOY crater in Reference 10), the crater is large relative to the block size and takes on an overall symmetrical, typical "crater-like" appearance. Figure 29 illustrates this.

b. Shape Characteristics

Crater shape characteristics are given in Table 6. The shape factor, F, is the measured volume divided by the quantity, $\pi R_a^2 D_a$ or $\pi (R_t')^2 D_t'$. Crater cross sections corresponding to various shape factors are also shown in Table 6. The ratio of crater depth to crater radius is also given in Table 6.

c. Excavated and Apparent Dimensions

The comparison of excavated and apparent crater dimensions is shown in Table 7. The ratio of apparent to excavated depth and radius is about 0.7. The ratio of apparent volume to excavated volume is about 0.4.

2. Upthrust and Ejecta

Crater lip crest data are summarized in Table 8. Each apparent lip dimension is the average of four profiles. True lip dimensions represent the average of

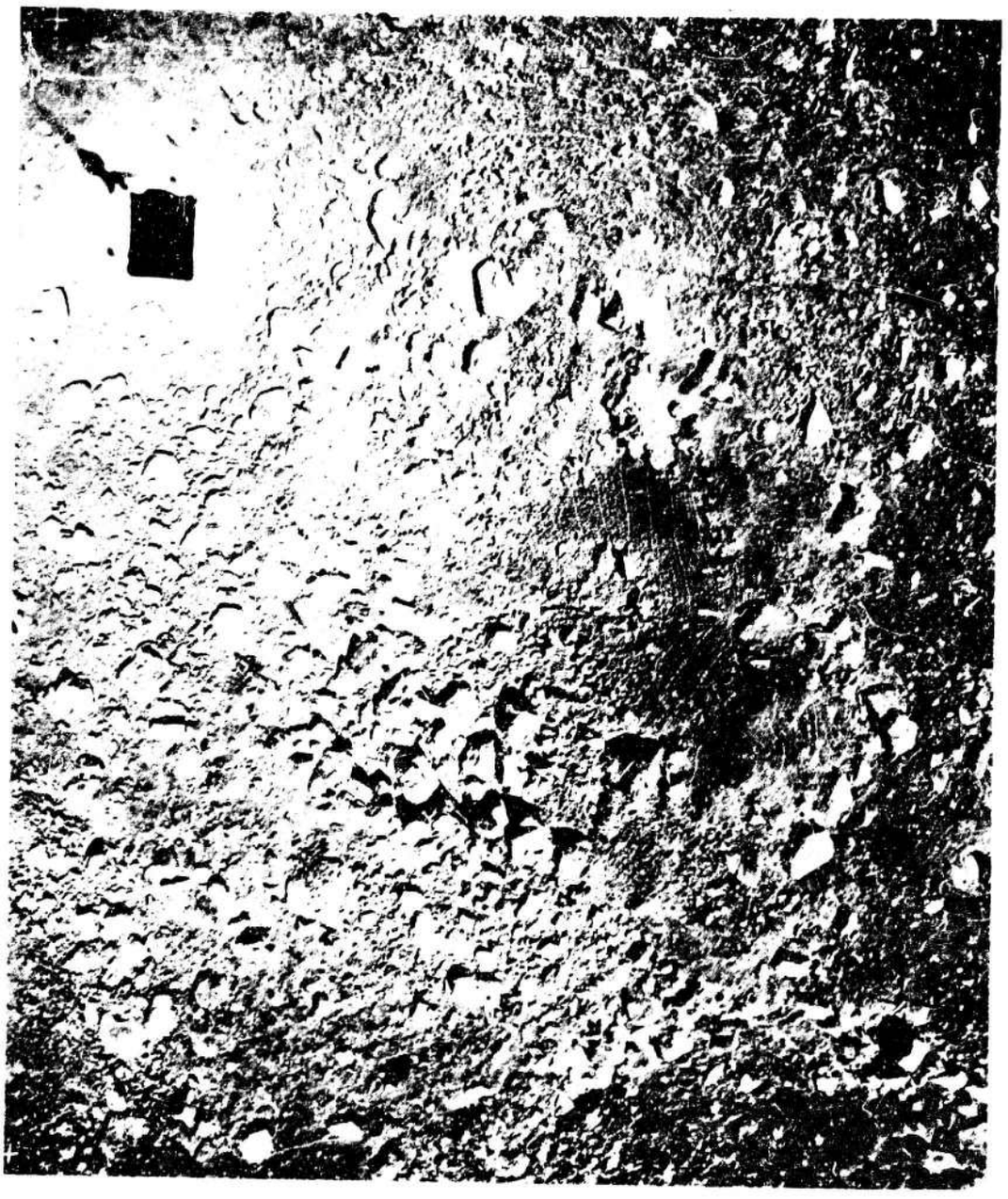

Figure 26. Aerial Photograph with Contours Superimposed for S4d.

Figure 27. Aerial Photograph with Contours Superimposed for LS.

OVERHEAD VIEW LOOKING E .ST

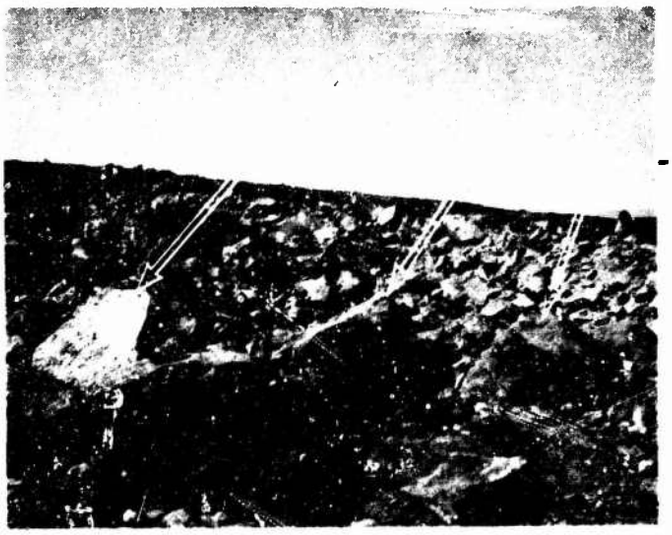

LOOKING WEST TOWARD CENTER OF CRATER. NOTE UPTHRUSTED BLOCKS IN FOREGROUND AT CRATERS EDGE.

Figure 28. Crater C2 Formed by a Fully-Buried Tangent Spherical Charge.

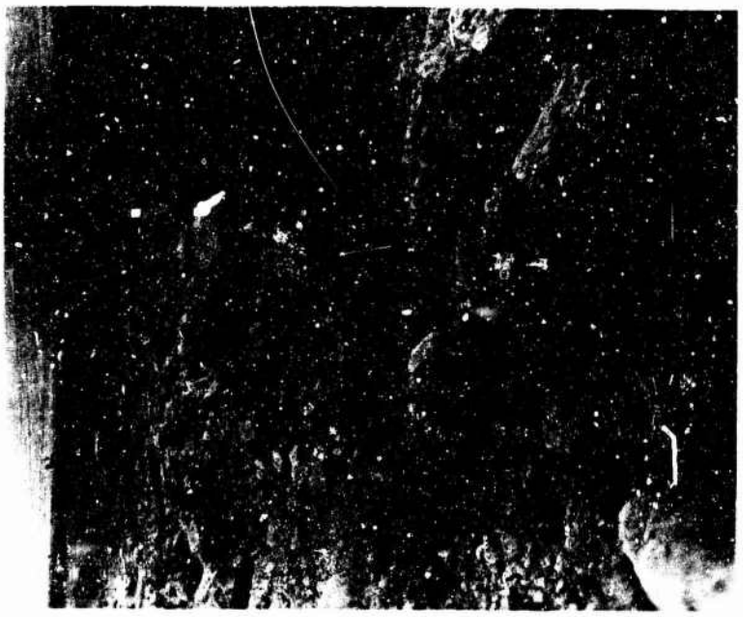

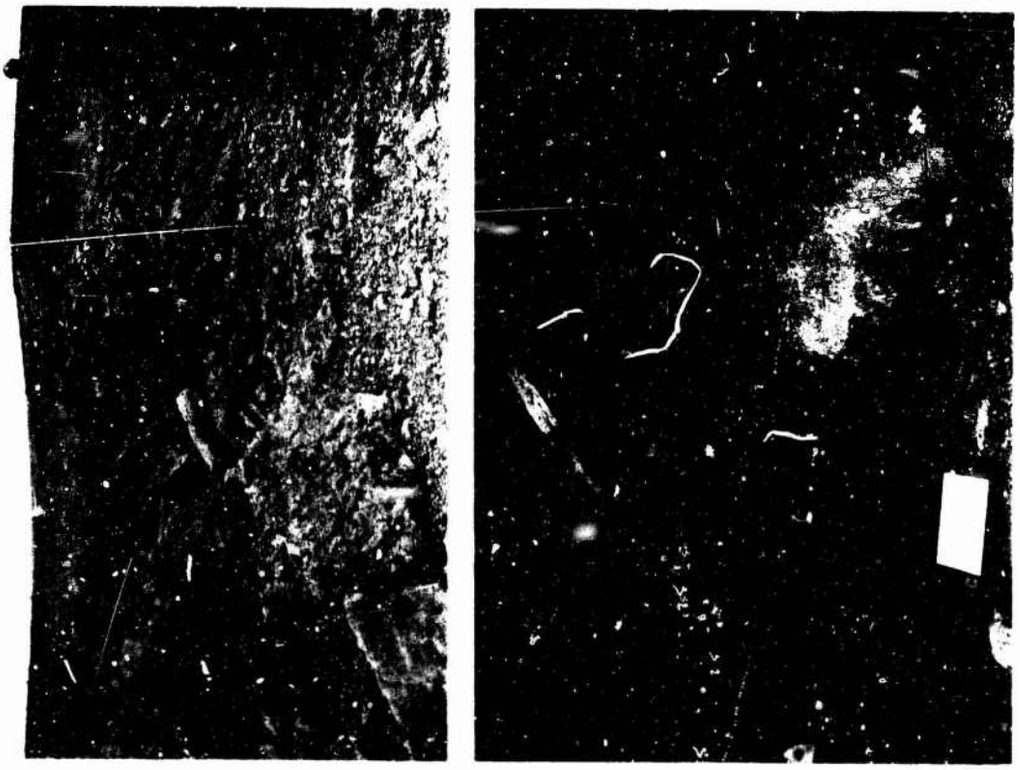

Figure 29. Photographs Showing Ejecta Distributed Adjacent to the S2a Crater.

Table 6

CRATER SHAPE CHARACTERISTICS

Shot	Shape Factor, F		Depth to Radius Ratio	
	Apparent	Excavated	Apparent D_a/R_a	Excavated D'_t/R'_t
S1(C1)	0.44	0.48	0.30	0.33
S2a	0.46	—	0.37	—
S2b	0.64	0.37	0.36	0.46
S3a	0.51	—	0.35	—
S3b	0.43	—	0.49	—
S3c	0.46	0.28	0.52	0.50
S4a	0.44	—	0.39	—
S4b	0.43	—	0.47	—
S4c	0.46	—	0.43	—
S4d	0.36	0.28	0.57	0.47
LS	0.59	0.46	0.30	0.38
H2	0.49	0.38	0.32	0.30
H1	0.55	0.42	0.29	0.24
C2	0.46	0.28	0.38	0.28
ST1	1.66	—	0.35	0.32
ST2a	1.50	—	0.28	—
ST2b	0.44	0.34	0.26	0.31
ST3a	1.33	—	0.27	—
ST3b	0.52	—	0.26	—
ST3c	0.36	0.35	0.26	0.29


RIGHT CIRCULAR CYLINDER F = 1.00

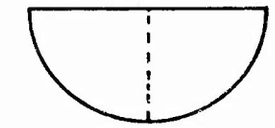
HEMISPHERE F = 0.67

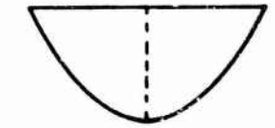
PARABOLOID OF REVOLUTION F = 0.50

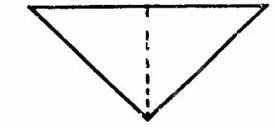
RIGHT CIRCULAR CONE F = 0.33

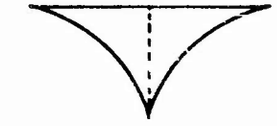
HYPOCYCLOID OF REVOLUTION F = 0.21

Table 7

EXCAVATED AND APPARENT CRATERS

Shot	Depth				Radius				Volume			
	Apparent D_a	Excavated D_t'	$\frac{D_t'}{D_a}$	$\frac{D_a}{D_t'}$	Apparent R_a	Excavated R_t'	$\frac{R_t'}{R_a}$	$\frac{R_a}{R_t'}$	Apparent V_a	Excavated V_t'	$\frac{V_t'}{V_a}$	$\frac{V_a}{V_t'}$
	(ft)	(ft)			(ft)	(ft)			(ft^3)	(ft^3)		
S1(C1)	3.6	5.3	1.5	0.7	12.1	16.0	1.3	0.8	733	2060	2.8	0.4
S2b	4.8	9.0	1.9	0.5	13.6	19.4	1.4	0.7	1802	3896	2.2	0.5
S3c	7.7	12.2	1.6	0.7	14.8	24.2	1.6	0.6	2413	6233	2.6	0.4
S4d	8.4	11.7	1.4	0.7	14.8	25.2	1.7	0.6	2081	6615	3.2	0.3
LS	5.6	9.1	1.6	0.6	18.7	23.8	1.3	0.8	3659	7527	2.0	0.5
H2	5.4	7.5	1.4	0.7	17.1	25.2	1.5	0.7	2417	5718	2.4	0.4
H1	3.0	4.1	1.4	0.7	10.2	17.3	1.7	0.6	536	1608	3.0	0.3
C2	5.3	7.3	1.4	0.7	14.0	25.8	1.8	0.5	1500	4189	2.8	0.4
ST1	1.3	1.7	1.3	0.8	3.7	5.4	1.5	0.7	37	—	—	—
ST2b	2.3	4.4	1.9	0.5	8.8	14.3	1.6	0.6	242	946	3.9	0.2
ST3c	3.5	4.9	1.5	0.7	12.3	16.8	1.4	0.7	560	1512	2.7	0.4
MEAN			1.5	0.7			1.5	0.7			2.8	0.4

Table 8

SUMMARY OF LIP CREST DATA

All lip crest dimensions are in feet. Successive shot lip dimensions shown were those measured after each shot and thus represent a cumulation of similar measurements from preceding shots.

Shot	H_{tl}	H_{tlc}	H_{al}	R_{al}	R_{ds}
S1(C1)	0.2	0.2	1.2	14.6	22.0
S2a	0.4	0.3	1.4	14.6	26.4
S2b	0.3	0.2	1.6	18.4	32.0
S3a	0.5	0.2	1.7	16.2	24.4
S3b	0.6	0.4	1.6	18.1	26.8
S3c	0.6	0.5	2.2	19.2	26.8
S4a	0.4	0.3	1.4	14.7	29.0
S4b	0.6	0.2	1.4	17.0	29.0
S4c	0.7	0.3	1.5	20.5	29.0
S4d	0.6	0.2	1.6	20.7	29.0
LS	0.8	0.6	1.8	22.6	47.3
H2	0.7	0.6	1.8	20.6	40.0
H1	0.3	0.3	1.1	14.3	35.1
C2	0.4	0.2	1.3	17.4	34.3
ST1	—	—	0.5	5.9	—
ST2a	0.1	0.1	0.5	12.9	18.0
ST2b	0.4	0.4	0.9	12.8	22.6
St3a(C3)	0.5	0.1	0.3	10.1	16.5
ST3b	0.5	0.3	1.1	11.6	20.5
ST3c	0.3	0.2	0.7	17.1	22.5

two to four profiles with the following exceptions: (1) lip dimensions for the S1(C1) crater result from only one upthrust profile and (2) true lip dimensions for the H2 crater are averages of eight profiles.

Permanent vertical and horizontal displacements of the rock surface adjacent to the H2 crater are shown in Table 9. Permanent vertical displacement data for all other craters are given in Table II.1 of Appendix II.

Observed ejecta data are tabulated in Table II.2 of Appendix II. These data are presented as graphs of ejecta thickness versus distance and are presented in Section IV. Ejecta data obtained from the missile survey and used for mass distribution determinations presented in Section IV, are tabulated in Table II.3 of Appendix II.

Masses and volumes associated with all MICE excavated craters are given in Table 10. Masses associated with excavated and apparent craters were obtained by multiplying measured volumes by a density of 170 pounds per cubic foot. The "fallback" volume is the difference between the excavated volume and the apparent crater volume ($V'_f = V'_t - V_a$). This volume actually represents a true fallback volume in addition to some portion of the volume of the ruptured region surrounding the true crater. The upthrust volume was converted to a mass by using a density of 150 pounds per cubic foot. This density was chosen arbitrarily by reasoning that the density in the upthrust region would likely be slightly less than the density for the <u>in situ</u> preshot material. The mass missing from the crater region was obtained by subtracting the "fallback" mass from the excavated crater mass ($M_m = M'_t - M'_f$).

Table 9

PERMANENT SURFACE DISPLACEMENTS ADJACENT TO THE H2 CRATER

All permanent ground motion data expressed in feet.

Radial	Pin 1			Pin 2			Pin 3			Pin 4			Pin 5		
	Dist. [a]	Vert. [b]	Hor. [c]	Dist. [a]	Vert. [b]	Hor. [c]	Dist. [a]	Vert. [b]	Hor. [c]	Dist. [a]	Vert. [b]	Hor. [c]	Dist. [a]	Vert. [b]	Hor. [c]
NE	20.1	+0.98	+0.11	23.0	+0.44	-0.05	26.0	+0.20	-0.03	33.3	+0.06	-0.03	46.1	+0.01	—
E	20.2	+0.36	+0.05	23.2	+0.23	+0.01	26.1	+0.16	-0.02	30.0	+0.11	-0.02	—	—	—
SE	—	—	—	—	—	—	26.1	+0.30	+0.03	34.9	+0.10	+0.01	46.1	+0.03	—
S	20.4	+0.62	+0.05	23.3	+0.45	+0.03	25.7	+0.17	+0.05	35.0	+0.07	+0.02	—	—	—
SW	—	—	—	—	—	—	26.0	+0.91	+0.55	36.1	+0.14	+0.12	46.1	+0.02	—
W	—	—	—	23.3	+0.38	+0.27	26.4	+0.14	+0.15	30.0	+0.15	+0.19	—	—	—
NW	—	—	—	—	—	—	—	—	—	34.5	+0.16	-0.06	46.1	+0.01	—
N	—	—	—	23.8	+0.32	-0.09	26.5	+0.15	-0.07	35.0	+0.04	-0.01	—	—	—

[a] Distance recorded is from preshot ground zero.
[b] Vertical Movements "+" = up, "-" = down.
[c] Horizontal Movements "+" = out, "-" = in.

Table 10

MASSES ASSOCIATED WITH CRATER AND EJECTA

Shot	Apparent Crater		Excavated Crater		"Fallback"		Upthrust		Ejecta [a]		Missing Crater Mass	Mass Non-accountable	$\frac{M_e}{M_m}$	Ejecta Measurement Area
	V_a (ft^3)	M_a (lb) x 10^5	V_t' (ft^3)	M_t' (lb) x 10^5	V_t' (ft^3)	M_t' (lb) x 10^5	V_u (ft^3)	M_u (lb) x 10^5	V_e (ft^3)	M_e (lb) x 10^5	M_m (lb) x 10^5	M_β (lb) x 10^5		D/R_a
S1(C1)	733	1.25	2060	3.50	1987	2.47	145	0.22	849	1.05	1.03	-0.24[b]	1.01	3.3
S2b	1802	3.06	3896	6.62	2094	2.60	210	0.32	1941	2.41	4.02	1.29	0.60	2.9
S3c	2411	4.09	6233	10.60	3822	4.74	368	0.54	3262	4.04	5.86	1.28	0.69	2.7
S4d	2081	3.54	6615	11.20	4534	5.62	494	0.74	2562[c]	3.18[c]	5.58	1.66	0.57	2.7
LS	3659	6.22	7527	12.80	3868	4.81	890	1.33	1794	2.23	7.99	4.43	0.28	2.1
H2	2417	11	5716	9.74	3299	4.10	866	1.29	1851	2.29	5.64	2.06	0.41	2.3
H1	536	0.91	1608	2.73	1072	1.33	231	0.35	535	0.66	1.40	0.39	0.47	3.9
C2	1500	2.55	4189	7.12	2689	3.33	425	0.64	1554	1.92	3.79	1.23	0.51	2.9
ST2b	242	0.41	946	1.61	704	0.87	181	0.27	616	0.76	0.74	-0.29	1.03	4.5
ST3c	560	0.95	1512	2.57	952	1.18	139	0.21	751[c]	0.93[c]	1.39	0.25	0.69	3.2

a Ejecta volume is cumulative for series shots.

b M_β cannot be negative because this means that more mass was accounted for than was missing from the crater. The negative value must reflect inaccuracies in assumed densities.

c Ejecta volume and mass are questionable due to direct influence of other nearby shots.

SECTION IV

DISCUSSION

Analysis, correlations, and comparisons of data, obtained from the applicable MTCE shots indicated in Table 3, are discussed in this section under "Successive Cratering," "Charge Geometry," and Coupling." Upthrust and ejecta data that apply to each of these types of cratering events are also discussed. The subsection titled "Crater Scaling" develops scaling relationships associated with surface craters formed by spherical and hemispherical charges in rock media; it also compares these relationships to similar craters in soil media.

1. Theory and Predictions

The survivability of hardened facilities is directly related to stress waves induced in the ground by both airblast and direct coupling of energy. Conservative estimates of offensive kill distances are the true crater dimensions. Therefore, both true and apparent crater dimensions are required on all shots. However, to measure true crater dimensions the apparent crater must be disturbed. Thus, this experiment included a single surface shot, a series of two, a series of three, and a final series of four shots so that the true crater is measured on the last shot of each series. True craters which were not measured are assumed to be of like dimensions as the excavated craters previously measured. A desired correlation is the one between true and apparent crater dimensions and the ground shock measurements described later in this report.

Crater scaling laws are currently highly argumentative. Crater data are derived from actual observations. Application of basic laws of physics and empiricism must be used to extrapolate to weapon yields of military interest. Reference 1 gives a detailed discussion of various scaling laws. To date, a single scaling law has not been found to relate crater dimensions for all possible yields. However, the scaling laws as given in Reference 11 are considered to predict dimensions which fit weapon yields of military significance for true surface bursts.

These laws ignore gravity, strength of the media, and several other factors. However, these laws give an accuracy of $\pm$ 25 percent for R_a and $\pm$ 35 percent for D_a. For this study the above laws have been used for predicting crater dimensions

when multiplied by the following factors for rock:

Dimension	Factor
R_a	0.8
D_a	0.7

An additional factor to reduce the crater dimensions from those of a true surface burst to those of a contact burst was also used. The factor was 0.68. Allowance must be made for the broken material resulting from the initial and succeeding shots when predicting the apparent crater dimensions of craters resulting from the second, third, etc., shots of a multiple cratering series.

Since such a paucity of information exists on multiple cratering and that which does exist is for very small charges in soil, little correlation can be made between previous experimental data and the data resulting from this experiment. However, two assumptions based on previous successive cratering data seem plausible:

(1) A curve of apparent crater dimensions versus number of shots fired becomes asymtotic after approximately four shots. Therefore, four shots were considered adequate for this experiment.

(2) Utilizing data from the MTCE experiment in rock, generally accepted scaling laws and data from other shots fired under similar conditions, the following crater dimensions for four multiple cratering shots are assumed.

After Shot No.	R_a(ft.)	D_a(ft.)
1	10.6	3.2
2	16.8	6.0
3	19.4	7.6
4	20.0	8.0

2. Successive Cratering

a. Crater Dimensions

Tables 11 and 12 show the increase in apparent and excavated size of successive craters. Increases in dimensions given in Table 13 were obtained by comparing excavated craters formed by separate series of successive charges and can only be assumed to apply to the growth of a crater formed by one successive series of shots along the same vertical axis.

Table 11

INCREASE IN APPARENT SIZE OF SUCCESSIVE CRATERS

	Half-Buried Spheres									Tangent Spheres				
Shot	S2a	S2b	S3a	S3b	S3c	S4a	S4b	S4c	S4d	ST2a	ST2b	ST3a(C3)	ST3b	ST3c
Maximum Crater Depth (ft)	4.0	4.8	4.0	6.0	7.7	4.0	5.8	5.9	8.4	1.9	2.3	1.2	2.4	3.3
Percent Increase Previous Shot	—	20	—	50	28	—	45	2	42	—	21	—	100	38
Percent Increase First Shot	—	20	—	50	92	—	45	48	110	—	21	—	100	175
Crater Radius (ft)	10.7	13.6	11.4	12.3	14.8	10.4	12.2	13.6	14.8	6.8	8.8	4.5	9.2	12.3
Percent Increase Previous Shot	—	27	—	8	20	—	8	11	10	—	29	—	104	34
Percent Increase First Shot	—	27	—	8	30	—	8	31	42	—	29	—	104	173
Crater Volume (ft^3)	672	1802	853	1233	2411	605	1178	1577	2081	139	242	25	324	560
Percent Increase Previous Shot	—	168	—	43	97	—	95	34	32	—	74	—	1196	73
Percent Increase First Shot	—	168	—	43	183	—	95	161	244	—	74	—	1196	2140

Table 12

INCREASE IN EXCAVATED SIZE OF SUCCESSIVE CRATERS

	Half-Buried Spheres				Tangent Spheres		
Shot	S1(C1)	S2b	S3c	S4d	ST1	ST2b	ST3c
Maximum Crater Depth (ft)	5.2	9.0	12.2	11.7	1.7	4.4	4.9
Percent Increase Previous Shot	-	70	36	0	-	159	11
Percent Increase First Shot	-	70	130	121	-	159	188
Crater Radius (ft)	16.0	19.4	24.2	25.2	5.4	14.3	16.8
Percent Increase Previous Shot	-	21	25	4	-	165	18
Percent Increase First Shot	-	21	51	58	-	165	211
Crater Volume (ft^3)	2000	3896	6233	6615	-	948	1512
Percent Increase Previous Shot	-	89	60	6	-	-	60
Percent Increase First Shot	-	89	202	221	-	-	-

Table 13

RANGE OF INCREMENTAL PERCENTAGES OF SIZE INCREASE
OF SUCCESSIVE CRATERS

All percentages given in this table refer to the incremental increase of a given dimension compared to Shot 1. Single values are given when only one set of data were available for comparison.

Half-Buried Spheres

	Shot	Depth		Radius		Volume	
		MTCE	OSO	MTCE	OSO	MTCE	OSO
APPARENT	2	20 to 50	56 to 93	8 to 27	15 to 24	43 to 168	70 to 102
	3	2 to 42	21	13 to 22	13	66 to 139	110
	4	62		12		83	
EXCAVATED	2	70		21		89	
	3	60		30		113	
	4	0		6		18	

Tangent Spheres

	Shot	Depth (MTCE)	Radius (MTCE)	Volume (MTCE)
APPARENT	2	21 to 100	29 to 104	74 to 1196
	3	75	69	944
EXCAVATED	2	158	165	—
	3	30	46	—

Comparable data presented in Table 11 and 12 exhibit a rather high degree of scatter; however, there are definite trends. Table 13 gives the range of increase in crater dimensions, which was obtained by comparing each incremental dimensional increase with the crater dimensions resulting from the first shot in a series. Increases in crater radius, depth, and volume are graphically illustrated in Figures 30, 31, and 32. The increase observed for the Oso argillite series craters (Reference 4) are comparable to increases shown for MTCE craters in these figures.

The increase in crater dimensions observed for craters formed by surface tangent spheres is illustrated in Figures 30, 31, and 32. However, Table 11 shows that the actual crater dimensions resulting from such charges are far less impressive. Apparent and excavated depths for craters formed by surface tangent charges are always less than half the apparent and excavated depths for craters formed by half-buried charges. This seems to hold for all craters in a three-shot series. Excavated and apparent volumes for craters formed by surface-tangent charges are also less than half, and, in most cases, less than one-quarter of the excavated and apparent volumes for craters formed by half-buried charges. The significant relative increase in crater dimensions resulting from the second tangent sphere undoubtedly results because the charge in effect is coupled to some degree. In other words, the initial tangent charge merely serves to excavate a placement hole for the second tangent sphere.

For surface-tangent spherical charges, the excavated depth of Shot 2 was 160 percent greater than the depth of Shot 1, and Shot 3 was 90 percent deeper than Shot 1. Because of the asymmetrical shape of crater ST1, the excavated profiles did not permit the determination of a valid excavated volume. Crater profiles for the series of three successive half-buried charges and the series of three successive surface-tangent charges are shown in Figure 33. This figure again illustrates the difference in the size of craters formed by half-buried and tangent charges. Half-crater profiles for craters formed by spherical half-buried and spherical tangent charges are shown in Figure 34.

The significant dimensions to be considered in evaluating the successive cratering technique as a kill mechanism are those associated with the excavated crater. The excavated crater profile represents a boundary at which the shock was intense enough to fracture and loosen the surrounding rock. The key dimension is excavated crater depth. This quantity increases in increments of

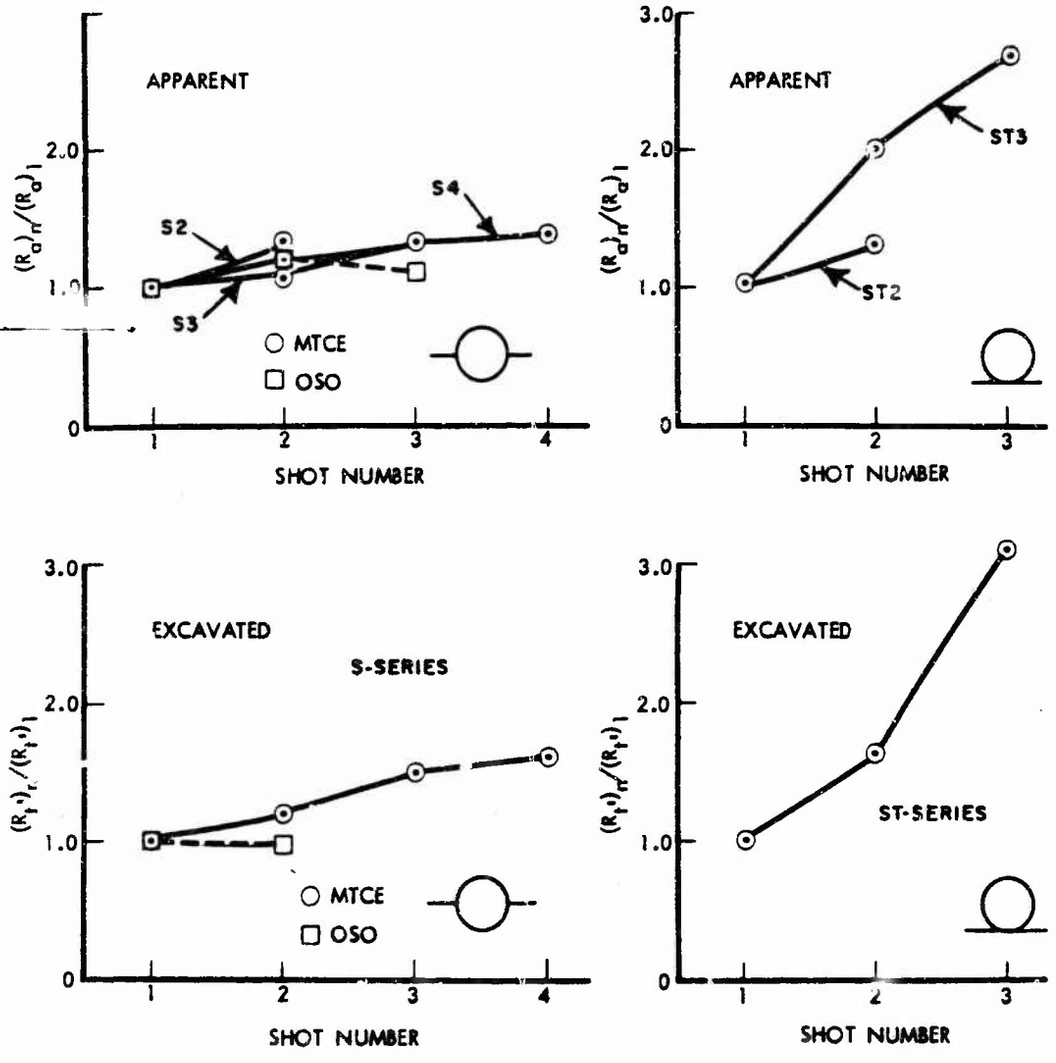

Figure 30. Increase in Crater Radius.

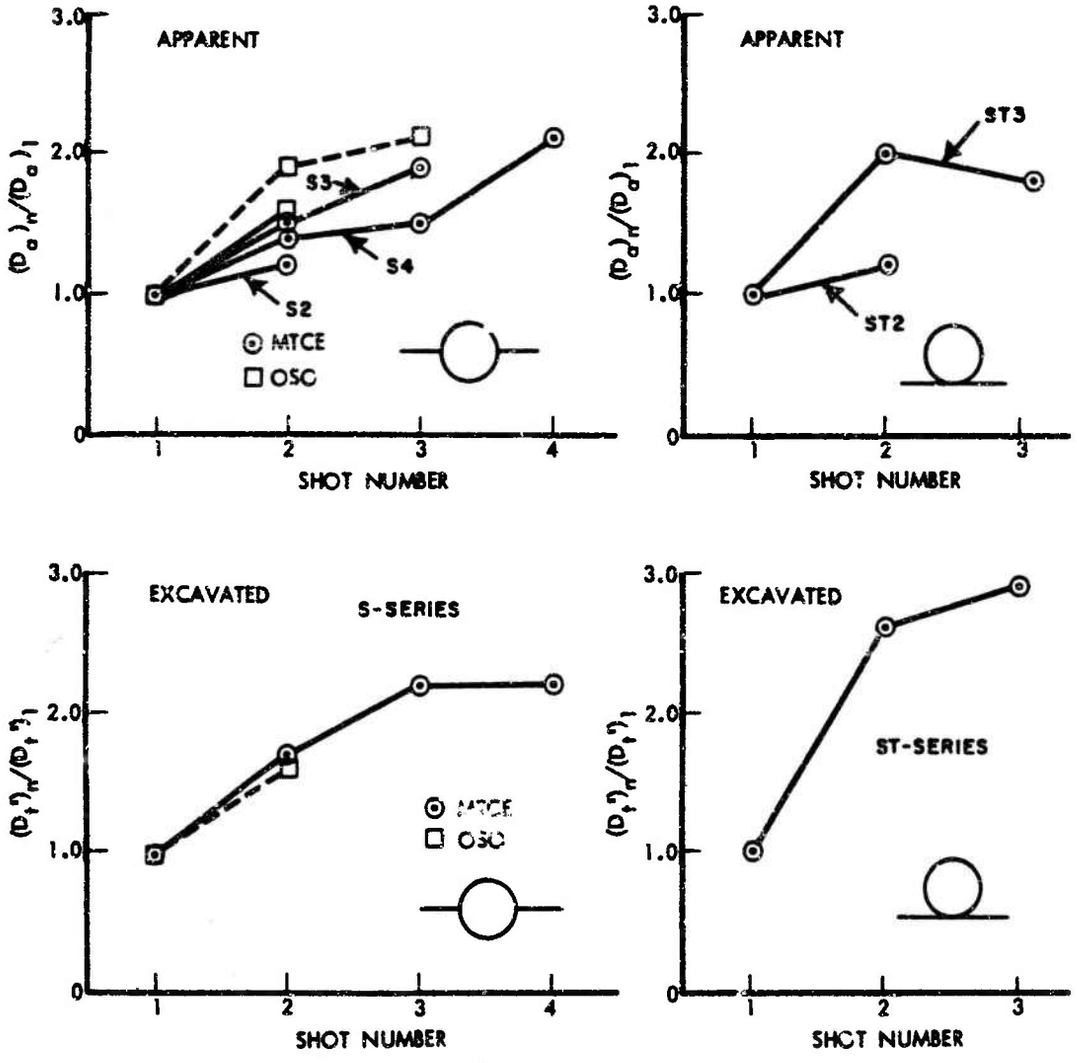

Figure 31. Increase in Crater Depth.

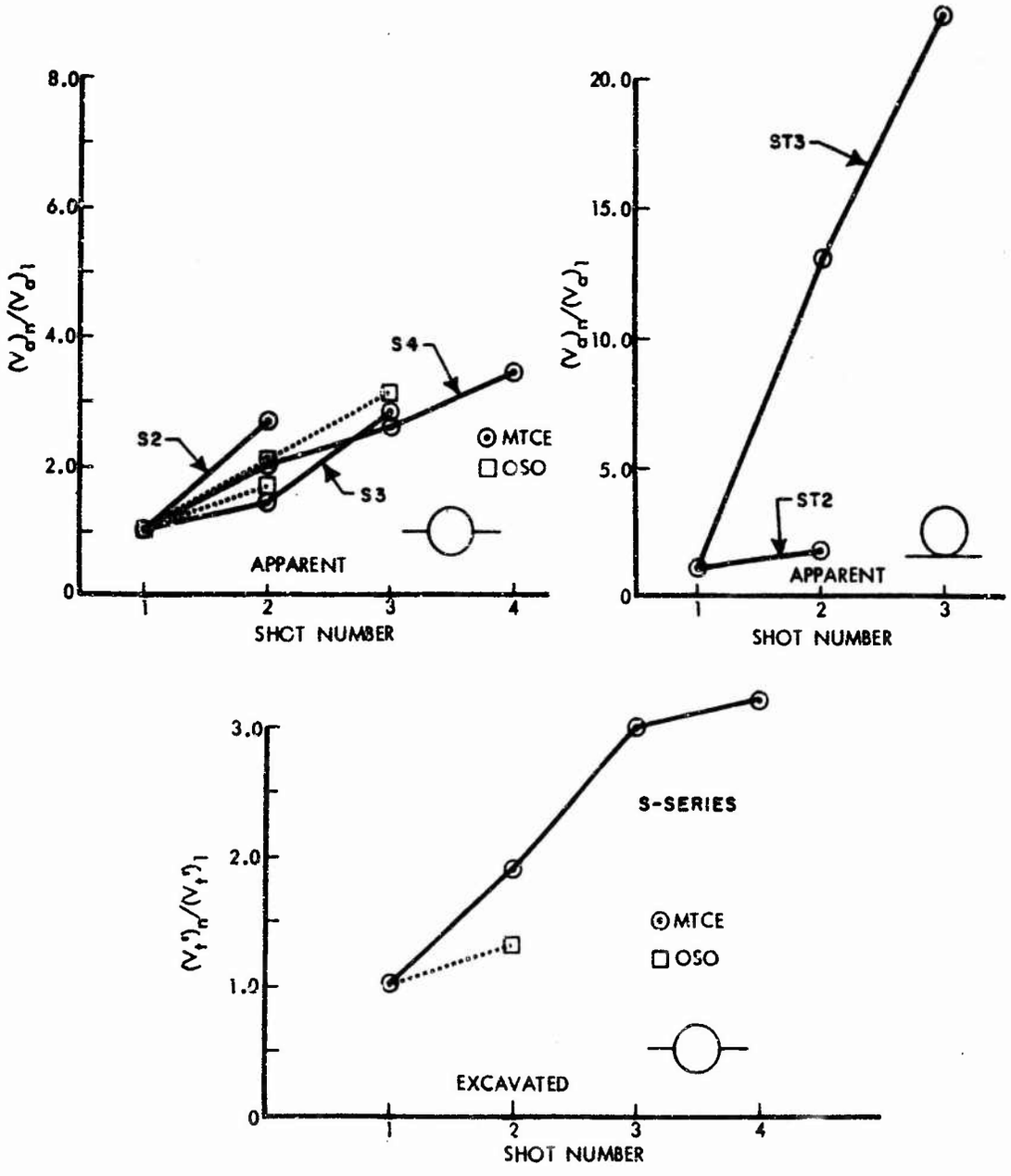

Figure 32. Increase in Crater Volume.

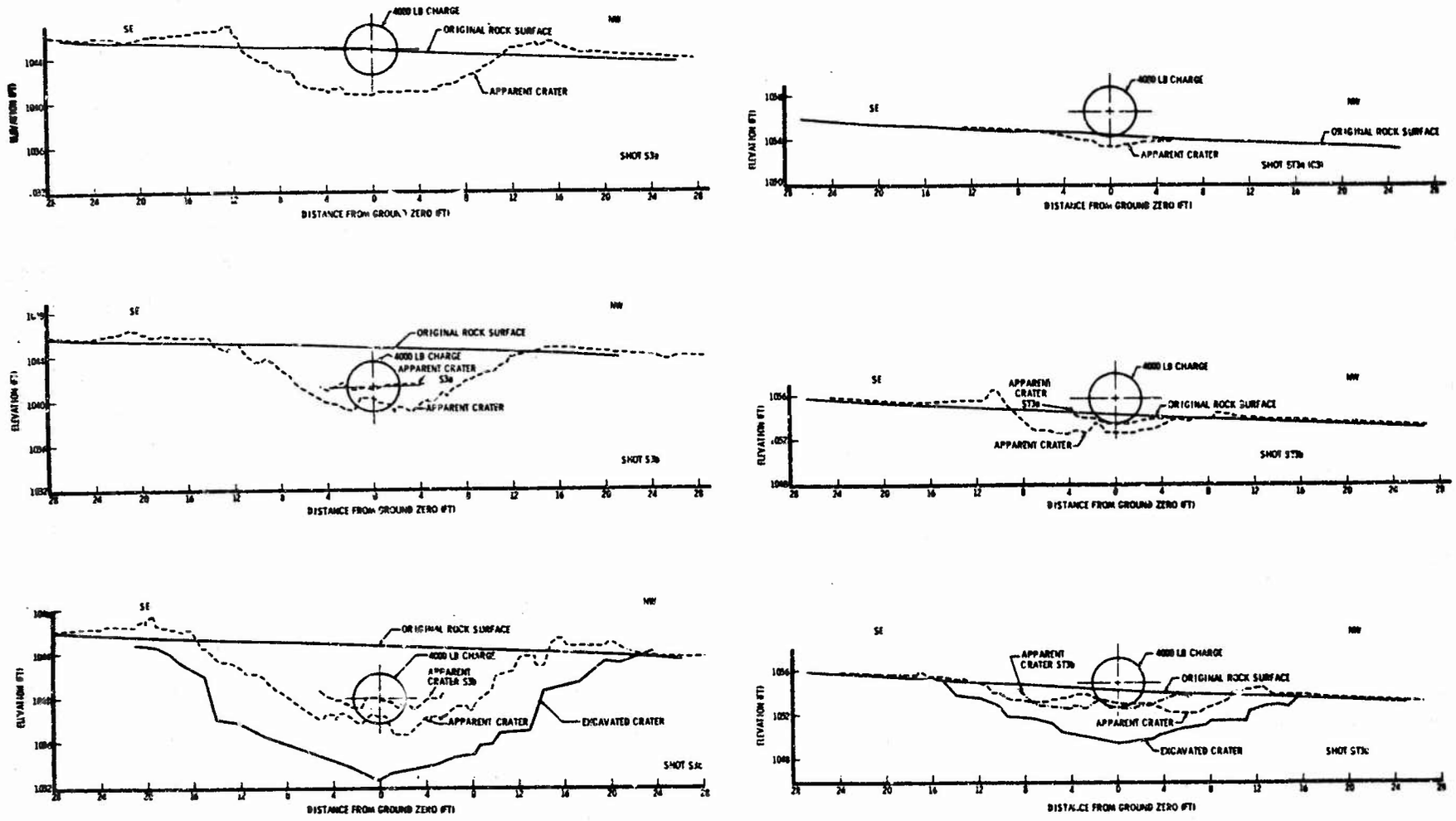

Half-Buried Spheres

Tangent Spheres

Figure 33. Profiles for Craters Formed by Successively Detonated Half-Buried Spheres and Similar Profiles for Tangent Spheres.

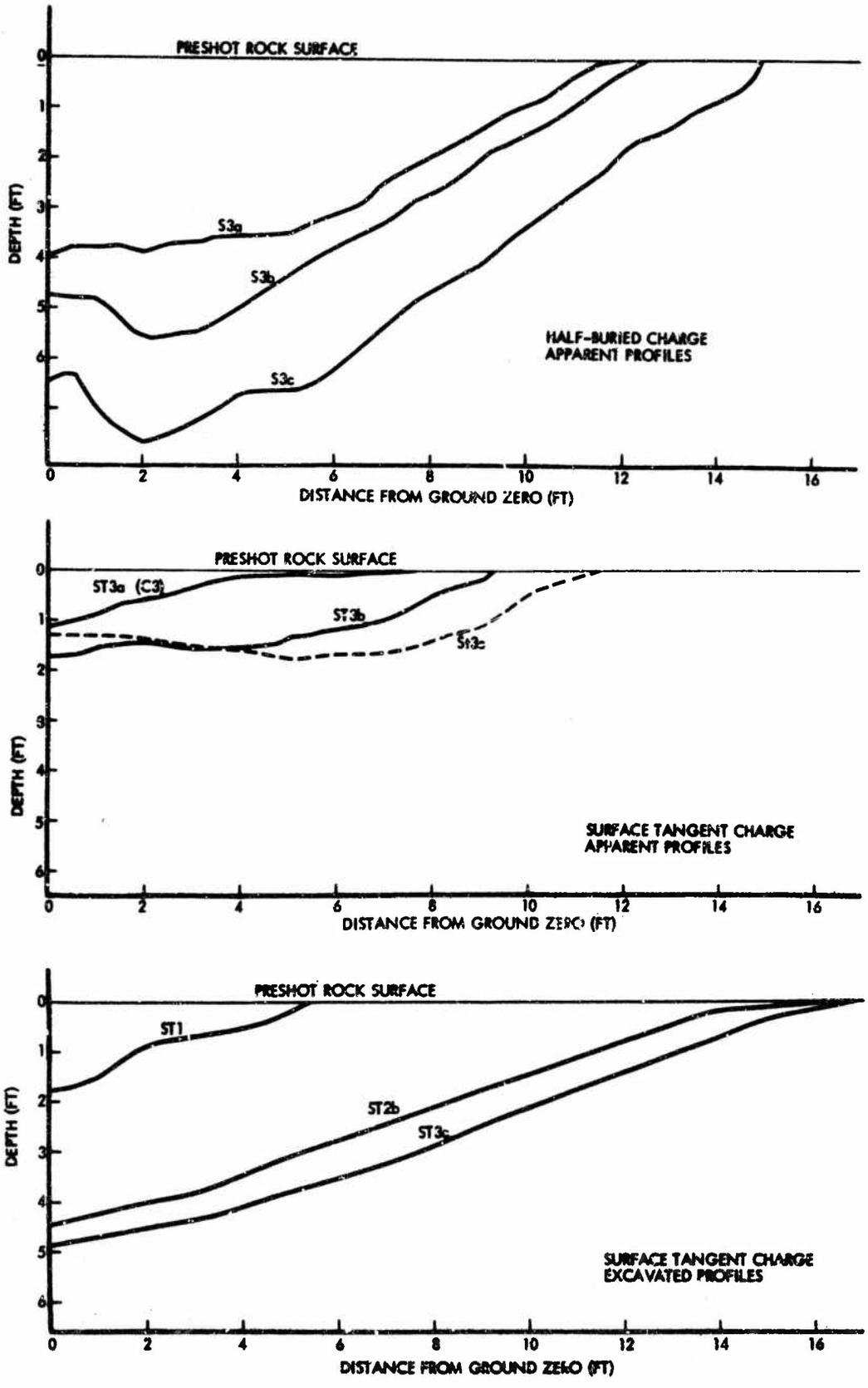

Figure 34. Profiles for Craters Formed by Half-Buried and Tangent 4000-Pound Spherical Charges.

70 percent and 60 percent for Shots 2 and 3, both relative to Shot 1. There was no increase in excavated depth measured after Shot 4. Figure 35 shows apparent crater profiles for the successive series of four 4000-pound half-buried spherical charges. Similar profiles are shown for the excavated crater in Figure 36.

The crater data from the series of half-buried charges might lead to the conclusion that excavated crater depth does not increase after the third shot. However, there is a discrepancy in the data that weakens this conclusion. Table 11 shows that the apparent crater depth resulting from the S3c shot was about 28 percent greater than the apparent crater depth resulting from the S3b shot. The apparent crater depth resulting from the S4c shot was only about 2 percent greater than the apparent crater depth resulting from the S4b shot. It is the apparent crater depth that determines the charge placement for each successive shot. Thus, for the S4-series shot, S4d was positioned in approximately the same place as shot S4c and resulted in no great increase in excavated crater depth above shot S3c's excavated crater depth.

An alternate approach to ascertaining the effectiveness of the fourth shot along the vertical axis would be to calculate the maximum excavated crater depths for those events where the excavated crater was not measured. The excavated depths may be calculated from apparent crater depths if a consistent apparent depth to excavated depth ratio exists for those events in which both depths were measured; namely events S2b, S3c, and S4d. For these three events the average ratio was 0.63 and is relatively consistent with a deviation of .009. The calculated excavated depths for events S2a, S3b, and S4c are 6.3, 9.6, and 9.4, respectively. The fourth shot in the S4 series therefore increased the depth from 9.4 to 11.7 feet or an increase of 24 percent which is significant. The MTCE crater data are not conclusive regarding the increase or lack of increase in the excavated crater depth after a third shot in a series. An additional 4-shot series would be required to provide conclusive data with which to answer this question.

Another line of reasoning can logically be followed when the data in Table 11 are studied. The fourth shot in the S4 series, while not increasing the excavated crater depth beyond that exhibited by the third shot in the S3 series, did increase its apparent crater depth by 42 percent over that resulting for the third S4-series shot. It is possible that a fifth shot might have increased the excavated crater depth.

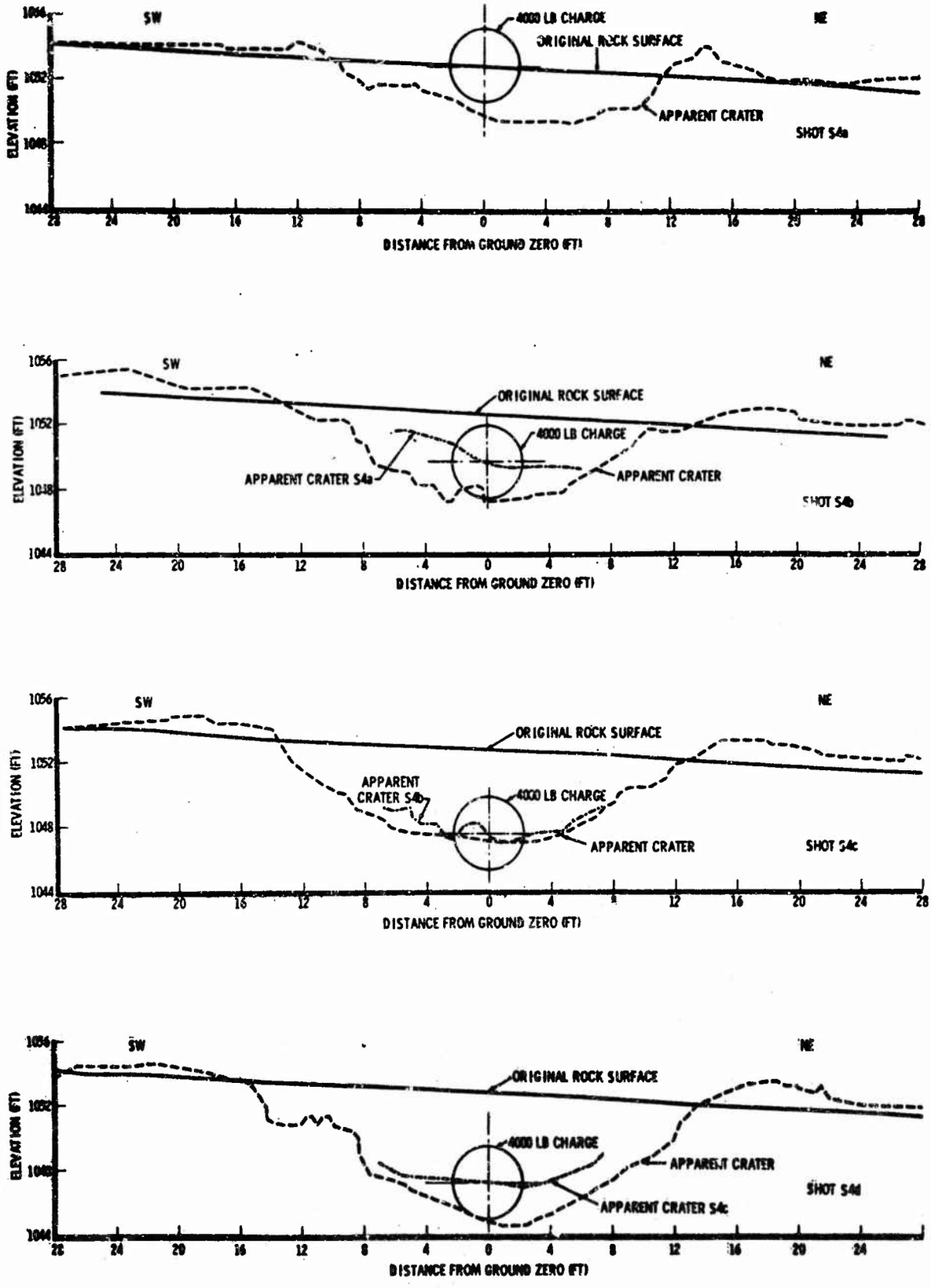

Figure 35. Apparent Crater Profiles for S4 Shot Series.

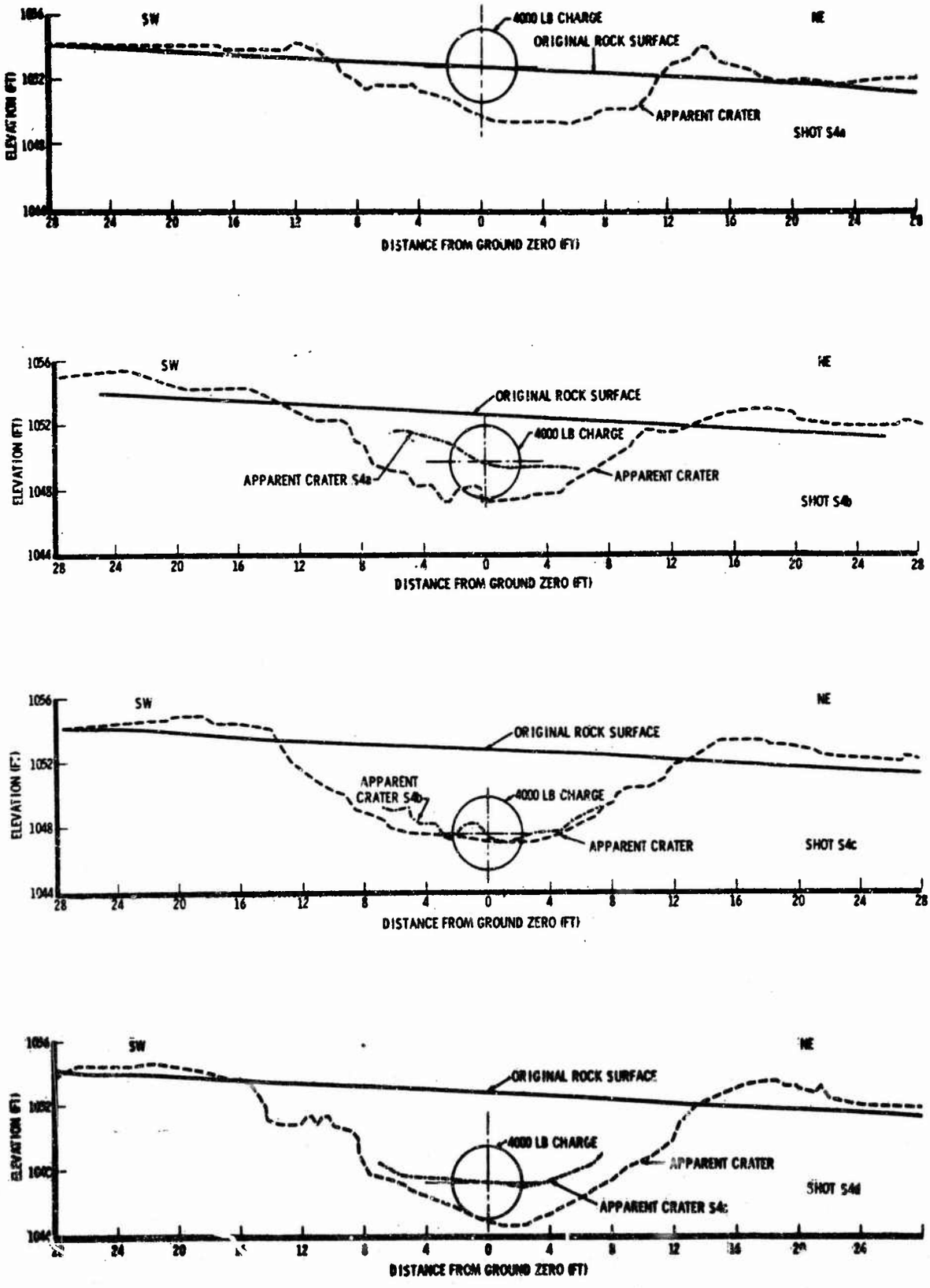

Figure 35. Apparent Crater Profiles for S4 Shot Series.

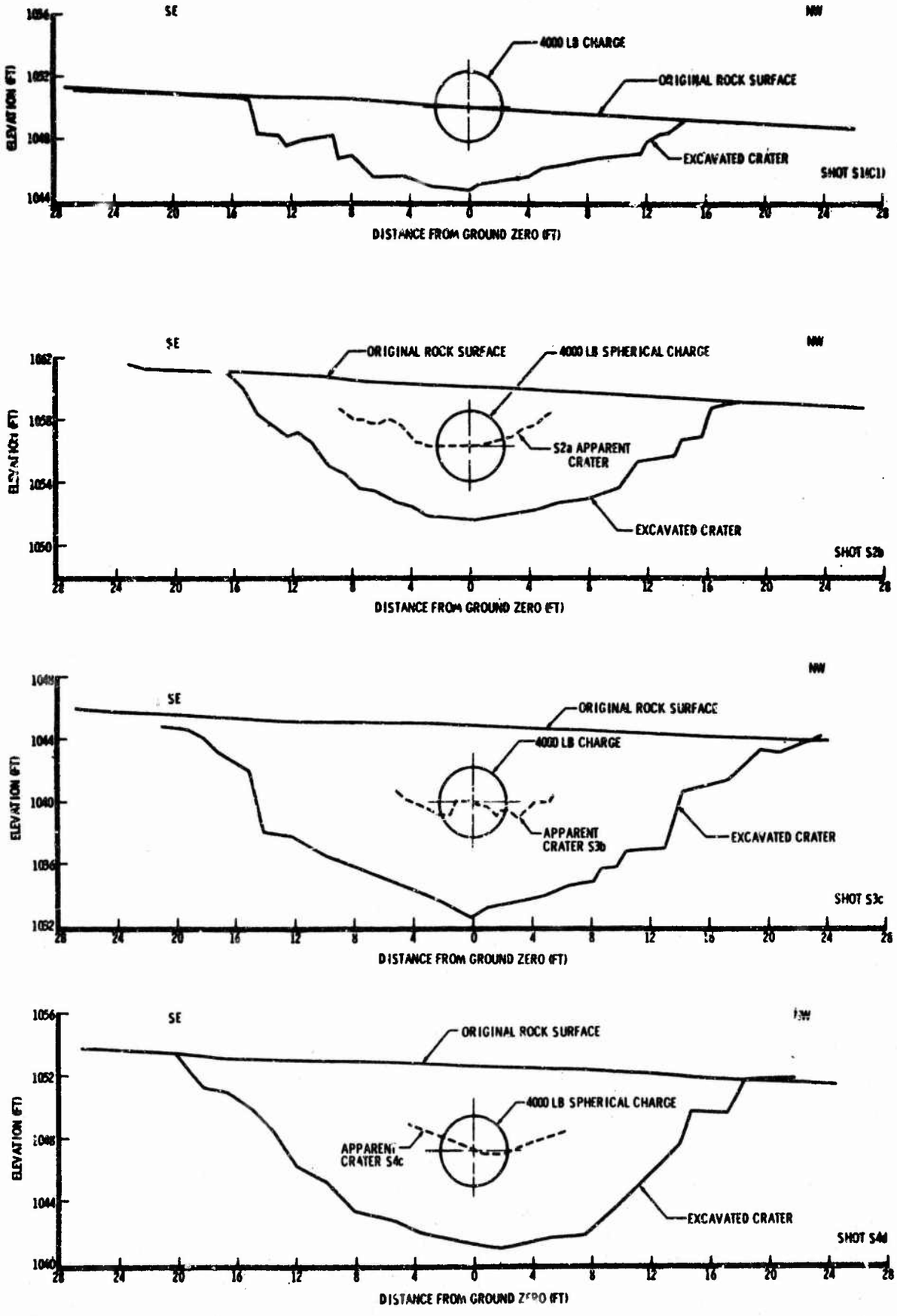

Figure 36. Excavated Crater Profiles for a 4-Shot Series.

The sequence of apparent depths exhibited by S4-series craters is compatible with a concept that would have one shot in a series fracturing rock and the following shot ejecting the rock. Again the MTCE successive cratering shots do not provide conclusive data on the validity of this concept. A five-shot series and a six-shot series would be required in the MTCE rock medium to obtain convincing data.

One of the primary objectives of the MTCE program was to ascertain whether crater size (excavated depth) is greater from a series of successively detonated charges (along a single vertical axis) or from a single charge comparable in energy to the sum of the series charges. This can be determined for charges in the MTCE weight class by comparing craters resulting from the LS shot and the S4d shot. Both craters resulted from the total expended energy of 16,000 pounds of TNT. The excavated crater depth was 9.1 feet for the LS crater and 11.7 feet for the S4d crater; therefore, the S4d excavated crater was 29 percent deeper than the excavated crater resulting from the LS shot. Crater profiles for the LS and S4d events are shown in Figure 37. The S4d apparent crater depth was about 50 percent greater than the apparent depth for the LS crater. (The S4d crater also exhibited apparent and excavated depths that were approximately 56 percent greater than similar dimensions for the H2, hemispherical, 16,000-pound surface shot.) However, it should be noted that the LS event was more efficient for moving and breaking rock than the combined S4 events. The LS apparent-crater volume was about 76 percent greater than the S4d crater volume. Half profiles for craters formed by the LS event and the S4 series are shown in Figure 38.

The shape factor for each apparent crater formed by a half-buried successive charge seems to be less than that of its predecessor. Data given in Table 6 indicate that the shape factor for the first shot in a series is about 0.45 (indicating a geometrical shape that is almost a paraboloid), and the apparent crater resulting from the third series shot exhibits a factor of about 0.46 (an almost parabolical shape). The shape factor for the excavated crater resulting from a series of shots is significantly less than that for its related apparent craters and appears to decrease with each successive shot. The shape factor for the excavated crater resulting from the third or fourth shot in a series is less than 0.30, so its shape approximates a cone. As expected, the ratio of crater depth to radius increases with each shot in a successive series within the range of 0.3 to 0.6. This ratio is about 0.5 for excavated craters.

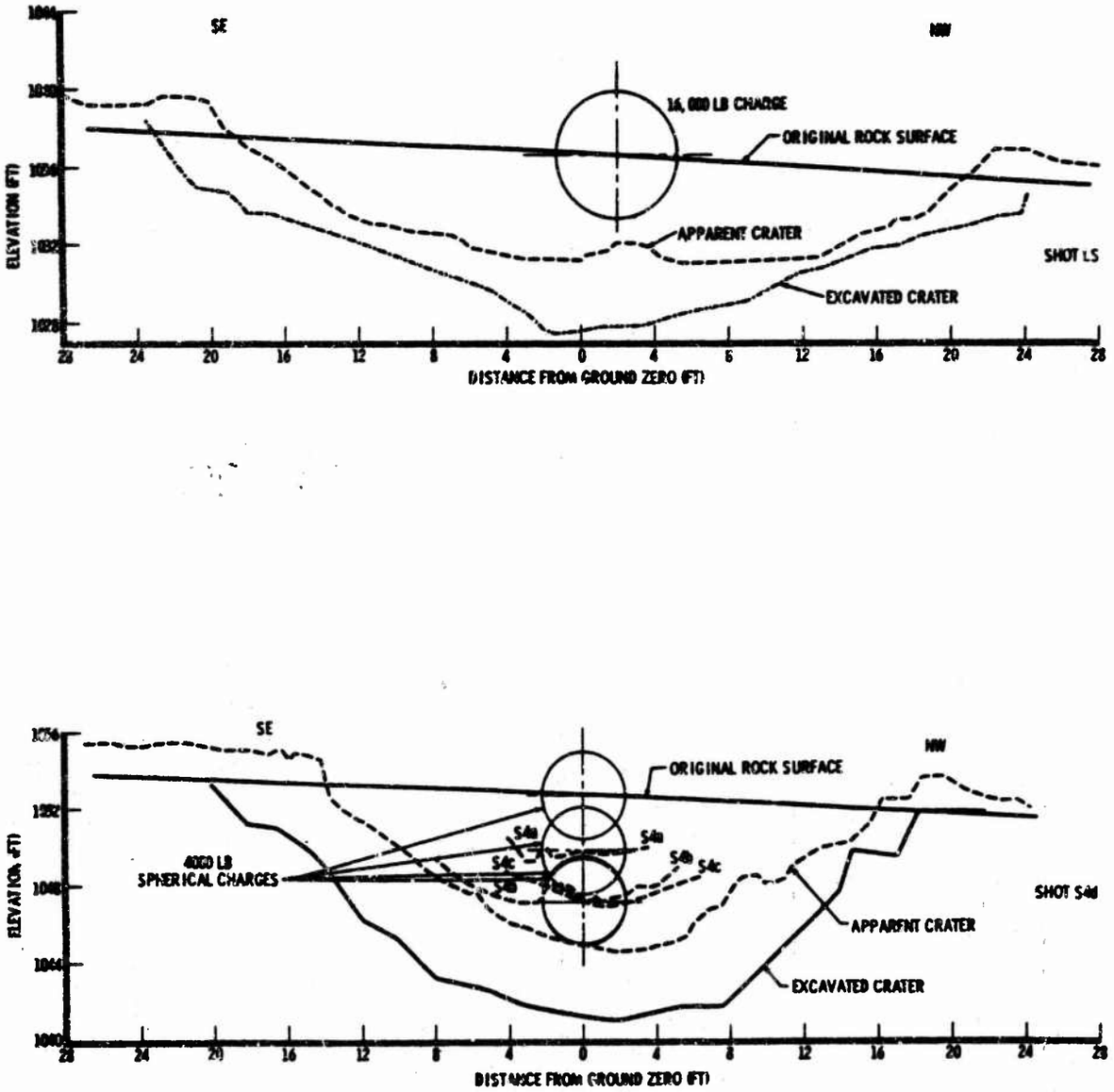

Figure 37. Crater Profiles for Events LS and S4.

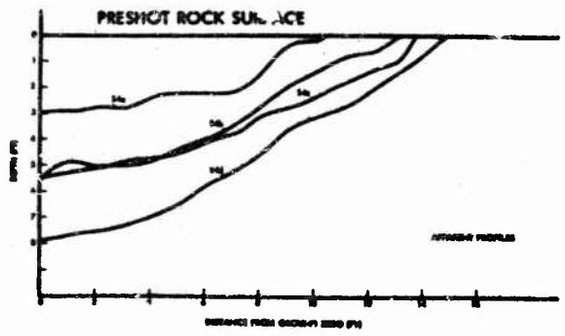

APPARENT

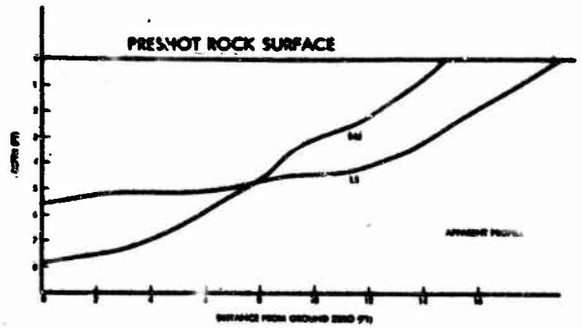

APPARENT

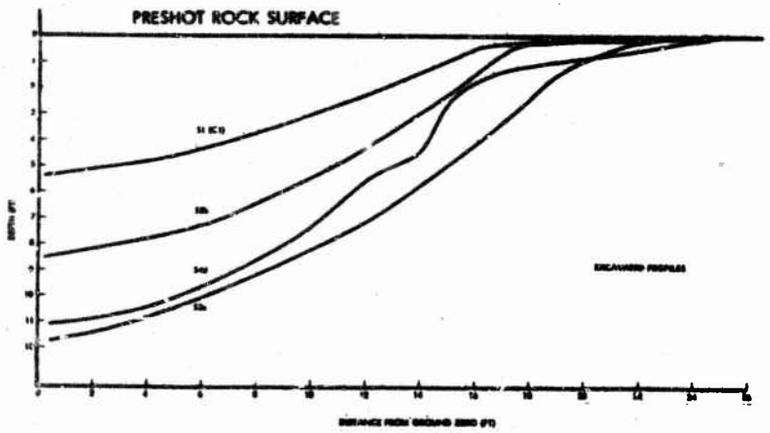

EXCAVATED

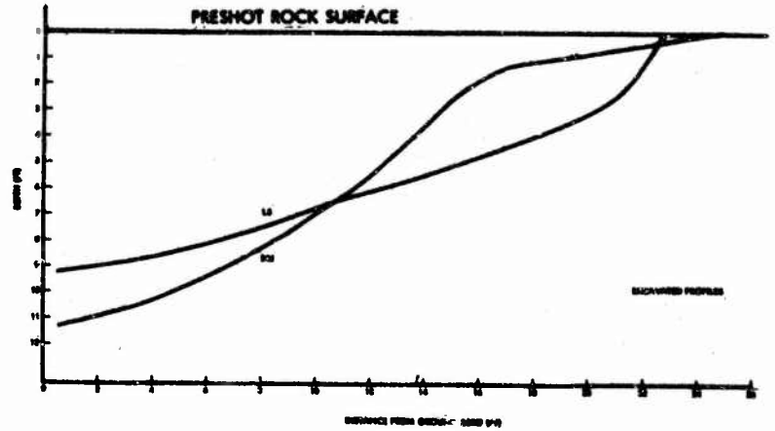

EXCAVATED

Figure 38. Profiles for Craters Formed by 4-Shot Series and LS Shot.

The apparent crater resulting from surface-tangent spheres exhibited shape factors ranging from 0.33 to 0.66 and no trend is noted. Excavated craters formed by surface-tangent charges were shaped like cones. The ratio of crater depth to radius was about 0.30 for excavated craters.

b. Rubble Thickness

Rubble thickness is comprised of material broken up in place, spall material from the walls of the crater plus fallback. Crater-depth quantities for all craters on which excavated measurements were made are given in Table 14. The actual burst depth listed is the position of the charges center-of-gravity relative to the original rock surface. It is interesting to note that tangent-spherical-charge centers of gravity were always above the original ground surface. In other words, the apparent crater depth at ground zero for craters formed by tangent spherical charges was always less than 2.2 feet. Crater dimensional data used in Group 1 are for the shots listed, but actually do not comprise a single successive series. Apparent crater dimensional data used in Group 2 are for the S4 and ST3 series; however, the excavated crater data include results from other craters, except for the final shot. The apparent data used in Group 3 represents the average for similar craters.

Several interesting observations can be drawn from Table 14. The actual vertical distance between the charge center of gravity and the excavated crater was about 6 feet (+1.4, -0.9) for the half-buried 4000-pound successive charges and about 5 feet (+0.8, -1.1) for the tangent successive charges. (Shots H1 and C2 also exhibited a similar dimension of about 5 feet.) When this dimension is divided by the charge weight raised to the 0.33 power, a value of about 0.37 results for the half-buried 4000-pound spheres and 0.31 results for the 4000-pound unburied tangent spheres. The 16,000-pound half-buried sphere and the surface hemisphere yielded a similar scaled value of 0.36. The fully-buried tangent (4000-pound sphere) and the surface 4000-pound hemisphere yield a value of 0.32 for this scaled dimension. Thus, the range of scaled values of the vertical distance from the center-of-gravity of the charge to the resulting excavated crater was 0.30 to 0.37. If the rock medium had been the same for all shots, one would expect this scaled value to be constant. This scaled value is related to the determination of the attenuating effect of the rubble on the shock and the prediction of crater dimensions resulting from successive cratering shots.

Table 14

CRATER DEPTH AND RELATED DIMENSIONS

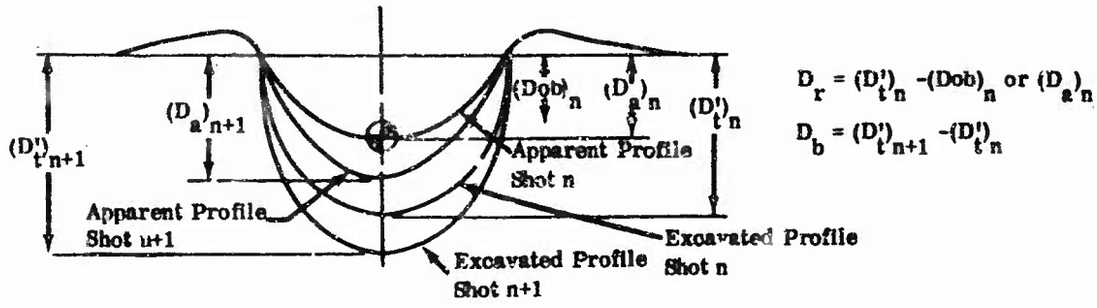

$D_r = (D'_t)_n - (Dob)_n$ or $(D_a)_n$

$D_b = (D'_t)_{n+1} - (D'_t)_n$

Shot	Actual Burst Depth	Rubble, D_r	Solid basalt, D_b	Actual Excavated Crater Depth, D'_t	$(D'_t)_{n+1} - (Dob)_{n+1}$ Actual	Mean	Scaled
	(ft)	(ft)	(ft)	(ft)	(ft)	(ft)	(ft/lb$^{0.33}$)
			GROUP 1				
S1(C1)	0	0	5.3	5.3	5.3		
S2b	3.9	1.4	3.7	9.0	5.1	6.0	0.37
S3c	4.8	4.2	3.2	12.2	7.4		
S4d	5.5	6.7	0	11.7	6.2		
			GROUP 2				
S4a	0	0	5.3	5.3	5.3		
S4b	3.1	2.2	3.7	9.0	5.9	6.0	0.37
S4c	5.5	3.5	3.2	12.2	6.7		
S4d	5.5	6.7	0	11.7	6.2		
			GROUP 3				
Sa	0	0	5.3	5.3	5.3		
Sb	3.6	1.7	3.7	9.0	5.4	6.0	0.37
Sc	4.8	4.2	3.2	12.2	7.4		
Sd	6.0	6.2	0	11.7	5.7		
			GROUP 1				
ST1	-2.2	0	1.7	1.7	3.9		
ST2b	-0.8	0.7	2.7	4.4	5.2	4.8	0.30
ST3c	-0.5	2.6	0.5	4.9	5.4		
			GROUP 2				
ST3a(C3)	-2.2	0	1.7	1.7	3.9		
ST3b	-1.3	0.8	2.7	4.4	5.7	5.0	0.31
ST3c	-0.5	2.7	0.5	4.8	5.4		
			GROUP 3				
STa	-2.2	0	1.7	1.7	3.9		
STb	-0.4	0.6	2.7	4.4	4.8	4.9	0.31
STc	-0.9	2.6	0.5	4.9	5.8		
LS	0	0	9.1	9.1	9.1	9.2	0.36
H2	-1.7	0	7.5	7.5	9.2		
H1	-1.0	0	4.1	4.1	5.1	5.1	0.32
C2	2.2	0	7.3	7.3	5.1		

Although the actual vertical distance between the charge center of gravity and the resulting excavated crater boundary remains roughly constant, the proportion of rubble and solid basalt making up this distance changes. As can be noted in Table 14, initially there is no rubble, only solid basalt between the charge and the vertical distance which later becomes the excavated crater depth. With successive shots, the proportion of the distance that is rubble increases and the proportion that is solid basalt decreases, until for Shot 4 there is only rubble between the charge and the excavated crater boundary. In other words, Shot 4 did not serve to expand the excavated crater boundary. This shows that sufficient rubble thickness attenuates the shock to such a degree that when it emerges from the rubble region it is no longer sufficiently intense to fracture and loosen surrounding rock for later excavation. The rather narrow range, within which the scaled vertical distance between the charge center of gravity and the excavated crater boundary falls for all MTCE craters, indicates that this scaled distance might represent a measure of the limiting distance beyond which the shock will not increase the excavated crater. Figure 39 shows actual distance of rubble and solid basalt through which the shock must travel for successive half-buried 4000-pound spherical and surface tangent 4000-pound spherical charges.

Strong shock measurements for the MTCE program were made on the S3 successive-shot series (Reference 11). Resulting data indicate that the shock intensity at the excavated crater boundary of Shot S3c was about 0.85 kilobars.

c. Ejecta Distribution

Observed data tabulated in Appendix II were used to make plots of ejecta thickness versus distance, as shown in Figure 40. The graph for the S4 successive shot series illustrates the erratic nature of the ejecta deposition resulting from these craters. This is due to the large boulders scattered on the ground surface adjacent to each crater.

Despite great variation in ejecta thickness and intermingling of ejecta-thickness curves for the S4 shot series, one can see the buildup of ejecta with each successive shot. The absolute amount of buildup appears to decrease with each successive shot--the greatest amount of material being deposited after Shot 1, and the least between Shots 3 and 4.

Ejecta thickness versus distance plots for the LS crater are also shown in Figure 40. The scatter is relatively small considering the type of ejecta

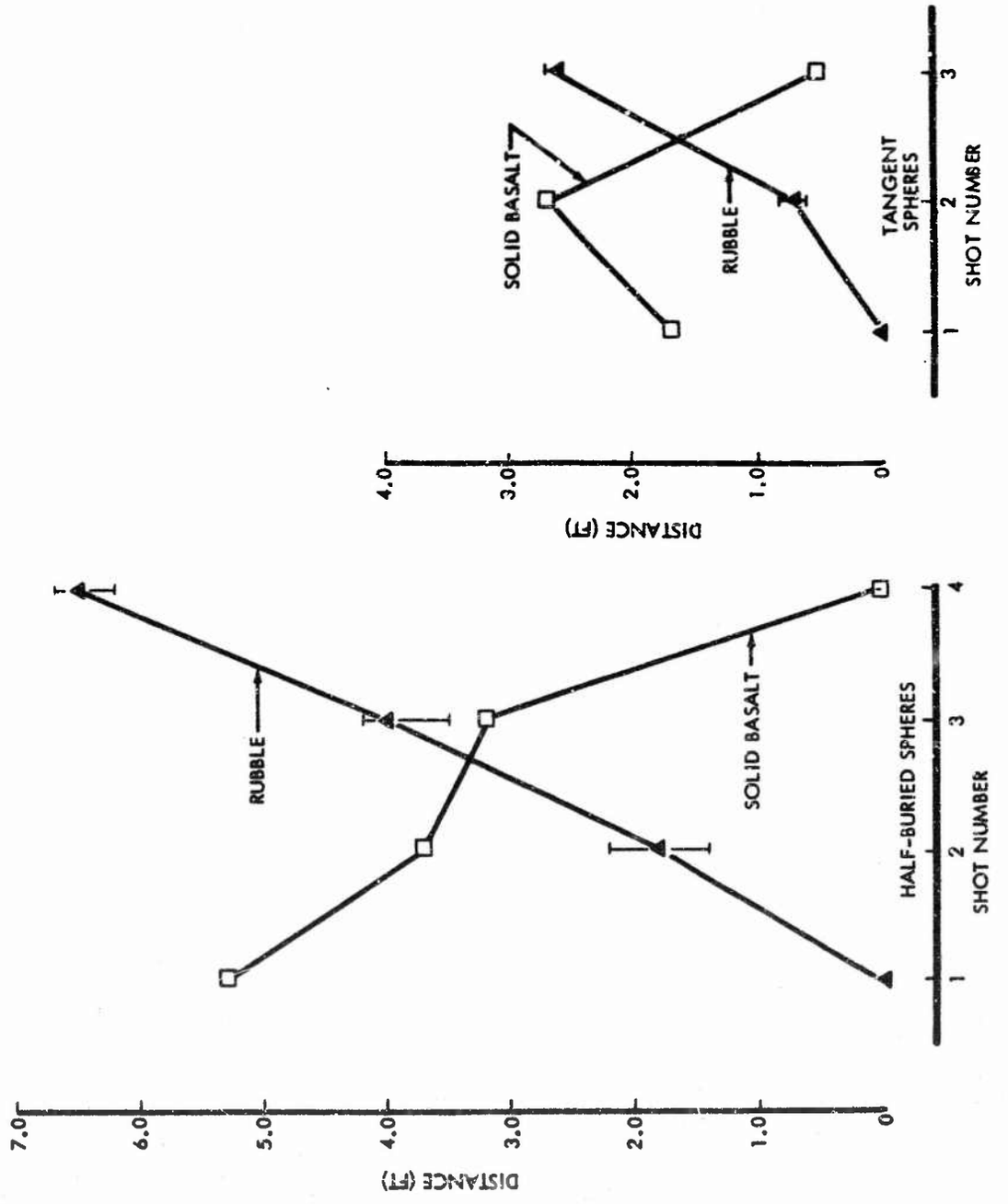

Figure 39. Rubble and Basalt Between Charge and Excavated Crater.

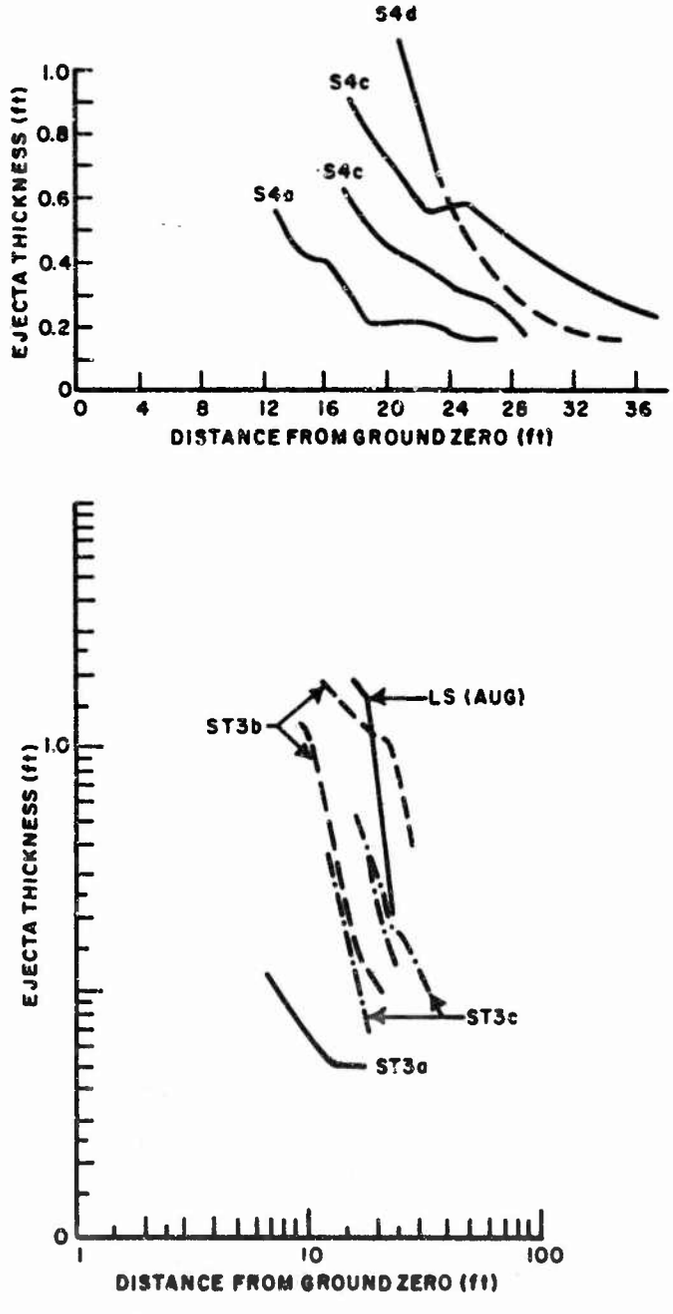

Figure 40. Ejecta Thickness as a Function of Distance for Successive Shots and for a Single Large Surface Shot.

that these curves represent. The mean ejecta thickness versus distance curves for the LS crater and the S4d crater are also plotted in Figure 40. At the same actual distance within about 30 feet from ground zero, the ejecta thickness for the LS crater is significantly greater than that for the S4d crater. The maximum ejecta thickness would be about 2 to 2.5 feet for the LS crater compared to about 1.5 feet for the S4d crater.

The ejecta thickness versus distance plots for the ST3 shot series, shown in Figure 40, also show a significant buildup between Shots 1 and 2. It should be noted, however, that few ejecta data were available for the ST3 crater series. Along certain radials there was a complete lack of ejecta. Single data points, representing an entire radial are not included in the graph in Figure 40. The lower absolute value of the ST3c curve shown in Figure 40 probably means that little or no ejecta were deposited along this radial for the ST3a and ST3b shots.

Mean ejecta thickness versus distance curves for S4 craters, are shown in Figure 41 as arithmetic plots. Ejecta-thickness curves shown for S4a, S4b, and S4c craters represent the average of three radials. The mean ejecta-thickness curve for the S4d craters represent only two radials. If additional data were available, it is felt that the outer portion of the S4d ejecta curve would not exhibit lesser absolute ejecta thicknesses than those exhibitied by the outer portion of the S4c curve. Thus, the doubtful portion of the S4d thickness curve is shown as a dashed line.

d. Upthrust

Vertical upthrust of the rock surface adjacent to the crater is illustrated in Figure 41 for craters resulting from the half-buried (S4) charge series and for craters resulting from the surface tangent (ST3) charge series. Upthrust of more than 1 foot was recorded along one radial on the S4d shot. Upthrust from one radial to the next varies significantly for a single shot. Figure 41 also shows average upthrust versus distance curves for each crater. Sufficient data were not available to plot a mean upthrust curve for the S4d crater. The initial shot in the S4 series contributed the greatest absolute amount of upthrust. Successive increments of upthrust contributed by the S4d and S4c shots were roughly equal.

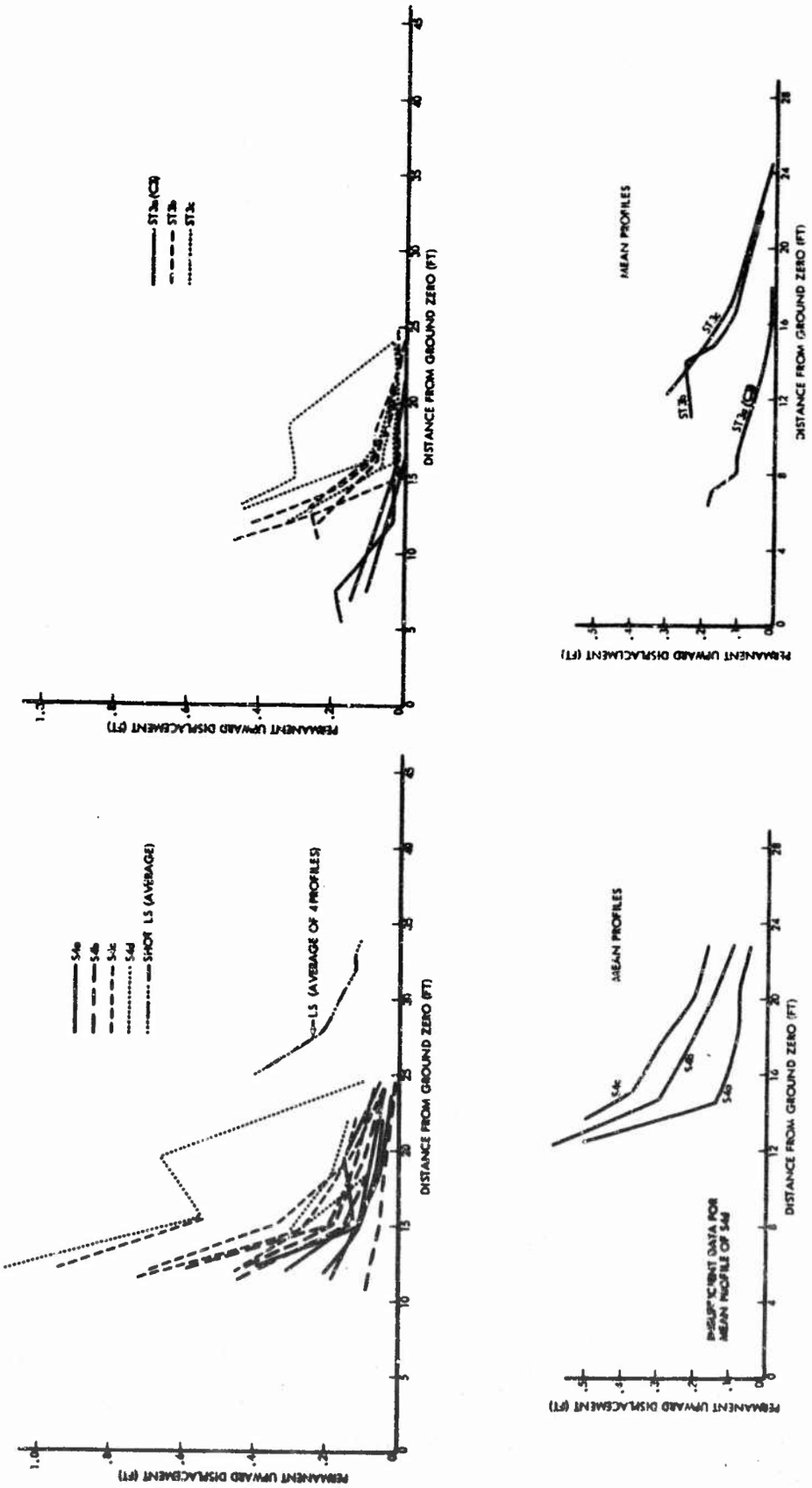

Figure 41. Permanent Vertical Upward Displacement Adjacent to Crater Resulting from Successive Shots.

Upthrust for the second shot in the ST3 series was greater than the upthrust resulting from the initial shot. Little additional upthrust was caused by the final (ST3c) shot.

Figure 41 also shows the mean upthrust for the four radials along which upthrust was measured on the LS crater. A comparison of this mean upthrust to the upthrust resulting from shot S4d shows a difference in the relative position at which upthrust occurred. This difference is due to the larger radius exhibited by the LS crater. Larger absolute upward displacements occurred for the S4d crater.

e. Reproducibility of Crater Dimensions

Table 15 gives an indication of the reproducibility of apparent crater dimensions for craters formed by 4000-pound TNT spheres in the basalt test medium. For half-buried spheres, data scatter is less than $\pm$ 10 percent for linear dimensions and about $\pm$ 20 percent for volume. Craters formed by tangent surface spheres exhibit a scatter of about $\pm$ 30 percent for radius, $\pm$ 25 percent for depth, and $\pm$ 90 percent for volume. The reproducibility of surface craters produced by half-buried 4000-pound spherical charges is illustrated graphically by the half-profiles shown in Figure 42. Because each half-profile shown is the average of two actual full profiles, there will be a difference between a radius read from Figure 42 and a corresponding radius given in Table 5 for the same crater. (Radii given in Table 5 represent an average of 16 readings.) To facilitate the comparison of half-profiles, each profile shown in Figure 42 has been plotted using the rock surface as a reference plane. Comments made here about the half-profiles given in Figure 42 also apply to similar figures in Section IV of this report.

Also shown in Figure 42 are averaged half-profiles for three craters formed by the second 4000-pound spherical charge in a series. The data from these craters exhibited a scatter of less than $\pm$ 10 percent for radius, $\pm$ 15 percent for depth, and $\pm$ 30 percent for volume.

3. Charge Geometry

a. Crater Dimensions

Craters resulting from hemispherical charges are slightly smaller than craters resulting from half-buried spherical charges of equal weight. Table 16 compares hemispherical-charge crater dimensions and volumes with similar crater

Table 15

REPRODUCIBILITY OF CRATER DIMENSIONS

Shot	Burst Position	Apparent Radius R_a(ft)	Apparent Depth[a] D_a(ft)	Apparent Volume V_a(ft^3)
S1(C1)	—○—	12.1	3.6	733
S2a	—○—	10.7	4.0	672
S3a	—○—	11.4	4.0	853
S4a	—○—	10.4	4.0	605
Mean		$11.2^{+0.9}_{-0.8}$	$3.9^{+0.1}_{-0.3}$	716^{+137}_{-111}
Standard Deviation		0.39	0.11	52.66
ST1	○	3.7	1.3	37
ST2a	○	6.8	1.9	139
ST3a(C3)	○	4.5	1.2	25
Mean		$5.0^{+1.8}_{-1.3}$	$1.5^{+0.4}_{-0.3}$	143^{+73}_{-42}
Standard Deviation		0.94	0.21	88.59

[a]Maximum crater depth

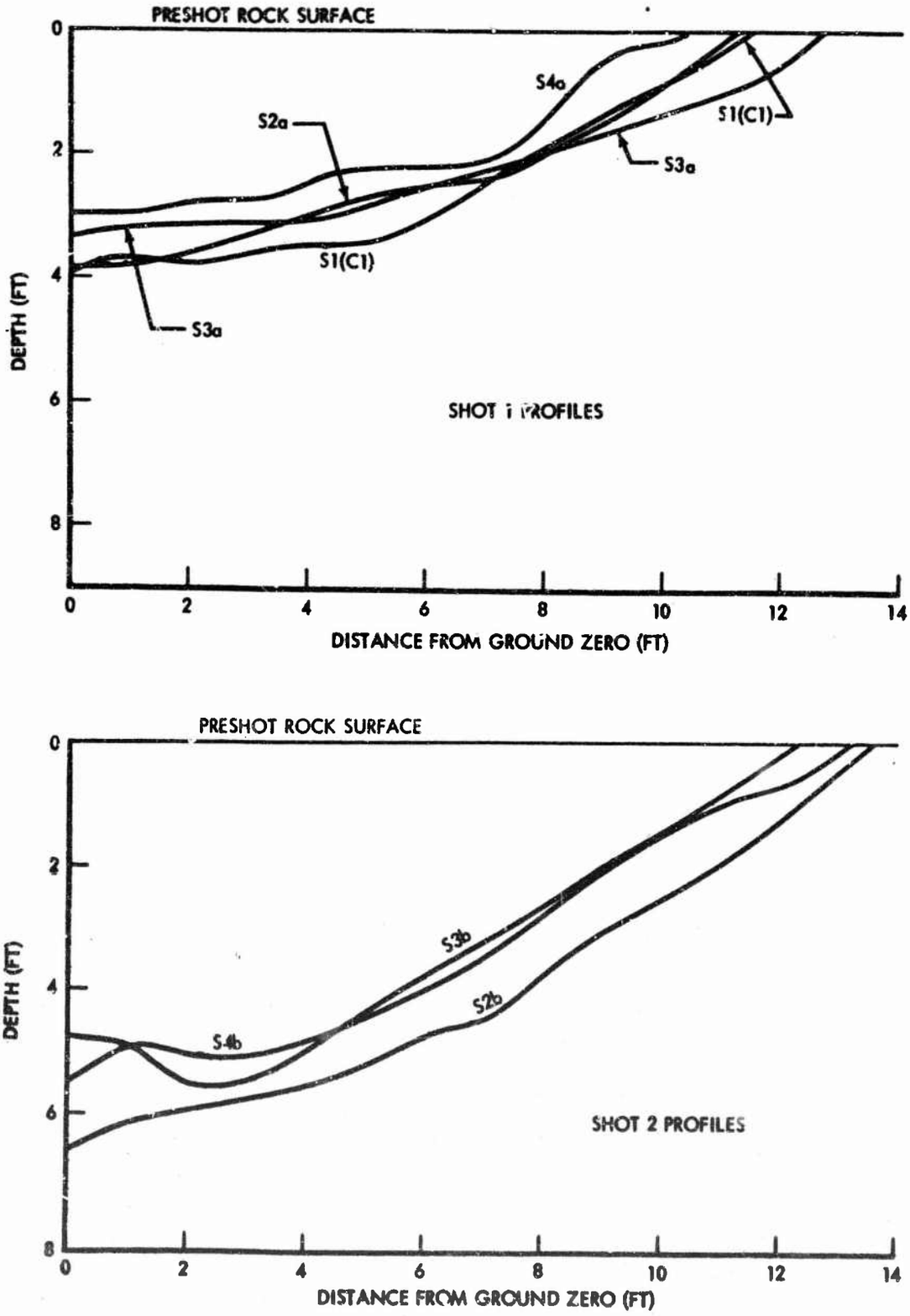

Figure 42. Average Apparent Profile Indicating Crater Reproducibility for Similar Shot Conditions.

Table 16

COMPARISON OF DIMENSIONS FOR CRATERS RESULTING FROM HEMISPHERICAL AND SPHERICAL HALF-BURIED CHARGES

All crater depths are maximum. Apparent dimensions compared for 4000-pound spheres are average of dimensions exhibited by craters S1(C1), S2a, S3a, and S4a. All comparisons are made to crater dimensions resulting from the spherical charge.

Shots	Apparent			Excavated		
	Radius	Depth	Volume	Radius	Depth	Volume
	(pct)	(pct)	(pct)	(pct)	(pct)	(pct)
Actual Crater Dimension						
16,000-pound sphere, LS; 16,000-pound hemisphere, H2	-09	-04	-34	+06	-18	-24
4,000-lb sphere; 4000-pound hemisphere, H1	-09	-23	-25	+08	-23	-22
Corrected Crater Dimensions						
16,000-pound sphere; LS; 16,000-pound hemisphere, H2	+12	+157	-32	+24	+34	-23
4,000-pound sphere; 4,000-pound hemisphere, H1	+13	+76	-23	+25	+32	-27

dimensions and volumes for half-buried spherical charges. Comparisons are nearly consistent for the 16,000- and 4000-pound shots. A crater in basalt resulting from a hemispherical charge will exhibit an apparent radius about 10 percent smaller, an apparent depth about 15 percent smaller, and an apparent volume about 30 percent smaller than a comparable half-buried spherical charge. Reference 6 indicates that the apparent radius and depth of craters formed in sand by 1-pound hemispherical charges were about 15 percent less than similar dimensions for craters formed by 1-pound spherical charges. Apparent crater volume was about 27 percent less for the hemispherical charge crater (See discussion in Section I.) For a hemispherical charge detonated on basalt, the excavated crater radius will be about 7 percent greater, the excavated crater depth about 20 percent smaller, and the excavated crater volume about 23 percent smaller than for a spherical-charge crater. Table 16 also shows the same comparison of crater dimensions (that is, hemispherical-charge craters related to half-buried spherical-charge craters) which have been corrected for the rock removed during the emplacement of the spherical charges. This comparison makes linear crater dimensions for the hemispherical charge crater appear greater than those for the half-buried spherical charge. However, the volume comparison changes only slightly, with the hemispherical apparent volume and excavated volume still remaining about 28 percent smaller and 25 percent smaller, respectively, than the apparent and excavated volume for a crater formed by a half-buried spherical charge. This small change in volume is due to the fact that the volume of material removed for charge placement is small relative to the crater volume. Dimensions of craters formed by hemispheres and half-buried spheres are so close that the additional effort involved in the half-burial placement of a TNT sphere in rock does not seem justified. However, these differences, when scaled to extremely large charges, could be quite significant. The similarity in shape and the nearness in actual size for the LS and H2 craters are illustrated in Figure 43. Half-crater profiles for both large and small spheres and hemispheres are shown in Figure 44. Again, the difference observed in craters resulting from hemispheres and half-buried spheres of equal energy release is negligible for charges in the 4000-pound to 16,000-pound weight category.

The LS apparent crater exhibited a shape factor of about 0.6 (between a paraboloid and a hemisphere), compared with a shape factor of 0.5 (paraboloid) for the H2 apparent crater. The LS excavated crater also exhibited a slightly larger shape factor than that for the H2 excavated crater (0.46 compared to 0.38).

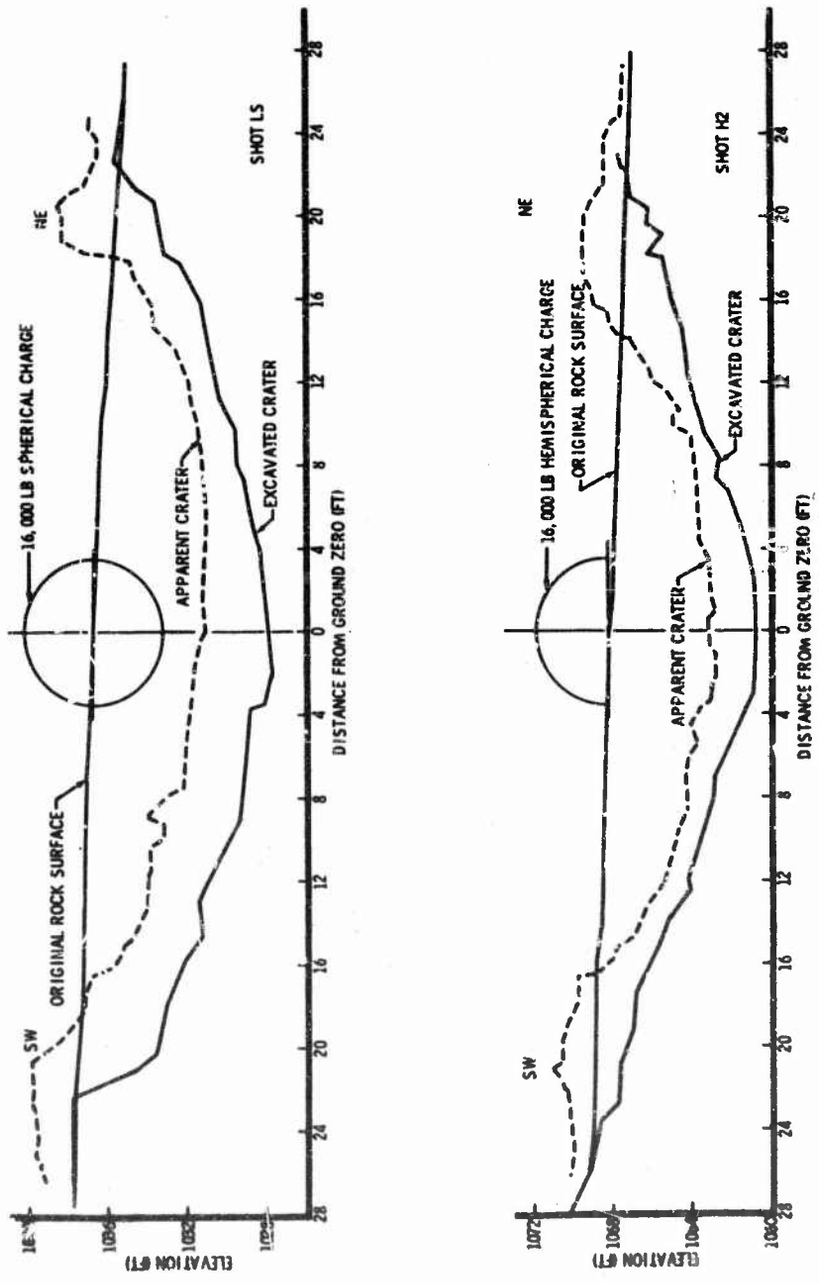

Figure 43. Profiles for the LS and H2 Craters.

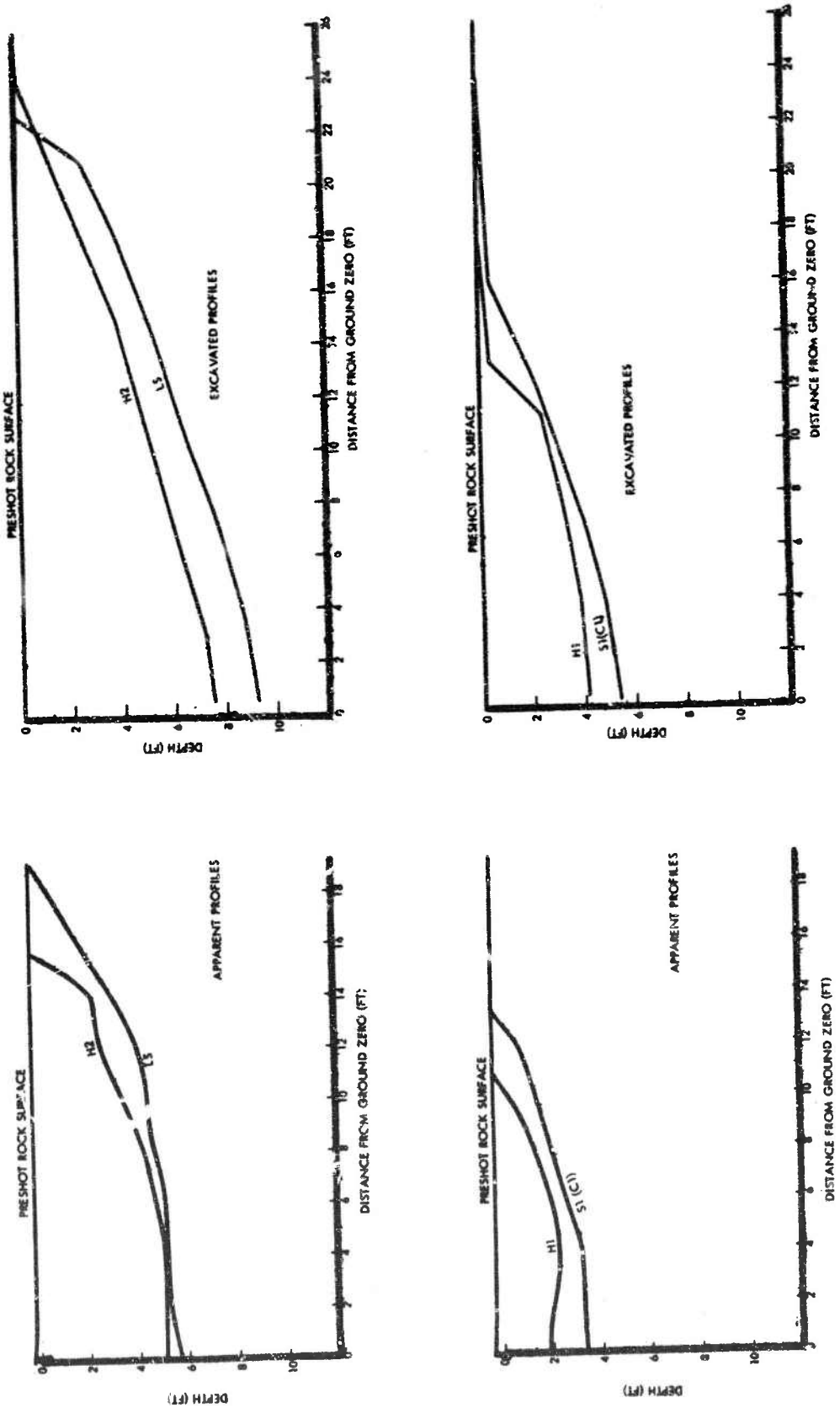

Figure 44. Profiles for Craters Formed by Spherical and Hemispherical Charges.

The ratio of apparent crater depth to radius was approximately 0.3 for both the LS and H2 craters. This ratio for the excavated dimensions was slightly higher for the LS crater (0.38 compared to 0.30).

The ratio of excavated dimension to apparent dimension was about 1.5 for radius, 1.6 for depth, and 2.2 for volume for half-buried spherical charges; 1.8 for radius, 1.4 for depth, and 3.0 for volume for hemispherical charges.

b. Cratering Effectiveness

Data related to the effectiveness of hemispherical and half-buried spherical charges in forming craters is given in Table 17 and plotted in Figure 45. Spherical charges ejected about 35 pounds of rock per pound of TNT to form the apparent crater. Hemispherical charges ejected about 25 pounds of rock per pound of TNT to form the apparent crater. The SAILOR HAT 500-ton hemispherical charge excavated over 50 pounds of rock per pound of TNT to form its apparent crater (Reference 14). The shock resulting from the MTCE spherical charges fractured, loosened, and in some way influenced about 85 pounds of rock per pound of TNT to form the region defined by the excavated crater boundary. The shock resulting from the MTCE hemispherical charges fractured, loosened, and in some way influenced about 65 pounds of rock per pound of TNT to form the region defined by the excavated crater boundary.

Cratering effectiveness for apparent surface craters formed by half-buried spherical charges is about 40 pounds of material per pound of TNT and remains relatively constant over a wide range of charge weight for both soil and rock (Figure 45). Cratering effectiveness for excavated surface craters formed in the same manner is about 100 pounds of material per pound of TNT for both soil and rock and also remained constant over a wide range of charge weights.

The cratering effectiveness of hemispherical charges in forming apparent craters in soil is on the order of 50 to 70 pounds of soil per pound of TNT. This is significantly higher than the 25 pounds of rock per pound of TNT mentioned previously.

c. Crater Lip Ratios

The ratio of the average apparent lip crest height to crater depth is given for rock and soil craters formed by spherical and hemispherical charges in Table 18 and plotted in Figure 46. This ratio lies between the limits of 0.17 and 0.36 regardless of charge shape or the geologic media in which the

Table 17

CRATERING EFFECTIVENESS FOR HEMISPHERES AND HALF-BURIED SPHERES

All charges were detonated at ground surface

HALF-BURIED SPHERES

Basalt				Playa			
Shot	Charge Weight W	M_a/W	M_t'/W	Shot	Charge Weight W	M_a/W	M_t/W
	(lb)	(lb/lb)	(lb/lb)		(lb)	(lb/lb)	(lb/lb)
OSO 1	64	87.7	---	E1a	8	27.8	---
OSO 2	64	135.1	276.34	E1b	8	21.8	---
S1(C1)	4,000	31.2	87.65	E1c	8	18.1	---
S2a	4,000	28.7	---	III-1A	64	36.3	103.1
S3a	4,000	36.2	---	III-1B	64	39.4	91.4
S4a	4,000	25.7	---	III-1C	64	34.5	94.9
LS	16,000	39.0	80.07	III-1D	64	42.8	87.9
Flat Top I	40,000	41.5	99.6	II-2A	256	36.1	98.1
				II-2B	256	35.3	---
				III-2A	1,000	42.8	106.6
				III-2B	1,000	50.1	116.3
				III-2C	1,000	42.8	106.6
				III-3A	6,000	40.7	90.4
				III-3B	6,000	43.6	---
				Flat Top II	40,000	46.5	89.8

HEMISPHERES

Basalt				Silt-Clay			
Shot	Charge Weight W	M_a/W	M_t'/W	Shot	Charge Weight W	M_a/W	M_t/W
	(lb)	(lb/lb)	(lb/lb)		(lb)	(lb/lb)	(lb/lb)
H2	16,000	25.8	60.7	9-29-59	10,063	58.3	---
H1	4,000	22.9	68.3	8-18-60	40,000	73.9	---
Sailor Hat	1,000,000	55.1	---	8-3-61	200,000	66.2	---
				7-17-64	1,000,000	50.0	---

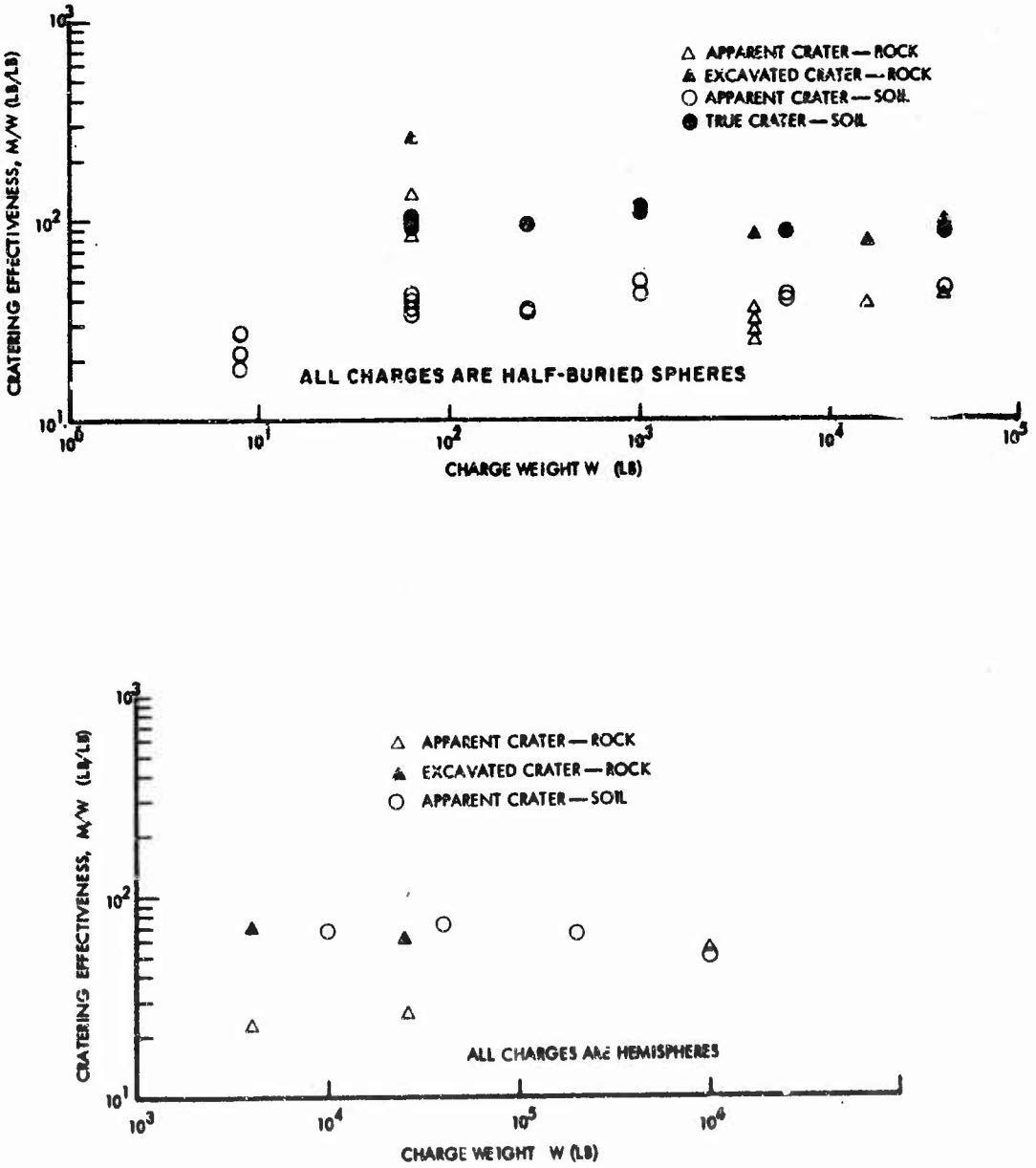

Figure 45. Cratering Effectiveness of Half-Buried Spherical Charges vs. Hemispherical Charges.

Table 18

RATIO OF LIP HEIGHT TO CRATER DEPTH FOR CRATERS FORMED BY HEMISPHERICAL AND HALF-BURIED SPHERICAL CHARGES

D_a is maximum crater depth, H_{al} is average apparent lip crest height.

HALF-BURIED SPHERES

Program	Charge Weight, W (lb)	Medium	$\frac{H_{al}}{D_a}$
Air Vent	64	Playa	0.24
	256	Playa	0.30
	1,000	Playa	0.20
	6,000	Playa	0.30
Flat Top	40,000	Playa	0.32
	40,000	Limestone	0.23
MTCE	4,000	Basalt	0.36
	16,000	Basalt	0.32

HEMISPHERES

Program	Charge Weight, W (lb)	Medium	$\frac{H_{al}}{D_a}$
Suffield	1×10^4	Silt Clay	0.17
	4×10^4	Silt Clay	0.22
	2×10^5	Silt Clay	0.27
	1×10^6	Silt Clay	0.19
Sailor Hat	1×10^6	Basalt	0.36
MTCE H2	16,000	Basalt	0.33
H1	4,000	Basalt	0.35

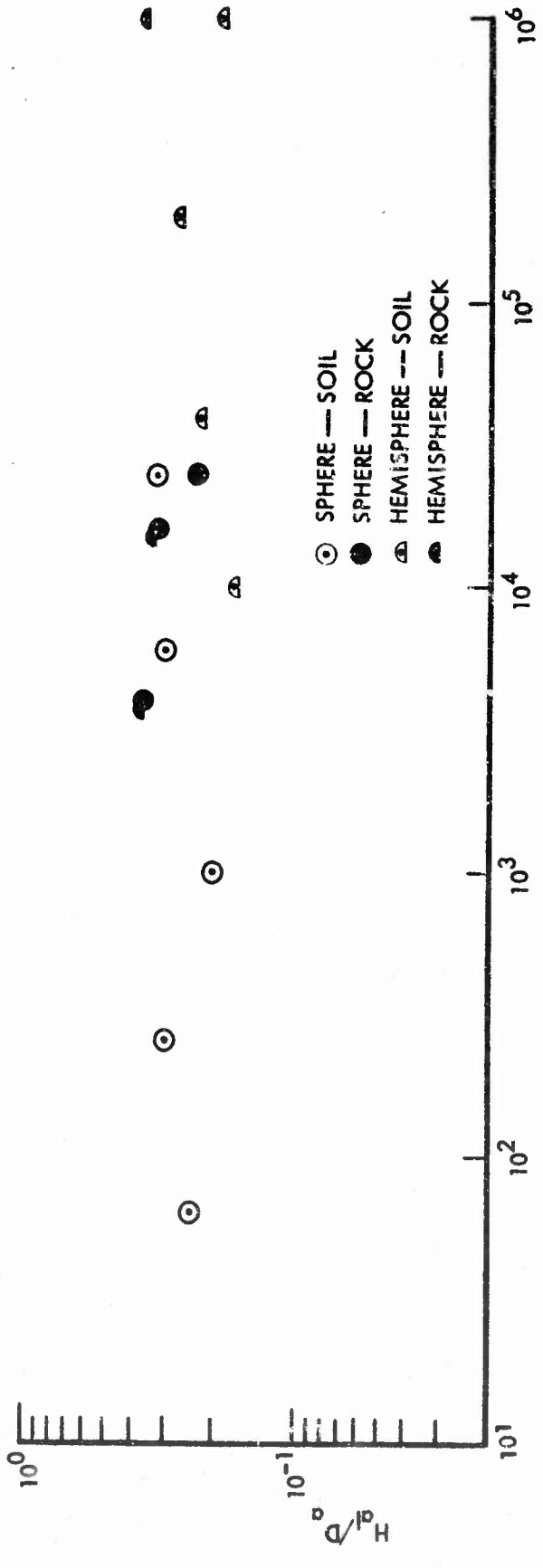

Figure 46. Ratio of Apparent Lip Crest Height to Apparent Crater Depth for Spherical and Hemispherical Charges.

crater is formed. This ratio is about 0.34 for both spherical and hemispherical charges in rock. The scatter in the value of this ratio appears to be about the same for both spherical and hemispherical charges in soil media.

d. Ejecta Distribution

The distribution of ejecta resulting from craters formed by spherical and hemispherical charges is shown in Figure 47. Comparisons given in this figure are for both 4000- and 16,000-pound charges.

Averaged ejecta distributions for a 4000-pound TNT sphere (S4a) and for a 4000-pound hemisphere (H1) are roughly comparable. Ejecta distribution plots for craters formed by the 16,000-pound spherical and hemispherical charges (LS and H2) are quite different. The LS crater exhibits ejecta distributions along 4 radials which are roughly the same. There is a tremendous difference between the ejecta distributions observed along the eight radials for the H2 crater. If the ejecta distribution observed along all H2 radials is averaged, the resulting distribution is quite different from that obtained in like manner for the LS crater. Such a comparison shows a definite tendency for the ejecta resulting from the H2 shot to be deposited over a larger area relative to the crater than that from the LS shot. At the same actual distance from ground zero within the first 30 feet, the average thickness of ejecta for the LS shot was significantly higher than the average ejecta thickness for the H2 shot.

The ratio of ejecta mass to missing crater mass is slightly greater for the H2 crater than for the LS crater. (See Table 11.) The annular region over which the ejecta mass was computed, extended to 1.1 and 1.3 crater radii from the crater edge for LS and H2 craters, respectively. This ratio of ejecta mass to missing crater mass seems, however, to be larger for the crater formed by the 4000-pound spherical charge than for the crater formed by the H1 charge. Thus, the tendency is conflicting; however, the reason for the apparent conflict may be the difference in the regions for each crater over which ejecta mass was computed

e. Upthrust

The permanent vertical and horizontal displacements adjacent to the H2 crater are plotted in Figure 48. Vertical upward displacements vary significantly from radial to radial. The maximum vertical upward displacement was on the order of 1 foot.

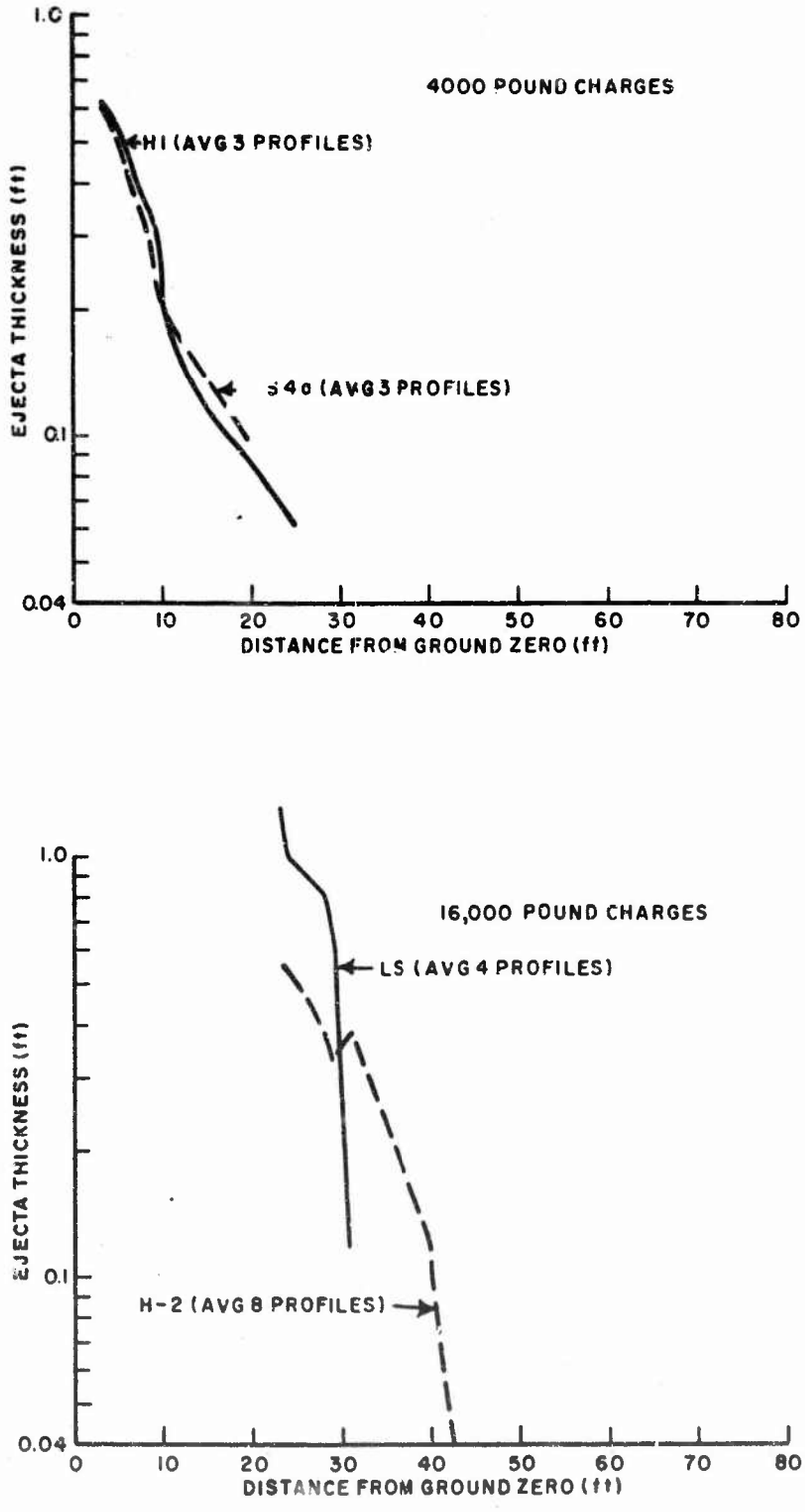

Figure 47. Ejecta Distribution for Craters Formed by Spherical and Hemispherical Charges.

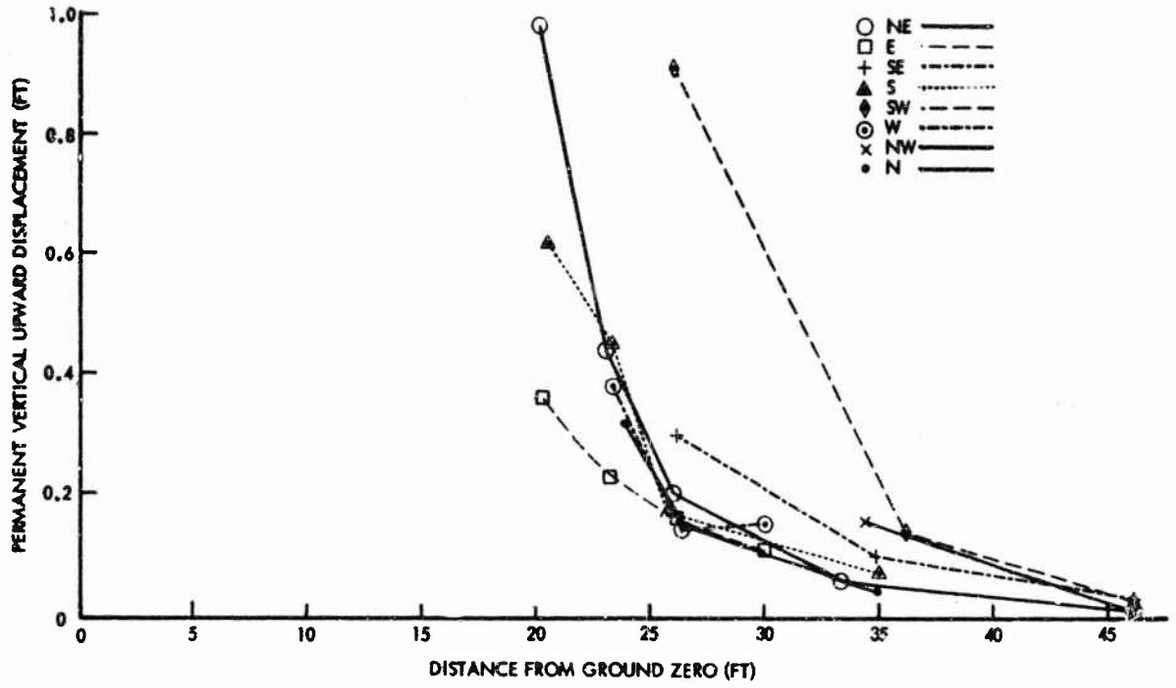

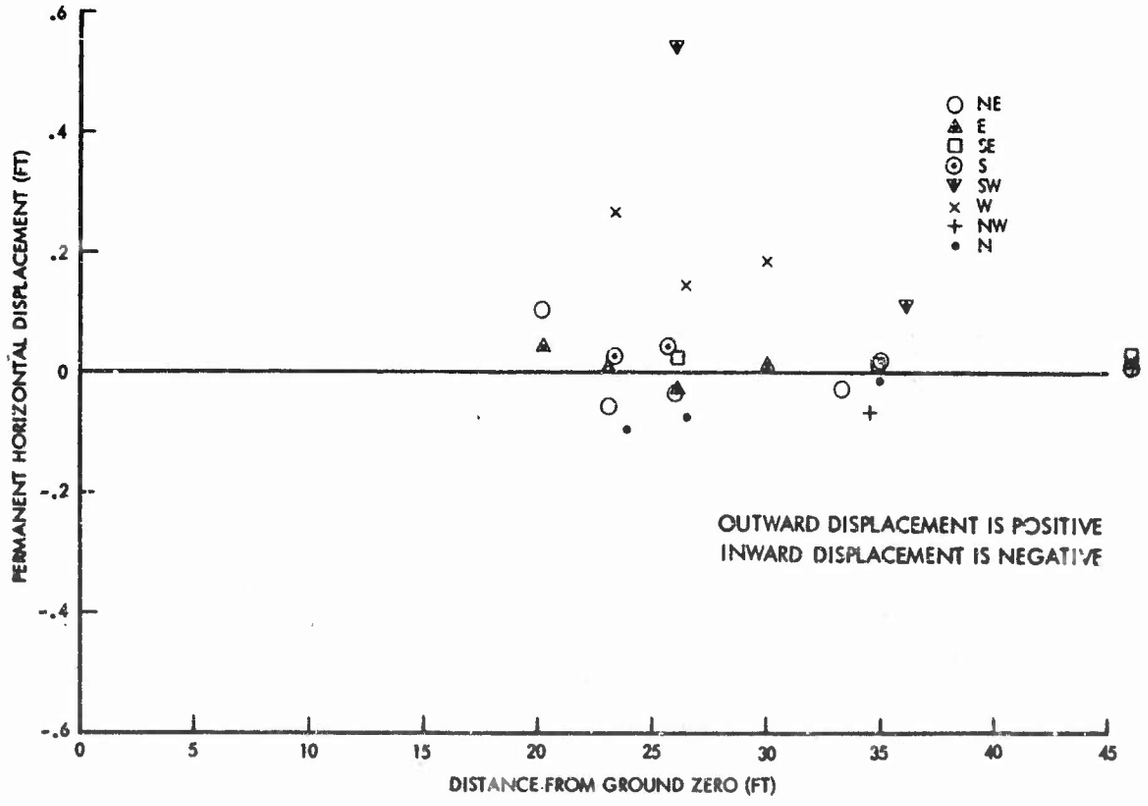

Figure 48. Permanent Vertical and Horizontal Displacements for H2 Crater.

Recorded horizontal permanent displacements were in both an inward and outward direction. Displacements inward toward the crater were generally observed in the region north of the crater. This means that the region bounded by the northwest and northeast radials shifted inward toward the crater a distance of something on the order of 0.1 foot. Most horizontal displacements were on the order of 0.1 foot; however, displacements along the west radial were consistently greater.

Permanent upward displacements for craters formed by spherical and hemispherical charges are plotted in Figure 49. The measurements along all radials encircling the LS charge are quite consistent. As observed for the ejecta thickness measurements on Crater H2, the upward displacements for the H2 crater vary significantly from radial to radial. Upward displacements from the LS and H2 craters are comparable although the position at which comparable displacements occur is closer to ground zero for the H2 shot because of its smaller crater.

Upward displacements for the craters formed by the 4000-pound spheres and hemispheres also vary greatly from radial to radial. It does appear, however, that upthrust for both types of craters is comparable. It is also interesting to note that maximum upthrust exhibited from craters formed by the 4000-pound spheres and hemispheres is about half of that exhibited for craters formed by 16,000-pound spheres and hemispheres.

4. Coupling

a. Crater Dimensions

Crater data for near-surface craters in basalt (MTCE) and playa (Air Vent, Reference 12) are given in Table 19. For the MTCE craters, the apparent crater formed by the fully buried charge exhibited a radius that was 20 percent greater than the crater radius from the half-buried charge and about 150 percent greater than the crater radius from the unburied surface tangent charge. Its depth was about 40 percent larger than the depth for the crater formed by the half-buried charge and about 150 percent greater than the depth for the crater formed by the tangent charge. The apparent volume for the crater formed by the fully buried charge was more than twice the volume resulting from the half-buried sphere and more than ten times the volume of the crater formed by the tangent sphere. Roughly, the same comparative relationships exist for the

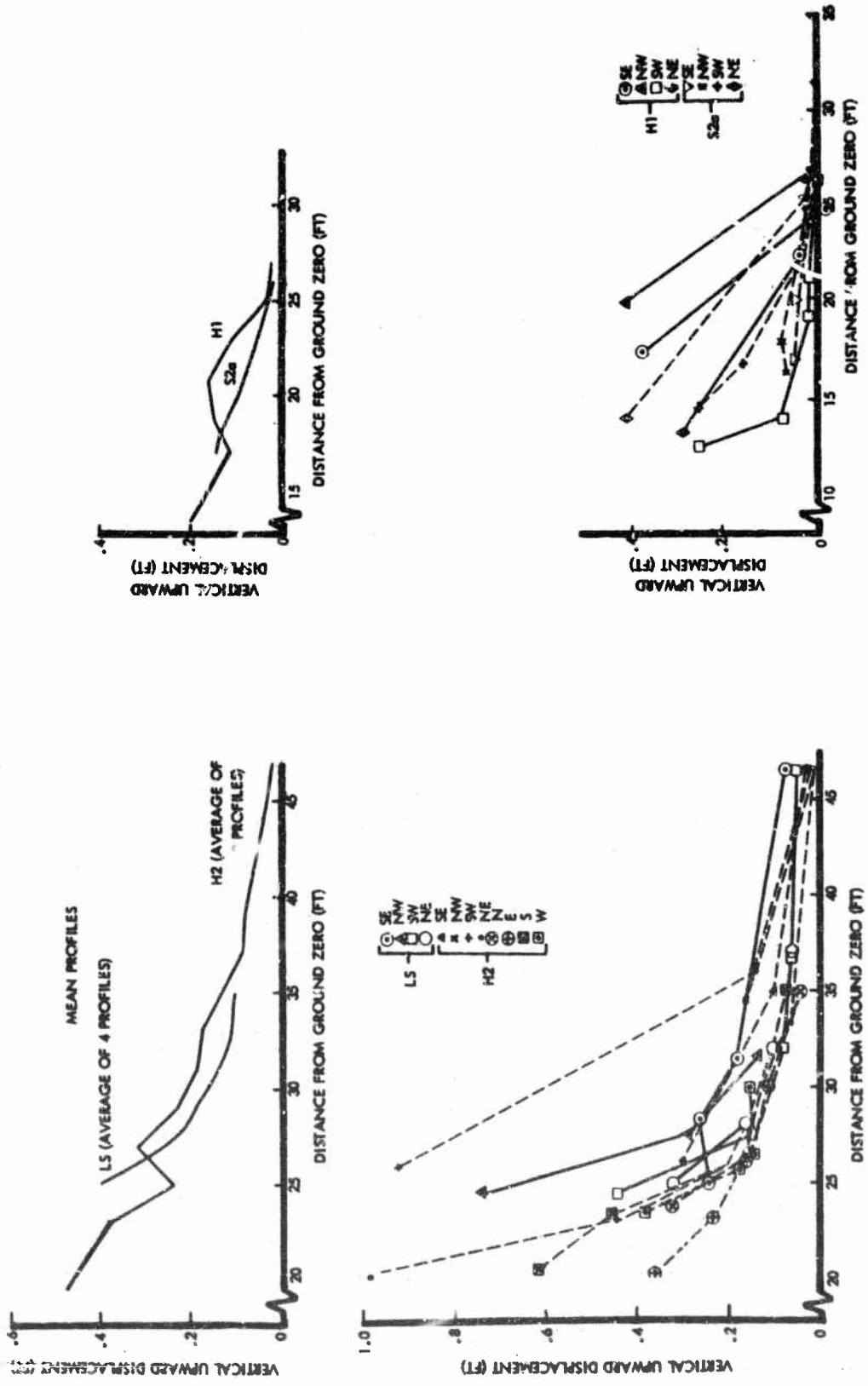

Figure 49. Permanent Vertical Upward Displacement for Craters Formed by Spherical and Hemispherical Charges.

Table 19

NEAR SURFACE CRATER DATA

Shot	Charge Weight	Burst Depth		Apparent Radius		Apparent Depth[a]		Apparent Volume		Excavated Radius		Excavated Depth[a]		Excavated Volume	
		Actual	Scaled	Actual	Scaled	Actual	Scaled	Actual	Scaled	Actual	Scaled	Actual	Scaled	Actual	Scaled
	(lb)	(ft)	($ft/lb^{1/3}$)	(ft)	($ft/lb^{1/3}$)	(ft)	($ft/lb^{1/3}$)	(ft^3)	(ft^3/lb)	(ft)	($ft/lb^{1/3}$)	(ft)	($ft/lb^{1/3}$)	(ft^3)	(ft^3/lb)
Basalt (MTCE)															
S1(C1)	4000	0	0	12.1	0.76	3.6	0.23	733	0.18	16.0	1.01	5.3	0.33	2960	0.52
S2a	4000	0	0	10.7	0.87	4.0	0.25	872	0.17	—	—	—	—	—	—
S3a	4000	0	0	11.4	0.72	4.0	0.25	853	0.21	—	—	—	—	—	—
S4a	4000	0	0	10.3	0.65	4.0	0.25	805	0.15	—	—	—	—	—	—
C2	4000	2.2	0.14	14.0	0.88	5.3	0.33	1500	0.38	19.3	1.22	7.3	0.46	4187	1.05
ST1	4000	-2.2	-0.14	3.7	0.23	1.3	0.08	37	0.01	5.4	0.34	1.7	0.11	—	—
ST2a	4000	-2.2	-0.14	7.3	0.46	1.9	0.12	139	0.03	—	—	—	—	—	—
ST3a(C3)	4000	-2.2	-0.14	4.5	0.28	1.2	0.08	25	0.01	—	—	—	—	—	—
Playa (Reference 12)															
AVII-1[b]	256	-0.86	-0.14	3.2	0.50	0.8	0.12	13.1	0.05	4.3[c]	0.68[c]	2.5[c]	0.39[c]	72.0[c]	0.28[c]
AVII-2A	256	0	0	5.5	0.87	2.4	0.38	95.5	0.37	6.8	1.07	4.4	0.69	259	1.01
AVII-2B	256	0	0	5.4	0.85	2.4	0.38	93.2	0.36	—	—	—	—	—	—
AVII-3	256	0.86	0.14	6.7	1.06	3.4	0.54	235	0.92	8.7	1.37	5.4	0.85	449	1.76

[a] Maximum Crater Depth
[b] True crater dimensions are approximate
[c] Dimensions are for true crater

excavated craters. (It should be noted here that a fully buried tangent spherical charge is not a fully coupled charge. Full coupling occurs at some depth below surface greater than that at which the uppermost edge of the charge is tangent to the surface.)

Apparent and excavated crater dimensions are plotted in Figure 50 as functions of actual burst depth for MTCE craters formed by near-surface, 4000-pound, TNT spherical charges. The relationship between the excavated crater and its associated apparent crater is interest. The excavated radius and depth for the crater formed by the fully buried charge and the half-buried charge are about 40 percent greater than corresponding dimensions for the apparent crater. Linear dimensions for the excavated crater are approximately the same as the linear dimensions of the apparent crater for the surface-tangent charge. The excavated volumes for the craters formed by the fully buried and half-buried charges were almost three times the volumes of the associated apparent craters. The significant differences in crater size observed when charges are detonated at slightly different positions relative to the rock surface is further illustrated by the crater profiles shown in Figures 51 and 52.

b. Craters in Rock and Soil

Scaled burst-depth plots for apparent craters in basalt (MTCE), desert alluvium, and playa are shown in Figure 53. This figure illustrates the reduced size of craters in rock as compared to craters in soil. (It should be noted here that although apparent craters in rock are smaller than apparent craters in soil, the cratering effectiveness is about the same for both rock and soil. See discussion under Charge Geometry.) Desert alluvium data were obtained from References 8 and 13 and represented a range of charge yield of 216 to 2.4×10^6 and 64 to 6000-pounds of TNT or equivalent, respectively. The apparent radius for craters formed in rock appears to be about 0.6 to 0.7 of the radius for similar craters (charge buried at the same scaled-burst depth) formed in soil. The apparent depth for craters formed in rock is about two-thirds of the depth for similar craters formed in soil. The apparent volume for craters formed in rock is about 0.35 to 0.40 times the volume for similar craters formed in soil.

Regarding the crater shapes, data given in Table 7 indicate that apparent crater shape factors are about the same (0.5) for craters formed by the half-buried charge and for the fully buried surface tangent charge. There is a

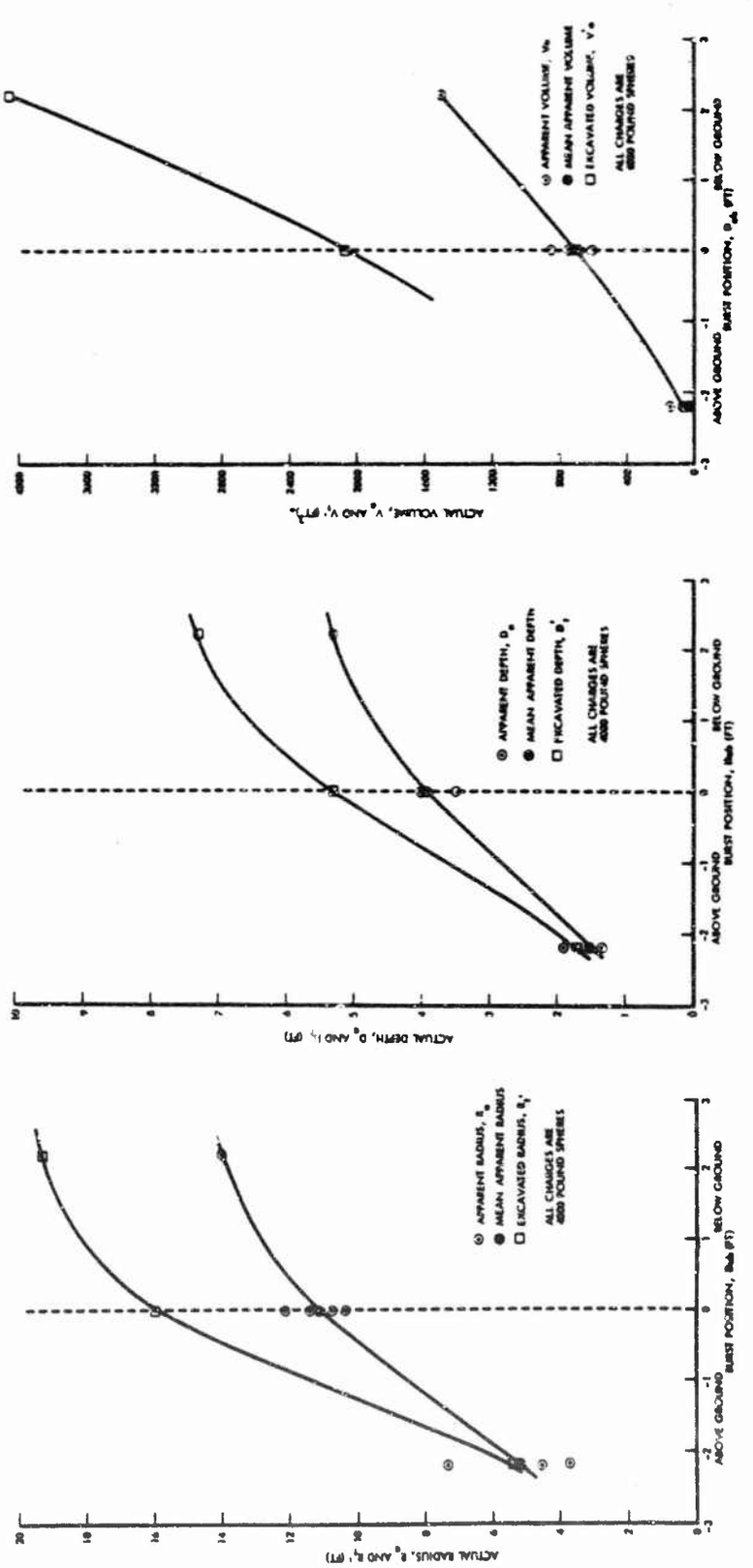

Figure 50. Apparent Crater Dimensions as Functions of Burst Depth for Surface and Near-Surface MTCE Craters.

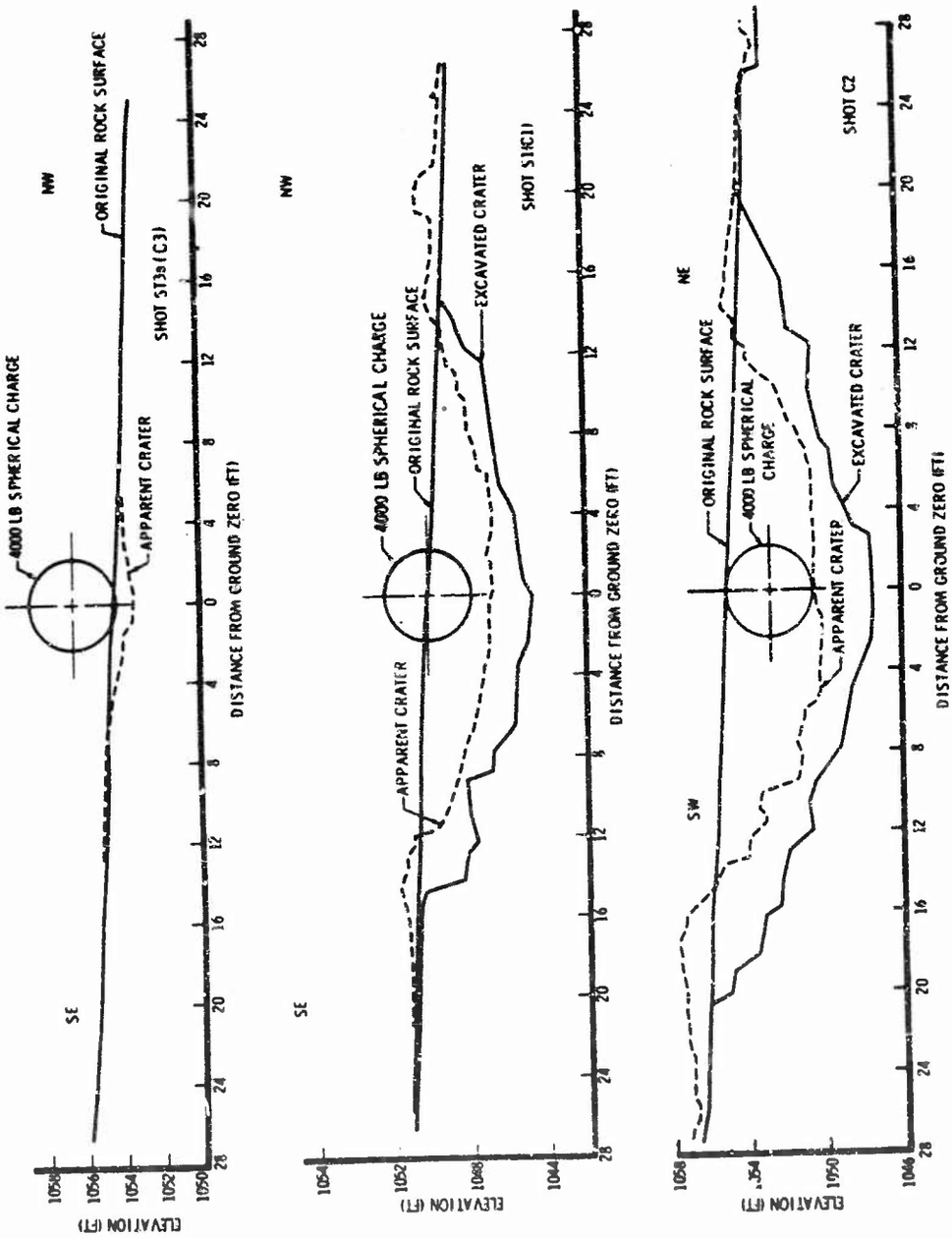

Figure 51. Profiles of Craters Formed by Surface and Near-Surface Charges.

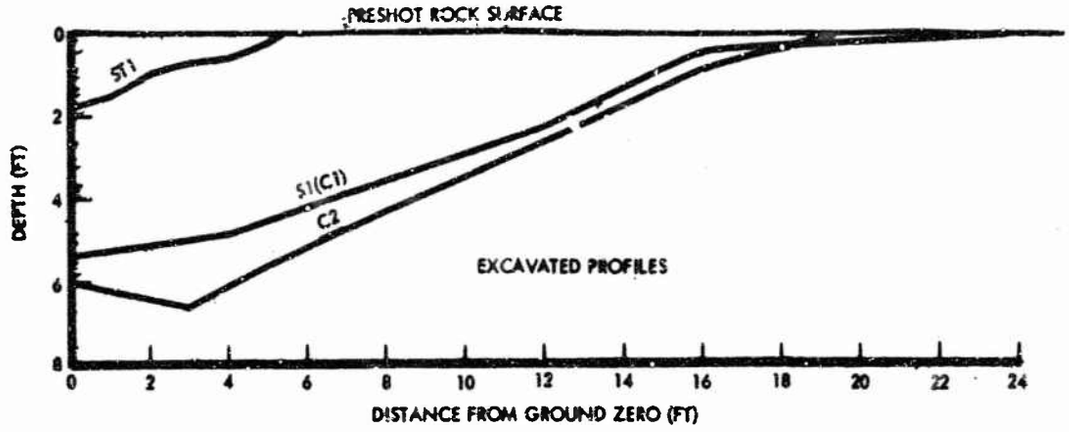

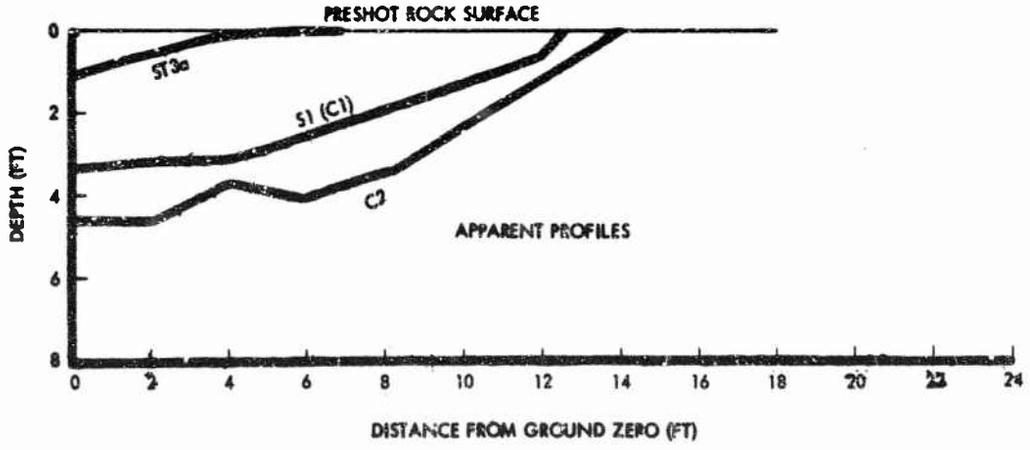

Figure 52. Half-Profiles for Craters Formed by Surface and Near-Surface Charges.

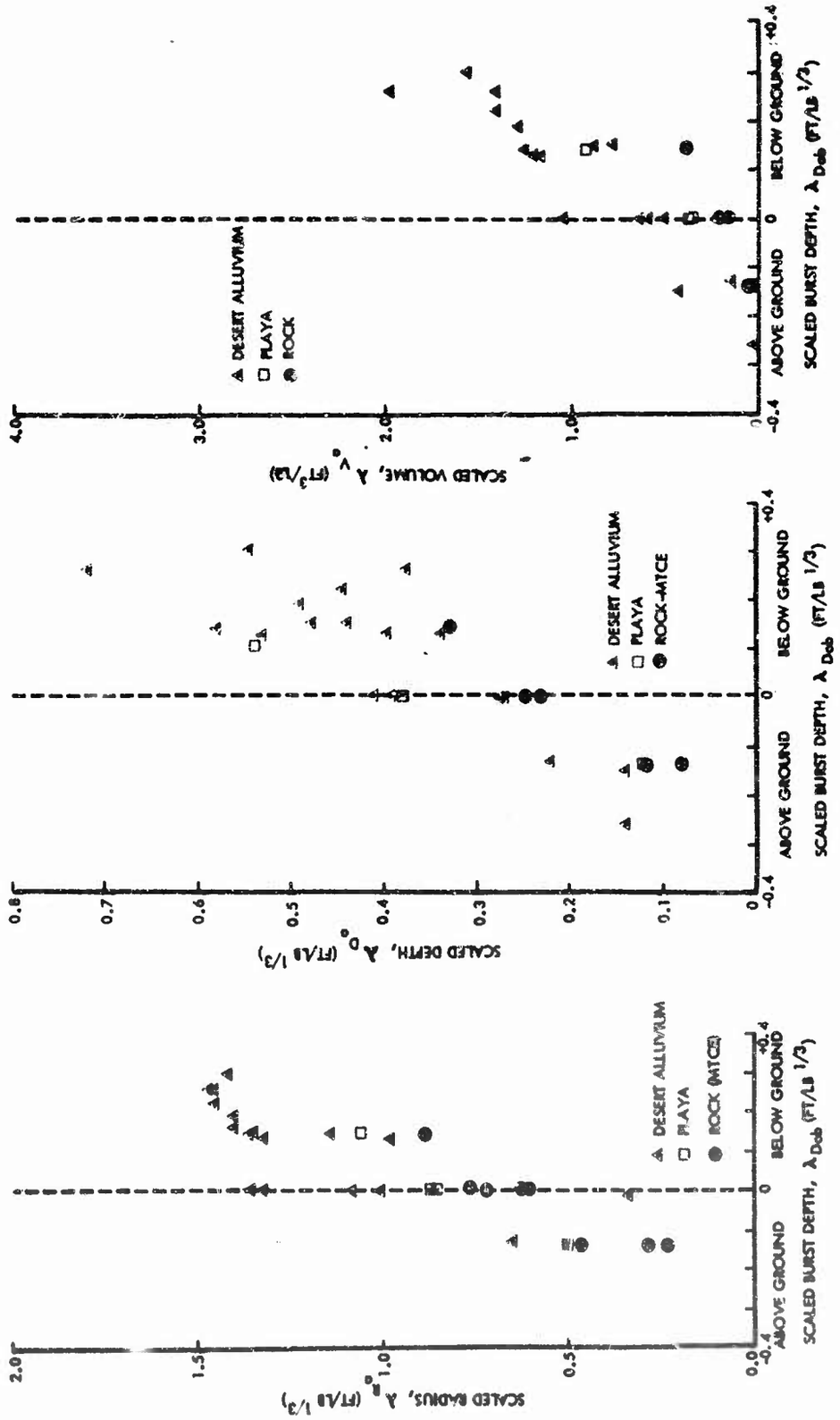

Figure 53. Scaled Apparent Crater Dimensions as Function of Scaled Burst Depth for Craters in Rock & Soil.

radical difference for apparent craters formed by above-surface tangent charges, these craters exhibiting shape factors from 0.33 to 0.66. The ratio of apparent crater depth to apparent crater radius increases as the center of the charge is moved downward. This ratio is about 0.25 for the surface tangent, about 0.3 for the half-buried, and about 0.4 for the fully buried spherical charges.

c. Ejecta Distribution

Neglecting the southeast radial for crater S4a because of the influence described of C2 ejecta, the ejecta thickness plots shown in Figure 54 indicate the larger ejecta thicknesses and the greater relative region over which the material is deposited for the C2 crater. Again as noted for most MTCE craters, the variation of ejecta thickness from radial to radial for craters formed by surface and near-surface charges is significant. Plots of ejecta thickness averaged for all radials on each shot show the relationship between the ejecta distribution for craters formed by surface and near-surface charges of the same energy release. These averaged ejecta distribution plots are also shown in Figure 54.

d. Upthrust

Permanent vertical upward displacement of the ground surface adjacent to craters formed by surface and near-surface shots are shown in Figure 55. The greatest displacement of the ground surface was caused by the fully buried sphere. This charge caused permanent upward displacements of the ground surface that were about twice those observed at the same distance from a half-buried charge, and about four times those observed at the same distances for a surface tangent charge. The average of maximum upthrust measurements made along each radial was approximately 0.5 feet for the fully buried charge, 0.25 for the half-buried charge, and less than 0.1 for the above-surface tangent charge.

5. Scaling

a. Craters

Table 20 presents data for surface craters in hard rock formed by half-buried spherical charges. In addition to the MTCE data, this table gives crater dimensions for the Oso experiment (Reference 4) and the Flat Top I experiment (Reference 14).

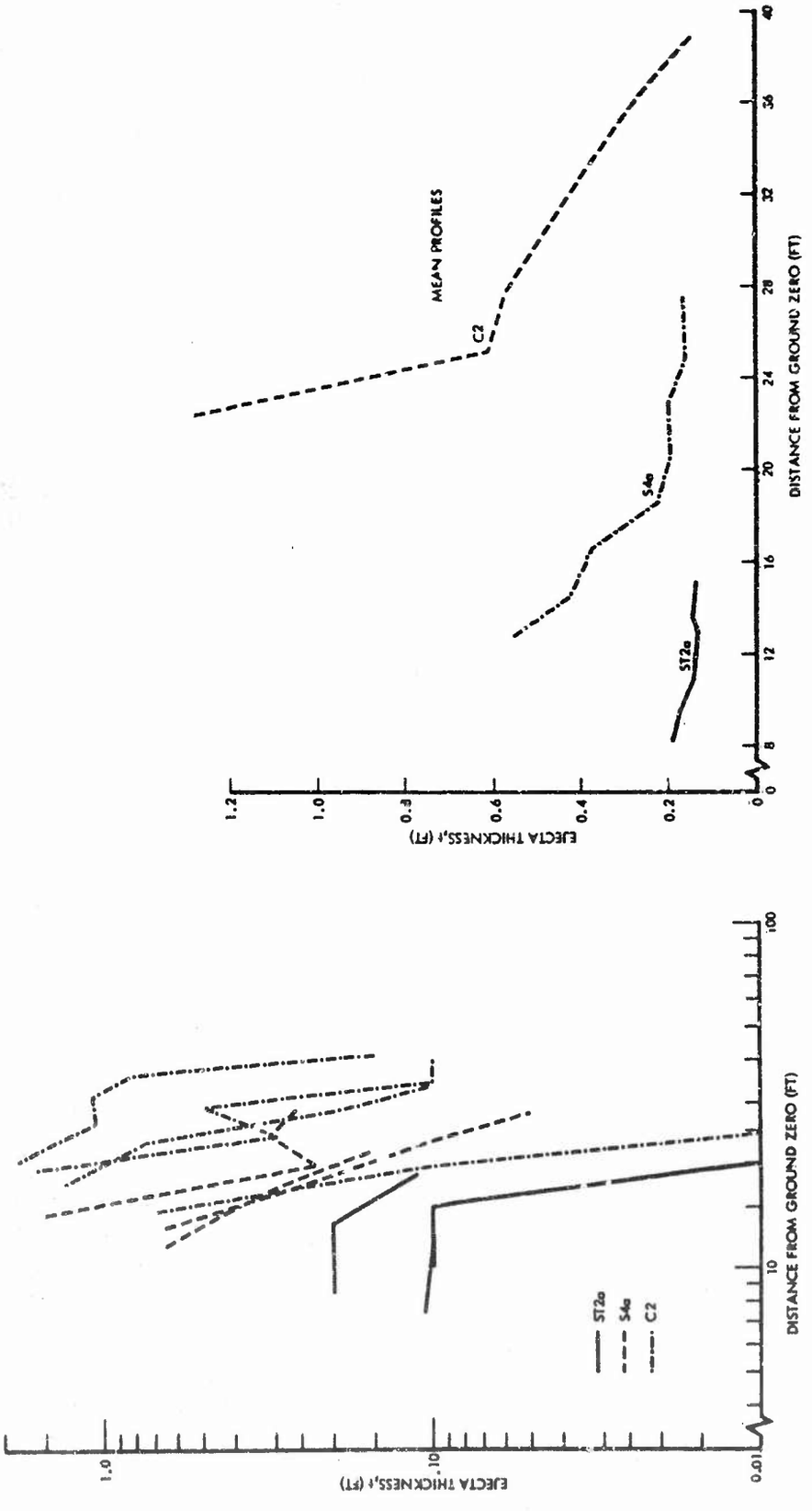

Figure 54. Ejecta Thickness for Surface and Near-Surface Craters.

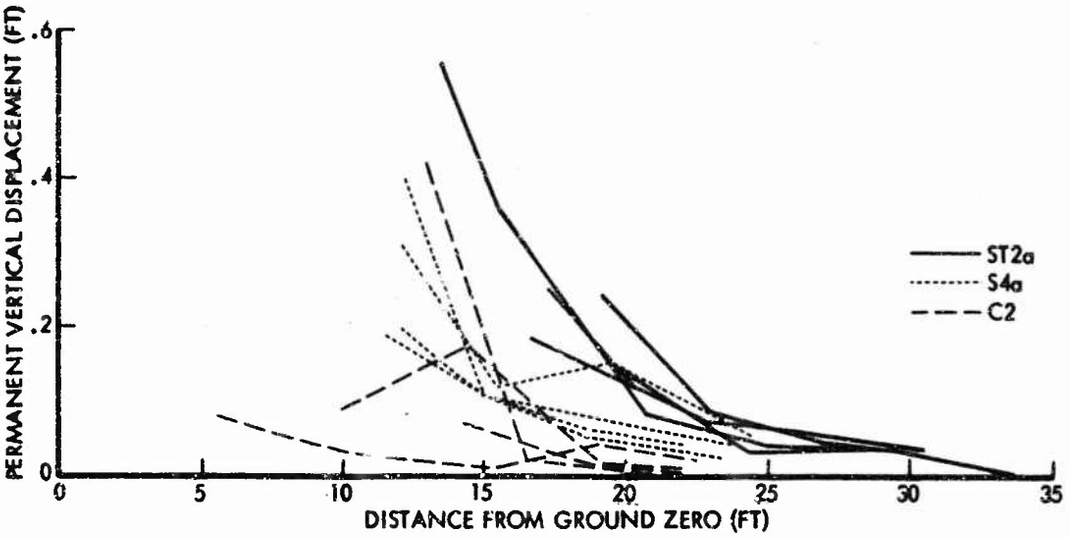

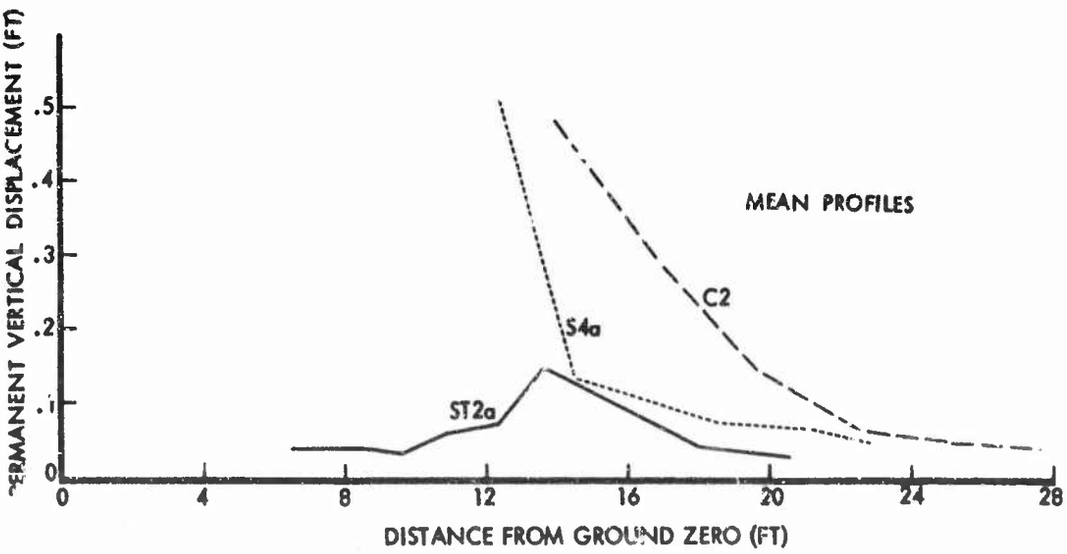

Figure 55. Permanent Vertical Displacement for Surface and Near-Surface Craters.

Table 20

HIGH EXPLOSIVE SURFACE CRATERS IN HARD ROCK
(HALF-BURIED SPHERICAL CHARGES)

Apparent crater depths listed are maximum depths. Flat Top 1 was detonated in limestone, all other charges were in basalt.

Shot	Charge Weight, W (lb)	Apparent Crater			Excavated Crater		
		Radius R_a(ft)	Depth D_a(ft)	Volume V_a(ft^3)	Radius R'_t(ft)	Depth D'_t(ft)	Volume V'_t(ft^3)
OSO 1[2]	64	3.8	1.4	36.2	—	—	—
OSO 2[2]	64	4.7	1.6	55.8	5.8	1.7	114.1
S1(C1)	4000	12.1	3.6	733	16.0	5.3	2060
S2a	4000	10.7	4.0	672	—	—	—
S3a	4000	11.4	4.0	853	—	—	—
S4a	4000	10.4	4.0	605	—	—	—
LS	16,000	18.7	5.6	3659	23.8	9.1	7527
Flat Top I[12]	40,000	27	12.7	1×10^4	38	14.5	2.4×10^4

Scaling relationships for apparent craters in hard rock formed by half-buried spherical charges are given in Figure 56. (It must be emphasized that all scaling relationships given in this section are valid only for the charge range over which they were derived.) Scaling relationships shown represent mathematical fits obtained by the method of least squares. Apparent crater scaling relationships are:

$$R_a = 1.30\ W^{0.27} \quad \text{(Deviation = 0.11)*}$$
$$D_a = 0.42\ W^{0.28} \quad \text{(Deviation = 0.17)}$$
$$V_a = 0.41\ W^{0.78} \quad \text{(Deviation = 0.34)}$$

*

$$\text{Deviation} = \sqrt{\sum_{i=1}^{n} \frac{1}{n} \left(\frac{Y_i - aW^b}{Y_i} \right)^2}$$

where n = number of points
a = constant
b = slope
W = charge weight
Y_i = ordinate value of data point of interest

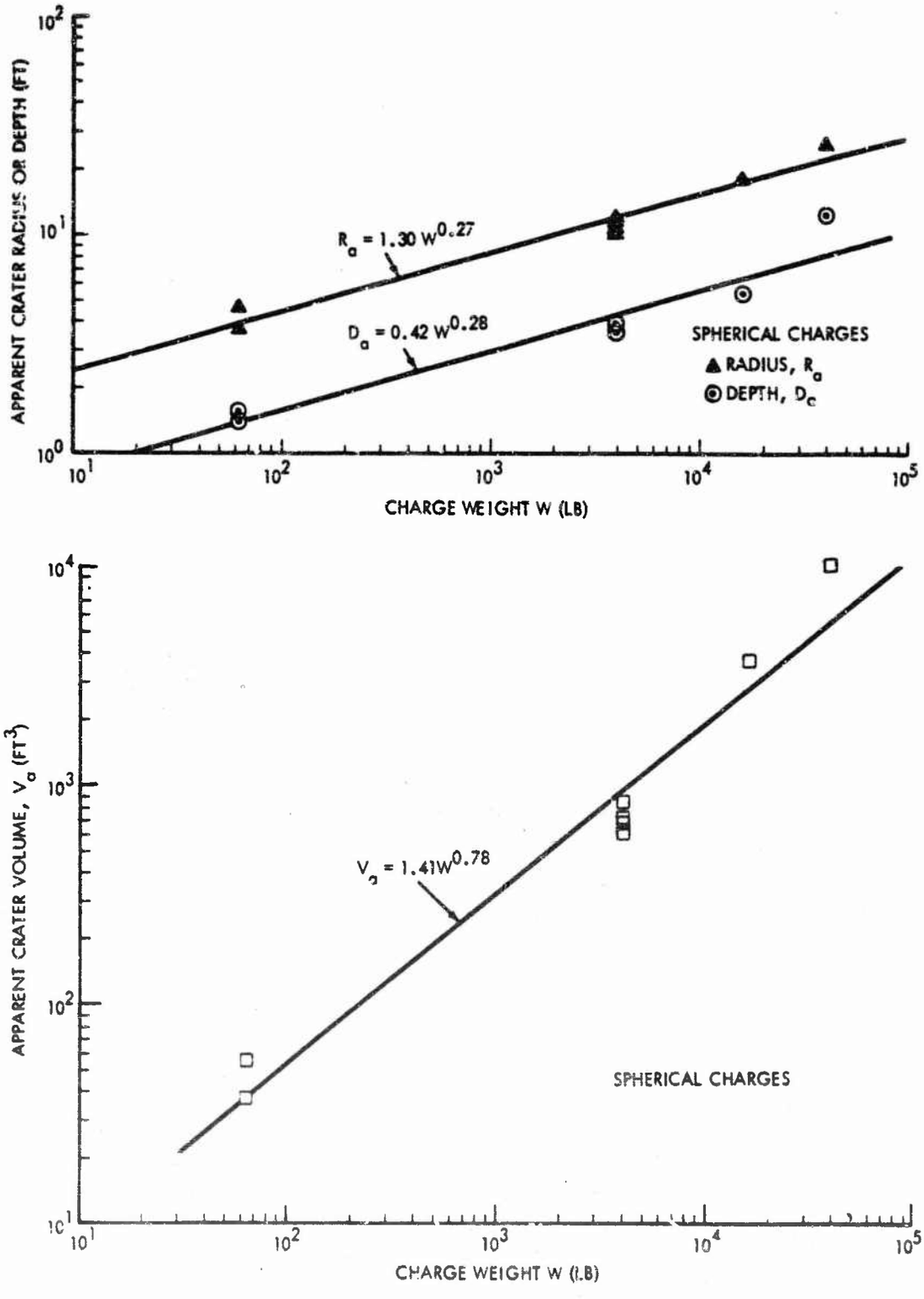

Figure 56. Scaling Relationships for Surface Apparent Craters in Hard Rock (Half-Buried Spherical Charges).

where radius and depth are in feet, volume is in cubic feet, and charge weight is in pounds. These exponents are nearly internally consistent, that is, the volume exponent is 0.78 as compared to 0.82 ($R_a^2 D_a$). For internal consistency the crater volume exponent should be equal to twice the radius exponent plus the depth exponent. If this is true then the crater is indeed characterized by a symmetrical circular shape.

The Flat Top I crater exhibits linear dimensions and a volume greater than that indicated by the scaling relationships shown in Figure 56. This seems reasonable inasmuch as the Flat Top I medium was a limestone having a lower density and compressive strength than those of the Yakima basalt and Oso argillite.

Scaling relationships, again determined by the method of least squares, are presented in Figure 57 for excavated surface craters formed in rock by spherical charges. Scaling relationships are as follows:

$$R'_t = 1.74\ W^{0.28} \text{ (Deviation = 0.09)}$$

$$D'_t = 0.42\ W^{0.32} \text{ (Deviation = 0.10)}$$

$$V'_t = 3.52\ W^{0.80} \text{ (Deviation = 0.24)}$$

The deviation from internally consistent exponents here is slightly greater (0.80 as compared to 0.88) than that for the apparent craters. Again, data for the Flat Top I crater fall above the scaling relationship; however, the difference here is not as much as that which was observed for apparent craters.

Table 21 gives existing dimensions for three craters formed by hemispherical charges detonated on the surface of hard rock. Apparent crater scaling relationships for these data are shown in Figure 58. These scaling relationships are:

$$R_a = 0.48\ W^{0.37} \text{ (Deviation = 0.001)}$$

$$D_a = 0.06\ W^{0.47} \text{ (Deviation = 0.03)}$$

$$V_a = 0.04\ W^{1.14} \text{ (Deviation = 0.03)}$$

Again the volume exponent is slightly less than the sum of twice the radius exponent and the depth exponent. One notes here that while apparent crater radius and depth for the half-buried spherical charges scaled approximately as the quarter root of charge weight, for hemispherical charges the apparent radius

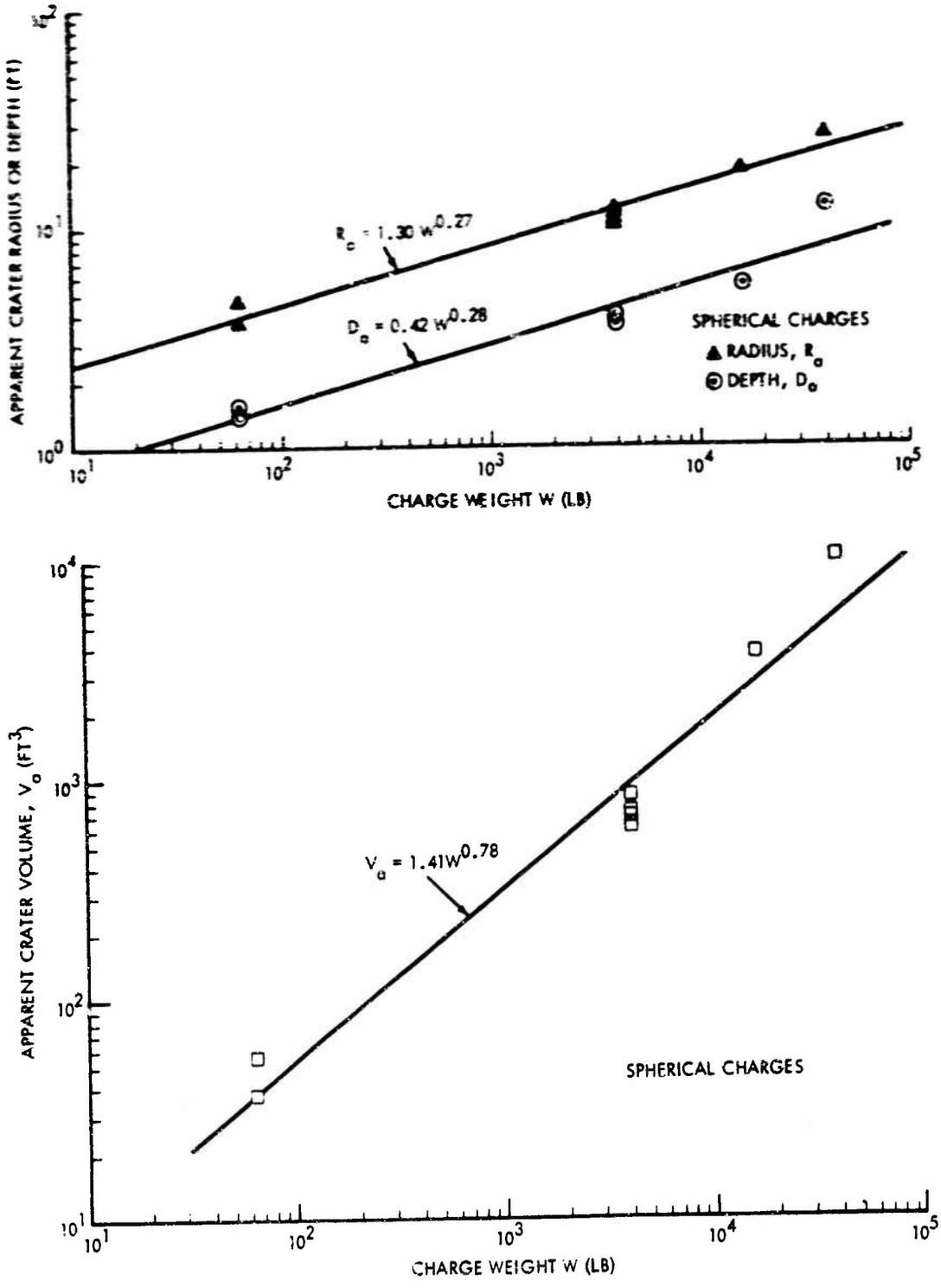

Figure 56. Scaling Relationships for Surface Apparent Craters in Hard Rock (Half-Buried Spherical Charges).

where radius and depth are in feet, volume is in cubic feet, and charge weight is in pounds. These exponents are nearly internally consistent, that is, the volume exponent is 0.78 as compared to 0.82 ($R_a^2 D_a$). For internal consistency the crater volume exponent should be equal to twice the radius exponent plus the depth exponent. If this is true then the crater is indeed characterized by a symmetrical circular shape.

The Flat Top I crater exhibits linear dimensions and a volume greater than that indicated by the scaling relationships shown in Figure 56. This seems reasonable inasmuch as the Flat Top I medium was a limestone having a lower density and compressive strength than those of the Yakima basalt and Oso argillite.

Scaling relationships, again determined by the method of least squares, are presented in Figure 57 for excavated surface craters formed in rock by spherical charges. Scaling relationships are as follows:

$$R'_t = 1.74\ W^{0.28} \quad \text{(Deviation = 0.09)}$$

$$D'_t = 0.42\ W^{0.32} \quad \text{(Deviation = 0.10)}$$

$$V'_t = 3.52\ W^{0.80} \quad \text{(Deviation = 0.24)}$$

The deviation from internally consistent exponents here is slightly greater (0.80 as compared to 0.88) than that for the apparent craters. Again, data for the Flat Top I crater fall above the scaling relationship; however, the difference here is not as much as that which was observed for apparent craters.

Table 21 gives existing dimensions for three craters formed by hemispherical charges detonated on the surface of hard rock. Apparent crater scaling relationships for these data are shown in Figure 58. These scaling relationships are:

$$R_a = 0.48\ W^{0.37} \quad \text{(Deviation = 0.001)}$$

$$D_a = 0.06\ W^{0.47} \quad \text{(Deviation = 0.03)}$$

$$V_a = 0.04\ W^{1.14} \quad \text{(Deviation = 0.03)}$$

Again the volume exponent is slightly less than the sum of twice the radius exponent and the depth exponent. One notes here that while apparent crater radius and depth for the half-buried spherical charges scaled approximately as the quarter root of charge weight, for hemispherical charges the apparent radius

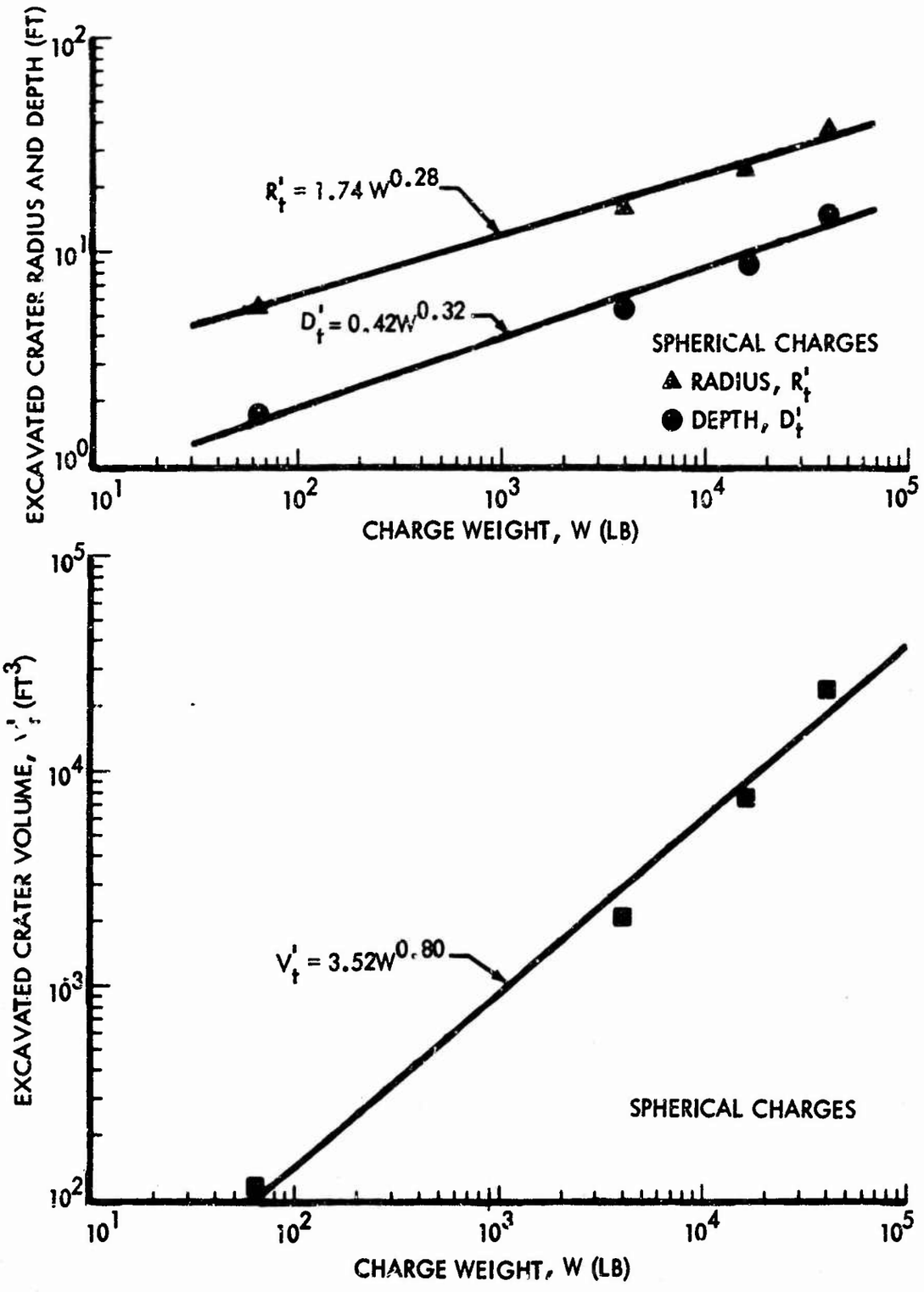

Figure 57. Scaling Relationships for Surface Excavated Craters in Hard Rock (Half-Buried Spherical Charges).

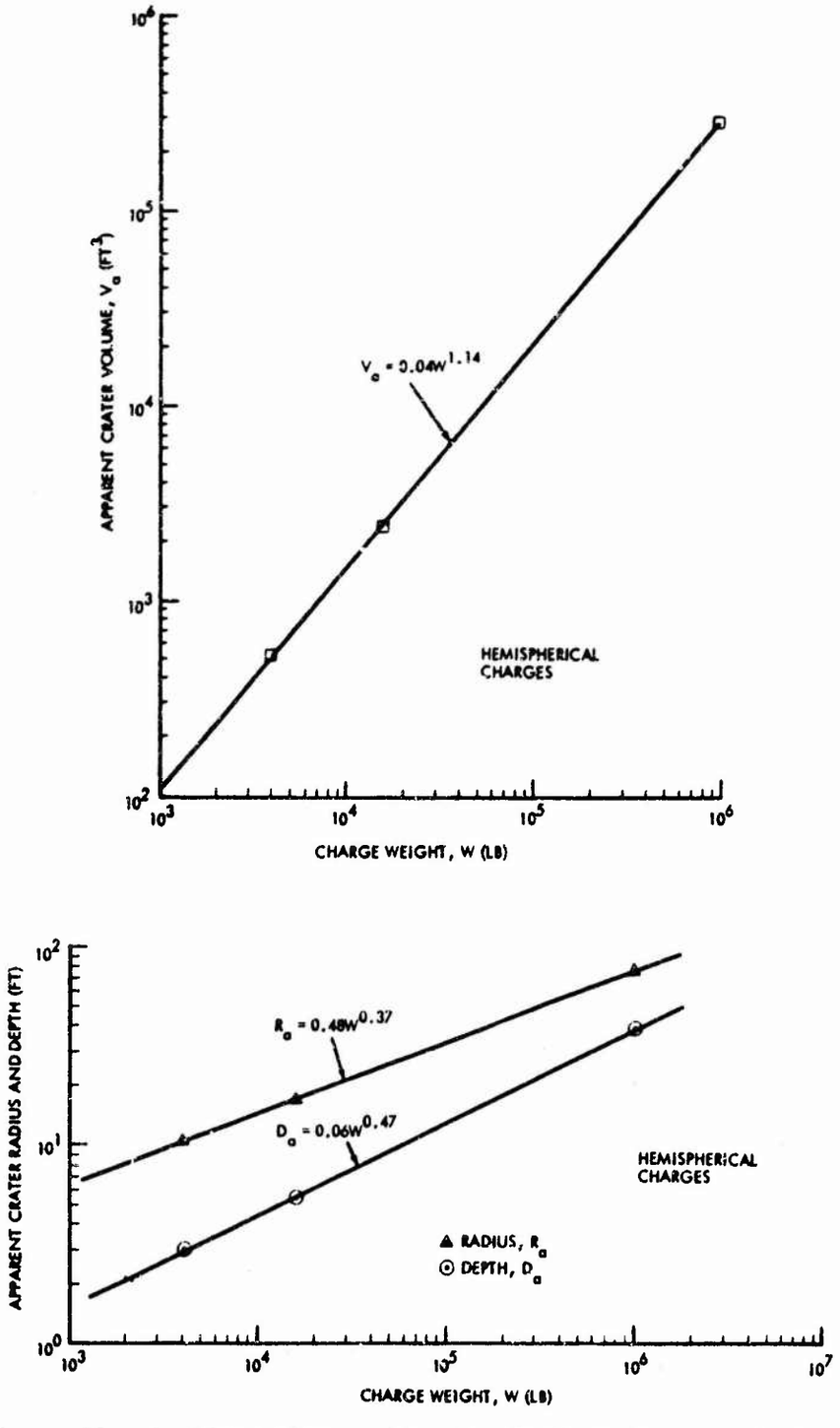

Figure 58. Scaling Relationships for Surface Apparent Craters in Hard Rock (Hemispherical Charges).

Table 21

HIGH-EXPLOSIVE SURFACE CRATERS IN HARD ROCK
(HEMISPHERICAL CHARGES)

Apparent depths listed are maximum depths. All charges were detonated in basalt.

Shot	Charge Weight W (lb)	Apparent Crater			Excavated Crater		
		Radius R_a(ft)	Depth D_a(ft)	Volume V_a(ft^3)	Radius R_t'(ft)	Depth D_t'(ft)	Volume V_t'(ft^3)
H2	16,000	17.1	5.4	2417	25.2	7.2	3868
H1	4,000	10.2	3.0	536	17.3	4.1	3299
Sailor Hat[13]	1×10^6	78.6	39.2	2.9×10^5	—	—	—

and depth scale as something greater than the cube root of charge weight. It is also somewhat unusual to find a set of scaling relationships for a given medium in which the crater depth scales by some exponent of charge weight that is greater than the scaling exponent of crater radius.

b. Craters in Rock and Soil

For comparison, data are included here on high-explosive surface craters in soil media (playa). Table 22 presents data for craters formed by half-buried spherical charges in playa (Reference 13). Scaling relationships for apparent craters in soil are shown in Figure 59. These scaling relationships are:

$$R_a = 0.70\ W^{0.38} \text{ (Deviation = 0.06)}$$

$$D_a = 0.40\ W^{0.33} \text{ (Deviation = 0.13)}$$

$$V_a = 0.22\ W^{1.09} \text{ (Deviation = 0.18)}$$

Also shown in Figure 59 are the scaling relationships developed for apparent surface craters in hard rock. The plot of scaling relationships for rock and soil shows that these curves are not parallel. This means that the ratio of crater dimensions for rock soil is not a constant. Thus, the conventional

Table 22

HIGH-EXPLOSIVE SURFACE CRATERS IN SOIL (HALF-BURIED SPHERICAL CHARGES)

All charges were fired in playa at the Nevada Test Site. Charges were positioned with their center of gravity coincident with the ground surface.

Program	Shot	Charge Weight, W	Apparent Crater			True Crater		
			Radius, R_a	Depth, D_a	Volume, V_a	Radius, R_t	Depth, D_t	Volume, V_t
		(lb)	(ft)	(ft)	(ft^3)	(ft)	(ft)	(ft^3)
Toboggan (Reference 15)	E1a	8	1.6	0.9	2.3	—	—	—
	E1b	8	1.5	0.7	1.8	—	—	—
	E1c	8	1.3	0.6	1.5	—	—	—
Air Vent (Reference 12)	III-1A	64	3.4	1.6	24.0	4.5	2.7	68.1
	III-1B	64	3.4	1.8	26.1	4.2	2.7	60.4
	III-1C	64	3.3	1.8	22.8	4.2	2.9	62.7
	III-1D	64	3.5	1.9	28.3	4.1	2.7	58.7
	III-2A	256	5.5	2.4	95.5	6.8	4.4	259.4
	III-2B	256	5.4	2.4	93.2	—	—	—
	III-2A	1,000	9.4	4.3	442	11.5	6.8	1.1×10^3
	III-2B	1,000	10.1	4.6	517	12.0	6.4	1.2×10^3
	III-2C	1,000	8.9	4.3	442	11.8	6.3	1.1×10^3
	III-3A	6,000	16.4	6.6	2,520	21.5	9.4	5.6×10^3
	III-3B	6,000	17.5	6.9	2,704	—	—	—
Flat Top (Reference 15)	II	40,000	35.3	12.9	2.32×10^4	38	15.2	4.48×10^4

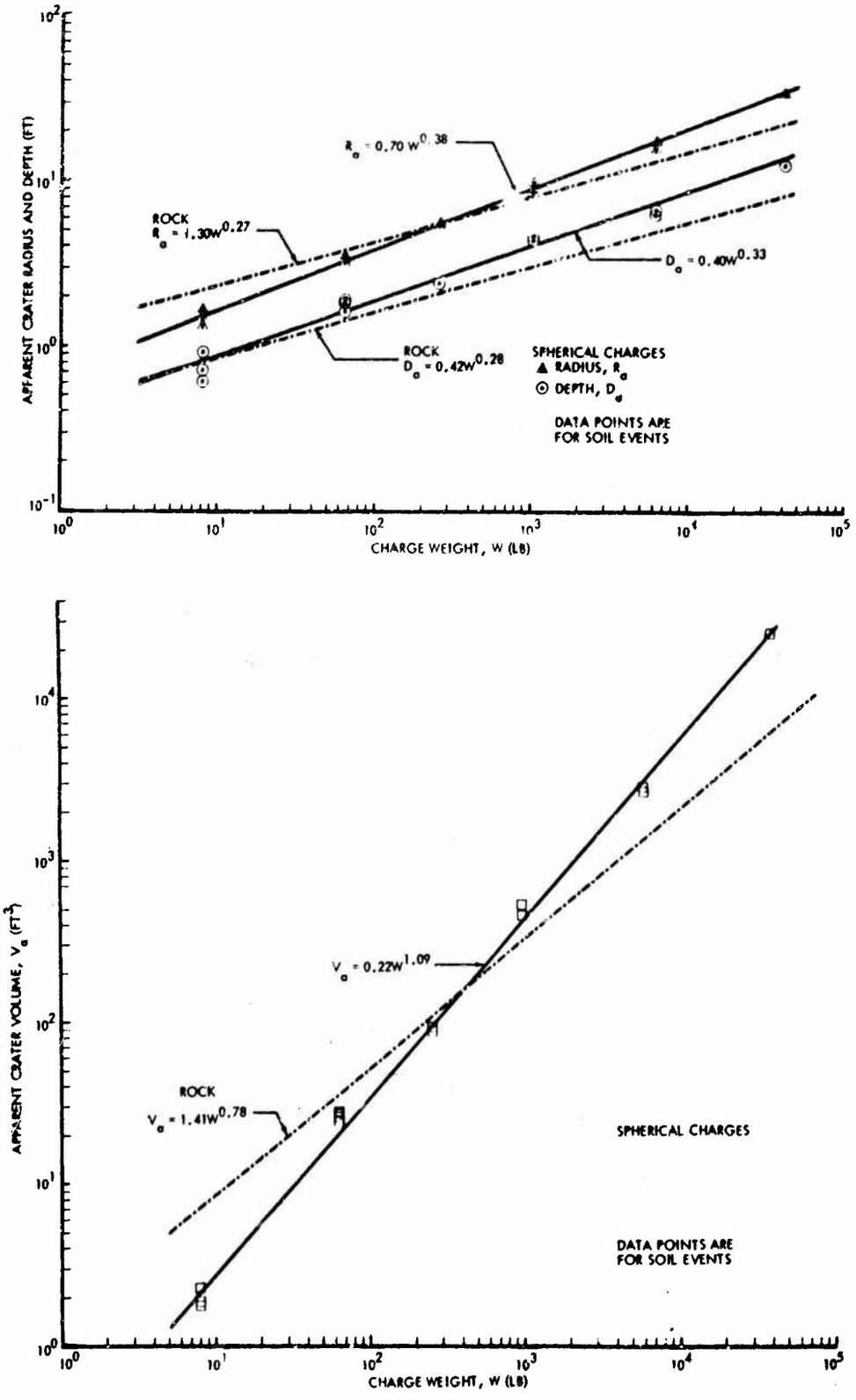

Figure 59. Scaling Relationships for Surface Apparent Craters in Soil (Half-Buried Spherical Charges).

ratio of 0.8 for linear dimensions of craters in rock and soil is not valid over the range of charge weight shown in Figure 59. Figure 59 indicates that the ratio of apparent radius of rock craters to apparent radius of soil craters varies from about 0.9, at a charge weight of 1,000-pounds, to about 0.7 for a charge weight of 40,000-pounds. The ratio of apparent depth of rock craters to apparent depth of soil craters varies from about 0.8 to about 0.6, and the ratio of apparent volume of rock craters to apparent volume of soil craters varies from 0.8 to 0.3 for the same range of charge weights.

Scaling relationships for true surface craters in soil are shown in Figure 60. These relationships are:

$$R_t = 1.01\ W^{0.35} \quad \text{(Deviation = 0.04)}$$

$$D_t = 0.92\ W^{0.27} \quad \text{(Deviation = 0.06)}$$

$$V_t = 0.92\ W^{1.02} \quad \text{(Deviation = 0.08)}$$

Also shown in Figure 60 are the scaling relationships of excavated craters in hard rock. Again these scaling curves for rock and soil on a log plot are not parallel and so the ratio between similar dimensions of rock and soil craters cannot be constant.

Table 23 presents available data for craters formed by hemispherical charges detonated on a silt clay medium at the Suffield Experimental Station in Canada (References 18 and 19). Scaling relations for these craters, shown graphically in Figure 61 are:

$$R_a = 0.51\ W^{0.40} \quad \text{(Deviation = 0.02)}$$

$$D_a = 1.63\ W^{0.20} \quad \text{(Deviation = 0.16)}$$

$$V_a = 1.04\ W^{0.96} \quad \text{(Deviation = 0.13)}$$

These relationships include the Snowball crater data. For comparative purposes scaling relationship without Snowball data are:

$$R_a = 0.48\ W^{0.41} \quad \text{(Deviation = 0.02)}$$

$$D_a = 1.10\ W^{0.25} \quad \text{(Deviation = 0.08)}$$

$$V_a = 0.47\ W^{1.04} \quad \text{(Deviation = 0.08)}$$

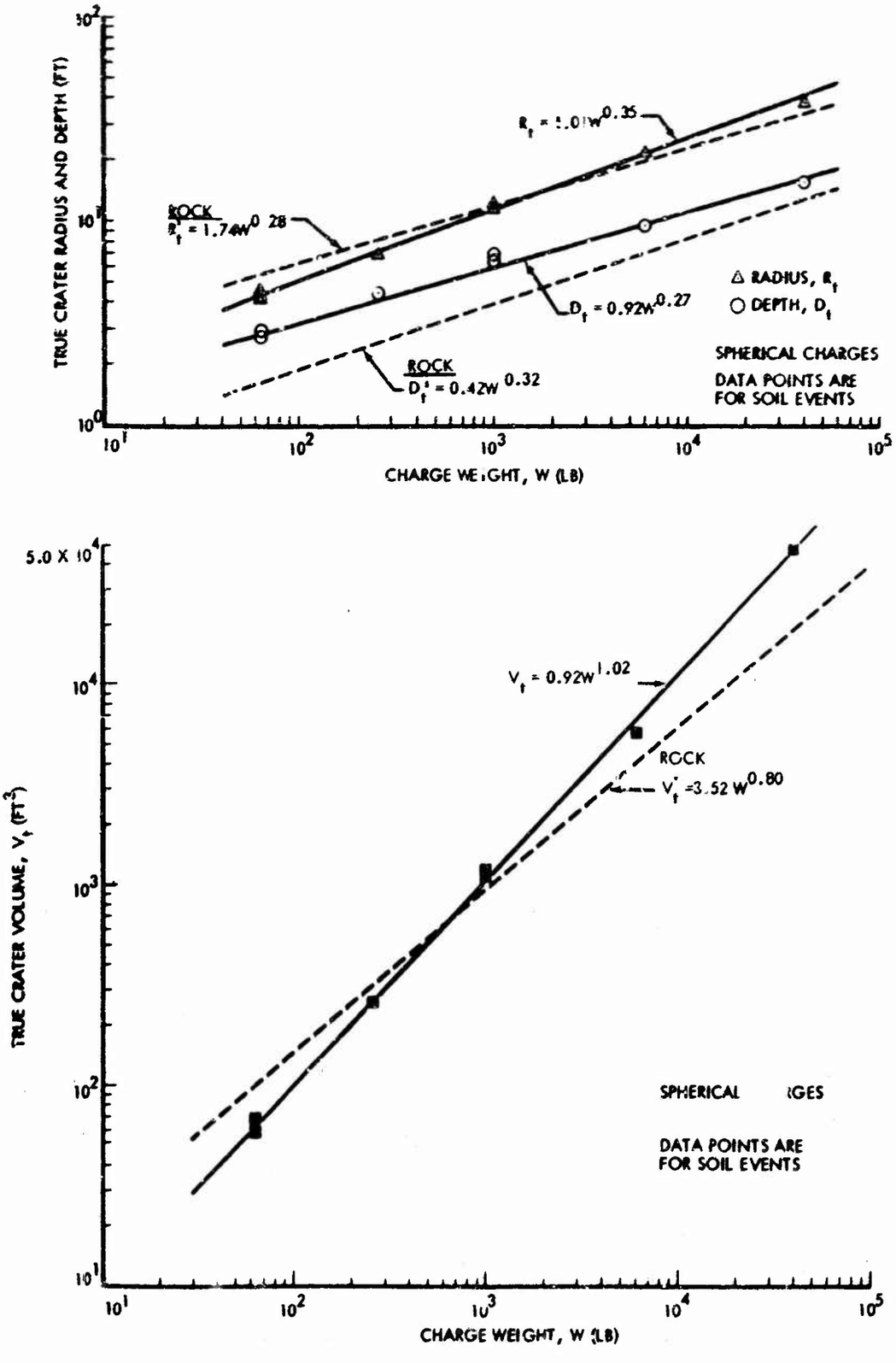

Figure 60. Scaling Relationships for Surface True Craters in Soil (Half-Buried Spherical Charges).

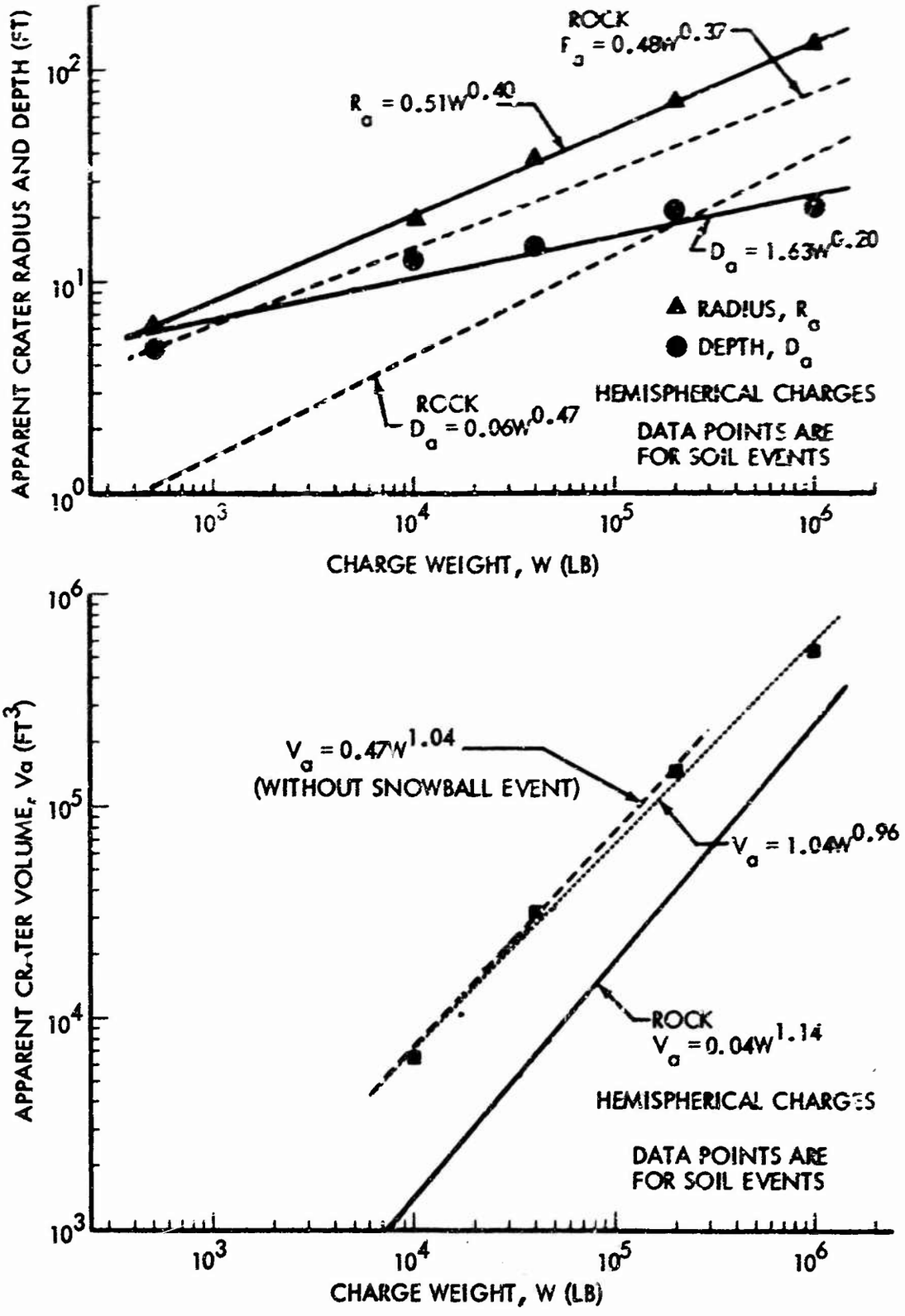

Figure 61. Scaling Relationships for Surface Apparent Craters in Soil (Hemispherical Charges).

Table 23

HIGH-EXPLOSIVE SURFACE CRATERS IN SOIL
(HEMISPHERICAL CHARGES)

All charges were hemispheres detonated on the surface of a silt clay soil at the Watching Hill Site of the Suffield Experimental Station. Data in table were taken from Reference 17 with the exception of Snowball data which were obtained from Reference 18.

Shot	Date	Charge Weight, W (lb)	Apparent Crater Radius R_a (ft)	Apparent Crater Depth D_a (ft)	Apparent Crater Volume V_a (ft^3)
H		512	6.2	4.8	—
	9-29-58	10,063	20	12.8	6390
	8-18-60	40,000	≅37.1	≅14.8	32,155
	8-8-61	200,000	70	≅21.1	144,160
	7-17-64	1,000,000	140	≅21	548,100

c. Ejecta

Ejecta thickness as a function of distance from ground zero is shown for 4000-pound and 16,000-pound spheres and hemispheres in Figure 62. Also shown are least-square fits to the average of various combinations of radials for which ejecta thickness was determined. For craters formed by hemispherical charges the following ejecta distribution relationships were derived:

H1: $t = 7.2 \times 10^3 D^{-3.63}$ $(12 < D < 36)$

H2: $t = 48.5 \times D^{-1.48}$ $(16 < D < 40)$

where t is ejecta thickness in feet and D is range from ground zero in feet.

The least-squares relationship shown above is not a good representation of ejecta distribution for crater H2 because ejecta thickness along the southeast and northwest radials was significantly greater than that measured along the other radials. For every radial the ejecta thickness decay with distance

Figure 62. Ejecta Thickness for Craters Formed by Half-Buried Spheres and Surface Hemispheres.

is actually greater than the negative 1.48 slo[illegible] cated above. A least-squares fit to an average ejecta thickness versus distance curve indicates $t \sim D^{-3.3}$. This is probably indicative of the real [illegible]ckness decay with distance.

For craters formed by spherical charges the following ejecta distribution relationships were derived:

S4a: $t = 2.8 \times 10^{2} D^{-2.36}$ $(11.5 < D < 29)$

LS: $t = 2.1 \times 10^{7} D^{-5.34}$ $(20 < D < 35)$

It is noted that the major portion of the mass of ejecta for craters in rock lies relatively close to the crater. This is shown in Figure 62 by the rapid drop-off of ejecta with distance, that is, the high negative exponent of distance. Crater H2 would also exhibit this rapid drop-off if individual fits were made to those radials exhibiting the high ejecta thickness and those exhibiting the low ejecta thickness.

Comparisons of ejecta mass distributions for MTCE craters with that for the Danny Boy nuclear crater are shown in Figure 63. These curves include the missile ejecta data given in Table II.3.

Fifty percent of the ejected material from the H1 shot was deposited between the crater edge and 1.7 crater radii, whereas the fifty percent distances were 1.9 and 2.0 for the Danny Boy crater and H2 crater, respectively. Ninety percent of the ejected material was deposited between the crater edge and 6.0, 2.7, and 2.9 crater radii for the H1, Danny Boy, and H2 craters, respectively. (It should be noted when making these comparisons that the Danny Boy nuclear crater resulted from charge placement at optimum depth from a cratering standpoint. The Danny Boy medium was a basalt similar to the MTCE medium.)

The most significar[illegible] ference noted in comparing mass distributions resulting from the large and small hemispherical charges was that ejected material was deposited over a larger area relative to the crater for the smaller charges.

A significant difference exists between the mass distribution curves for the large (LS) and small (S4a) half-buried charges. Fifty percent of the ejected material was distributed between the crater edge and 1.2 crater radii for the LS crater. The fifty percent distance for the S4a crater was 1.9 crater radii.

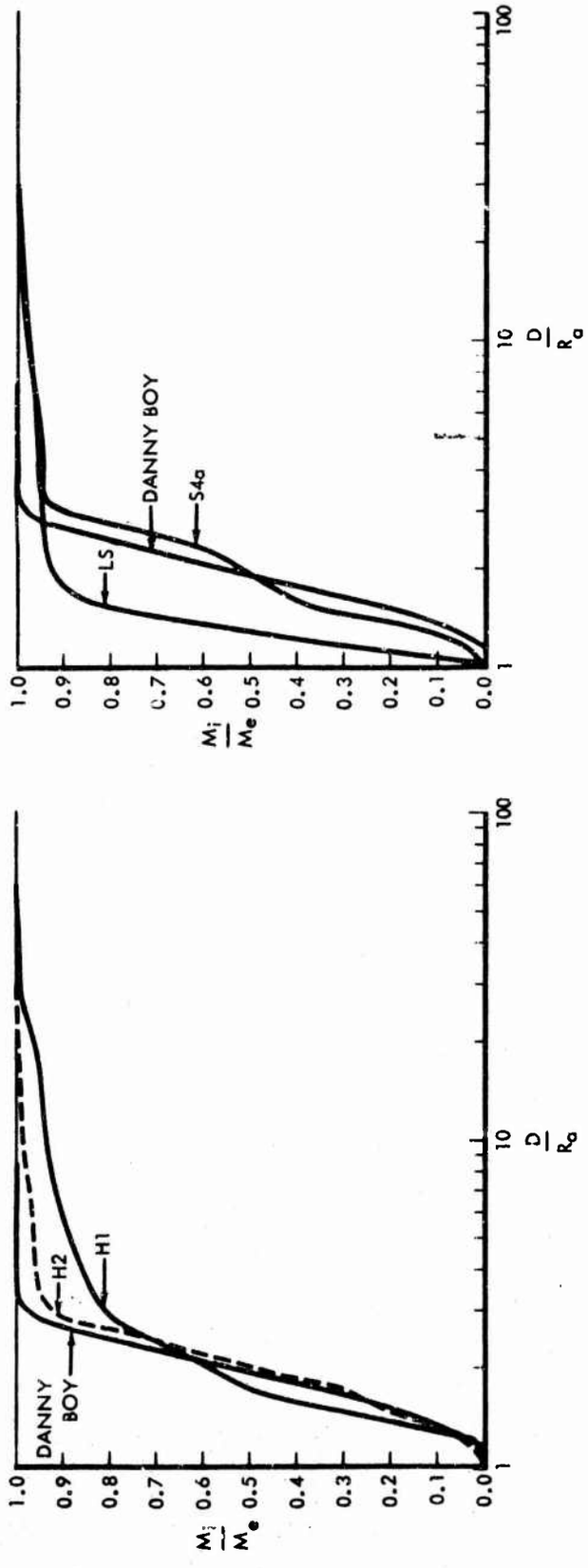

Figure 63. Comparison of Ejecta Mass Distribution for MTCE High-Explosive Craters and Danny Boy Nuclear Crater.

The 90 percent distance was 1.7 and 3.0 for the LS and S4a craters, respectively. The Danny Boy nuclear crater exhibited a mass distribution curve that differed significantly from the LS crater. On a relative basis, ejected material was deposited much closer to the crater edge for the LS crater than was observed for the Danny Boy crater.

d. Discrete Missiles

As mentioned above, the mass distribution curves shown in Figure 63 include the missile data given in Table II.3. The missile data were included in ejecta thickness versus distance plots used to compute total ejecta mass. The missile data represented 35 percent and 15 percent of the total rock mass ejecta for the H2 and H1 craters, respectively. The missile data represented 7 percent and 5 percent of the ejecta from the LS and S4a craters, respectively. Scrutiny of the mass distributions shown in Figure 63 will show that these percentages are logical.

e. Upthrust

Actual vertical displacements of the rock surface adjacent to the LS and S2a crater are shown in Figure 64. It appears that at similar relative distances upthrust for the LS crater is twice that for crater S2a. Also shown in Figure 64 is a plot of scaled vertical displacement versus scaled distance. Displacement and range have been scaled by charge weight to the 0.3 power. (This exponent is the mean for the scaling exponents determined for apparent and excavated crater depths.) This scaling relationship appears to hold over a scaled range of from 1.5 to 1.9.

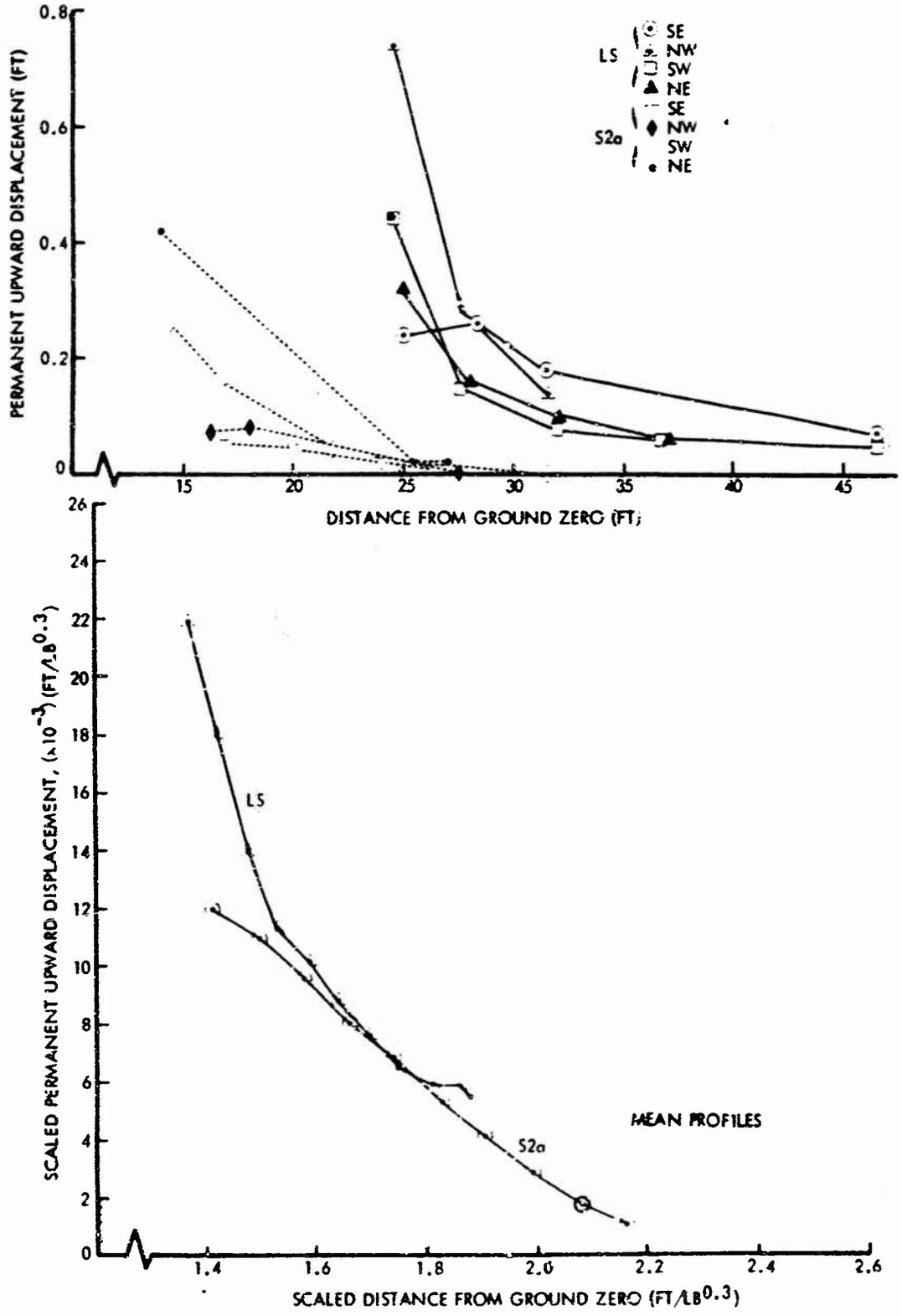

Figure 64. Actual and Scaled Permanent Vertical Displacement of Ground Surface Adjacent to LS and S2a Crater.

SECTION V

CONCLUSIONS AND RECOMMENDATIONS

1. Conclusions

These conclusions apply specifically to the charge weights, burst conditions, and geologic media related to the MTCE project.

a. Successive Cratering

Depending on the approach used, the fourth shot in a series of half-buried successive shots along the same vertical axis may or may not appreciably increase the excavated crater depth. If the measured excavated crater depth from the third shot of a three-shot series is assumed to be equal to the excavated crater depth of the third shot in a four-shot series (which was not measured), then there is no increase in the excavated crater depth as the result of the fourth shot. However, there is actually a decrease in the measured excavated crater depth from the third shot in the three-shot series to the fourth shot in the four-shot series (Table 5), undoubtedly due to the inhomogeneity of the jointed basalt media. Alternatively, if there exists a constant ratio between the measured apparent and excavated crater depths for a single shot, which appears to be true, then an excavated crater depth for the third shot in the four-shot series calculated from this ratio indicates that there will be a 24 percent increase in the excavated crater depth from the third to fourth shot in a successive series. Because of the discrepancy in the results drawn from the same data, it is apparent that the data provided by the MTCE project are not conclusive.

The excavated depth for the crater formed by a four-shot series was about 30 percent greater than the excavated depth for a crater formed by the surface burst of a single half-buried spherical charge equal in energy release to the total of the four-shots in the series and 63 percent greater than the excavated crater depth for a crater formed by the surface burst of a single hemispherical charge of equal energy release.

The absolute dimensions for craters resulting from surface tangent spherical charges were significantly less than similar dimensions for craters formed by half-buried spherical charges. For example, the depth for each apparent and excavated crater in a three-shot series for those craters formed by surface tangent charges was less than half the depth for similar craters formed by half-buried charges.

Shot-to-shot dimensional incremental increases are greater, however, when compared to Shot 1, for craters formed by a series of surface tangent spherical charges than for craters formed by a series of half-buried spherical charges.

The vertical distance between the center-of-gravity of the charge and the resulting excavated crater boundary is about 6 feet for half-buried, 4000-pound spherical charges regardless of the crater, in a four-shot series, in which this quantity is measured. The portion of this distance that is solid basalt decreases with each successive shot and the portion of this distance which is rubble increases with each successive shot.

The shape factor of the excavated crater formed by a series of half-buried spherical charges decreases with each successive charge. This shape factor is less than 0.3 after the third and fourth charge in a four-shot series.

The ejecta thickness was greater at the same distance from ground zero for the crater formed by a 16,000-pound half-buried surface charge than for the first crater resulting from a four-shot series of 4000-pound half-buried charges. At a distance of about 25 feet from ground zero the ejecta thickness resulting from the 16,000-pound surface charge was about three times that for the 4000-pound crater at the same distance.

The upthrust of the rock surface adjacent to the crater builds up in rather consistent and uniform increments with each successive shot in a series. The average upthrust resulting from the final shot in the four-shot series was significantly less than that which resulted from each of the preceding shots.

b. Charge Geometry

Craters formed by hemispherical charges are slightly smaller than craters formed by half-buried spherical charges of the same weight. The apparent crater formed by the hemispherical charge exhibits a radius about 10 percent smaller, a depth about 15 percent smaller, and a volume about 30 percent smaller than those for a crater resulting from the spherical charge. For the hemispherical charge, the excavated crater radius was about 5 percent greater, the excavated crater depth about 20 percent smaller, and the excavated crater volume about 25 percent smaller than those for a crater formed by a spherical charge.

Apparent and excavated craters formed by the 16,000-pound half-buried spherical charge exhibited larger shape factors than like craters formed by the hemispherical charge.

The ratio of excavated to apparent crater dimension was about 1.5 for radius, 1.6 for depth, and 2.6 for volume for half-buried spherical charges; and 1.6 for radius, 1.4 for depth, and 2.8 for volume for hemispherical charges.

Half-buried spherical charges exhibited an apparent cratering effectiveness of about 35 pounds of rock per pound of TNT; surface hemispherical charges exhibited an apparent cratering effectiveness of about 25 pounds of rock per pound of TNT. The shock resulting from a spherical charge fractured, loosened, and in someway influenced about 85 pounds of rock per pound of TNT to form the region defined by the excavated crater; the shock resulting from a hemispherical charge fractured, loosened, and in someway influenced about 65 pounds of rock per pound of TNT to form the region defined by the excavated crater.

The relative distribution of ejected material on the rock surface adjacent to the crater formed by the 16,000-pound half-buried charge differed significantly from the relative distribution of ejected material observed for the crater formed by a 16,000-pound hemispherical charge resting on the rock surface. There appears to be a definite tendency for ejecta resulting from the hemispherical charge to be deposited over a larger area relative to the crater than the area over which the material was deposited for the half-buried spherical charge.

Upward displacements of the rock surface adjacent to the crater were comparable for craters formed by both the half-buried spherical and the surface hemispherical charges. Maximum upward displacements on the order of 0.8 foot were observed for craters formed by 16,000-pound charges of both types. Maximum upthrust resulting from 4000-pound charges was about half of that resulting from 16,000-pound charges.

c. Coupling

The apparent crater formed by the fully buried, 4000-pound spherical charge exhibited a radius that was 2.5 times as great, a depth that was 2.5 times as great, and a volume that was more than 10 times as great as the equivalent dimensions and volume for an apparent crater formed by the unburied, surface-tangent 4000-pound spherical charge. About the same comparative relationships hold for excavated crater dimensions.

The excavated radius and depth for the crater formed by both the fully buried and the half-buried 4000-pound spherical charges are about 40 percent

greater than similar dimensions for the apparent crater. The excavated crater volume was about three times the apparent volume. Linear dimensions for the excavated crater are approximately the same as linear dimensions of the apparent crater for the surface-tangent, 4000-pound charges.

In the near-surface region, and at the same scaled burst depth, the ratio of rock crater dimensions to soil crater dimensions is about 0.6 for radius, 0.7 for depth, and about 0.35 for volume.

The fully buried, 4000-pound spherical charge caused permanent upward displacements of the ground surface adjacent to the crater that were about twice those observed at the same distance from a half-buried, 4000-pound spherical charge and about four times those observed at the same distance for an unburied, surface-tangent, 4000-pound spherical charge.

d. Scaling

Apparent surface craters in rock formed by half-buried spherical charges exhibit the following scaling relationships:

	Deviation		Deviation
$R_a = 1.30\ W^{0.27}$	± 0.11	(Soil, $R_a = 0.70\ W^{0.38}$)	± 0.06
$D_a = 0.42\ W^{0.28}$	± 0.17	(Soil, $D_a = 0.40\ W^{0.33}$)	± 0.13
$V_a = 1.41\ W^{0.78}$	± 0.34	(Soil, $V_a = 0.22\ W^{1.09}$)	± 0.18

Excavated surface craters formed in rock by half-buried spherical charges exhibit the following scaling relationships:

	Deviation		Deviation
$R'_t = 1.74\ W^{0.28}$	± 0.09	(Soil true crater, $R_t = 1.01\ W^{0.35}$)	± 0.04
$D'_t = 0.42\ W^{0.32}$	± 0.10	(Soil true crater, $D_t = 0.92\ W^{0.27}$)	± 0.06
$V'_t = 3.52\ W^{0.80}$	± 0.24	(Soil true crater, $V_t = 0.92\ W^{1.02}$)	± 0.08

Apparent surface craters in rock formed by hemispherical charges exhibit the following scaling relationships:

	Deviation		Deviation
$R_a = 0.48\ W^{0.37}$	± 0.0001	(Soil, $R_a = 0.51\ W^{0.40}$)	± 0.02
$D_a = 0.06\ W^{0.47}$	± 0.03	(Soil, $D_a = 1.63\ W^{0.20}$)	± 0.16
$V_a = 0.04\ W^{1.14}$	± 0.03	(Soil, $V_a = 1.04\ W^{0.96}$)	± 0.13

The ratio dimensions for craters in rock to crater dimensions in soil is not a constant. Within the charge weight range of 1000 to 40,000 pounds, the ratio of apparent radius of rock craters to apparent radius of soil craters decreases from 0.9 to 0.7. For apparent depth, this ratio decreases from 0.8 to 0.6, and for apparent volume it decreases from 0.8 to 0.3.

The erratic nature of the distribution of ejecta resulting from craters in rock and the limited upthrust data obtained from this experiment prohibit the determination of meaningful scaling relationships for ejecta thickness and upthrust.

Fifty percent of the ejected material was deposited between the crater edge and 1.7 crater radii for the H1 shot. This 50 percent distance was 2.0 crater radii for the H2 crater, 1.2 crater radii for the LS crater, and 1.9 crater radii for the S4a crater.

2. Recommendations

The following suggestions are made for future cratering experiments in hard rock:

Ejecta should be sampled continuously along concentric rings rather than along radials. Resulting data would be similar to that obtained from the missile survey. Ejecta data of this type are far more meaningful and useful than the erratic data obtained by sampling along arbitrarily selected radials.

The number of upthrust measurements should be greatly increased on any future cratering experiments in hard rock. Again, it is suggested that permanent ground motions be measured continuously along concentric circles. Permanent ground motion stations should be designed to provide both vertical and horizontal data. A combination of this and the above suggestion applied to craters formed by differing charge weights should result in sufficient data for which meaningful scaling relationships can be developed.

An additional five-shot and six-shot successive series of 4000-pound charges should be fired at the MTCE test site to provide data on the enhancement or lack of enhancement of the excavated crater after the third shot.

APPENDIX I

CRATER PHOTOGRAPHS, PROFILES, AND TOPOGRAPHIC MAPS

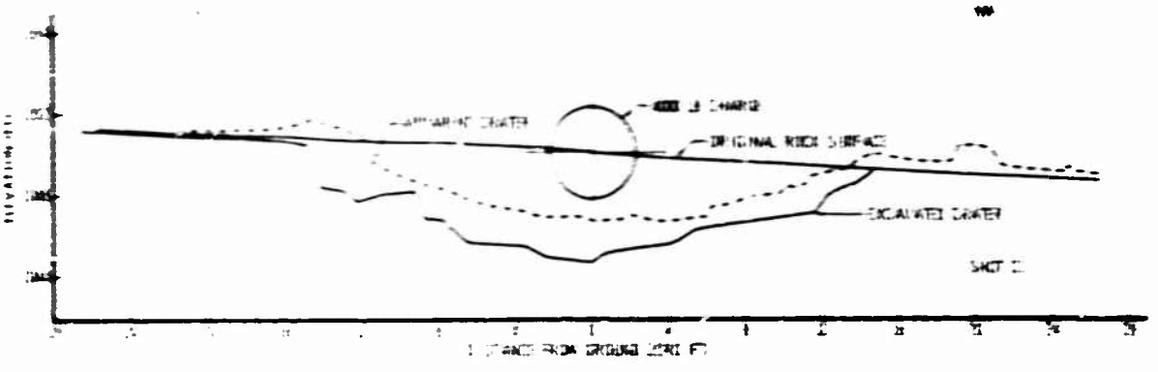

Figure C-1. Photograph and Profile of Crater S1(D).

COMPILED BY
AMERICAN AERIAL SURVEYS, INC.
564 S. STEWART DR.
COVINA, CALIFORNIA

CONTOUR INTERVAL 0.2'

Figure I-2. Topographic Map of Crater S1(C1).

COMPILED BY
AMERICAN AERIAL SURVEYS, INC.
564 S. STEWART DR.
COVINA, CALIFORNIA

CONTOUR INTERVAL 0.2'

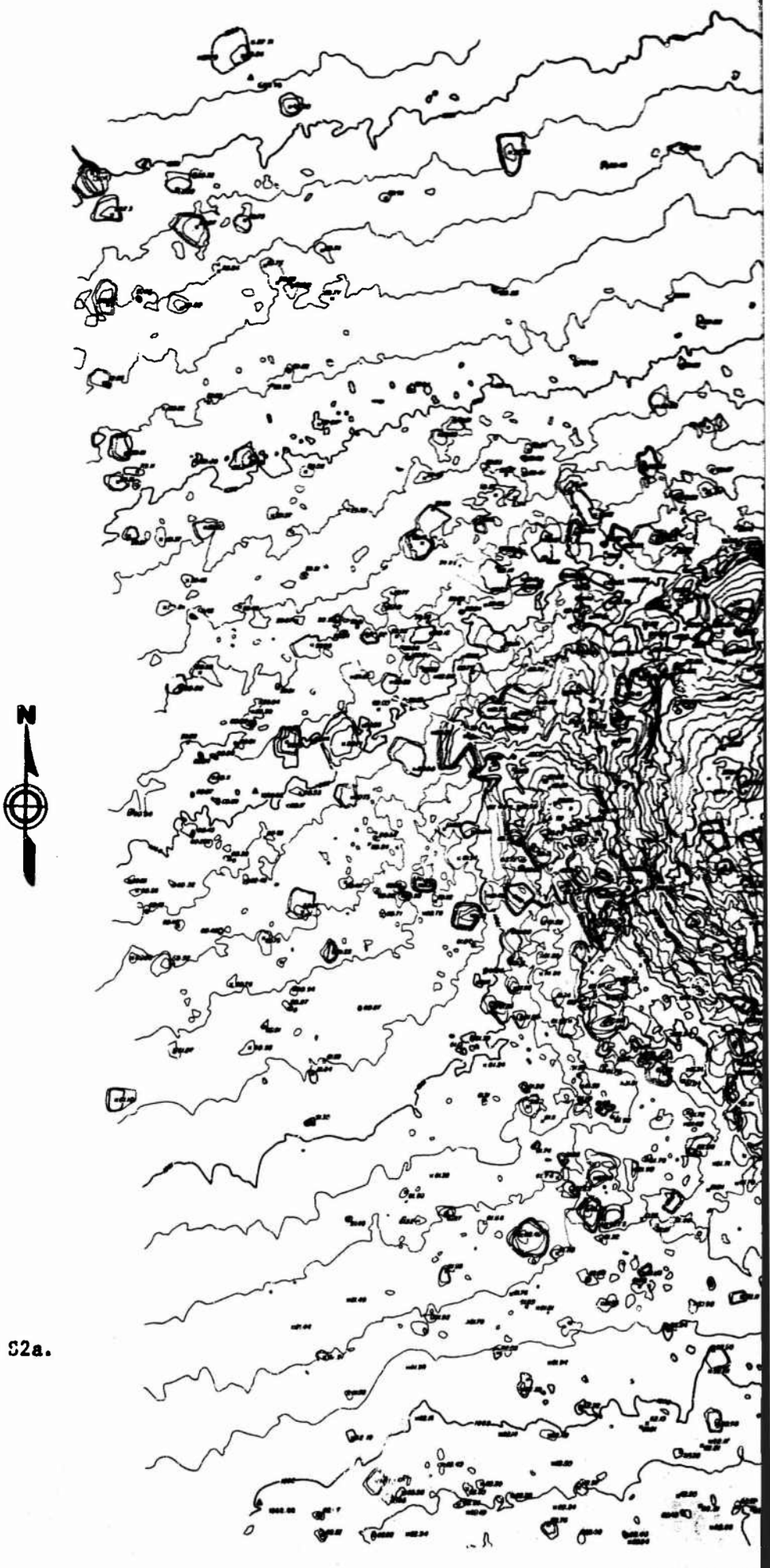

Figure I-3. Topographic Map of Crater S2a.

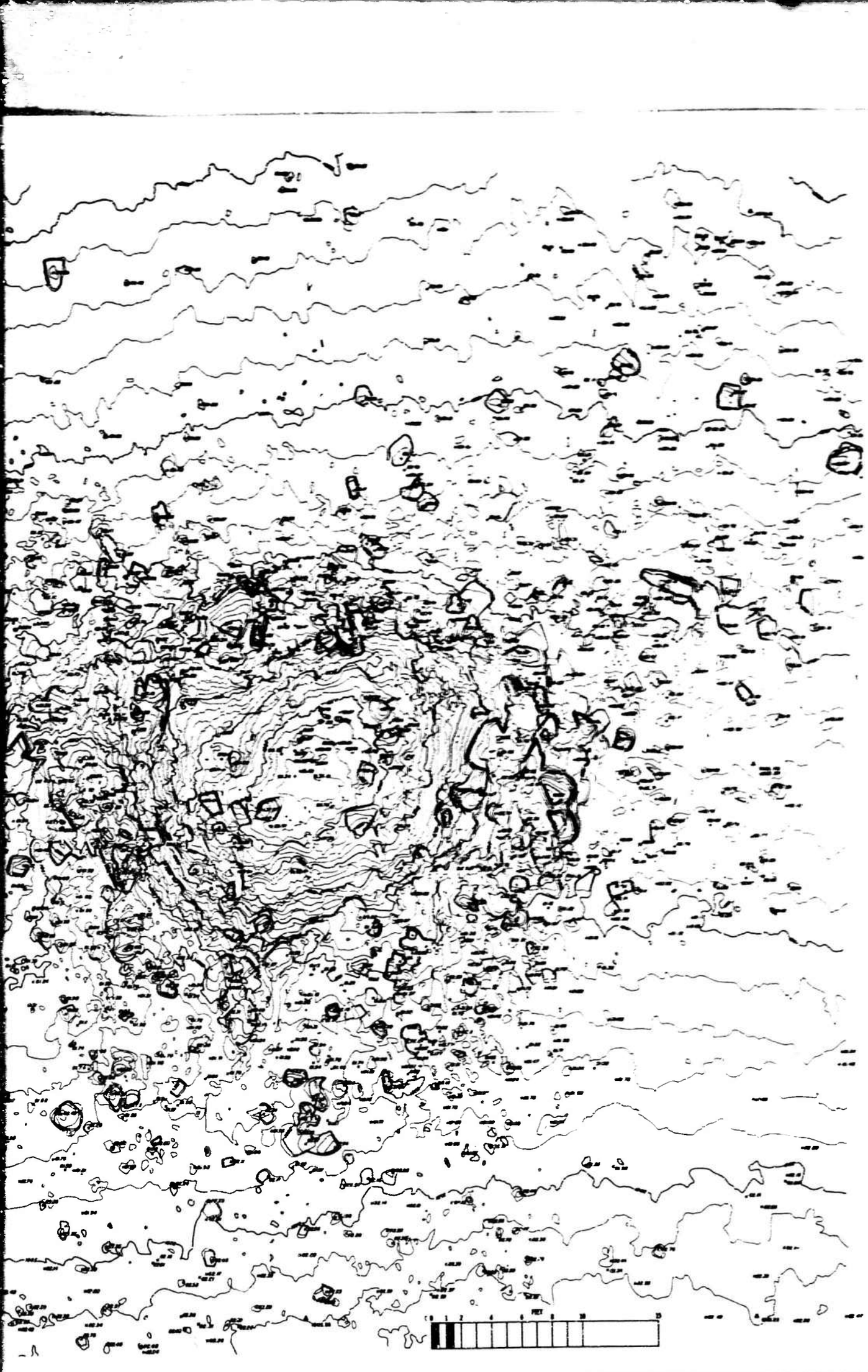

2

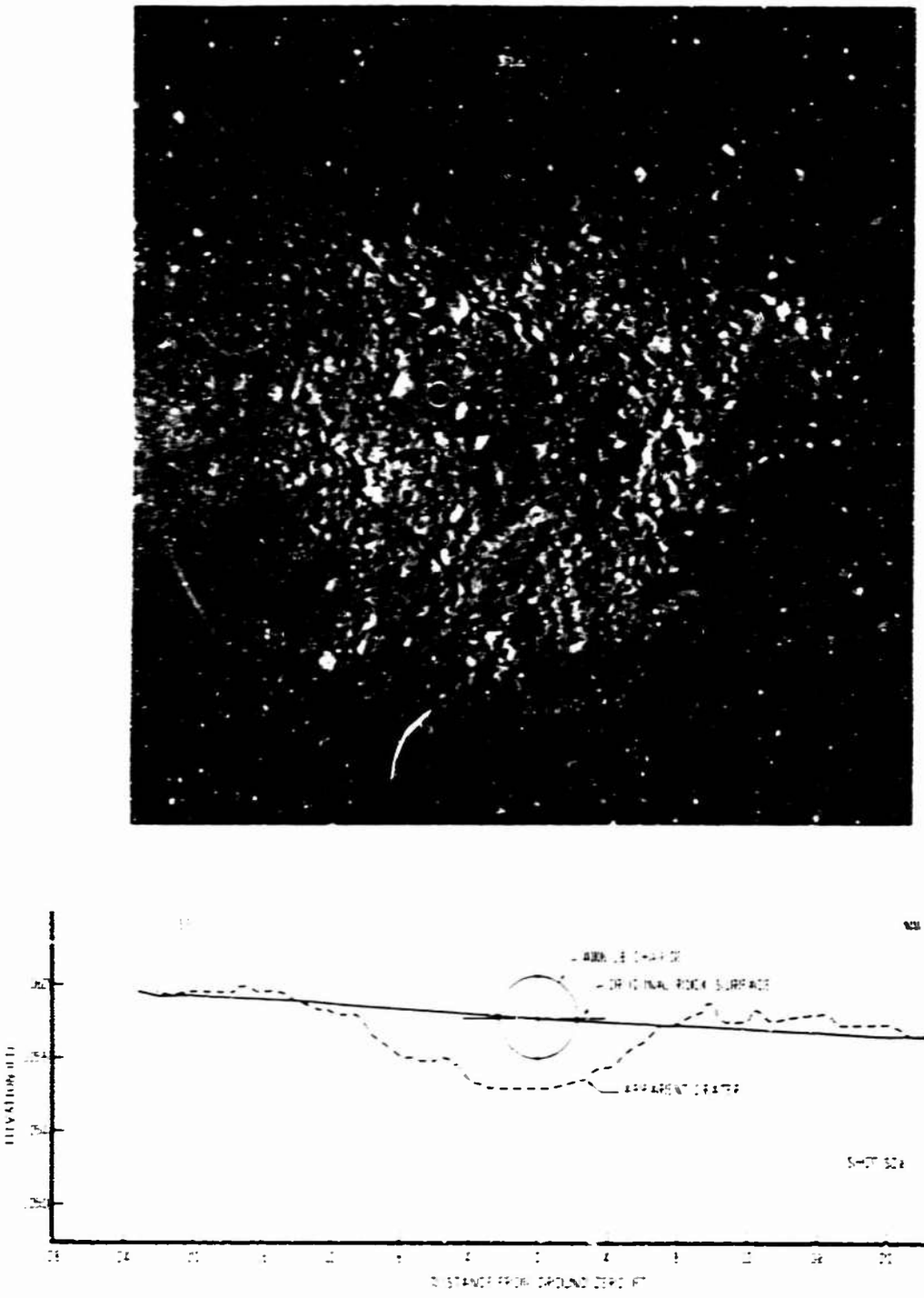

Figure I-4. Photograph and Profile of Crater S2a.

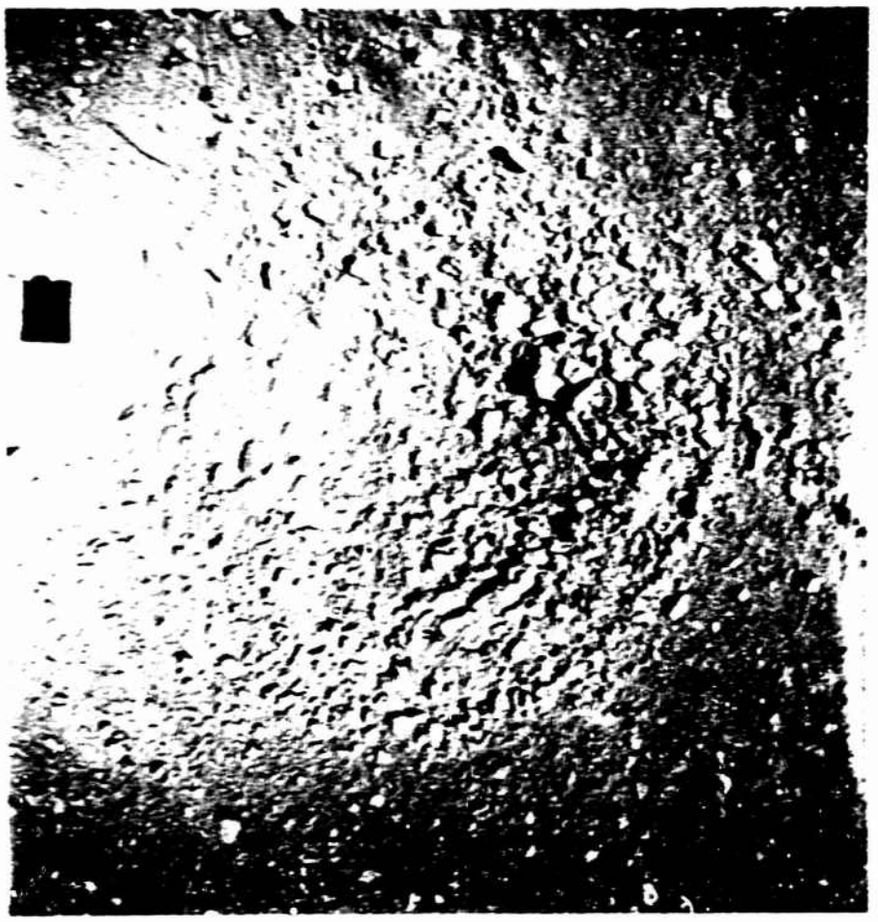

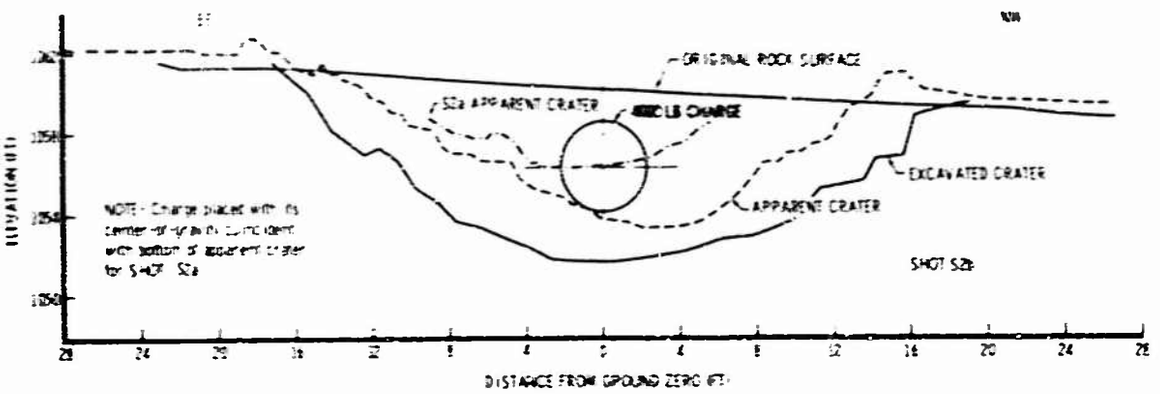

Figure I-5. Photograph and Profile of Crater S2b.

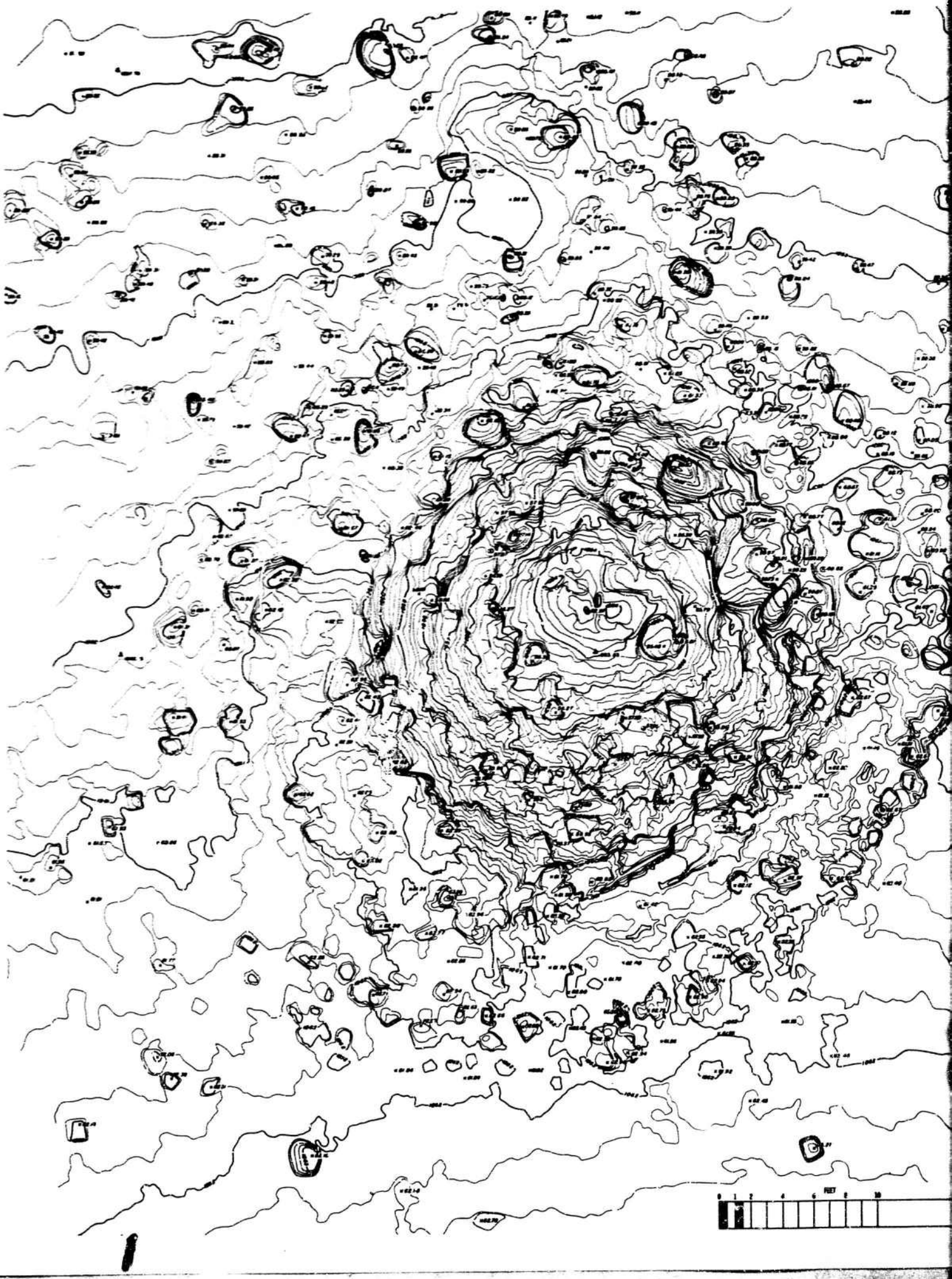

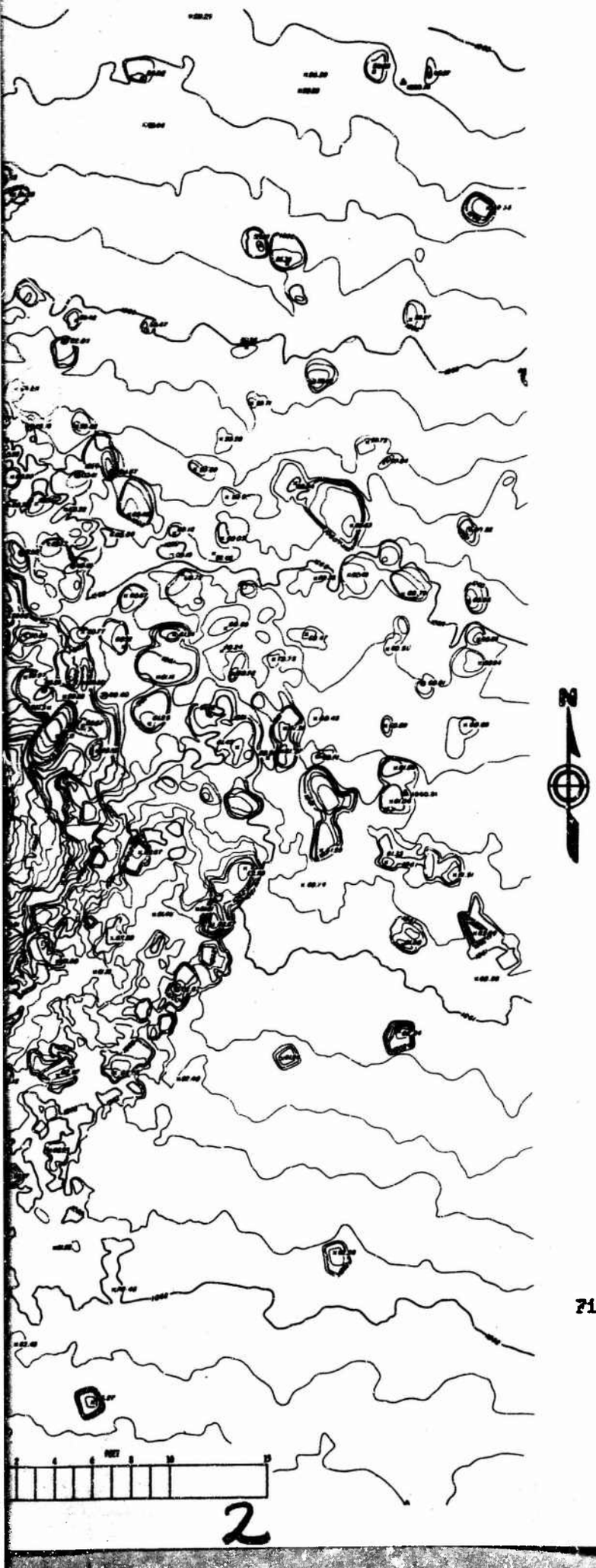

COMPILED BY
AMERICAN AERIAL SURVEYS, INC.
564 S. STEWART DR.
COVINA, CALIFORNIA

CONTOUR INTERVAL 0.2'

Figure I-6. Topographic Map of Crater S2b.

COMPILED BY
AMERICAN AERIAL SURVEYS, INC.
564 S. STEWART DR.
COVINA, CALIFORNIA

CONTOUR INTERVAL 0.2'

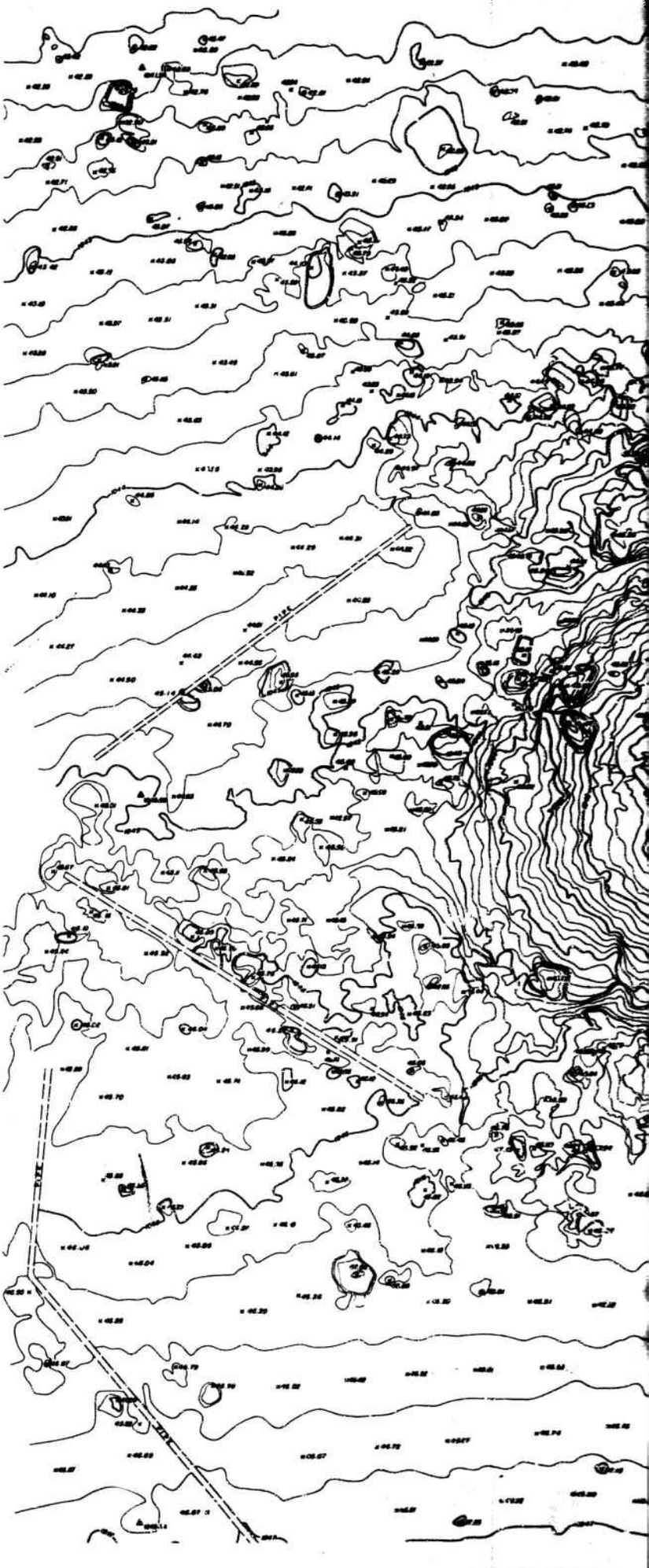

Figure I-7. Topographic Map of Crater S3a.

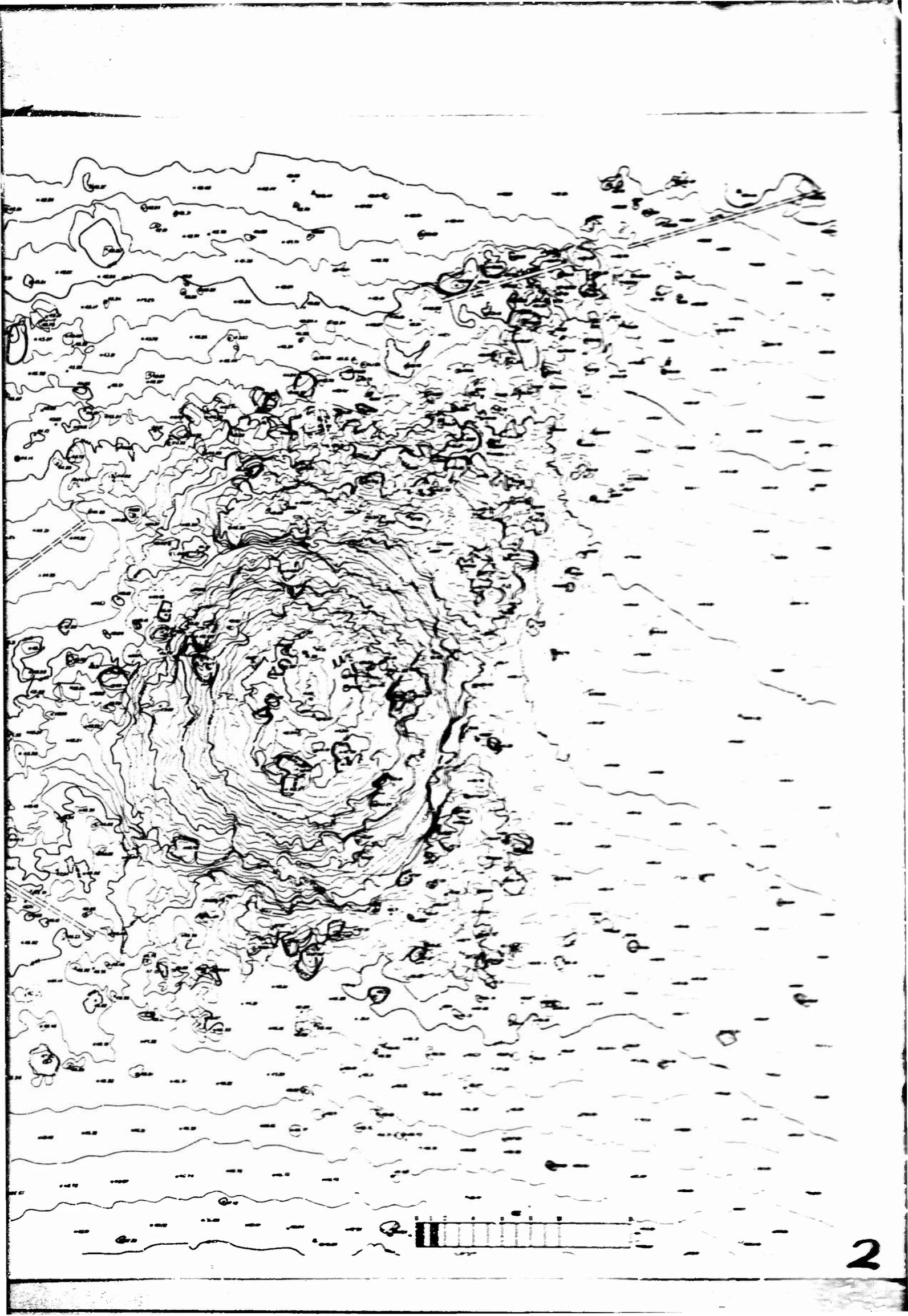

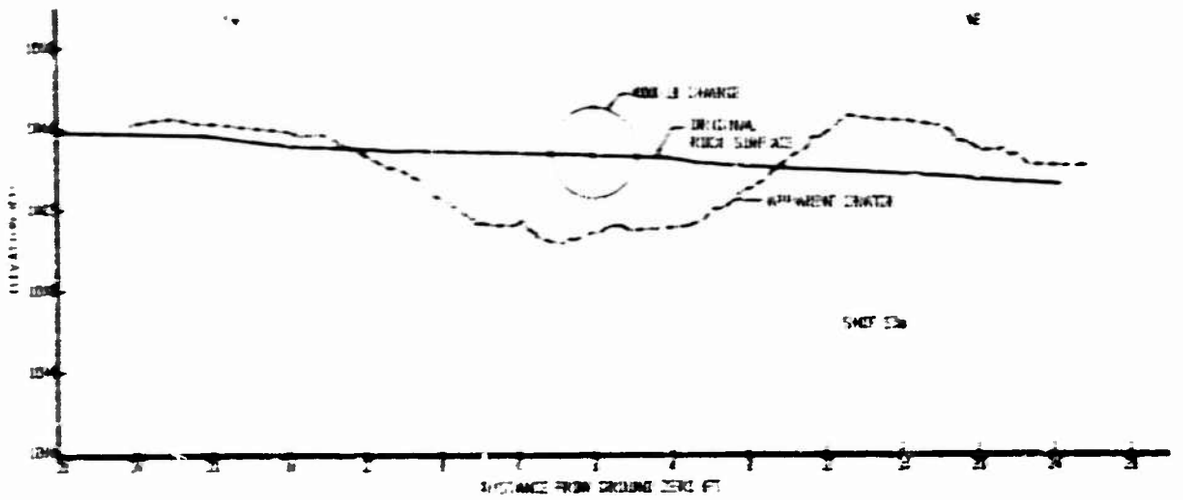

Figure D-1. Photograph and Profile of Crater 5Ba.

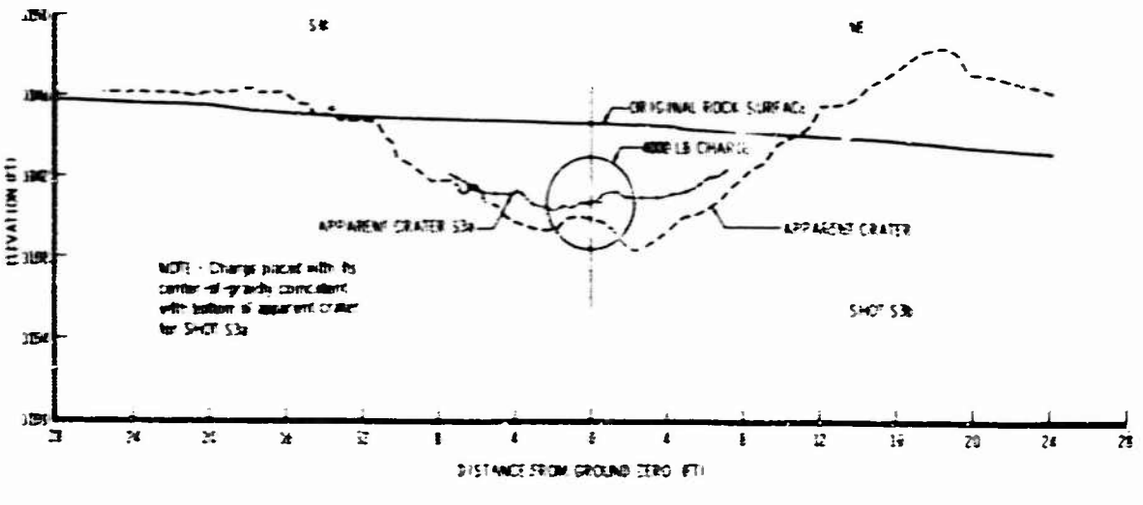

Figure 1-9. Photograph and Profile of Crater S3b.

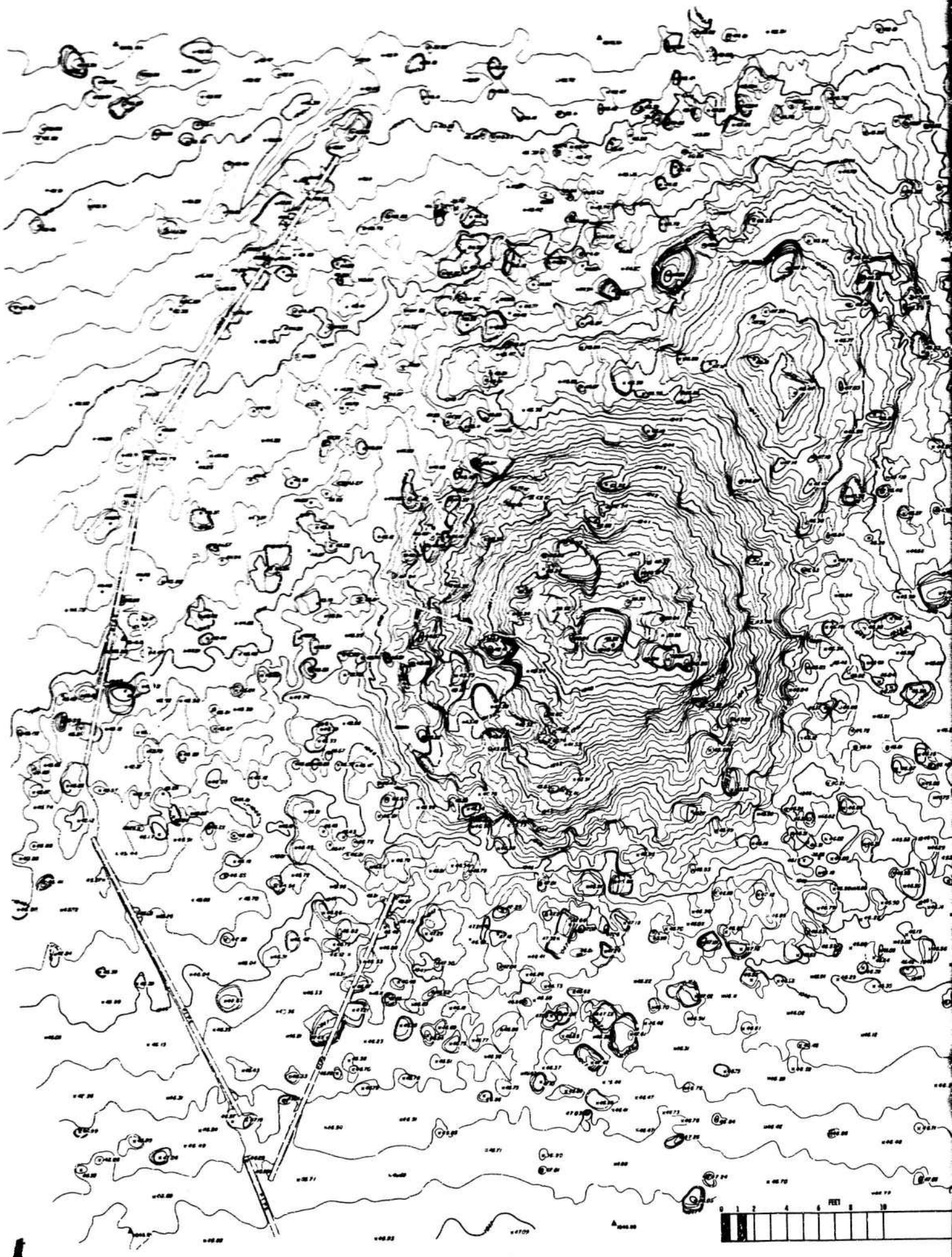
FEET
0 1 2 4 6 8 10

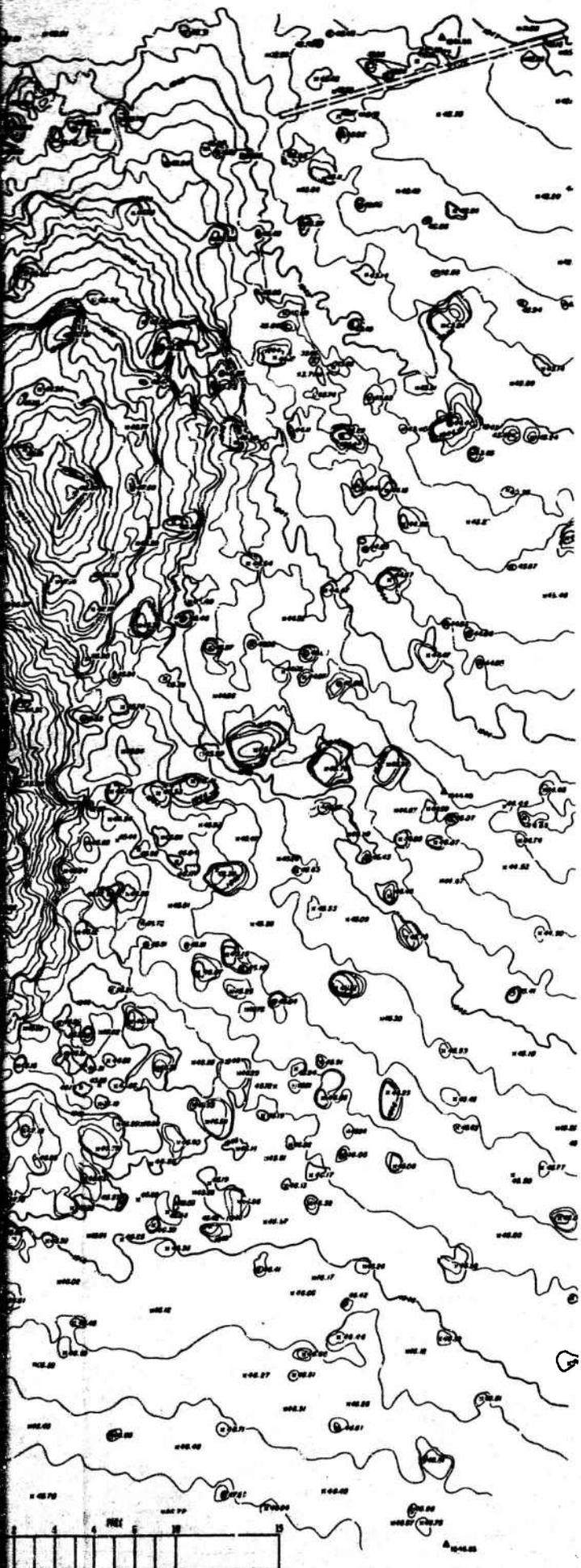

COMPILED BY
AMERICAN AERIAL SURVEYS, INC.
564 S. STEWART DR.
COVINA, CALIFORNIA

CONTOUR INTERVAL 0.2'

Figure I-10. Topographic Map of Crater S3b.

2

COMPILED BY
AMERICAN AERIAL SURVEYS, INC.
564 S. STEWART DR.
COVINA, CALIFORNIA

CONTOUR INTERVAL 0.2'

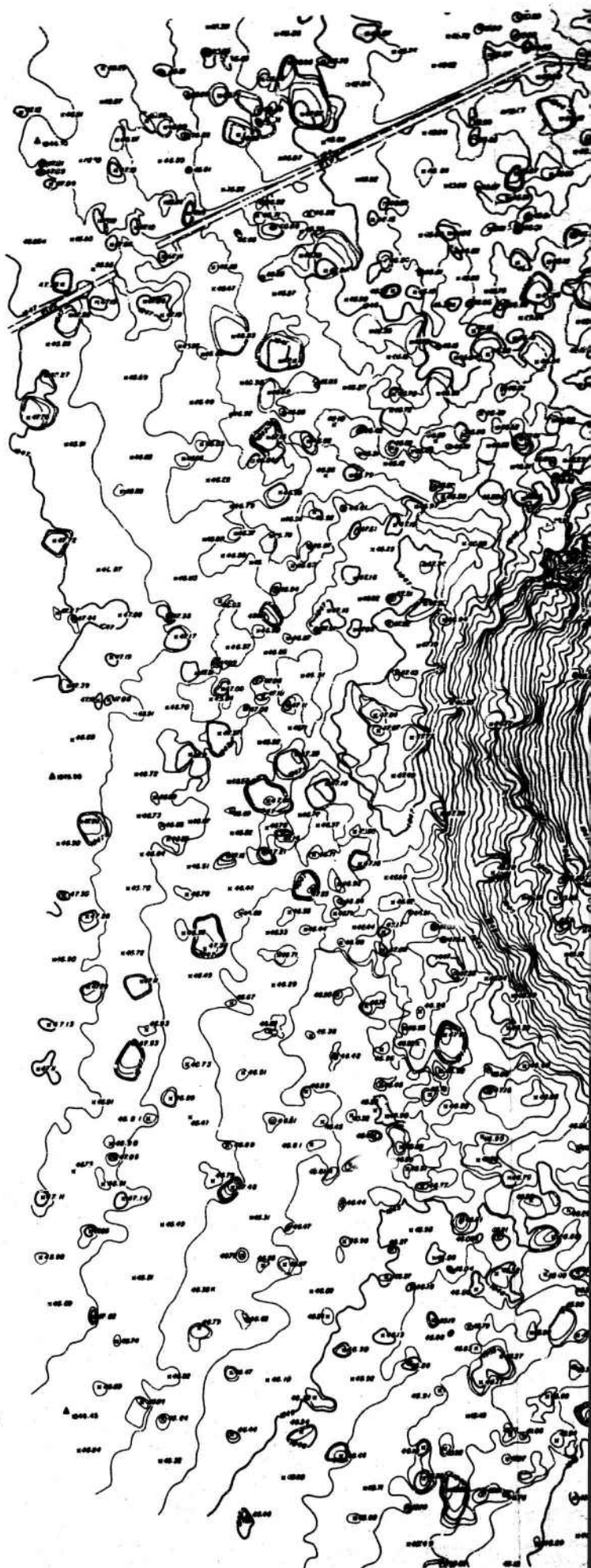

Figure I-11. Topographic Map of Crater S3c.

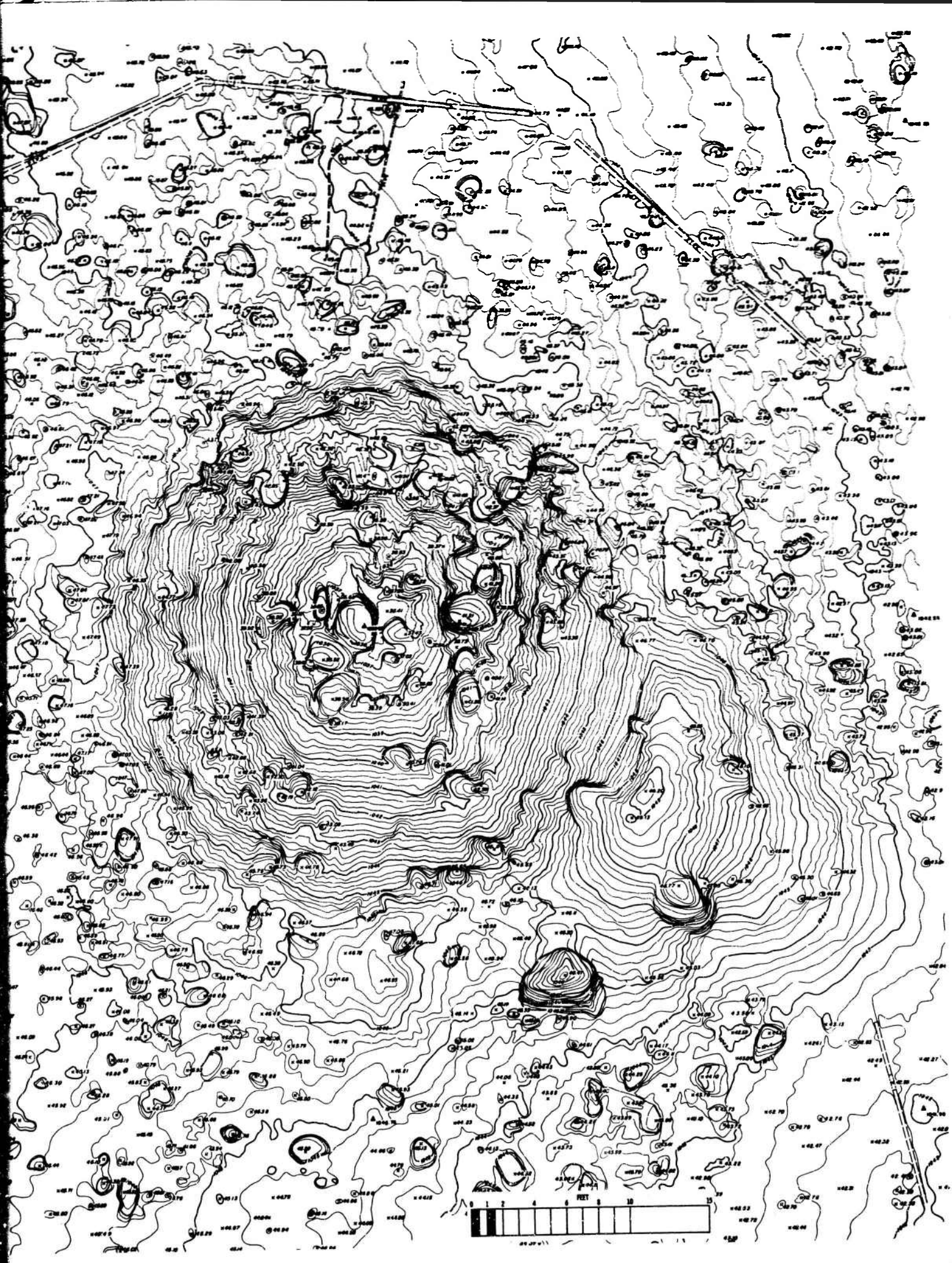
0 1 2 4 6 8 10 15
FEET

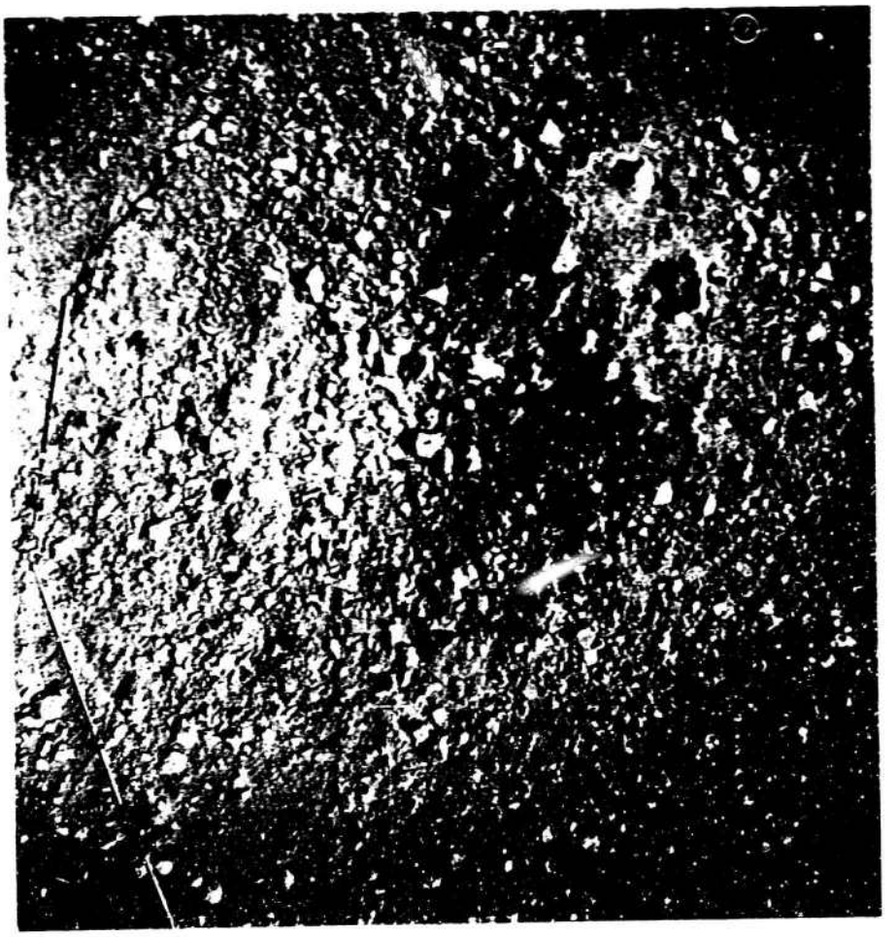

SW NE

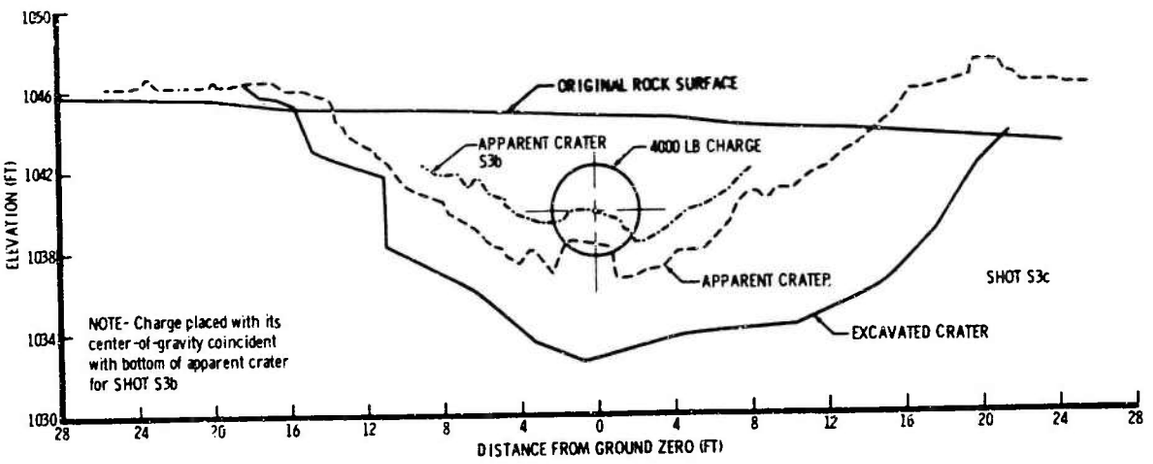

Figure I-12. Photograph and Profile of Crater S3c.

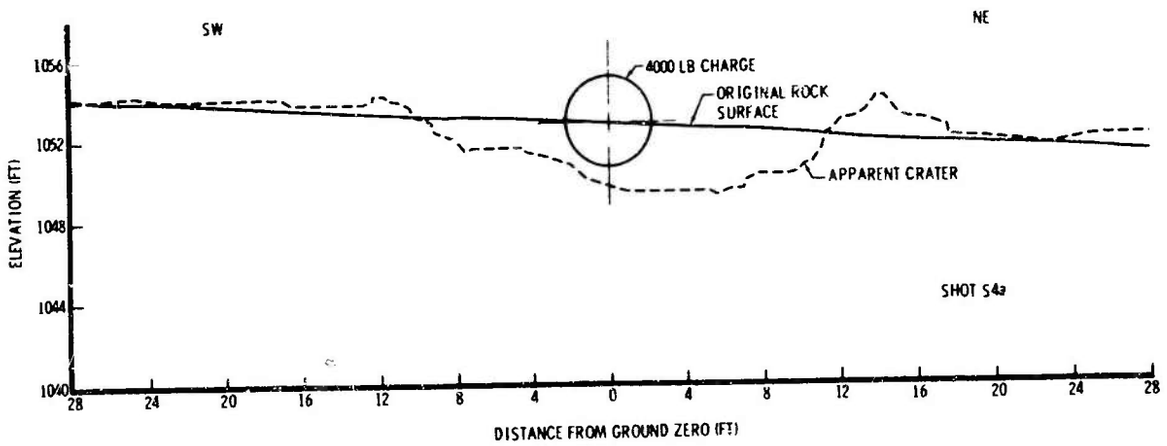

Figure I-13. Photograph and Profile of Crater S4a.

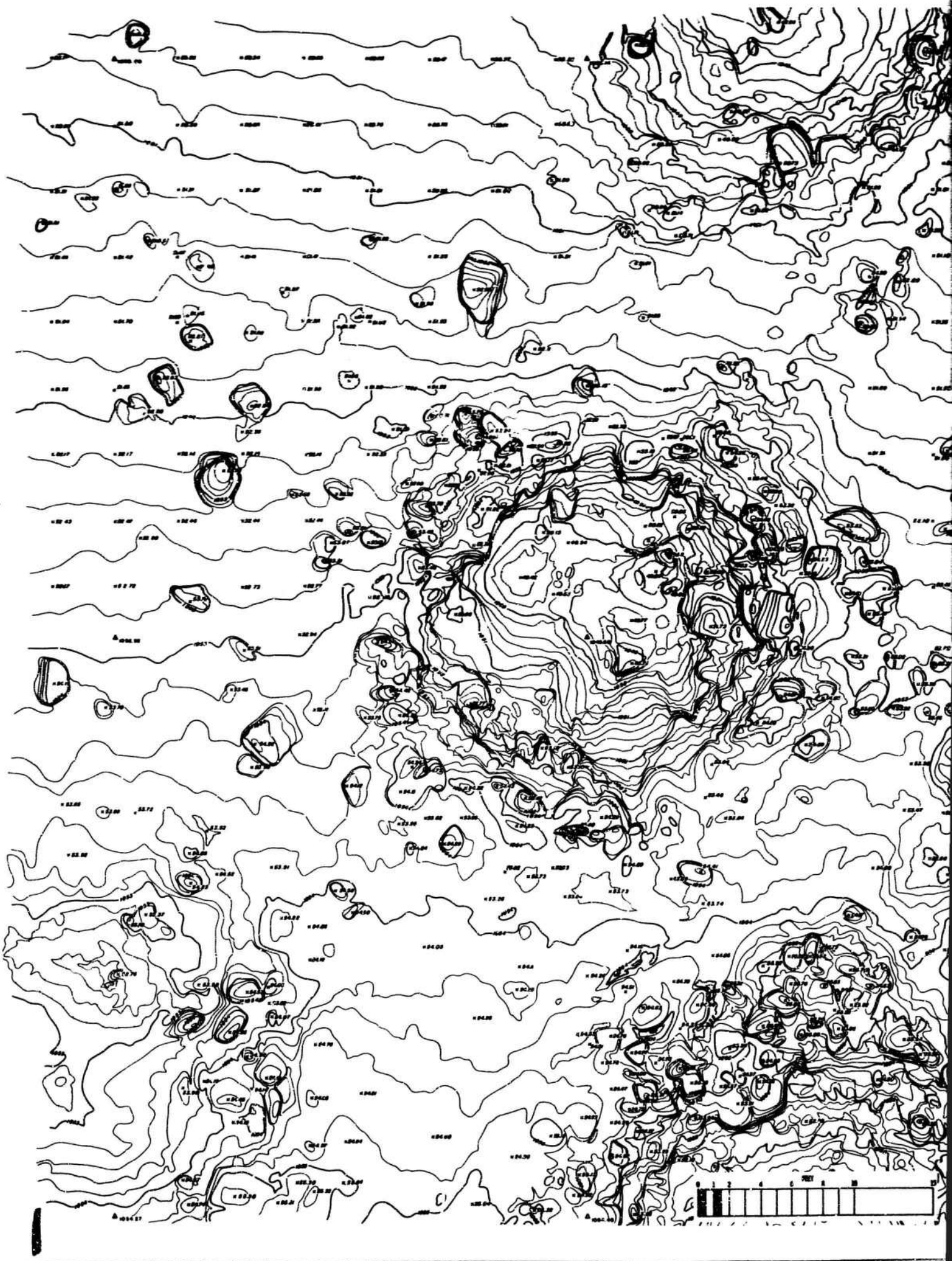

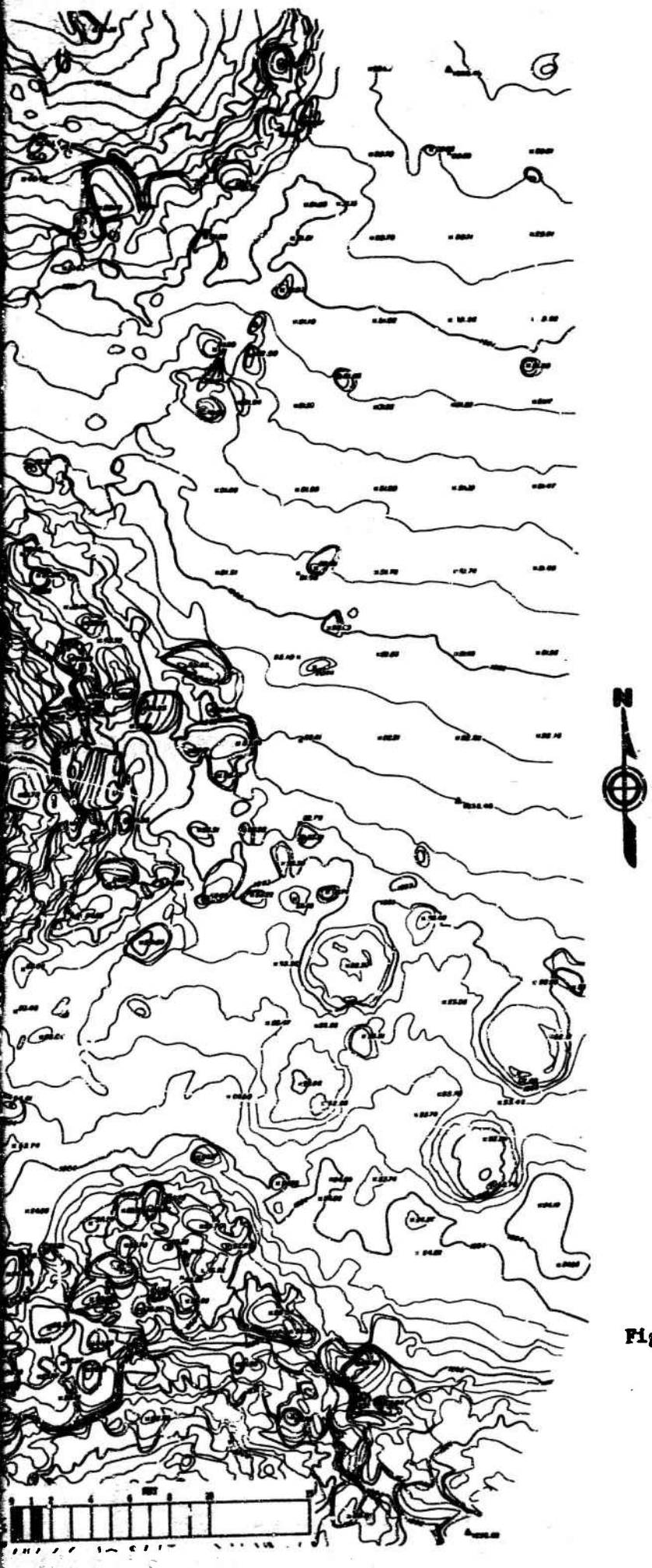

COMPILED BY
AMERICAN AERIAL SURVEYS, INC.
564 S. STEWART DR.
COVINA, CALIFORNIA

CONTOUR INTERVAL 0.2'

Figure I-14. Topographic Map of Crater S4a.

2

COMPILED BY
AMERICAN AERIAL SURVEYS, INC.
564 S. STEWART DR.
COVINA, CALIFORNIA

CONTOUR INTERVAL 0.2'

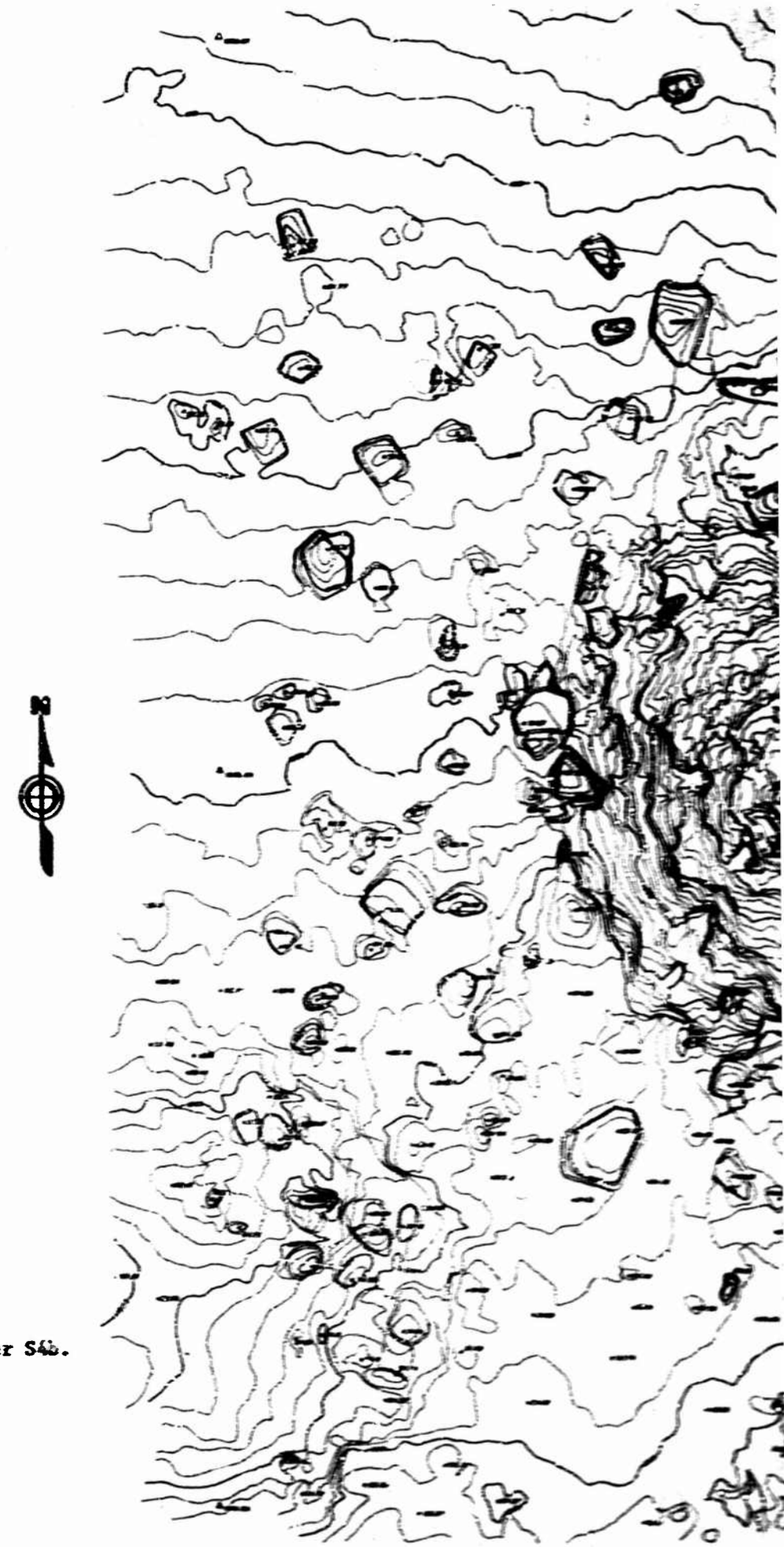

Figure I-15. Topographic Map of Crater S4b.

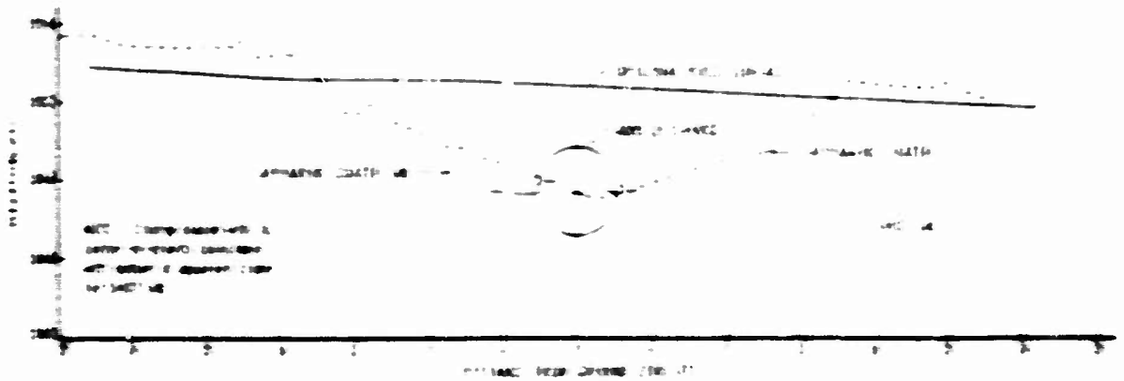

COMPILED BY
AMERICAN AERIAL SURVEYS, INC.
564 S. STEWART DR.
COVINA, CALIFORNIA

CONTOUR INTERVAL 0.2'

Figure I-18. Topographic Map of Crater Sec.

2

COMPILED BY
AMERICAN AERIAL SURVEYS, INC.
564 S. STEWART DR.
COVINA, CALIFORNIA

CONTOUR INTERVAL 0.2'

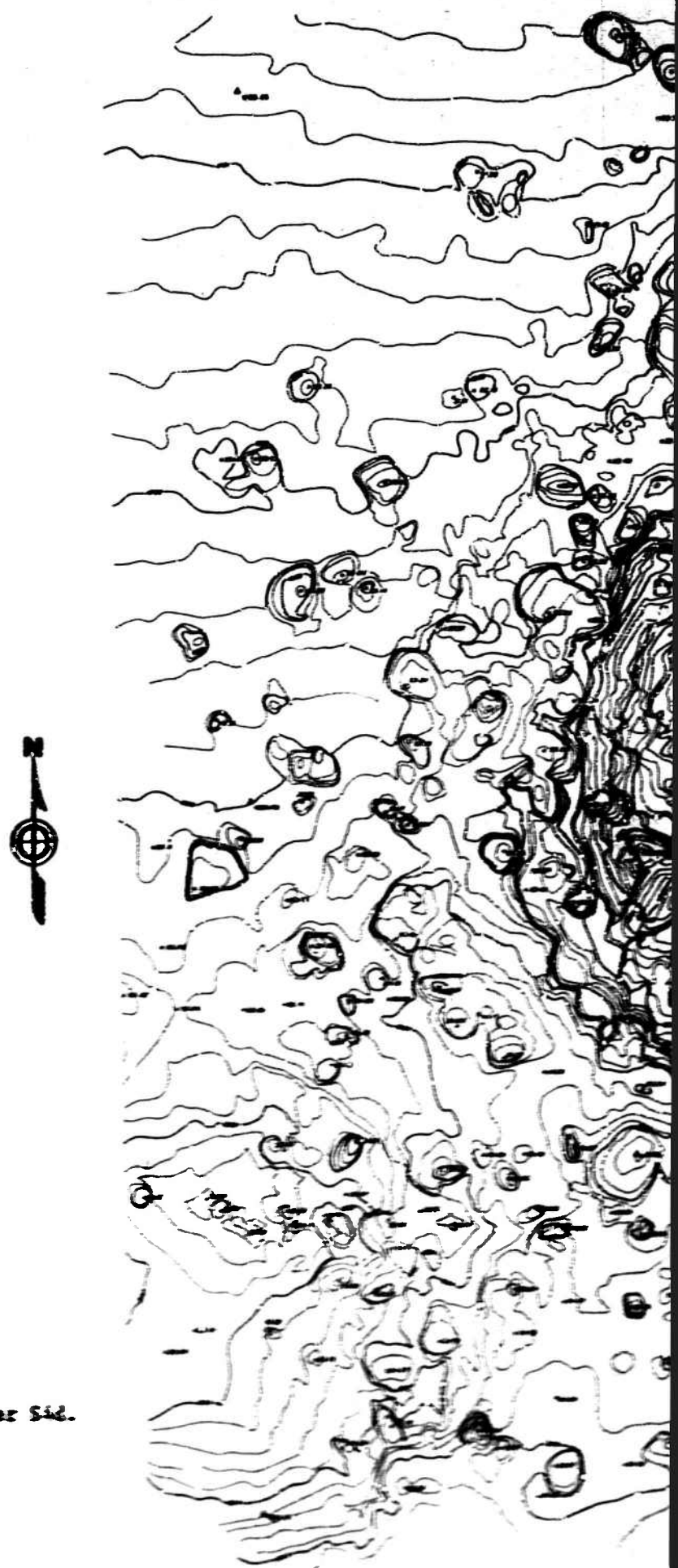

Figure I-19. Topographic Map of Crater Sid.

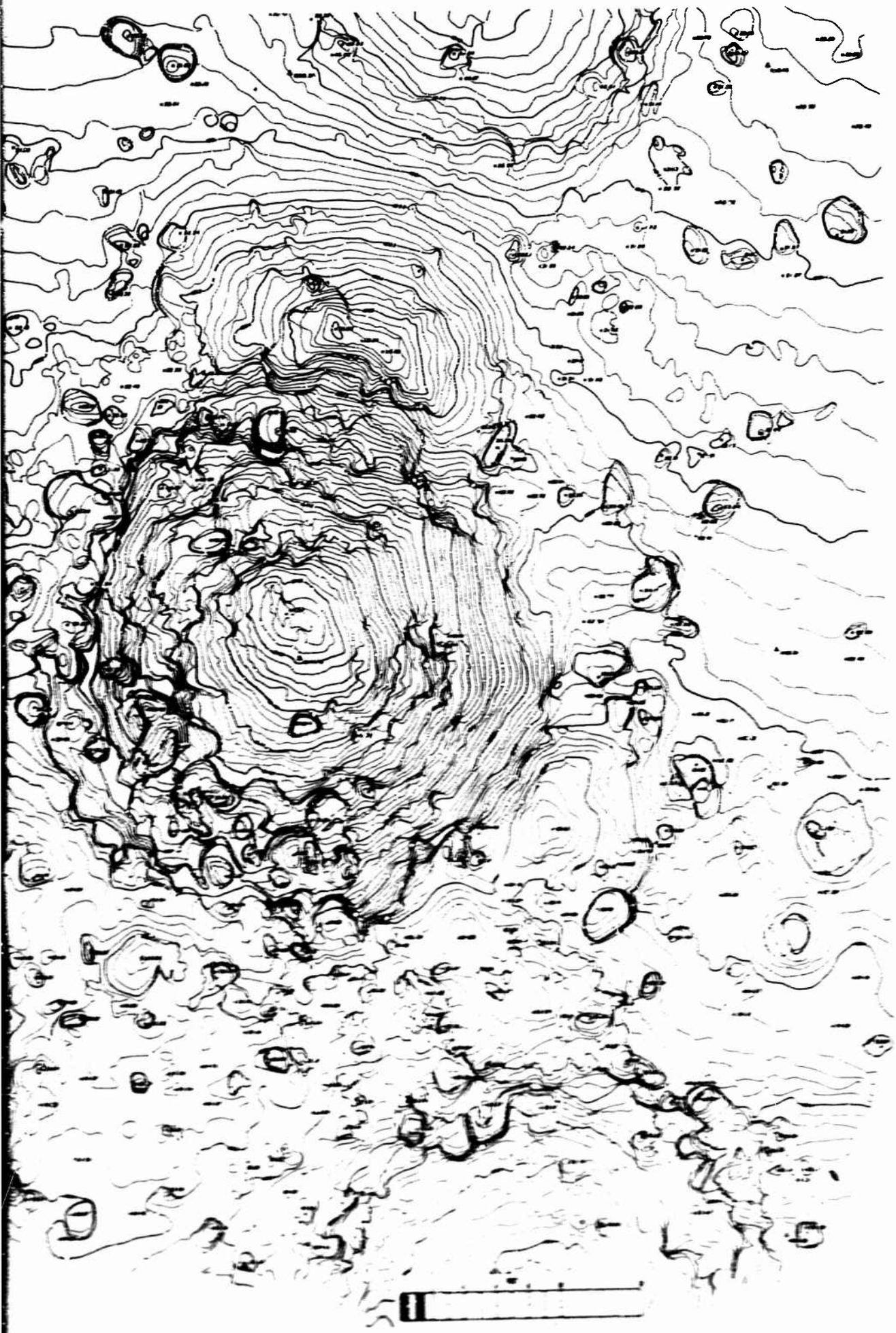

2

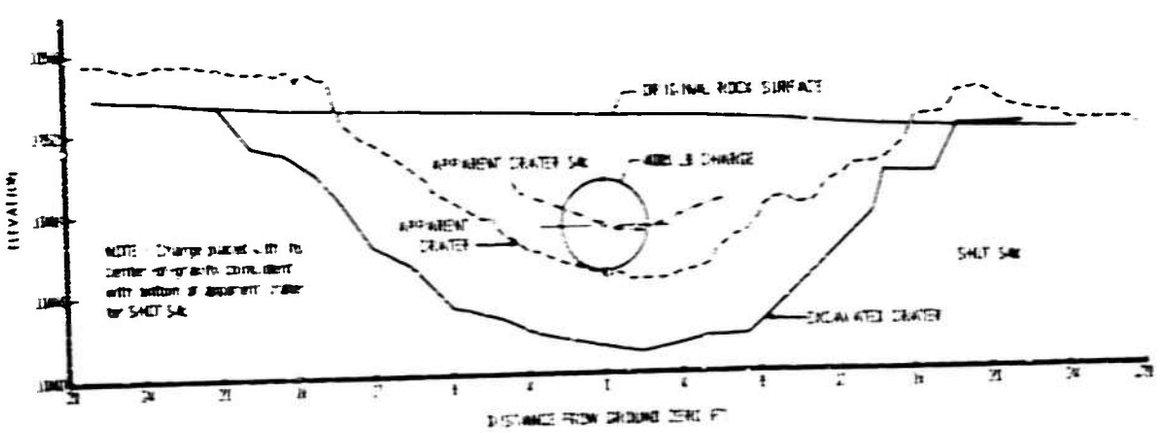

Figure I-20. Photograph and Profile of Crater 548.

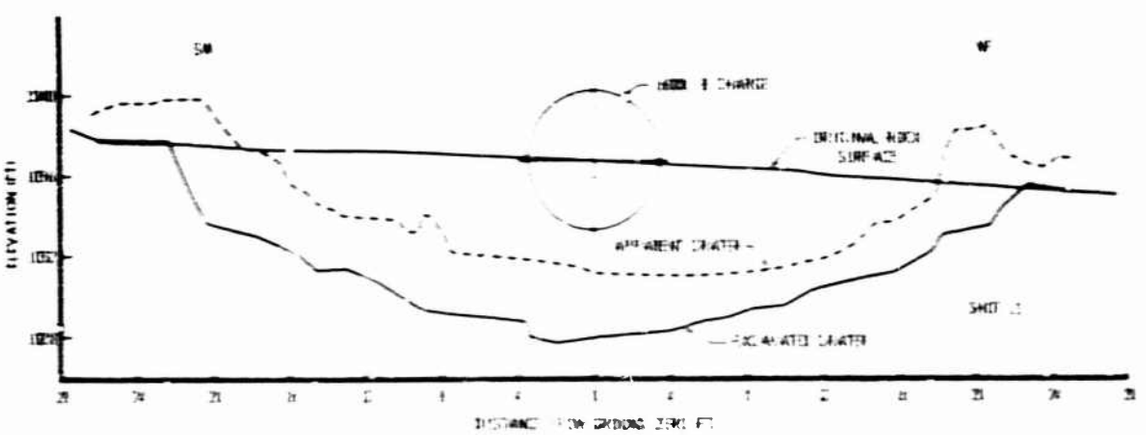

Figure 2-21. Photograph and Profile of Crater 2.

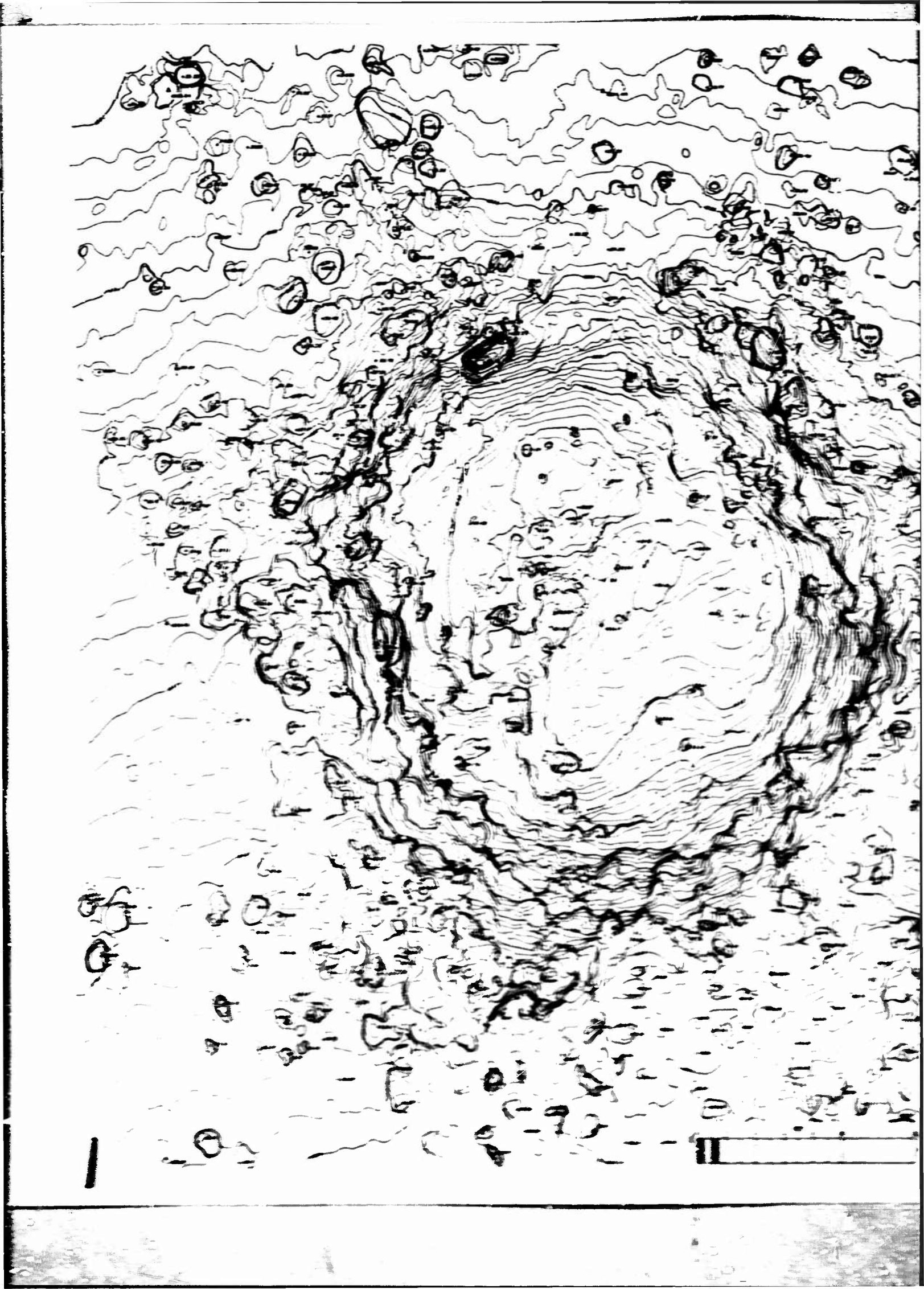

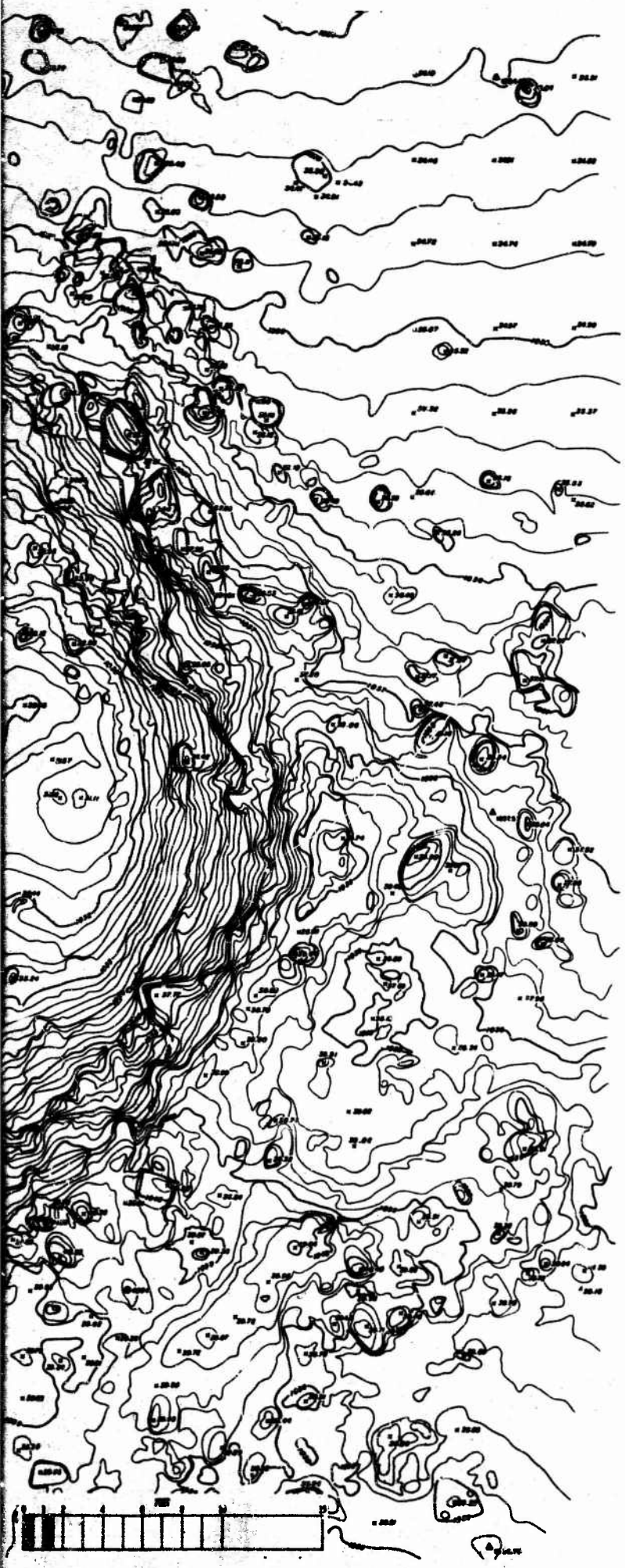

COMPILED BY
AMERICAN AERIAL SURVEYS, INC.
564 S. STEWART DR.
COVINA, CALIFORNIA

CONTOUR INTERVAL 0.2'

N

Figure I-22. Topographic Map of Crater LS.

2

COMPILED BY
AMERICAN AERIAL SURVEYS, INC.
564 S. STEWART DR.
COVINA, CALIFORNIA

CONTOUR INTERVAL 0.2'

Figure I-23. Topographic Map of Crater H2.

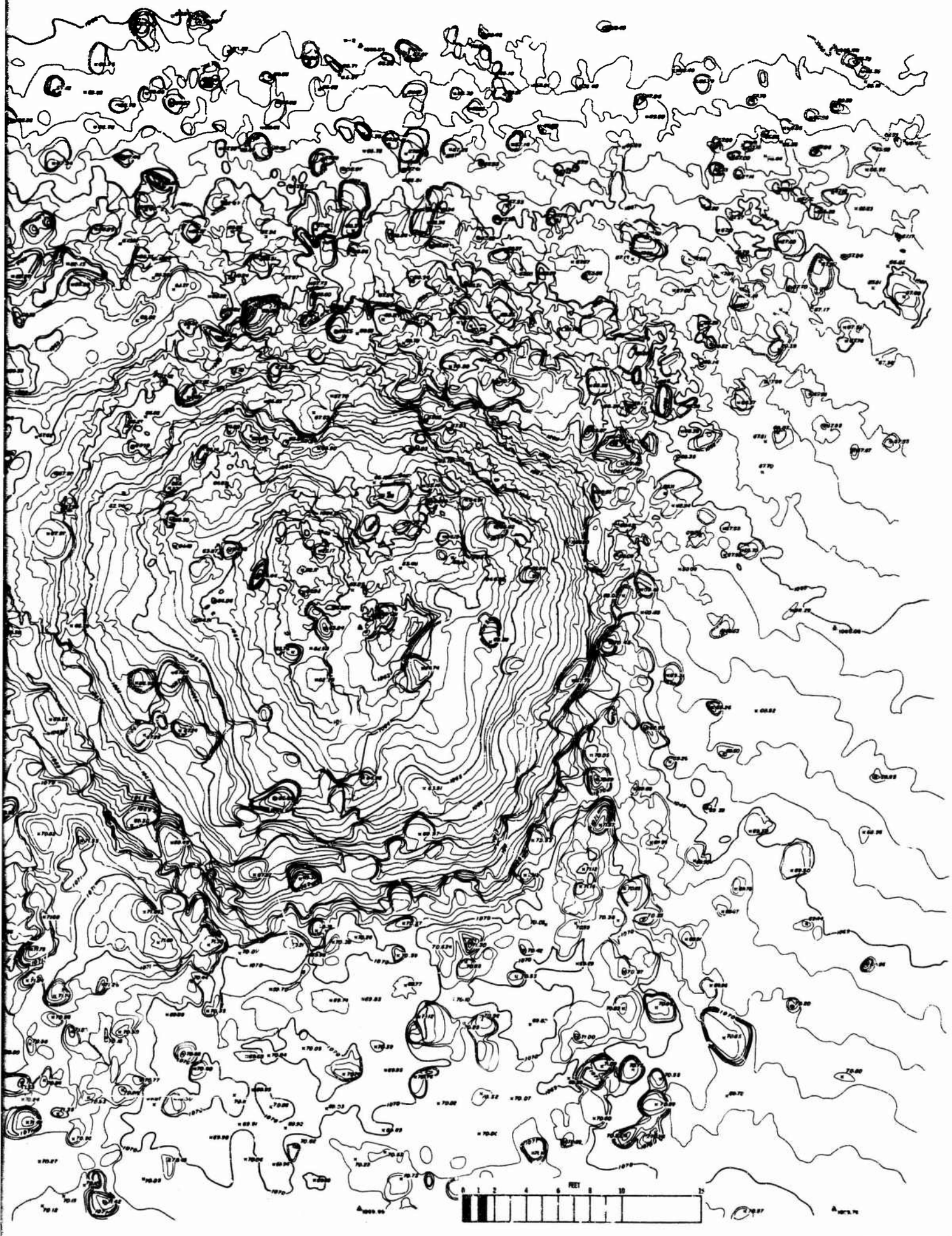
FEET

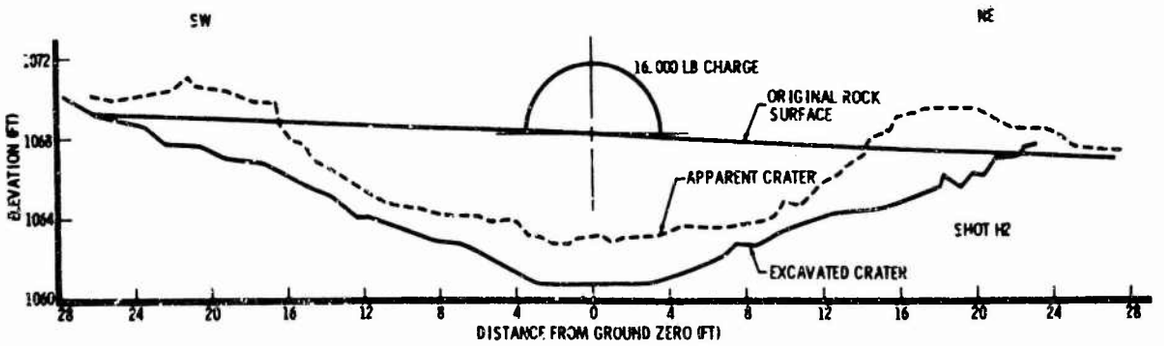

Figure I-24. Photograph and Profile of Crater H2.

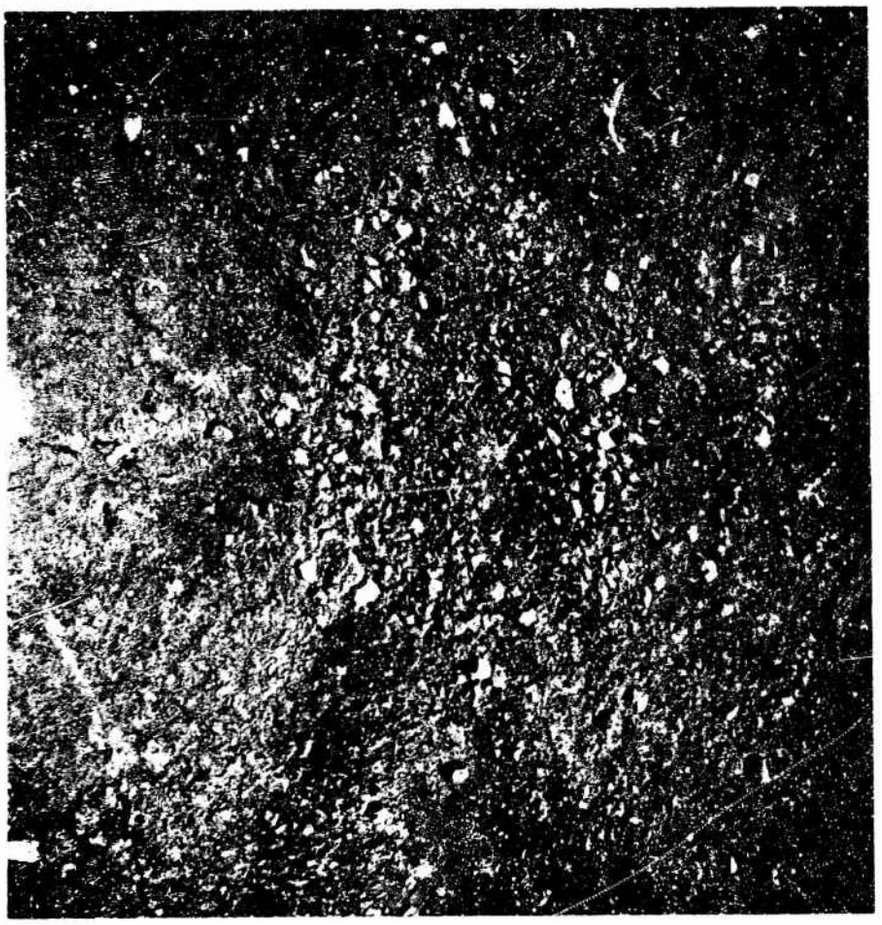

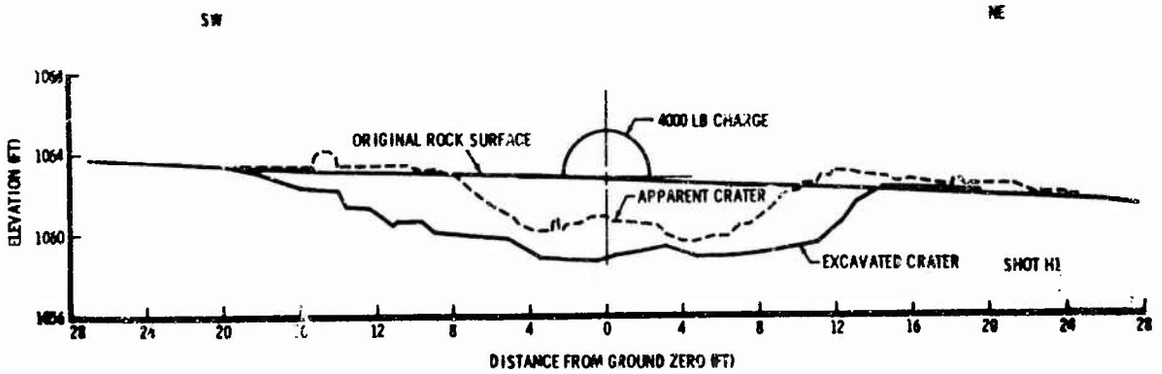

Figure I-25. Photograph and Profile of Crater H1.

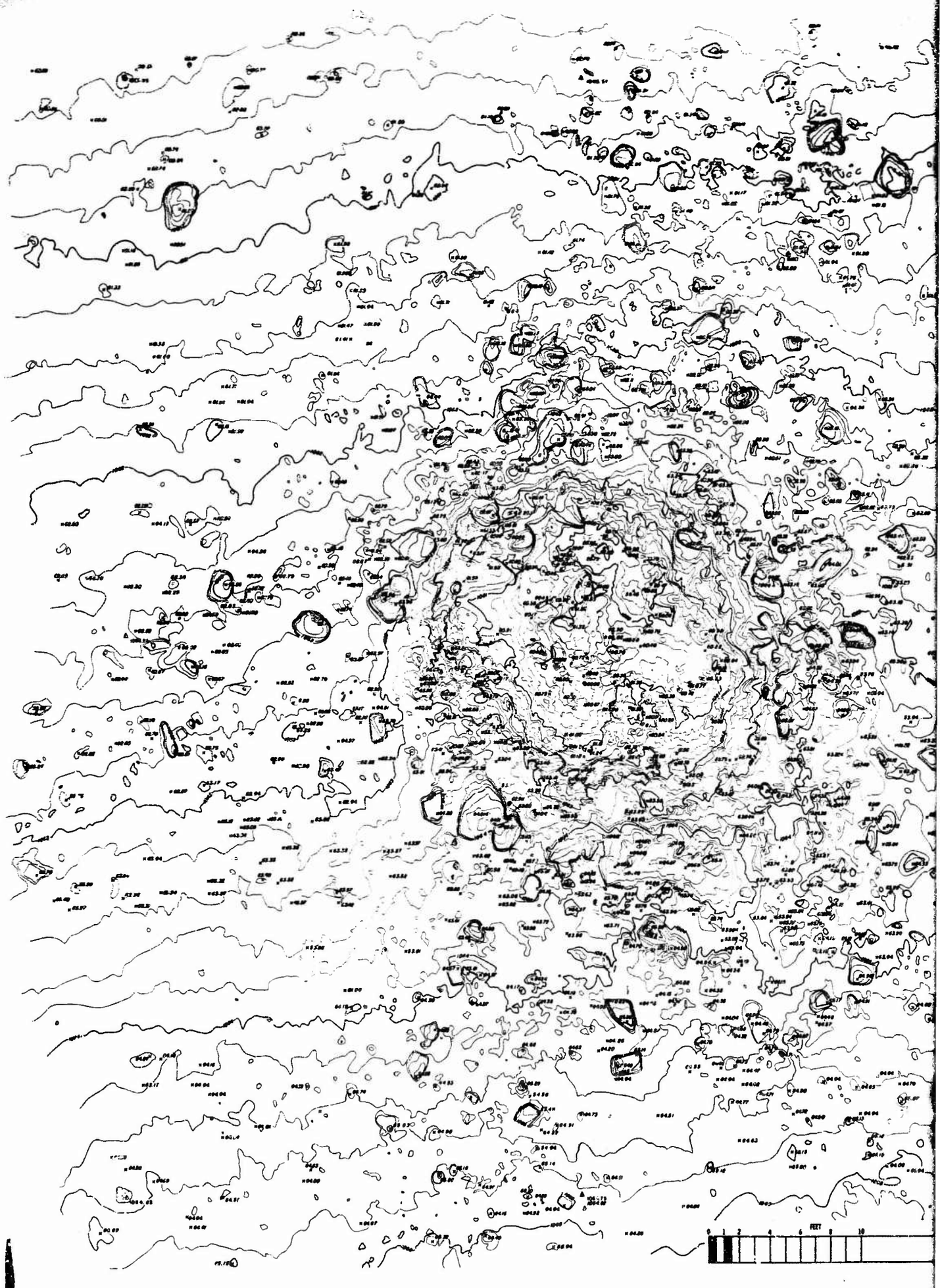
0 1 2 4 6 8 10
FEET

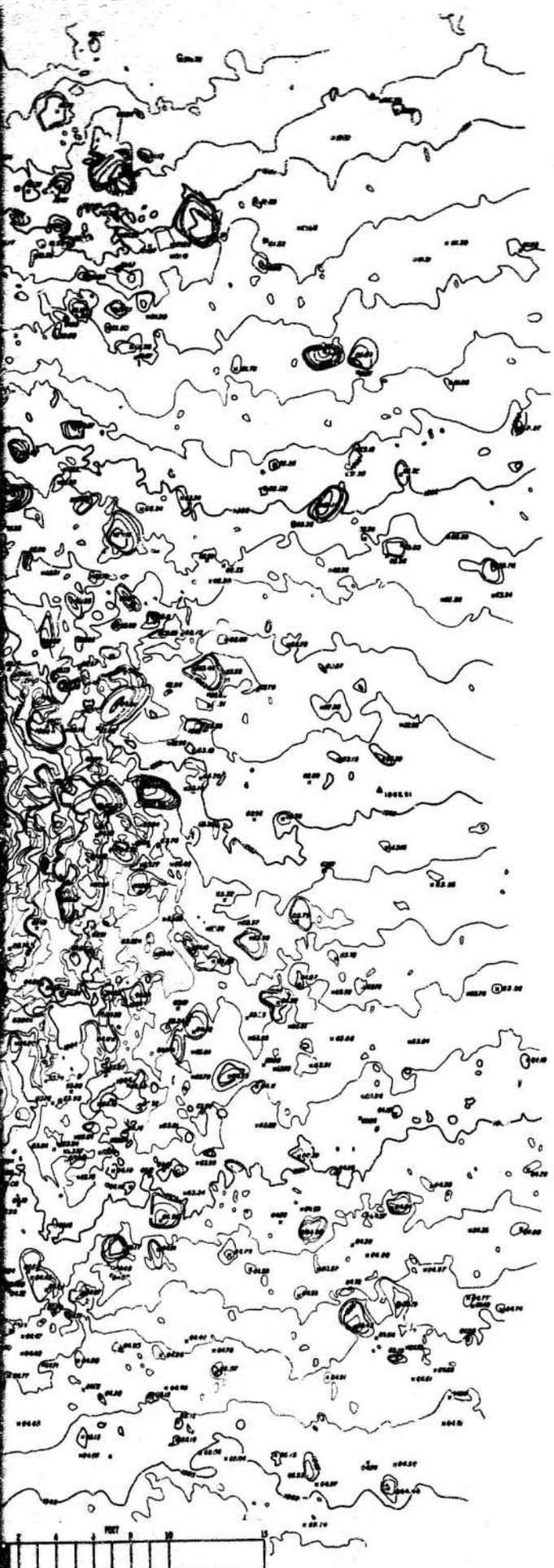

COMPILED BY
AMERICAN AERIAL SURVEYS, INC.
564 S. STEWART DR.
COVINA, CALIFORNIA

CONTOUR INTERVAL 0.2'

Figure I-26. Topographic Map of Crater H1.

COMPILED BY
AMERICAN AERIAL SURVEYS, INC.
564 S. STEWART DR.
COVINA, CALIFORNIA

CONTOUR INTERVAL 0.2'

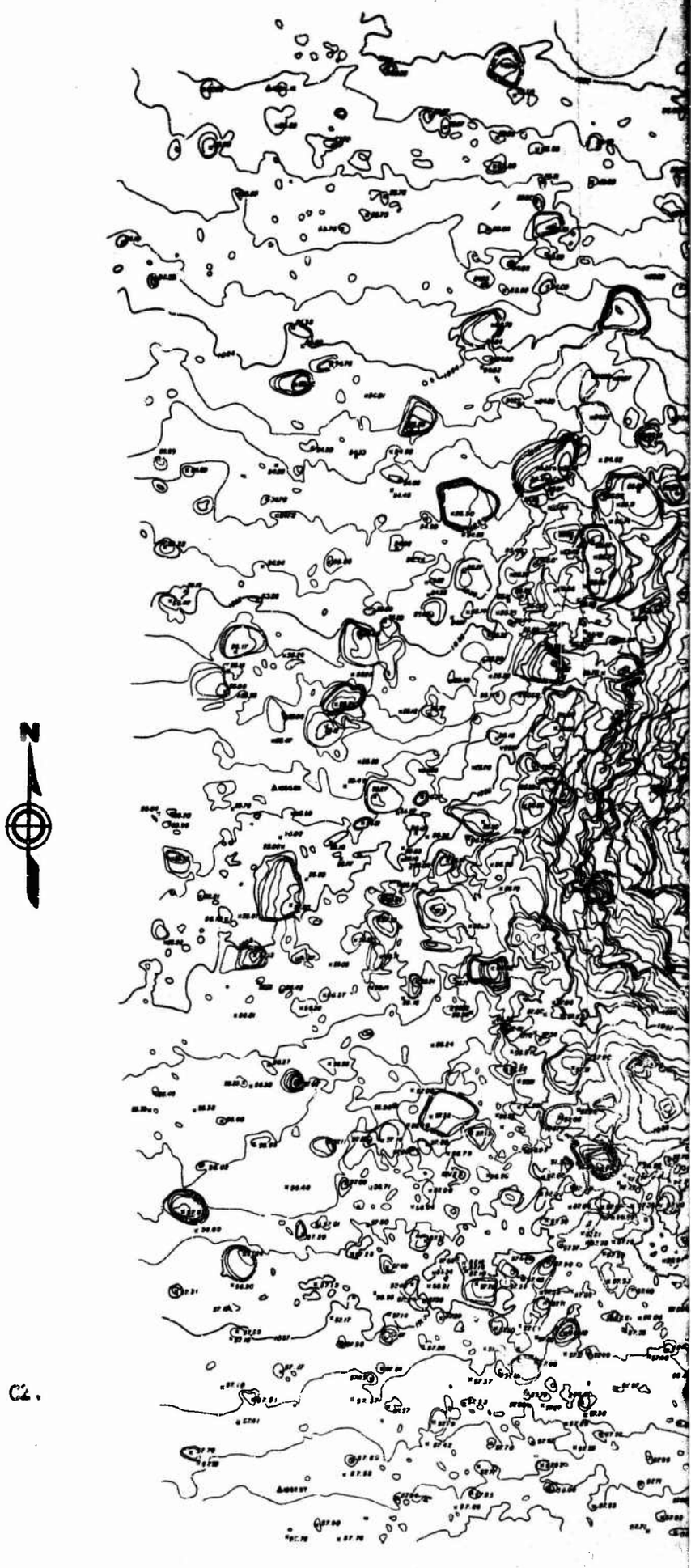

Figure I-27. Topographic Map of Crater C4.

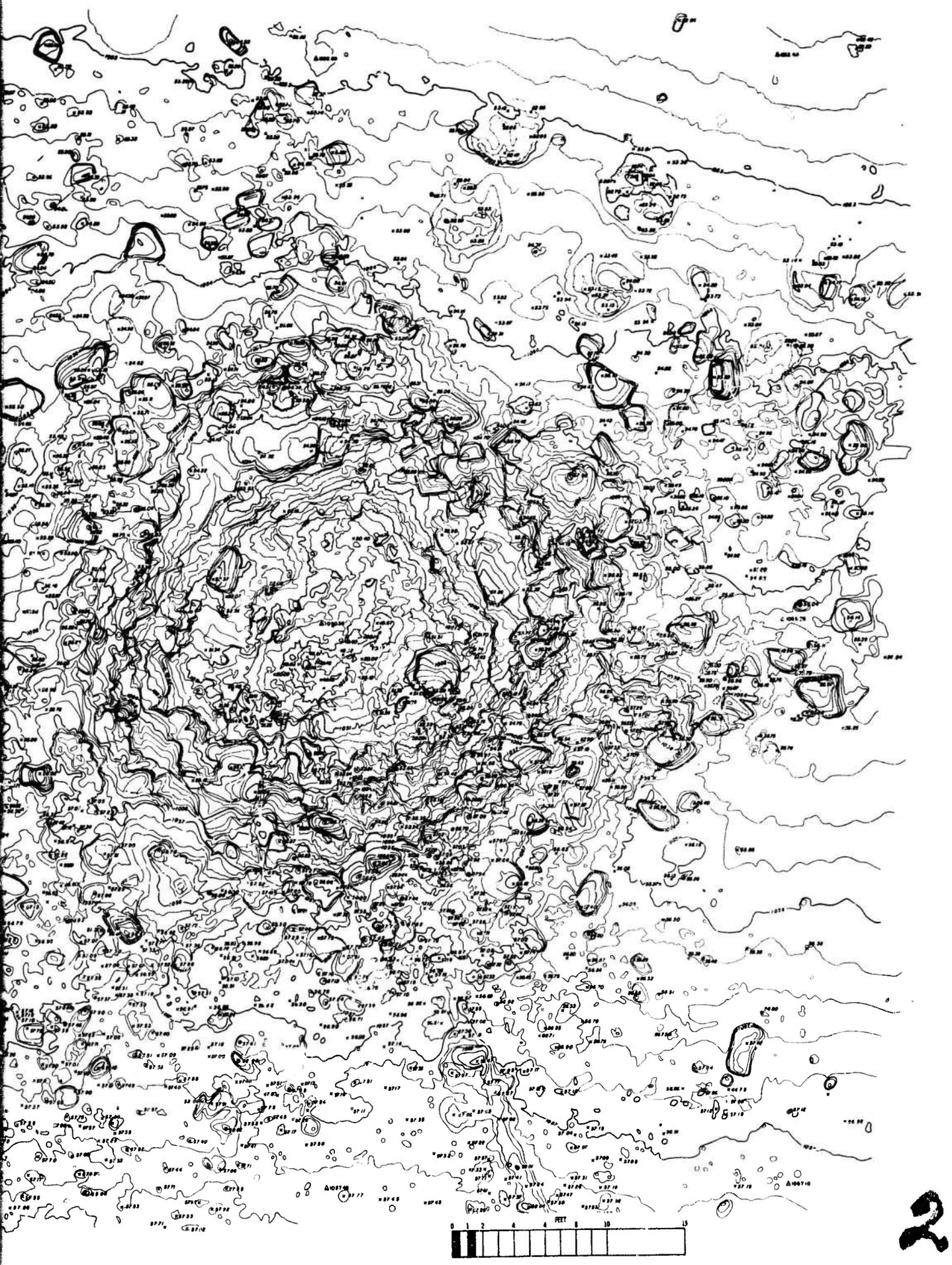
FEET
0 1 2 4 6 8 10 15

SW NE

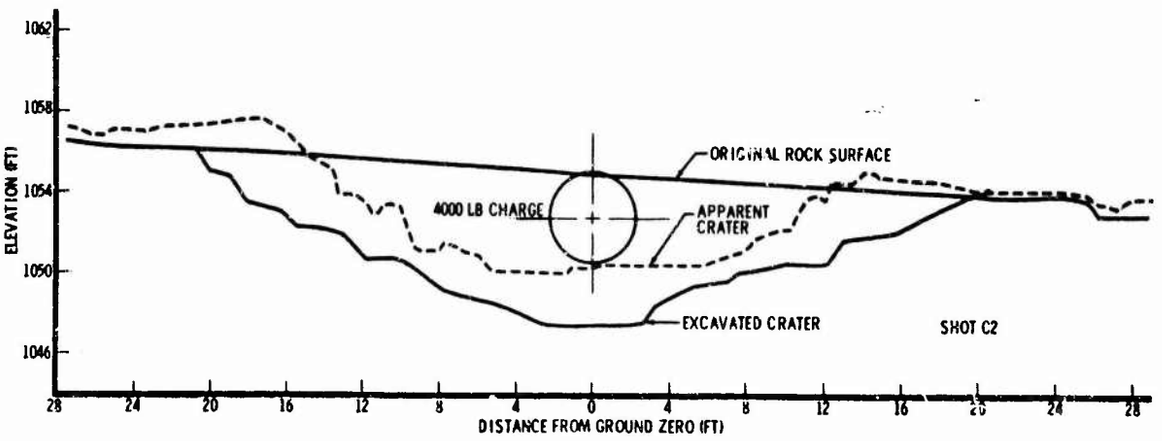

Figure I-28. Photograph and Profile of Crater C2.

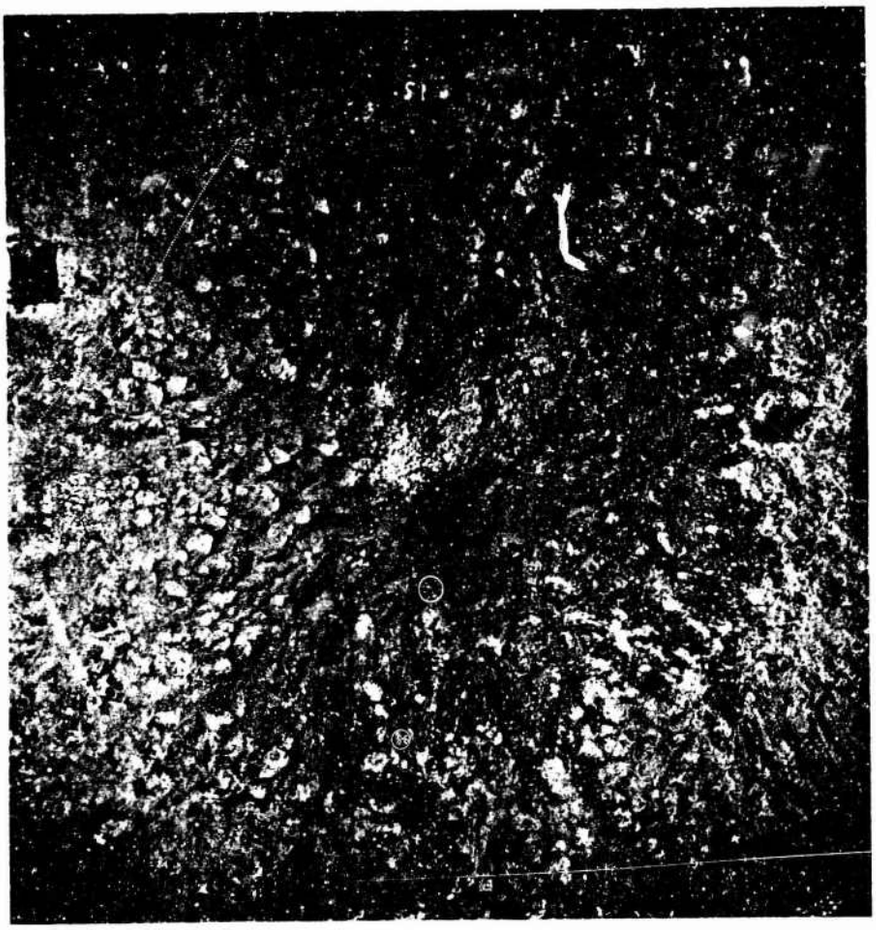

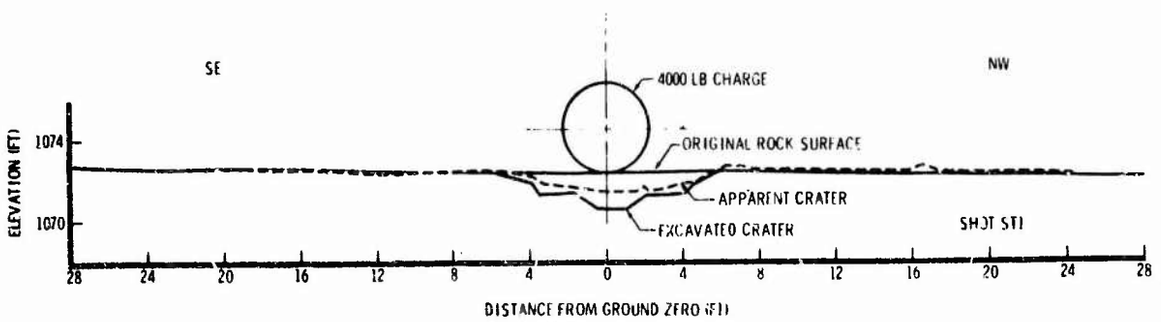

Figure I-29. Photograph and Profile of Crater ST1.

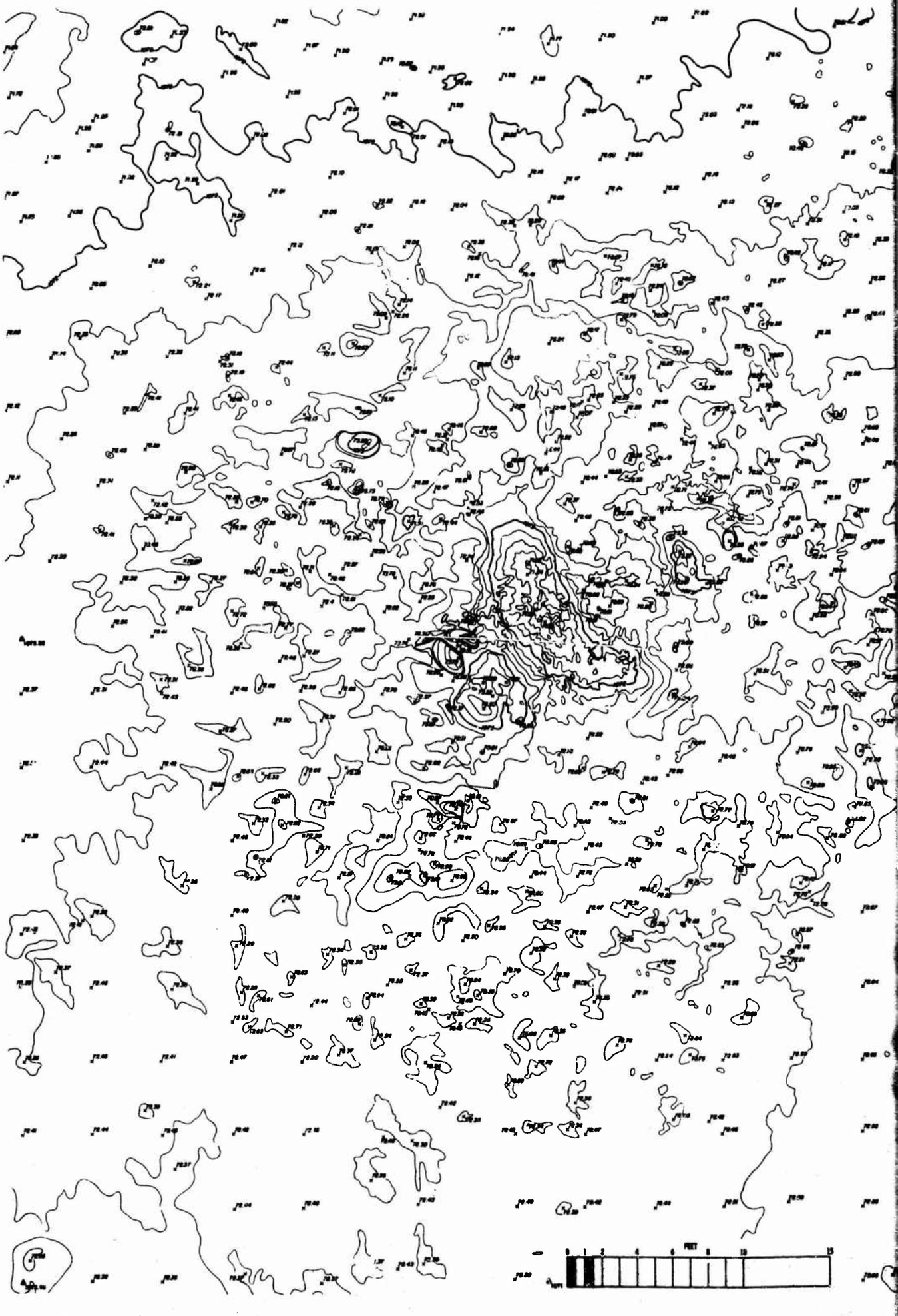
0
1
2
4
6
8
10
15
FEET

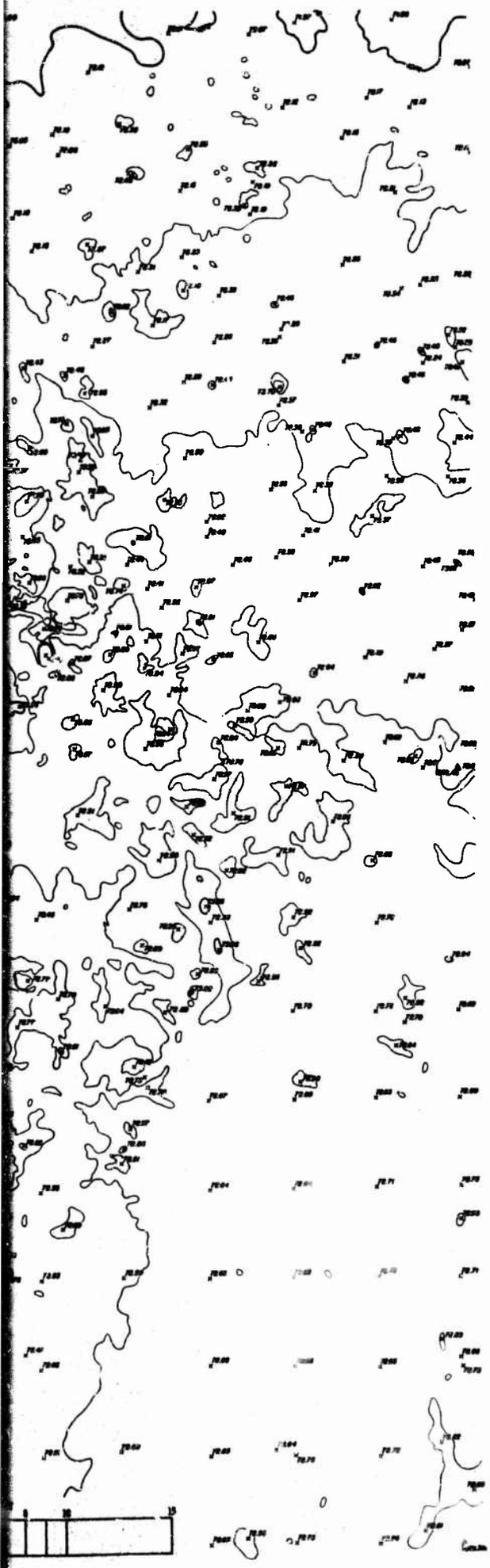

COMPILED BY
AMERICAN AERIAL SURVEYS, INC.
564 S. STEWART DR.
COVINA, CALIFORNIA

CONTOUR INTERVAL 0.2'

Figure I-30. Topographic Map of Crater ST1.

2

COMPILED BY
AMERICAN AERIAL SURVEYS, INC.
564 S. STEWART DR.
COVINA, CALIFORNIA

CONTOUR INTERVAL 0.2'

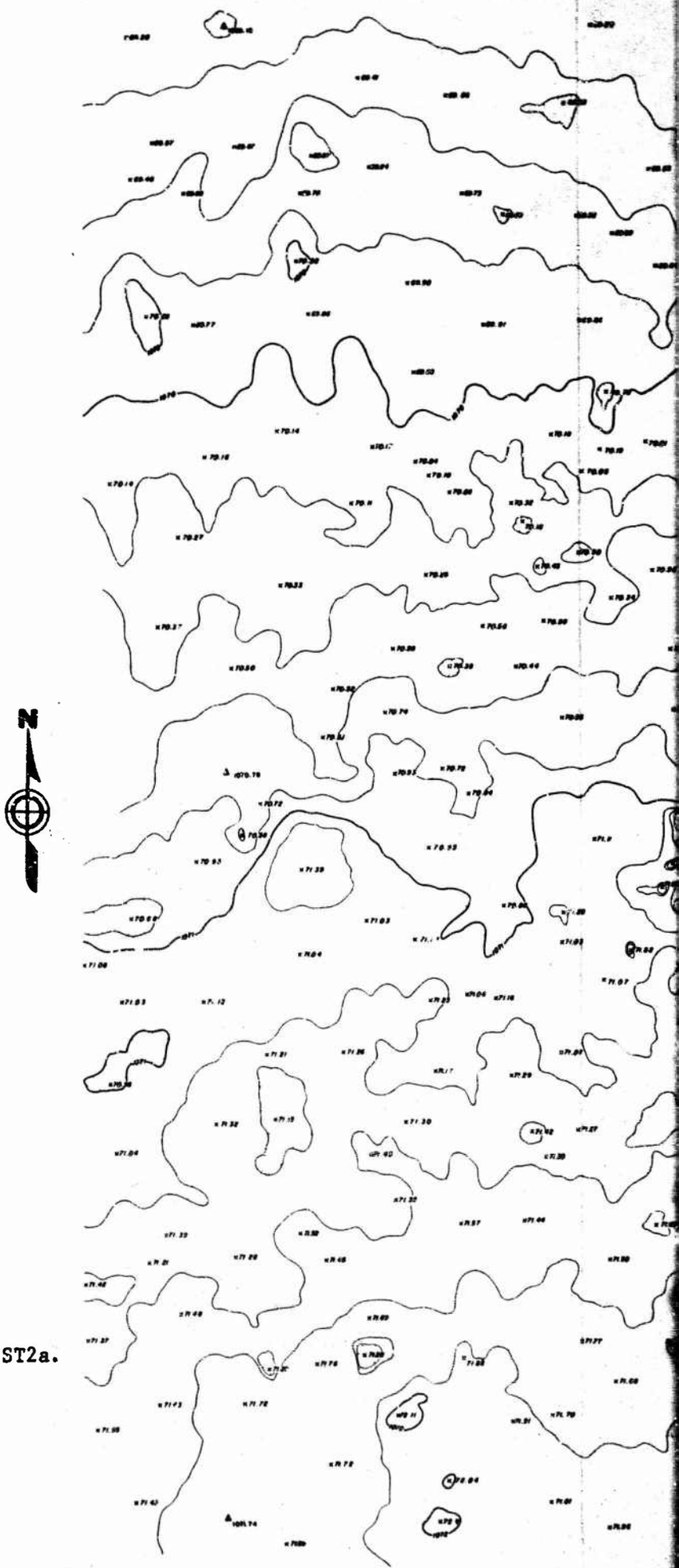

Figure I-31. Topographic Map of Crater ST2a.

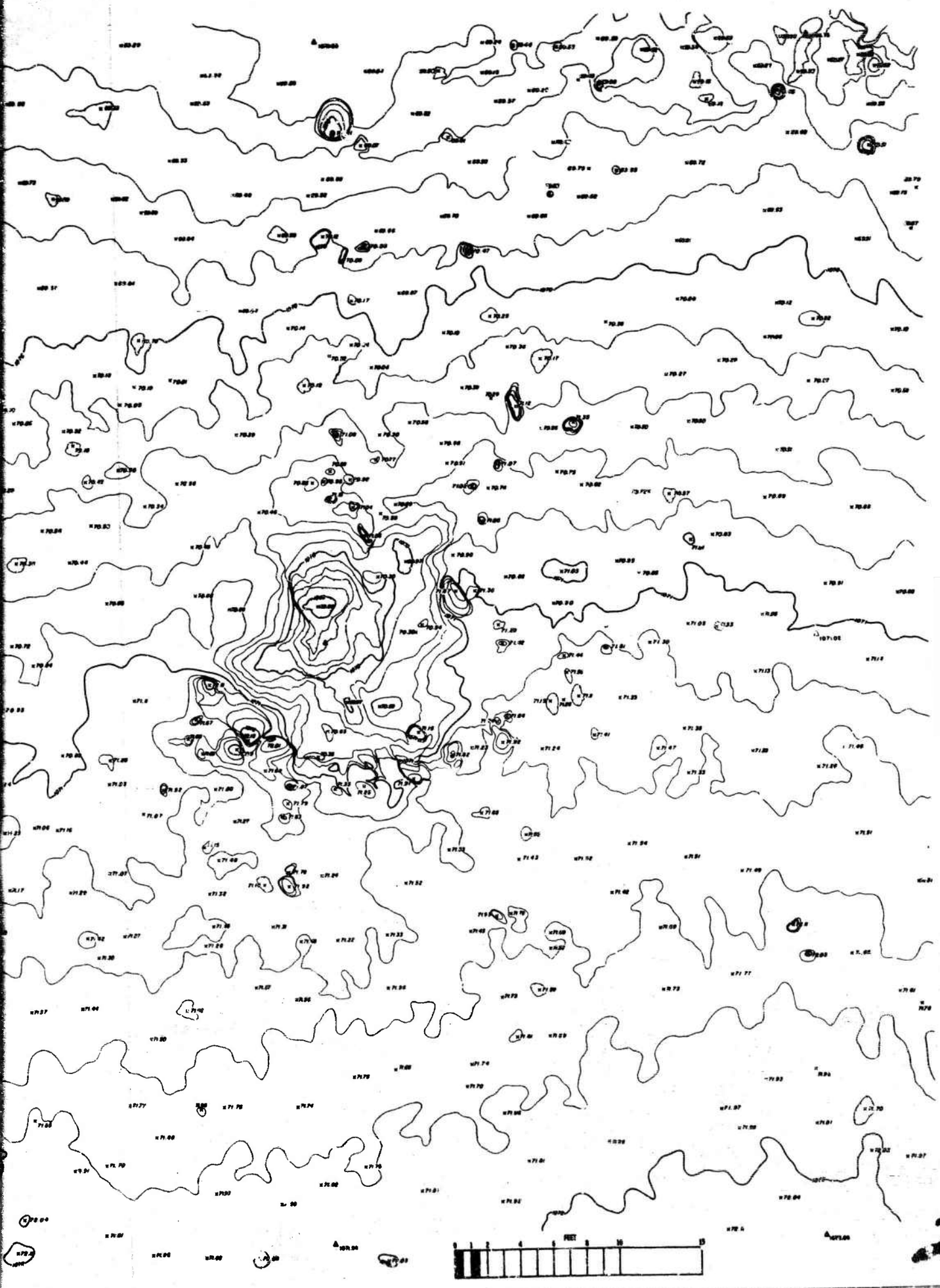
FEET
0
4
8
16
24

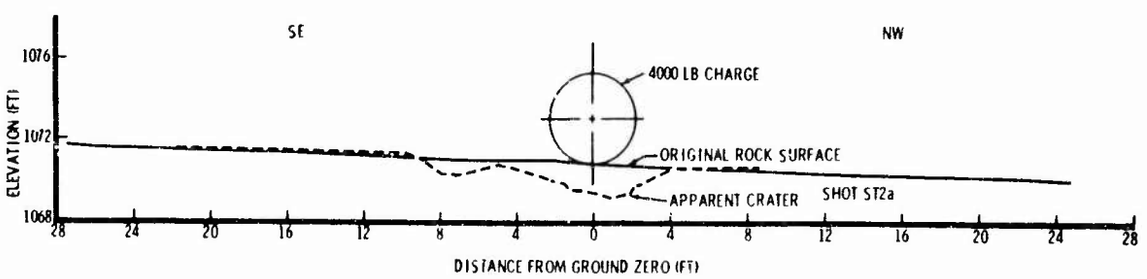

Figure I-32. Photograph and Profile of Crater ST2a.

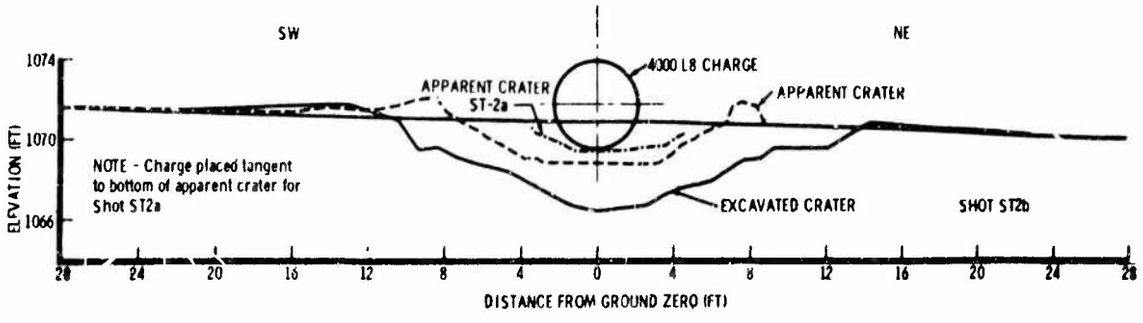

Figure I-33. Photograph and Profile of Crater ST2b.

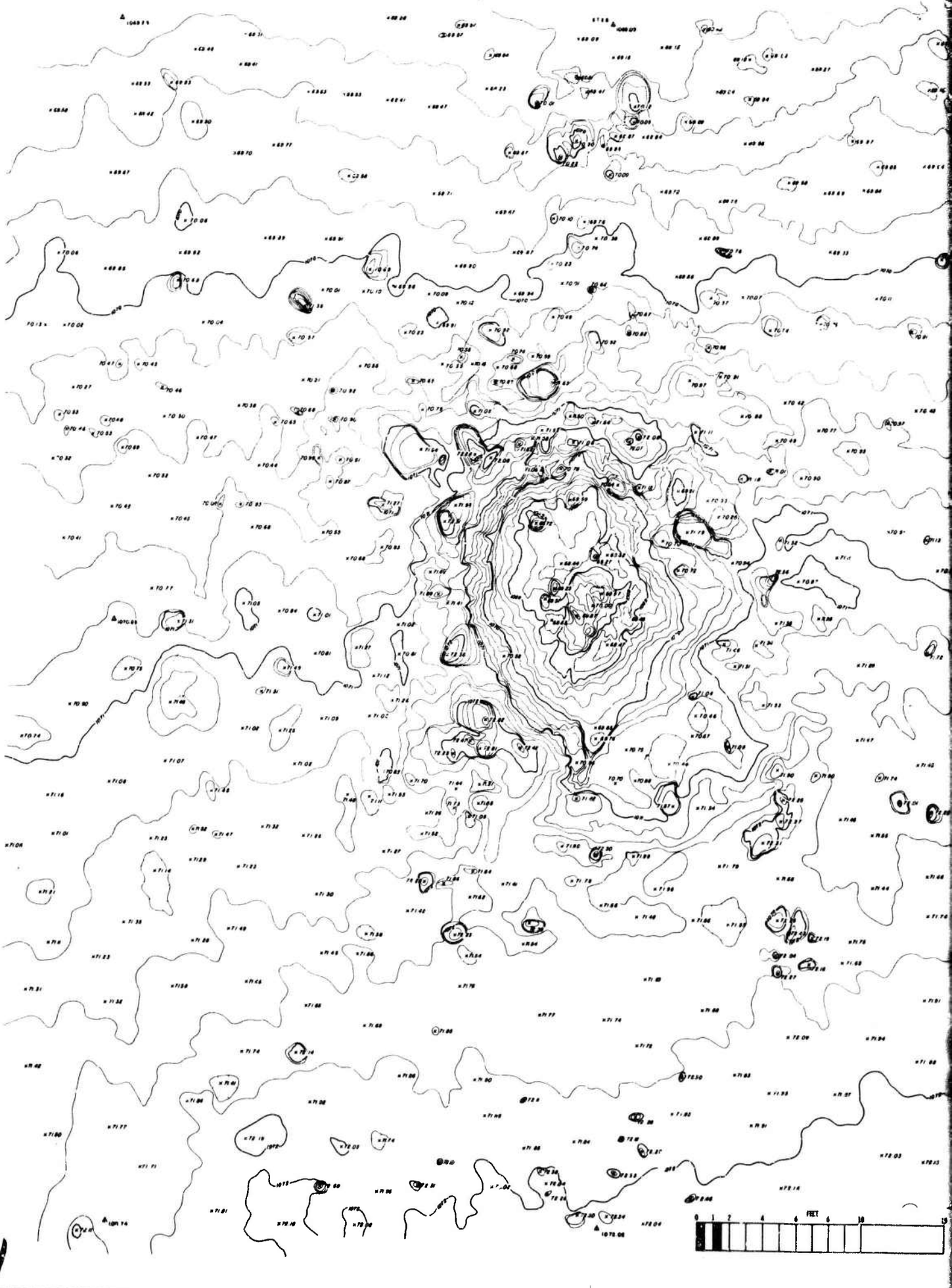
FEET

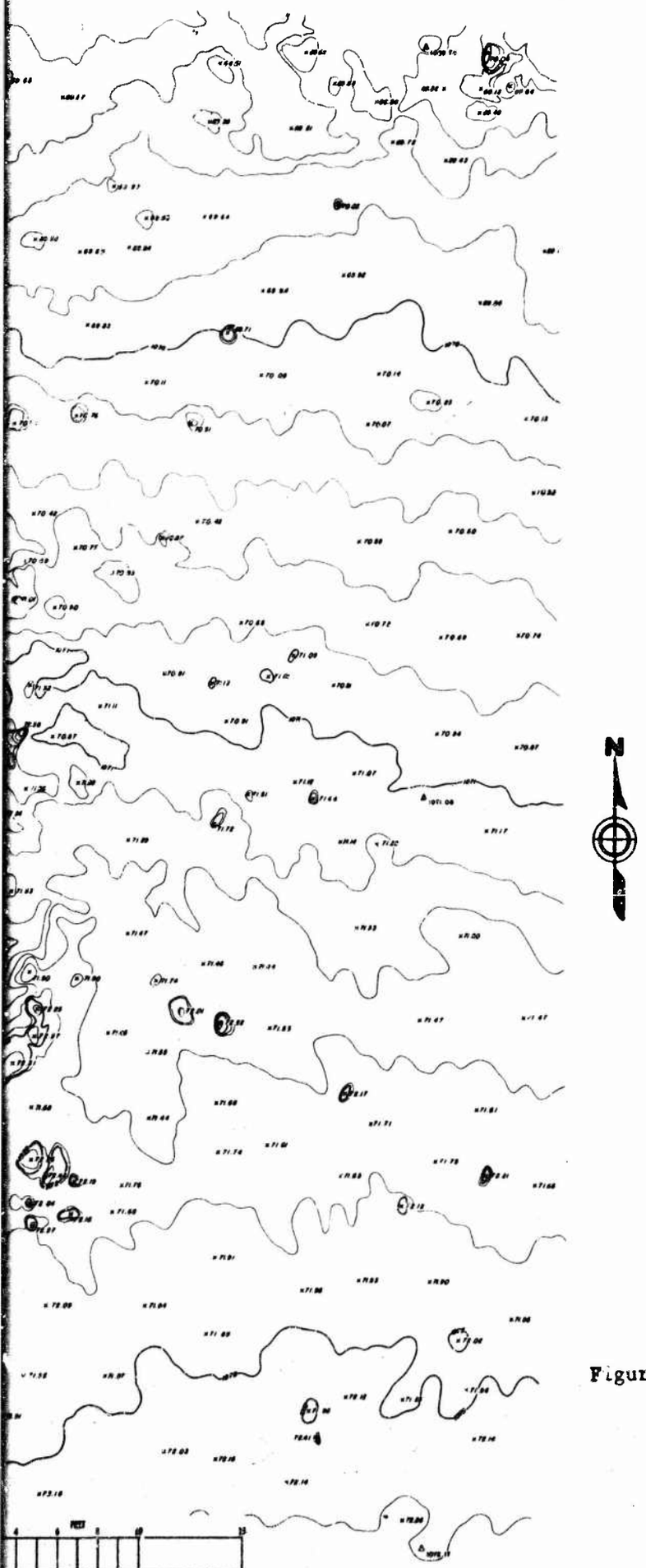

COMPILED BY
AMERICAN AERIAL SURVEYS, INC.
564 S. STEWART DR.
COVINA, CALIFORNIA

CONTOUR INTERVAL 0.2'

Figure I-34. Topographic Map of Crater ST2b.

2

COMPILED BY
AMERICAN AERIAL SURVEYS, INC.
564 S. STEWART DR.
COVINA, CALIFORNIA

CONTOUR INTERVAL 0.2'

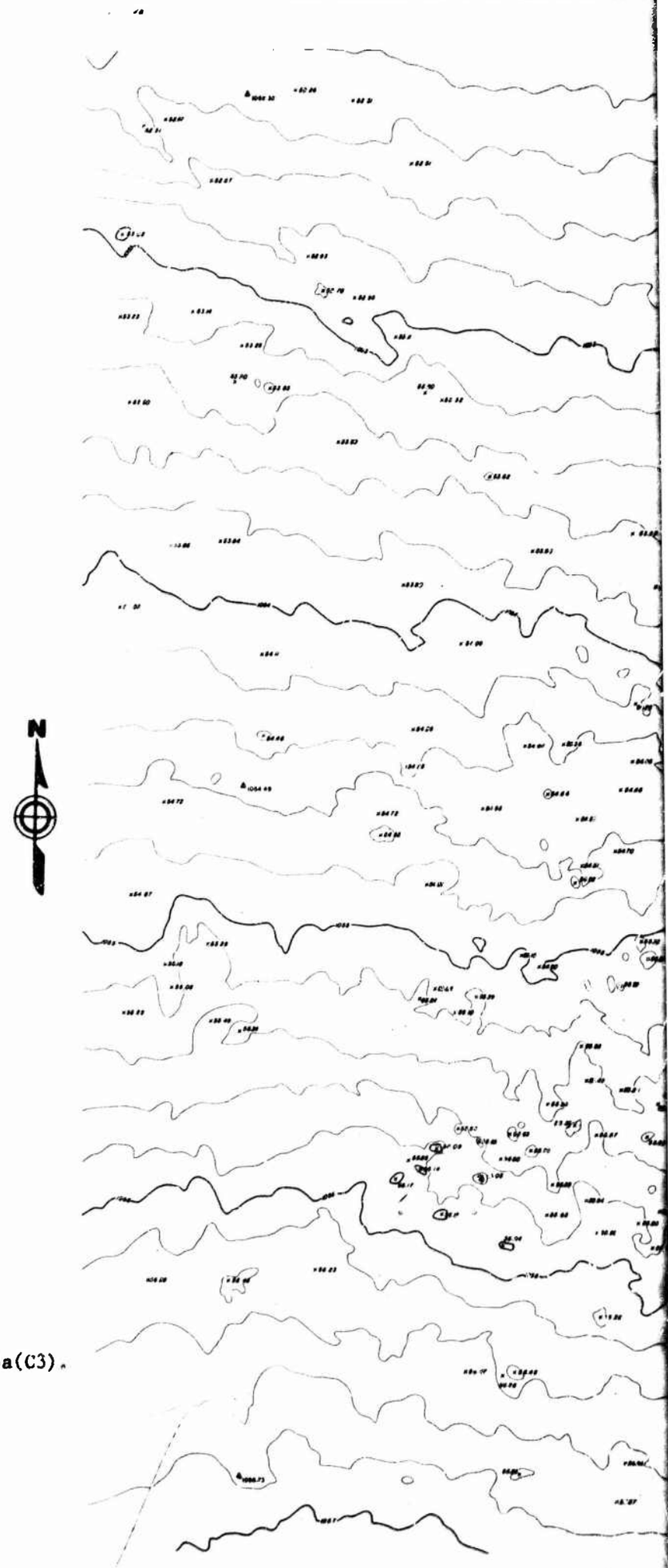

Figure I-35. Topographic Map of Crater ST3a(C3).

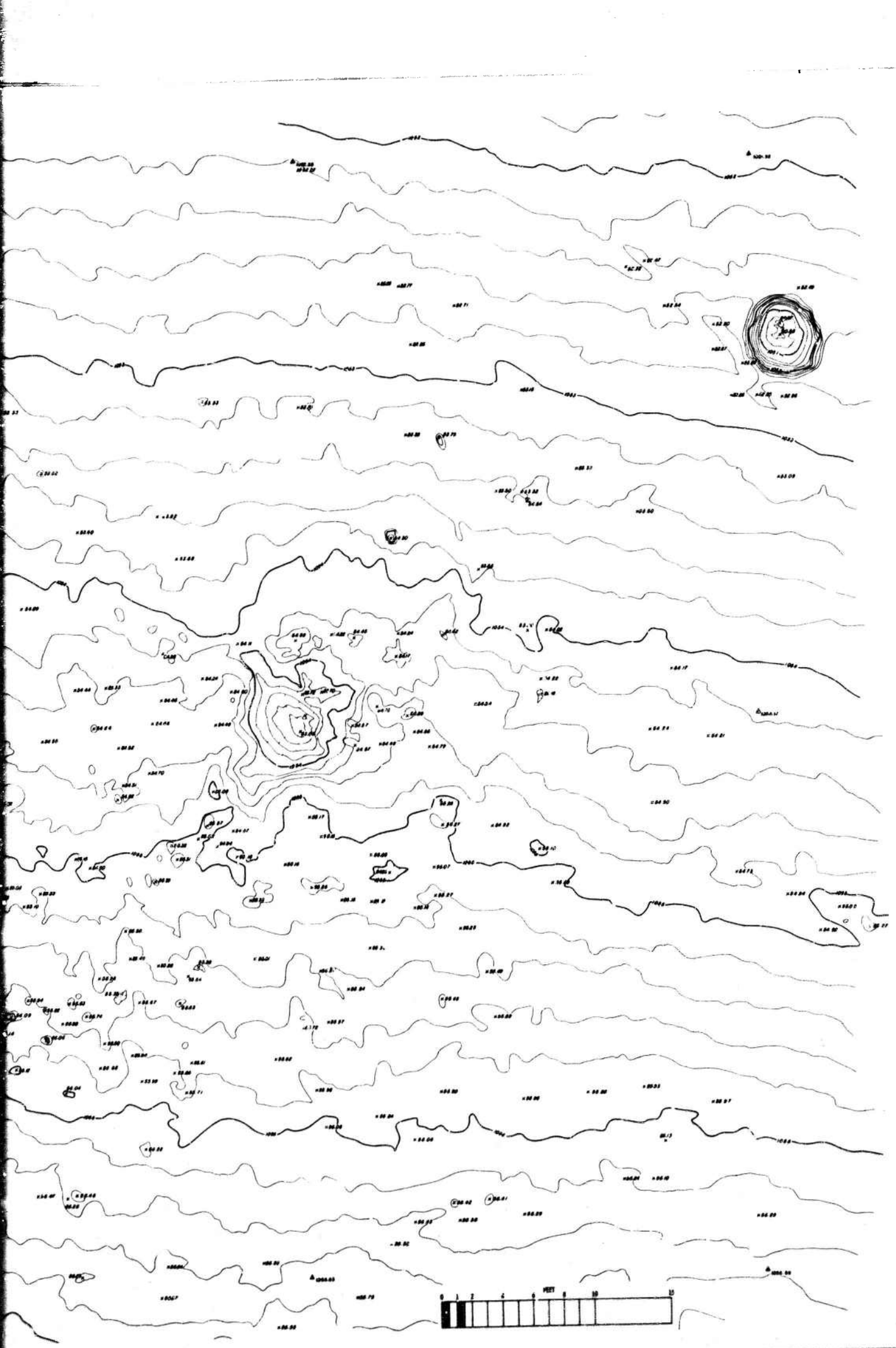

2

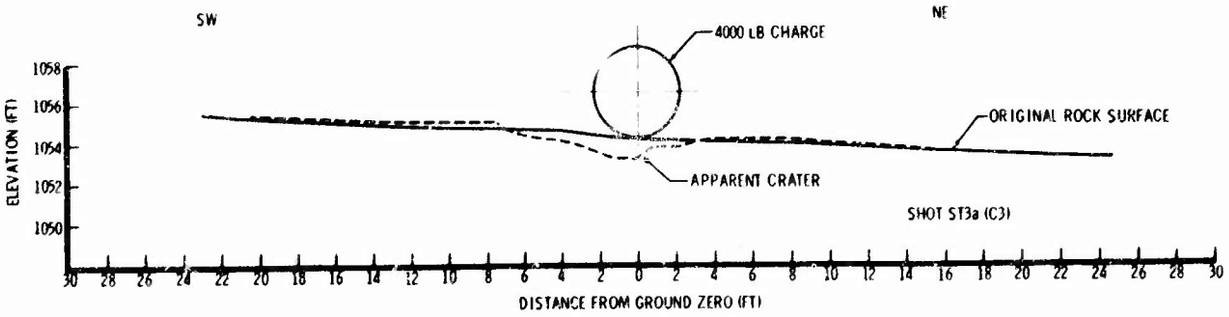

Figure I-36. Photograph and Profile of Crater ST3a(C3).

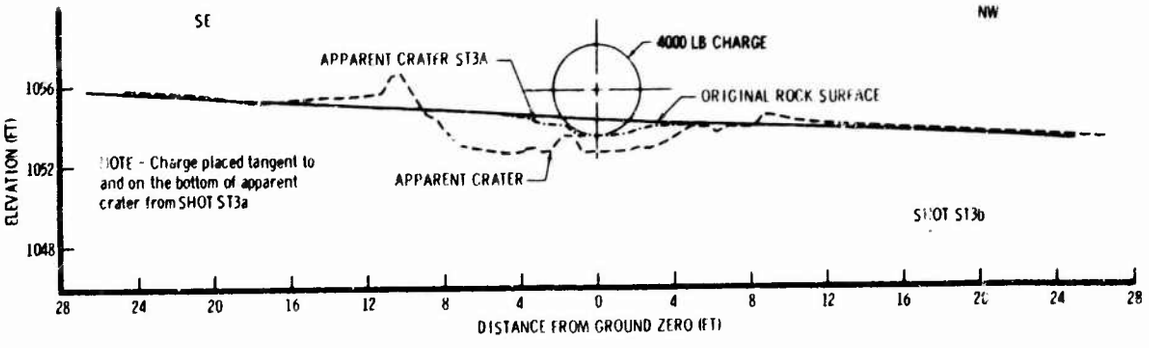

Figure I-37. Photograph and Profile of Crater ST3b.

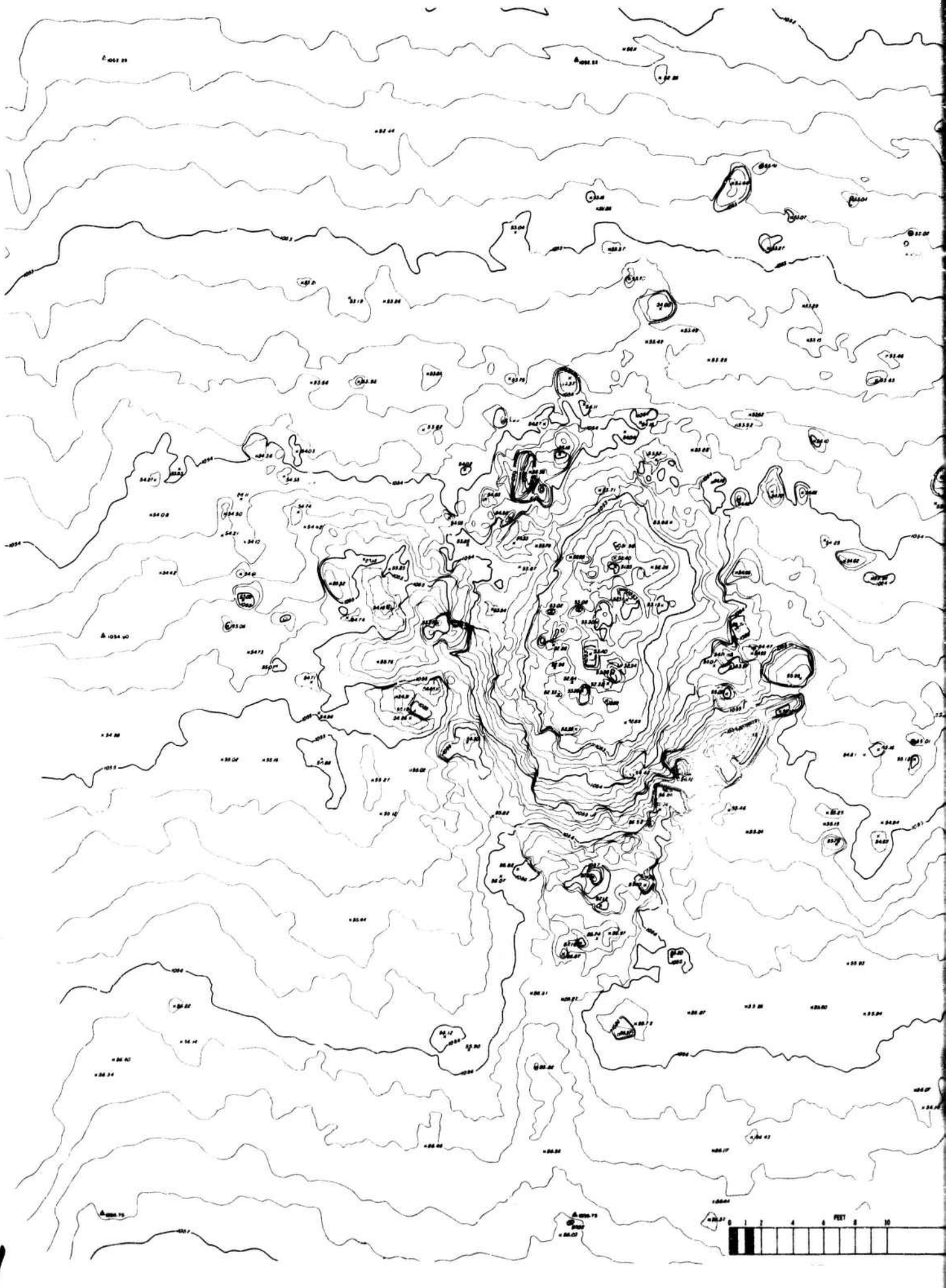
0 1 2 4 6 8 10
FEET

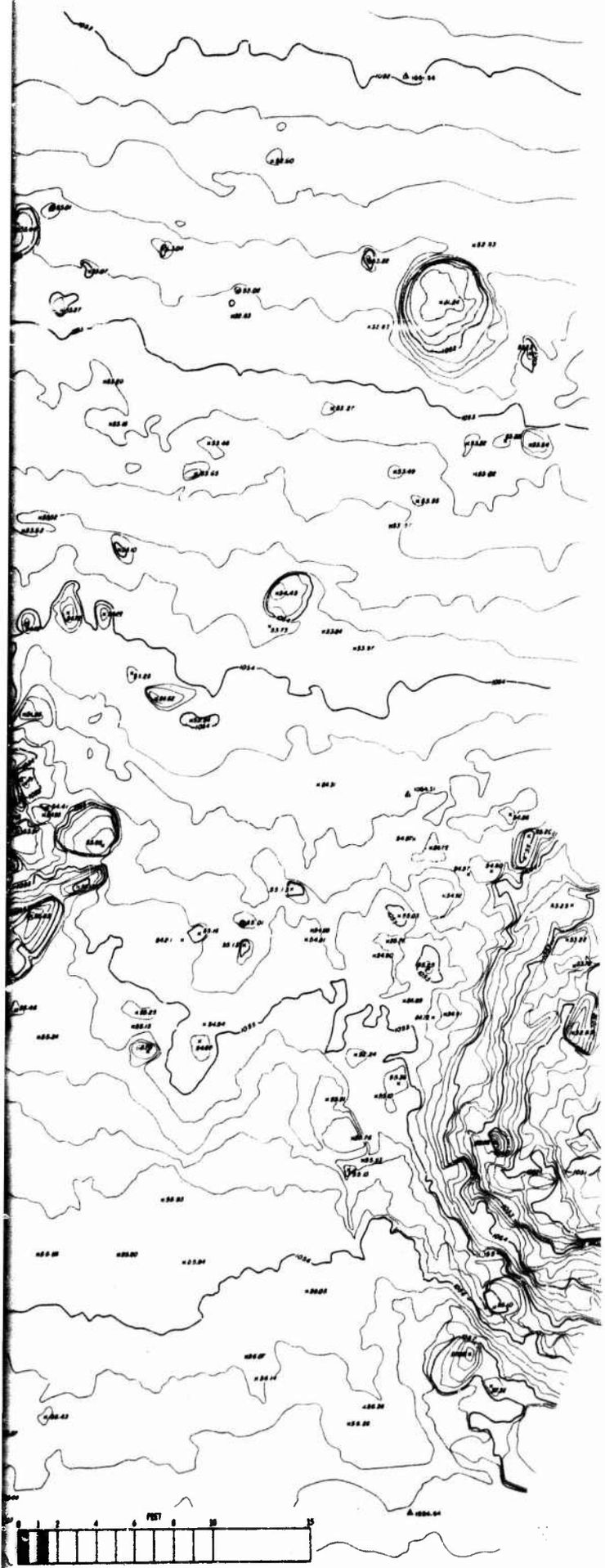

COMPILED BY
AMERICAN AERIAL SURVEYS, INC.
564 S. STEWART DR.
COVINA, CALIFORNIA

CONTOUR INTERVAL 0.2'

Figure I-38. Topographic Map of Crater ST3b.

2

COMPILED BY
AMERICAN AERIAL SURVEYS, INC.
564 S. STEWART DR.
COVINA, CALIFORNIA

CONTOUR INTERVAL 0.2'

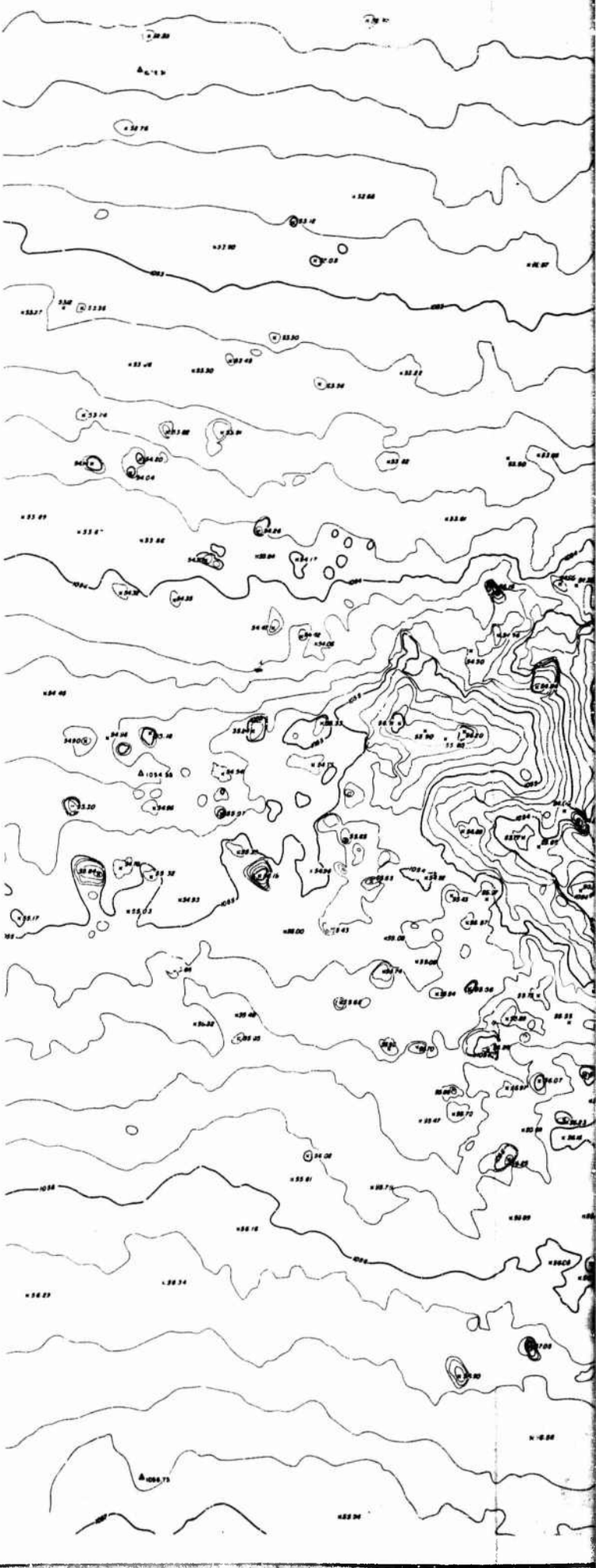

Figure I-39. Topographic Map of Crater ST3c.

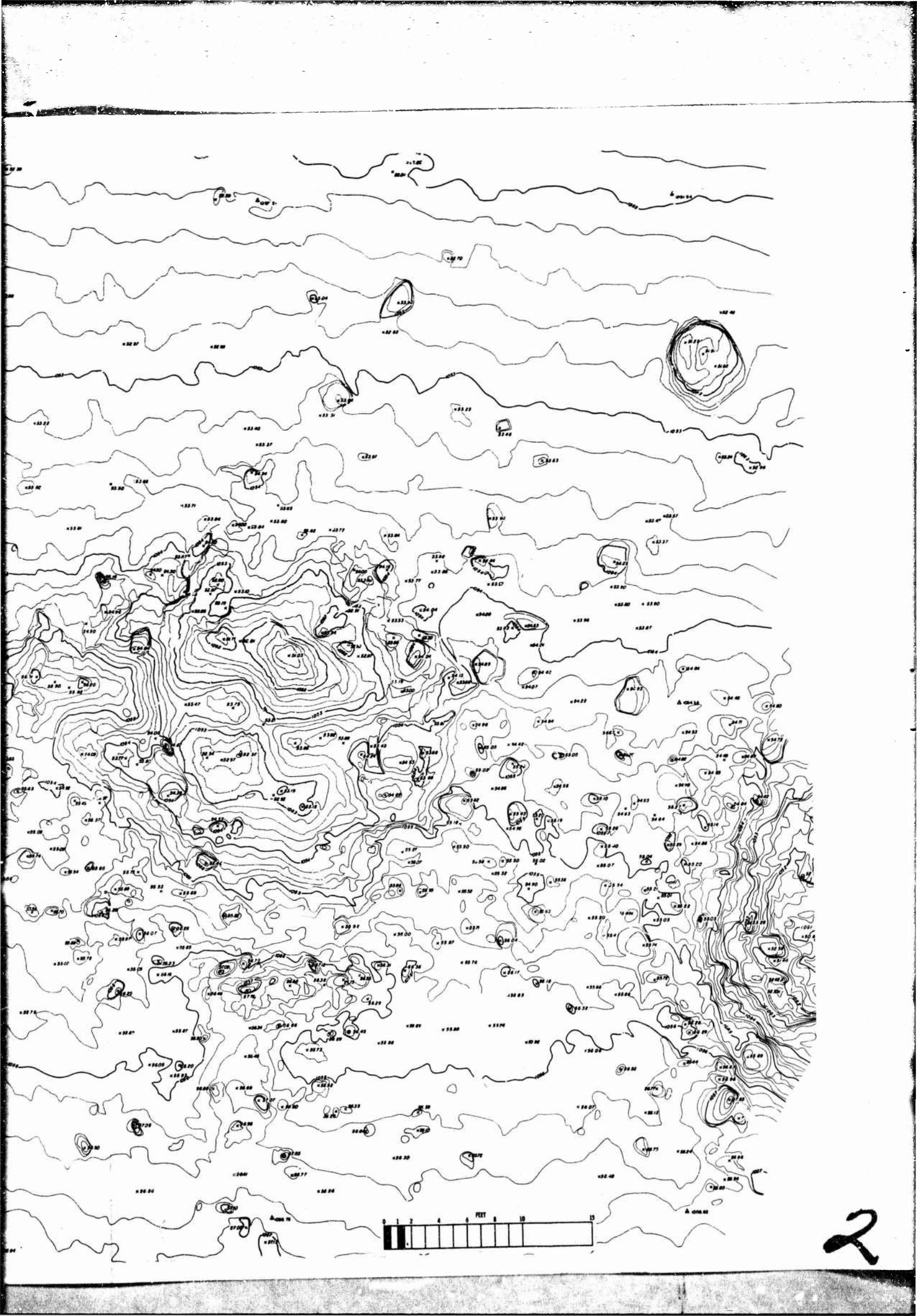

2

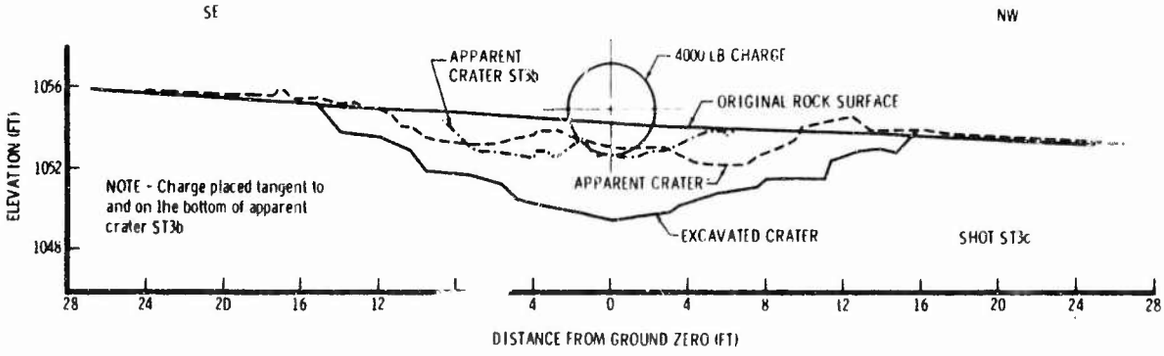

Figure I-40. Photograph and Profile of Crater ST3c.

This page intentionally left blank.

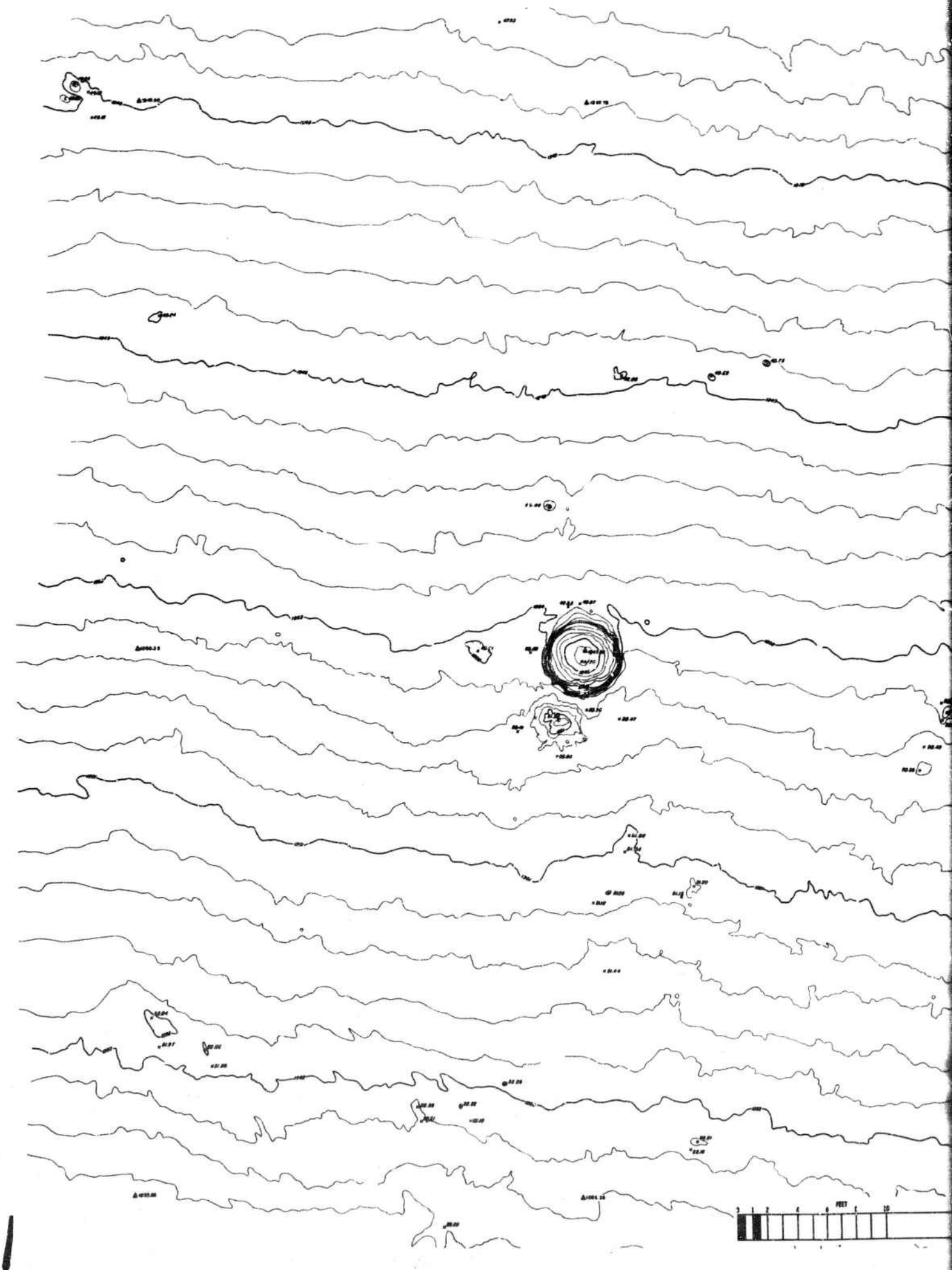
FEET

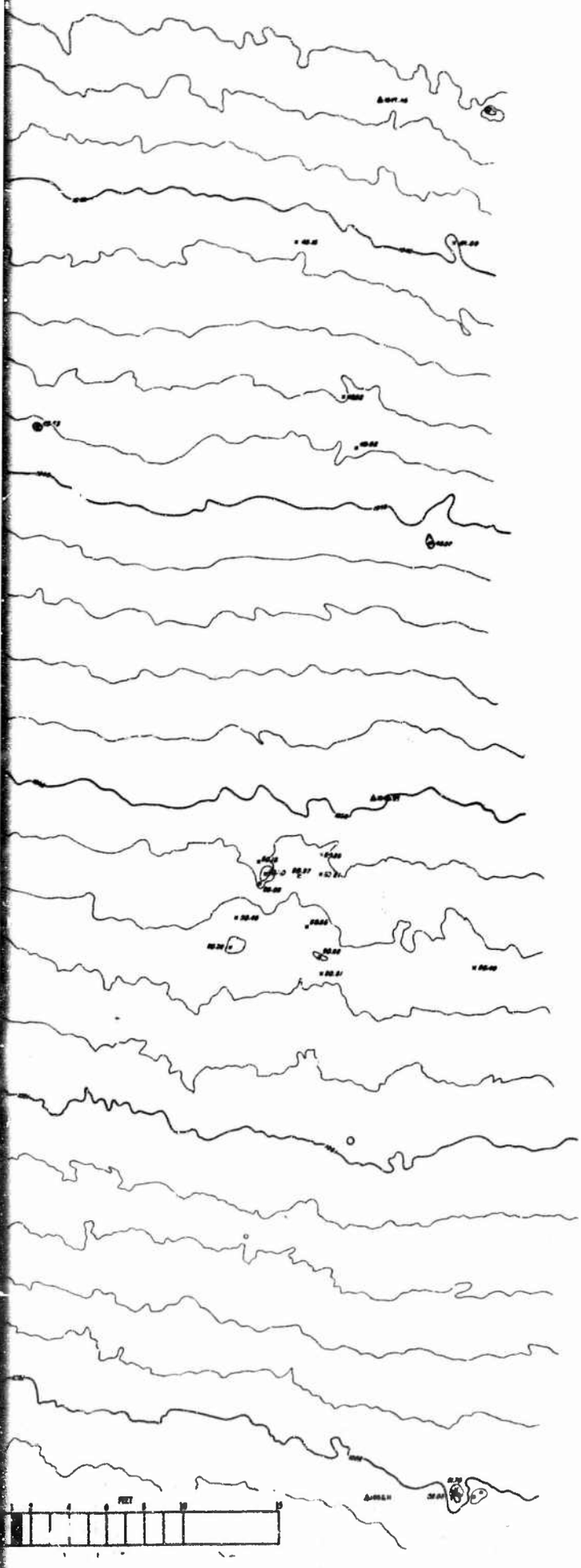

COMPILED BY
AMERICAN AERIAL SURVEYS, INC.
564 S. STEWART DR.
COVINA, CALIFORNIA

CONTOUR INTERVAL 0.2'

Figure I-41. Preshot Topographic Map of Shot S1(C1) Region.

COMPILED BY
AMERICAN AERIAL SURVEYS, INC.
564 S. STEWART DR.
COVINA, CALIFORNIA

CONTOUR INTERVAL 0.2'

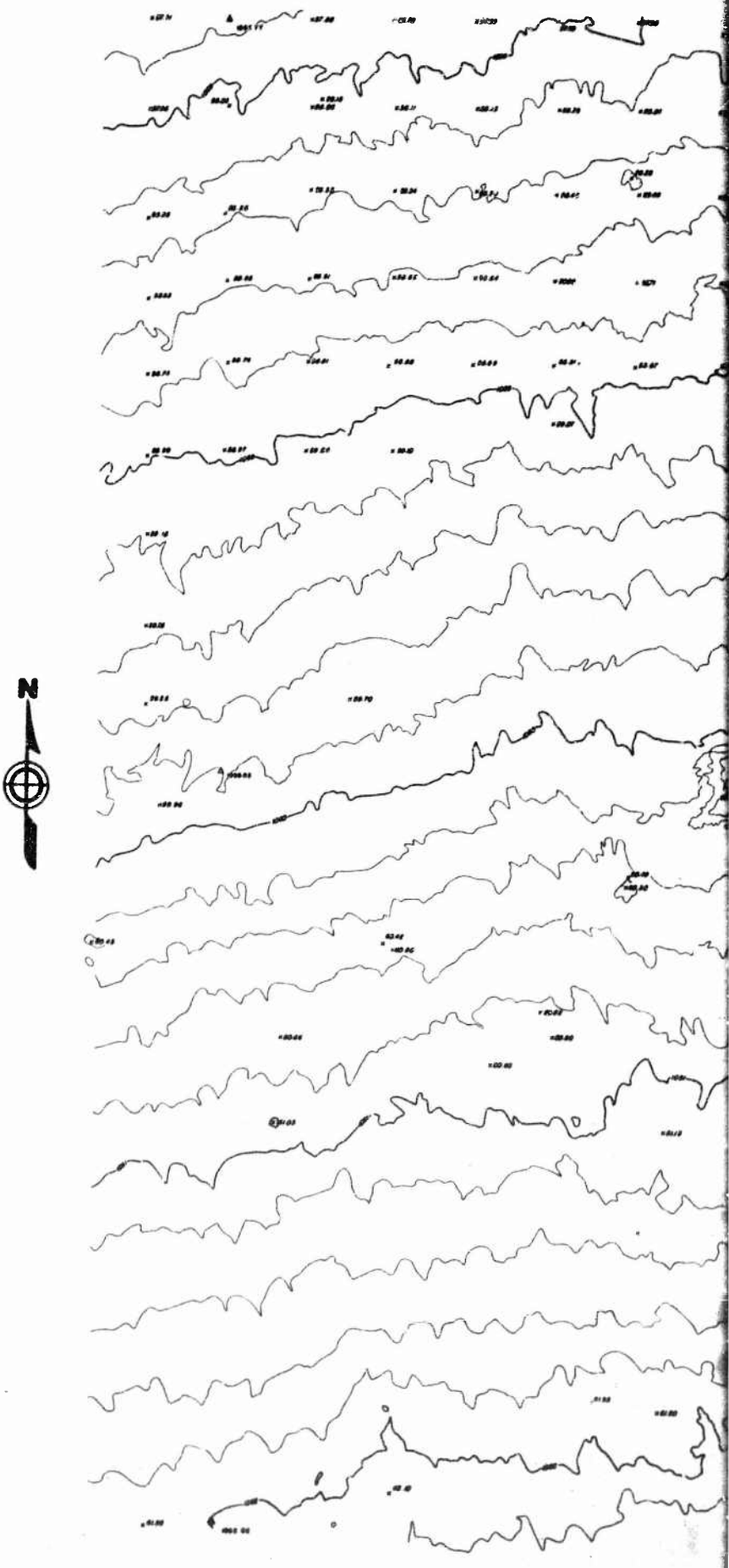

Figure I-42. Preshot Topographic Map of Shot S2a Region.

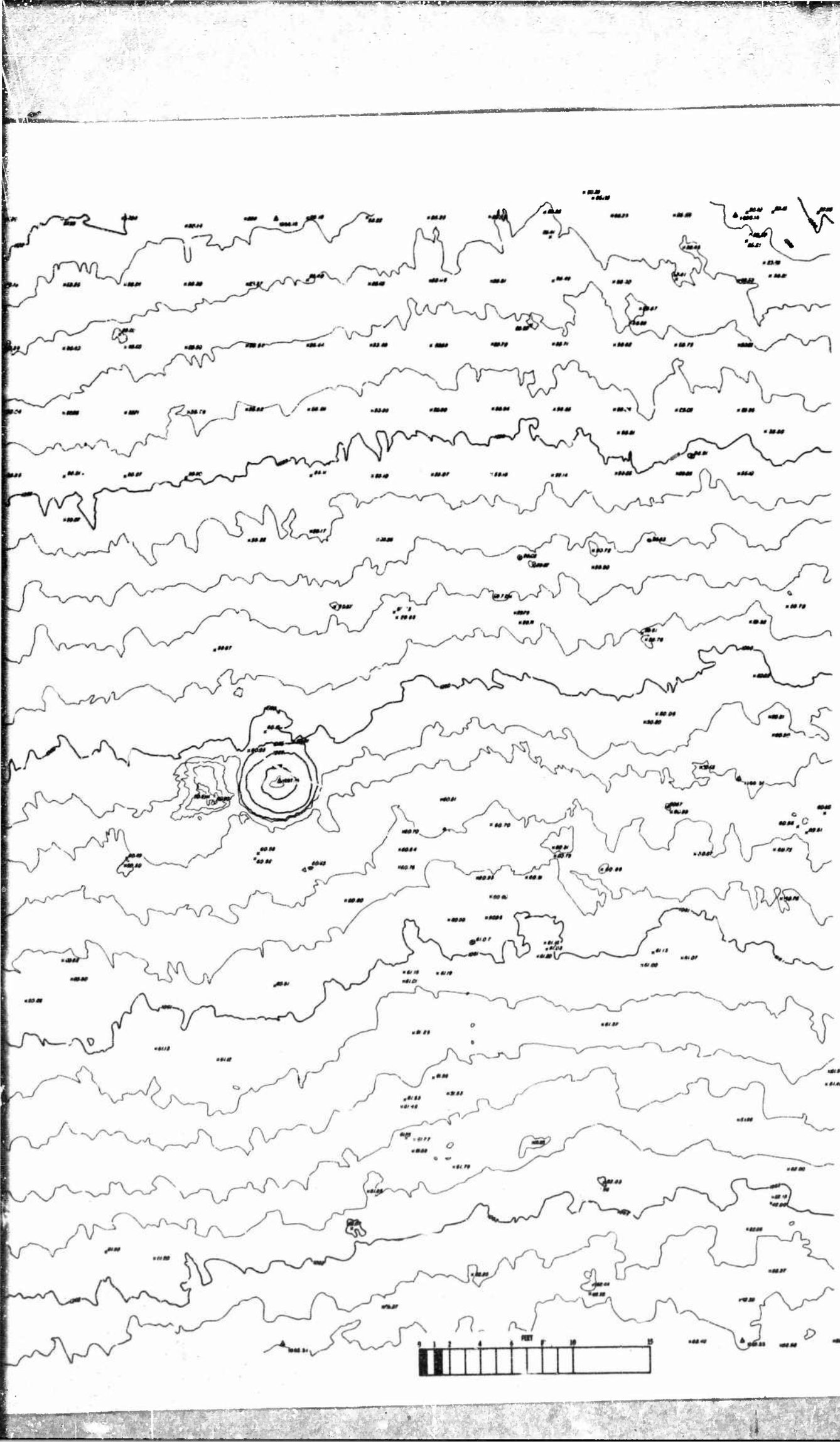
FEET

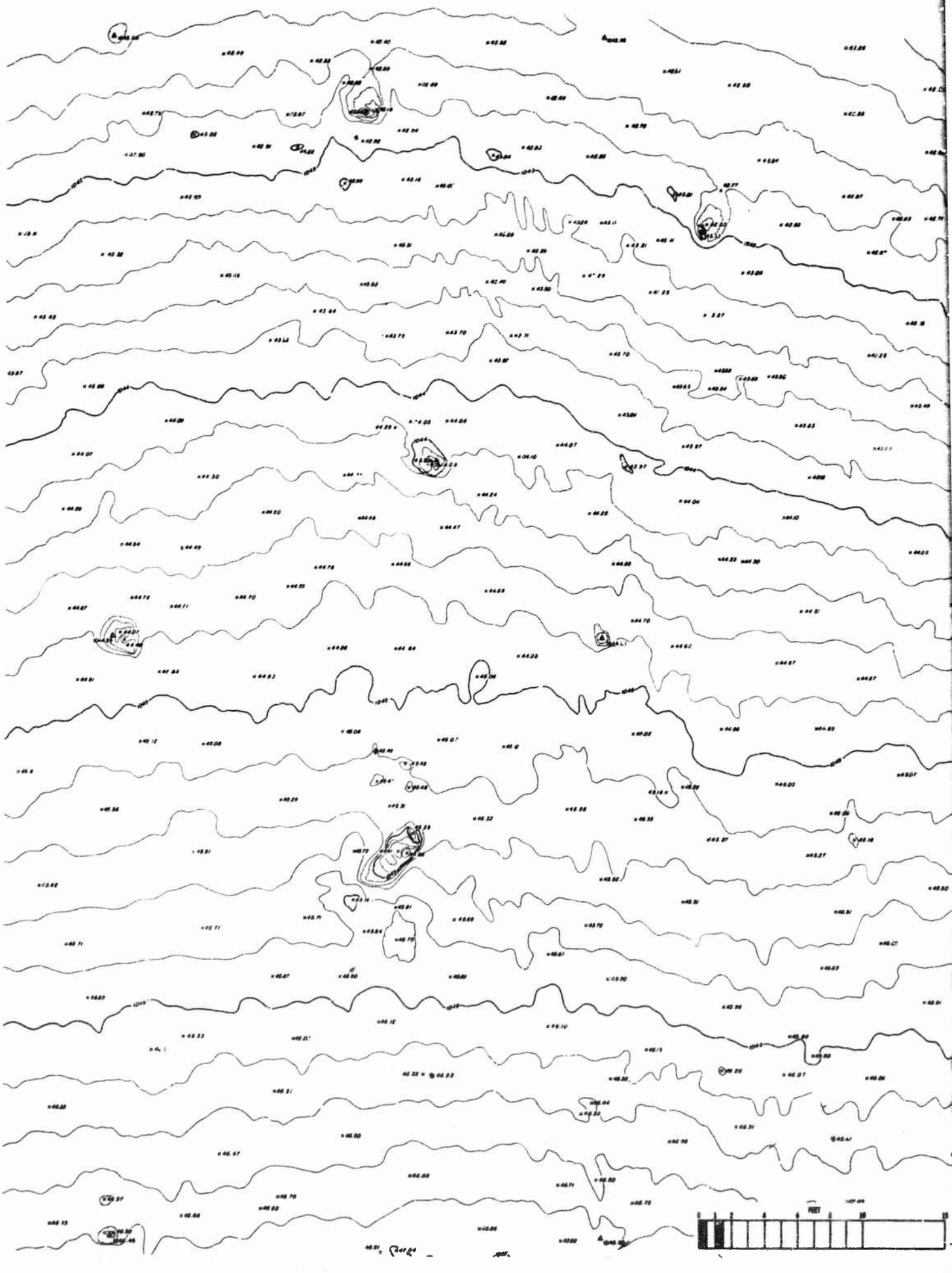
FEET

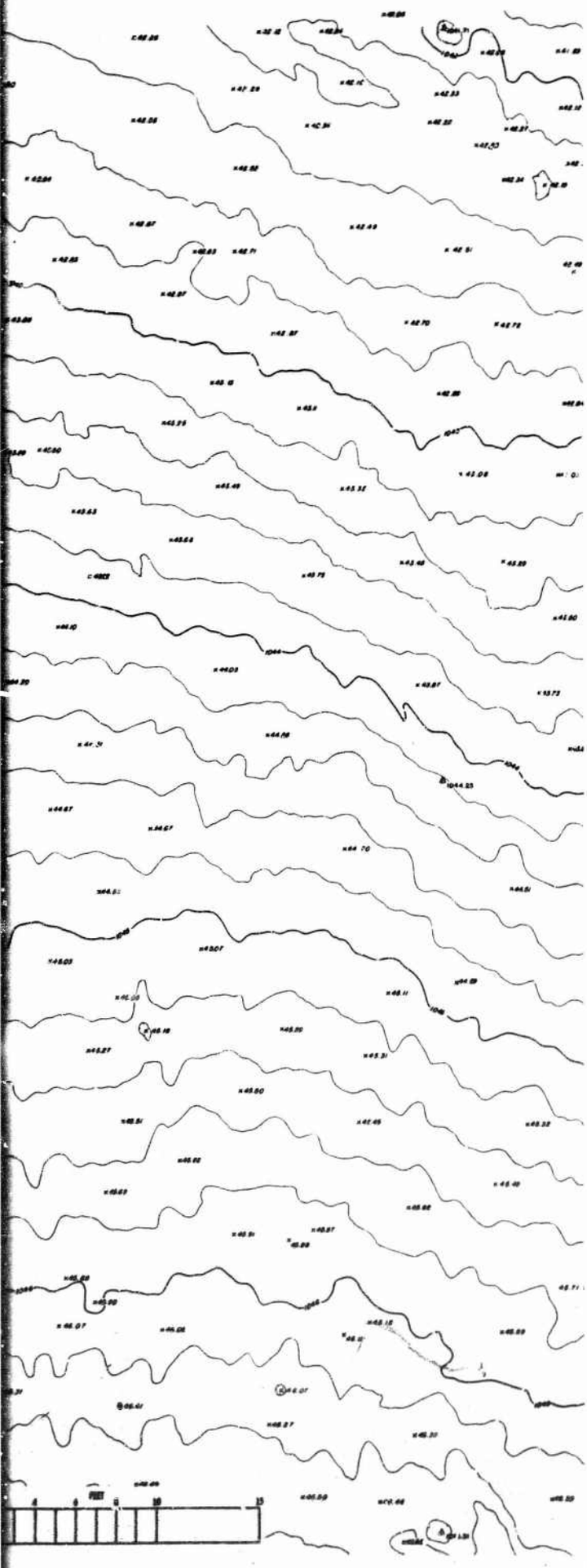

COMPILED BY
AMERICAN AERIAL SURVEYS, INC.
564 S. STEWART DR.
COVINA. CALIFORNIA

CONTOUR INTERVAL 0.2'

Figure I-43. Preshot Topographic Map of Shot S3a Region.

2

COMPILED BY
AMERICAN AERIAL SURVEYS, INC.
564 S. STEWART DR.
COVINA, CALIFORNIA

CONTOUR INTERVAL 0.2'

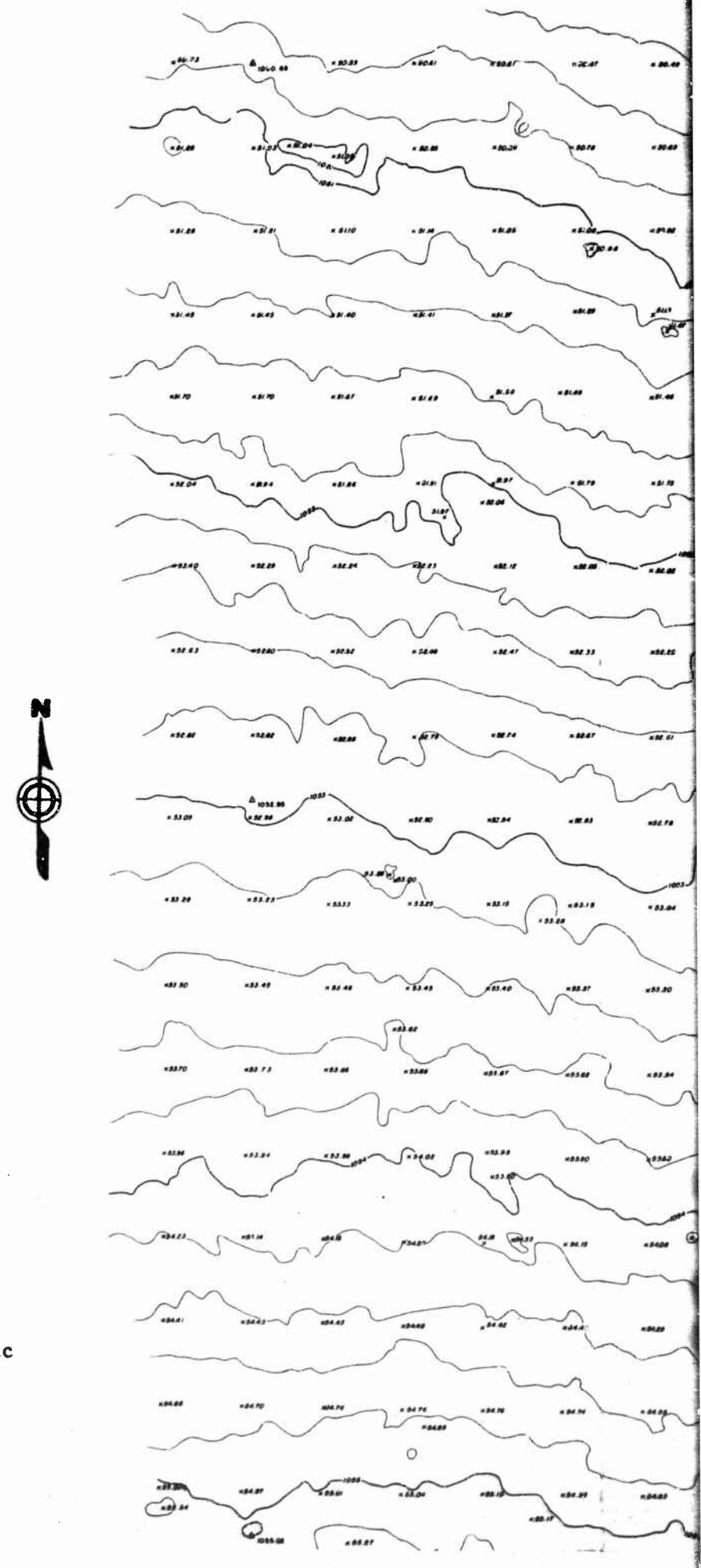

Figure I-44. Preshot Topographic Map of Shot S4a Region.

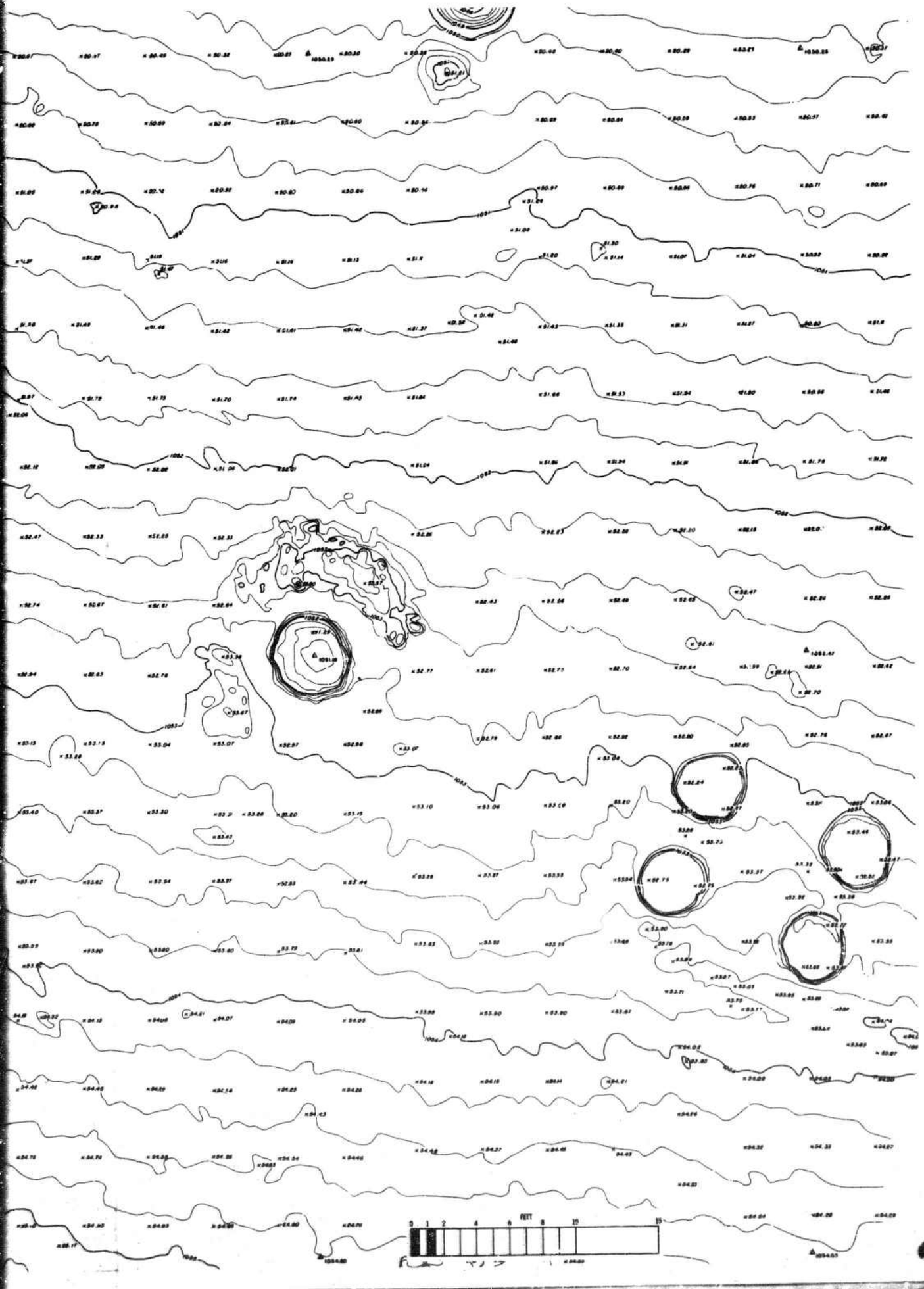

2

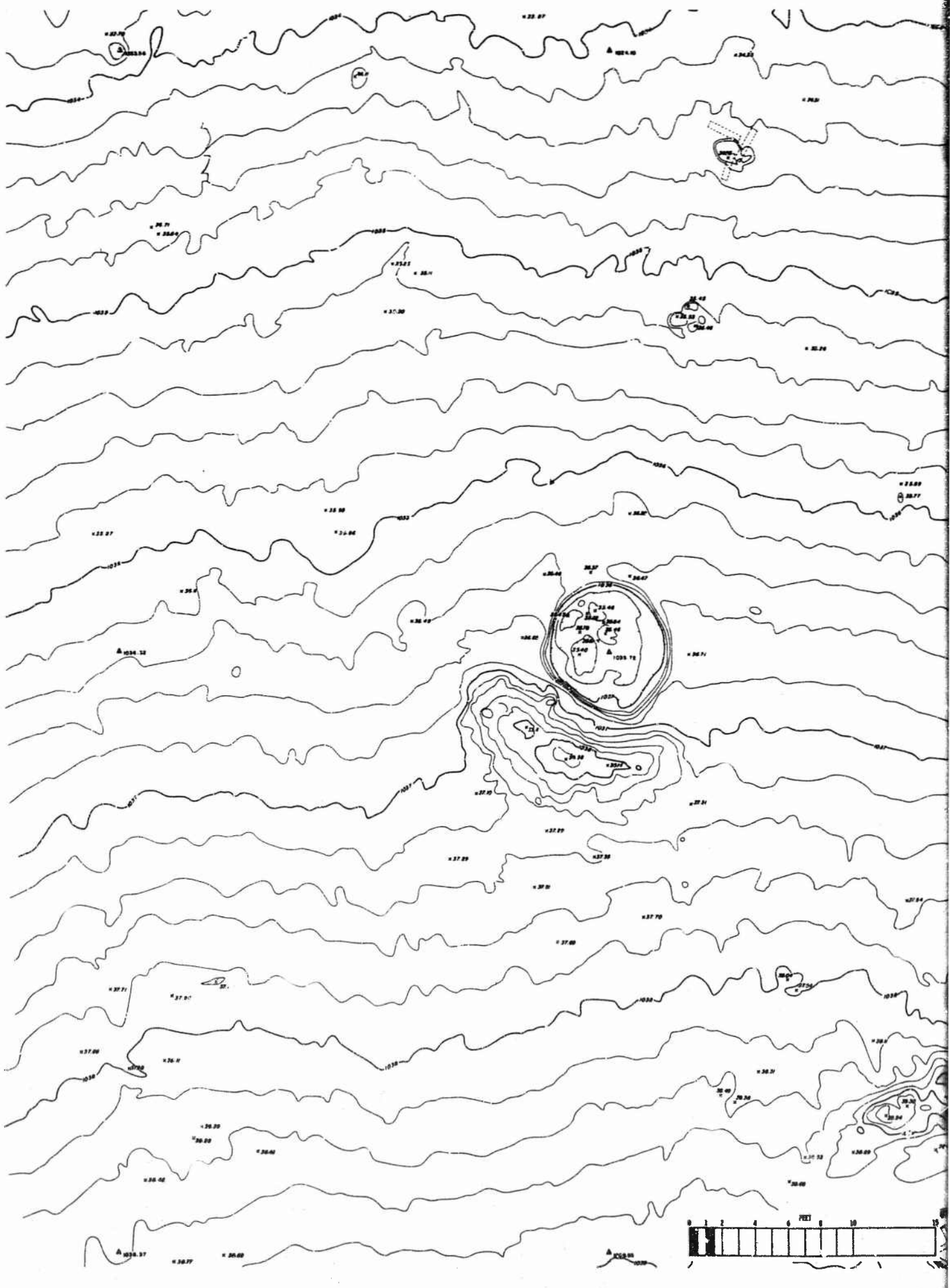
FEET
0
2
4
6
8
10
15

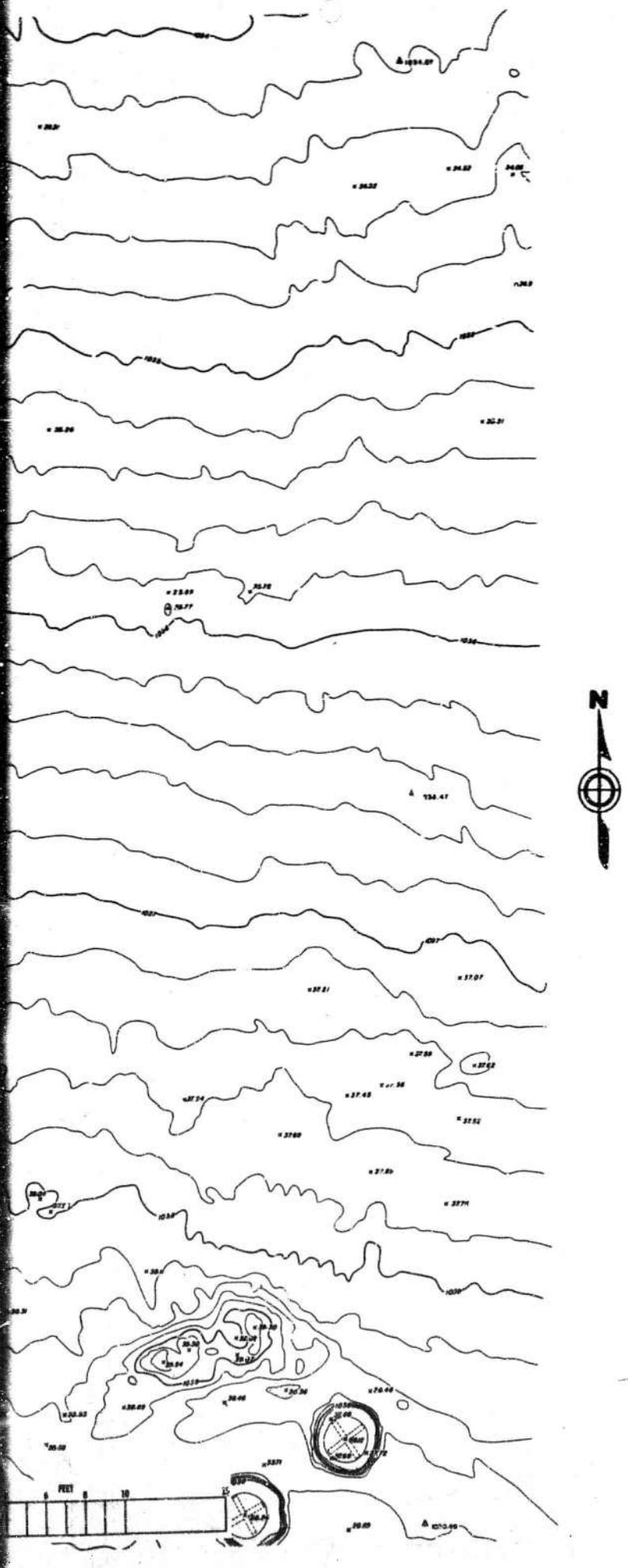

COMPILED BY
AMERICAN AERIAL SURVEYS, INC.
564 S. STEWART DR.
COVINA, CALIFORNIA

CONTOUR INTERVAL 0.2'

Figure I-45. Preshot Topographic Map of Shot LS Region.

2

COMPILED BY
AMERICAN AERIAL SURVEYS, INC.
564 S. STEWART DR.
COVINA, CALIFORNIA

CONTOUR INTERVAL 0.2'

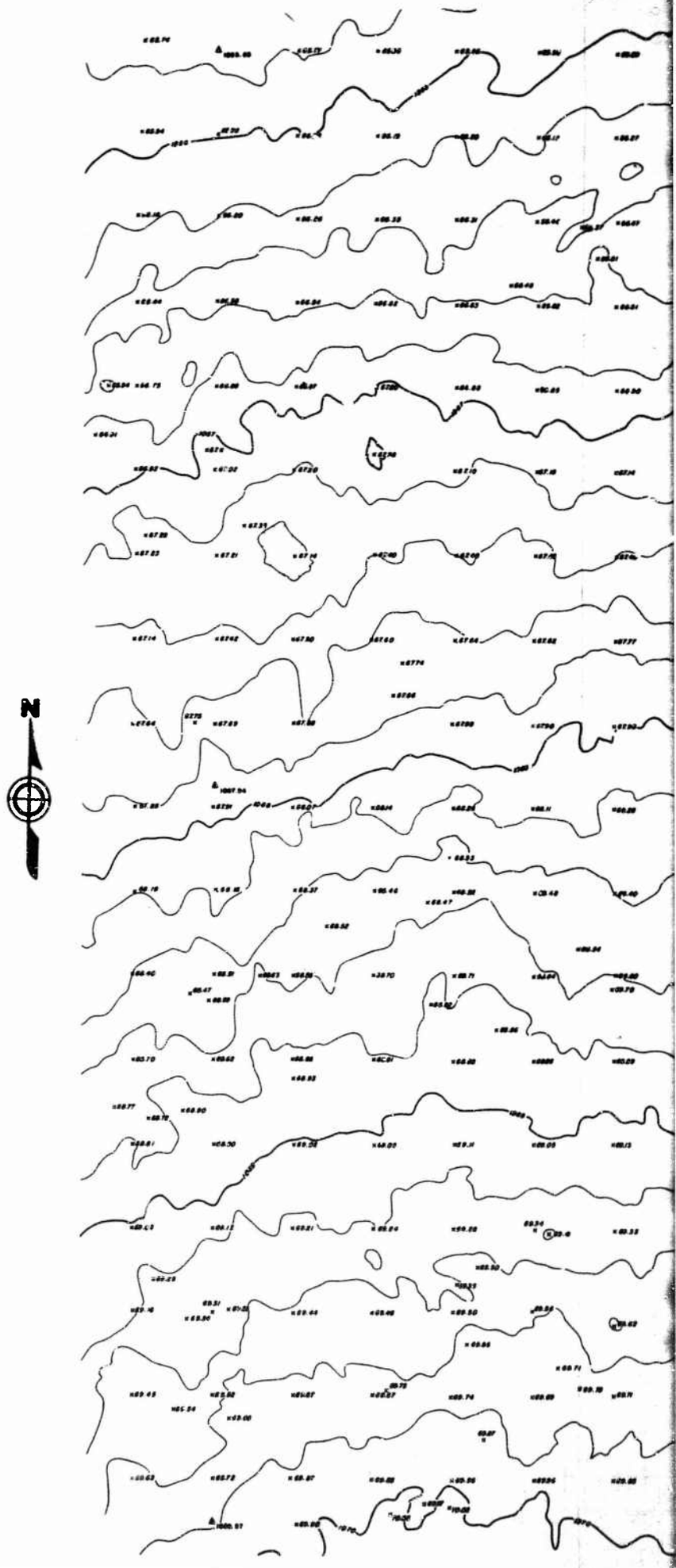

Figure I-46. Preshot Topographic Map of Shot H2 Region.

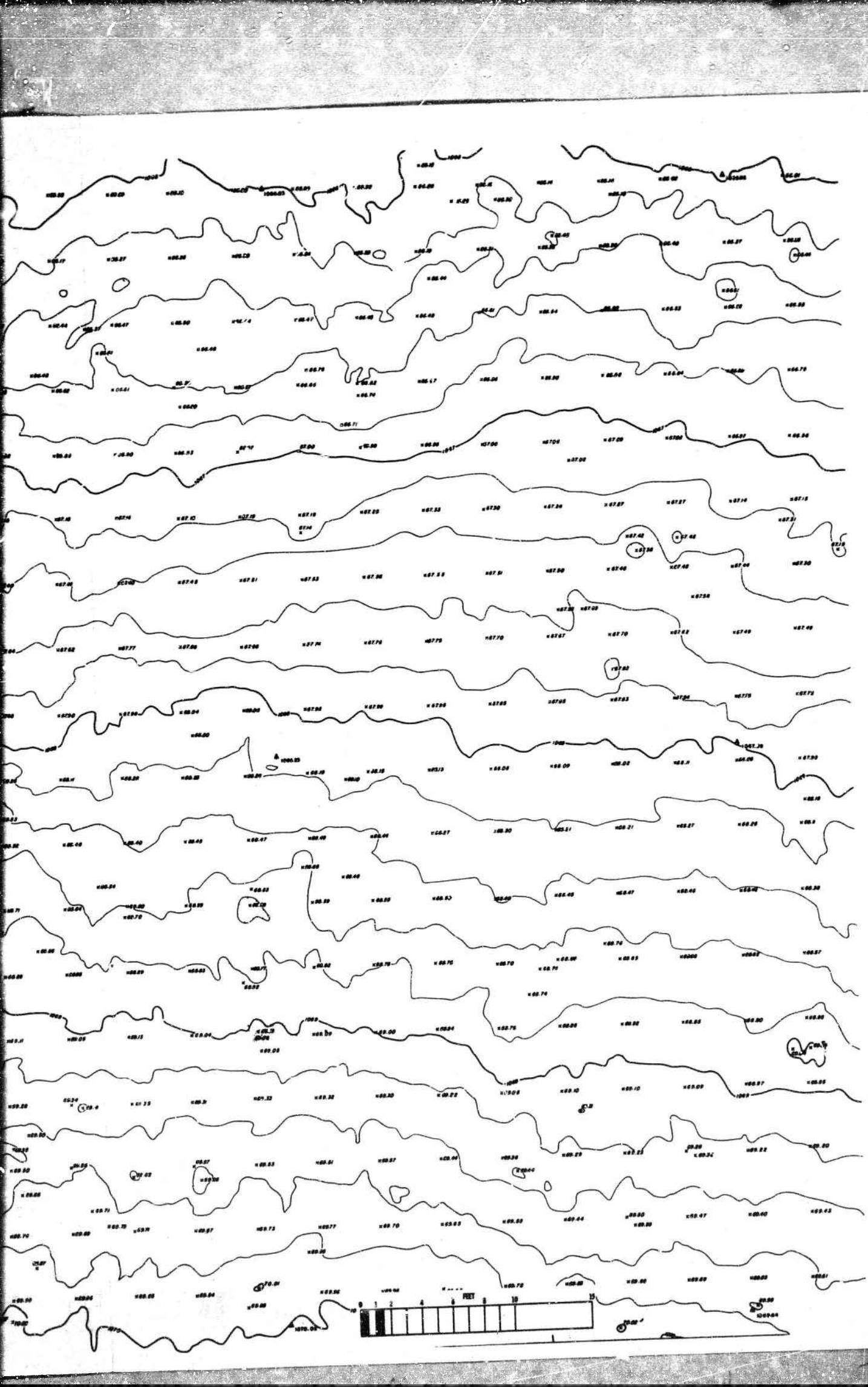

2

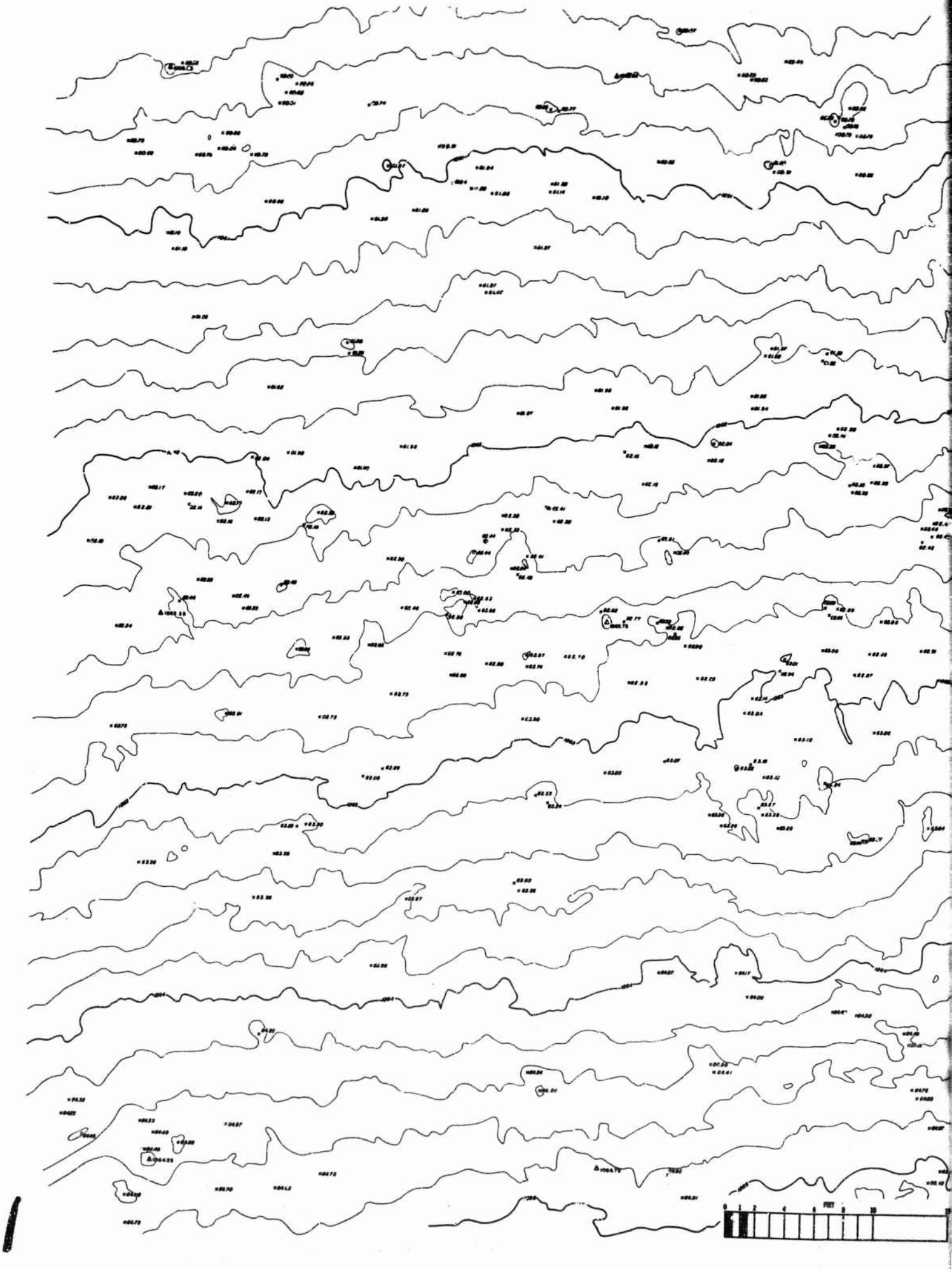

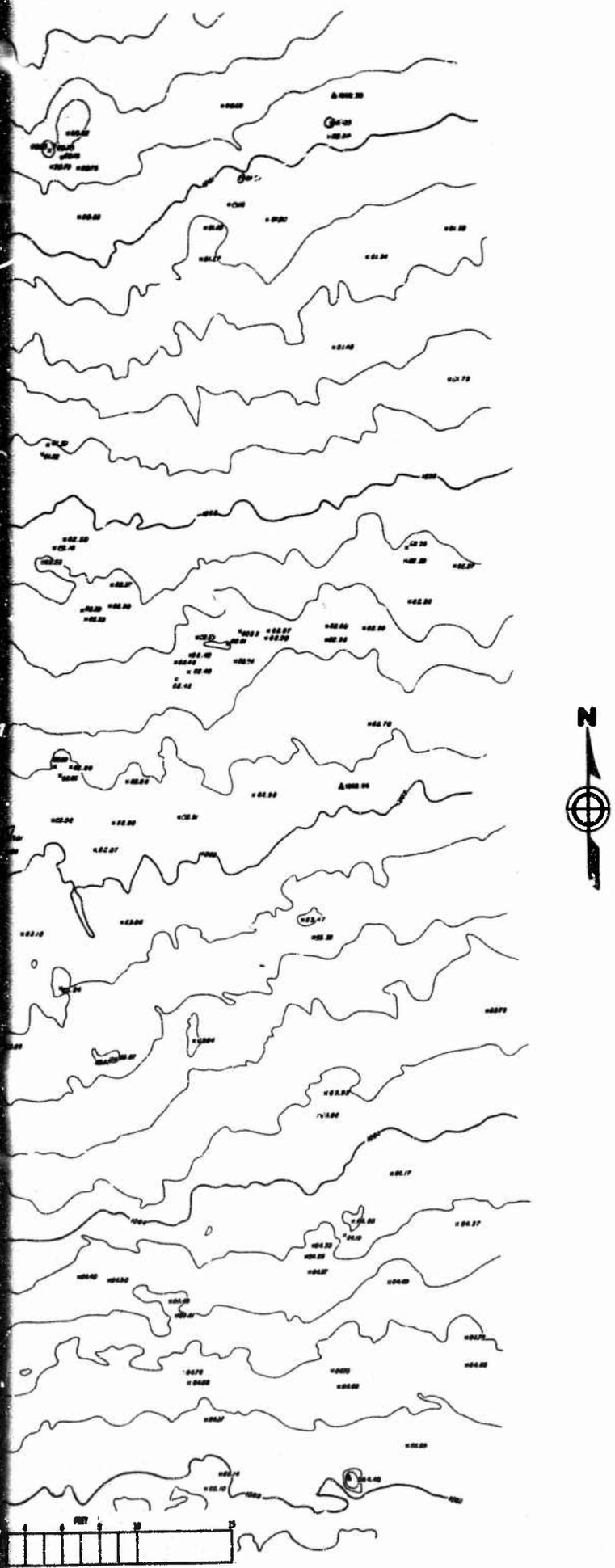

COMPILED BY
AMERICAN AERIAL SURVEYS, INC.
564 S. STEWART DR.
COVINA, CALIFORNIA

CONTOUR INTERVAL 0.2'

Figure I-47. Preshot Topographic Map of Shot Hl Region.

2.

COMPILED BY
AMERICAN AERIAL SURVEYS, INC.
564 S. STEWART DR.
COVINA, CALIFORNIA

CONTOUR INTERVAL 0.2'

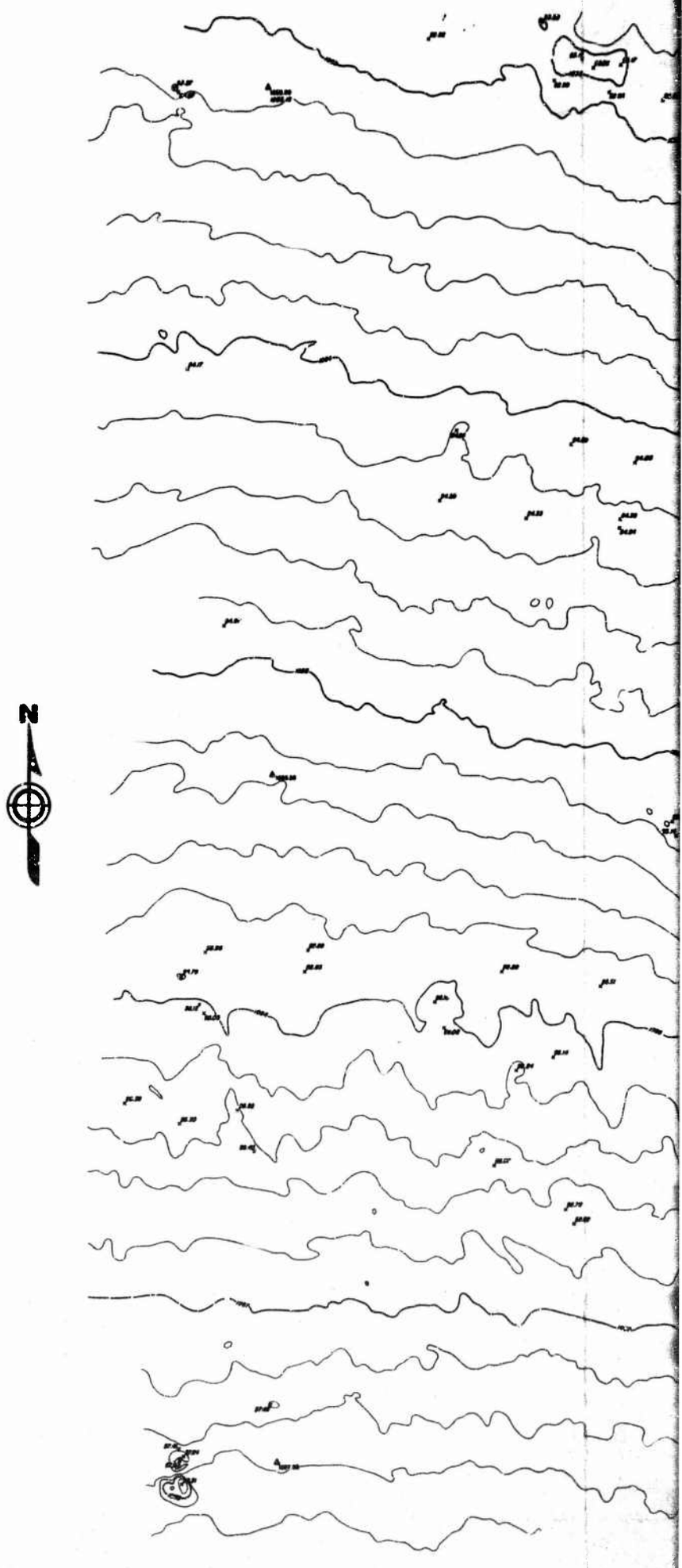

Figure I-48. Preshot Topographic Map of Shot C2 Region.

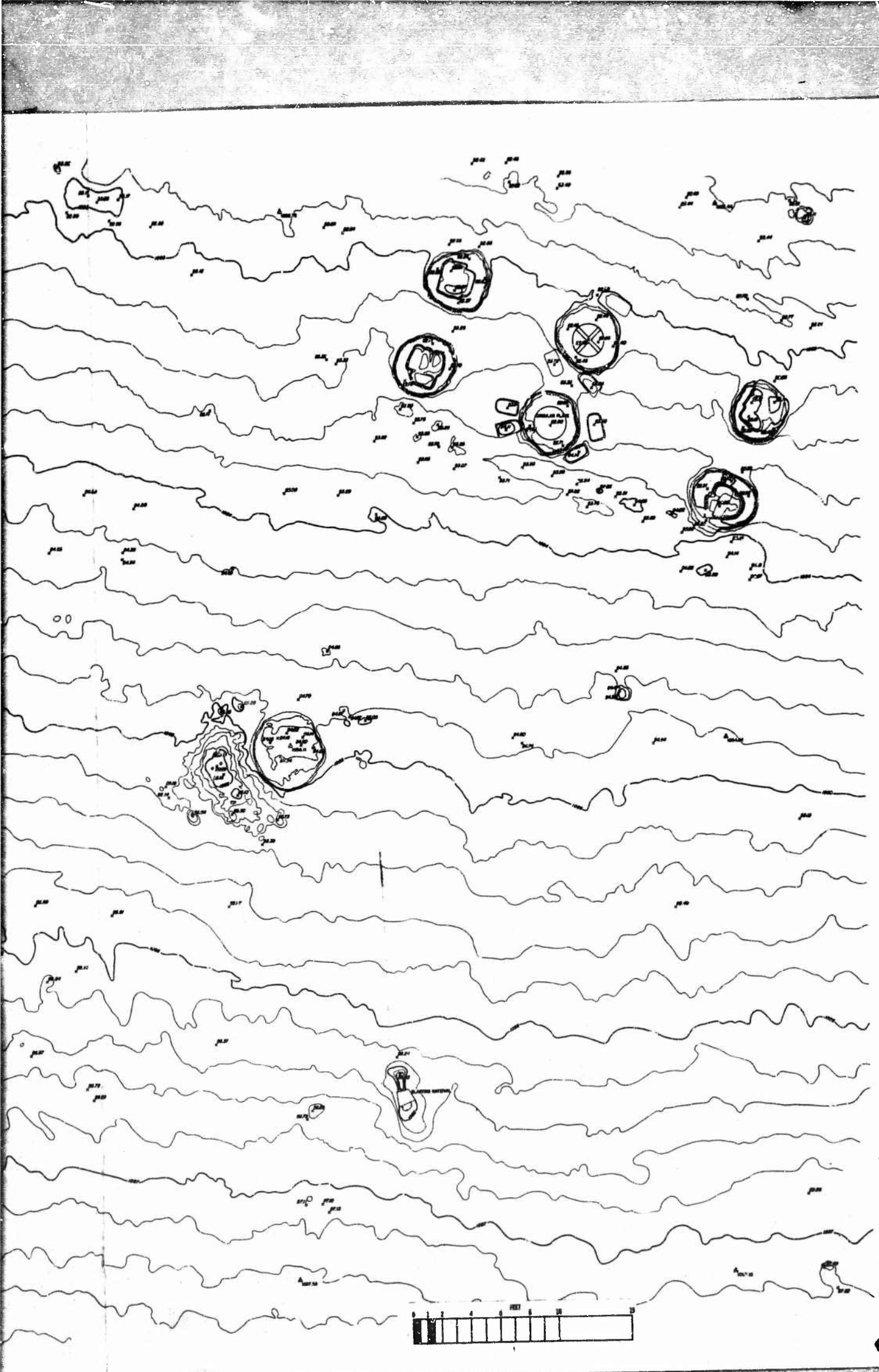

2

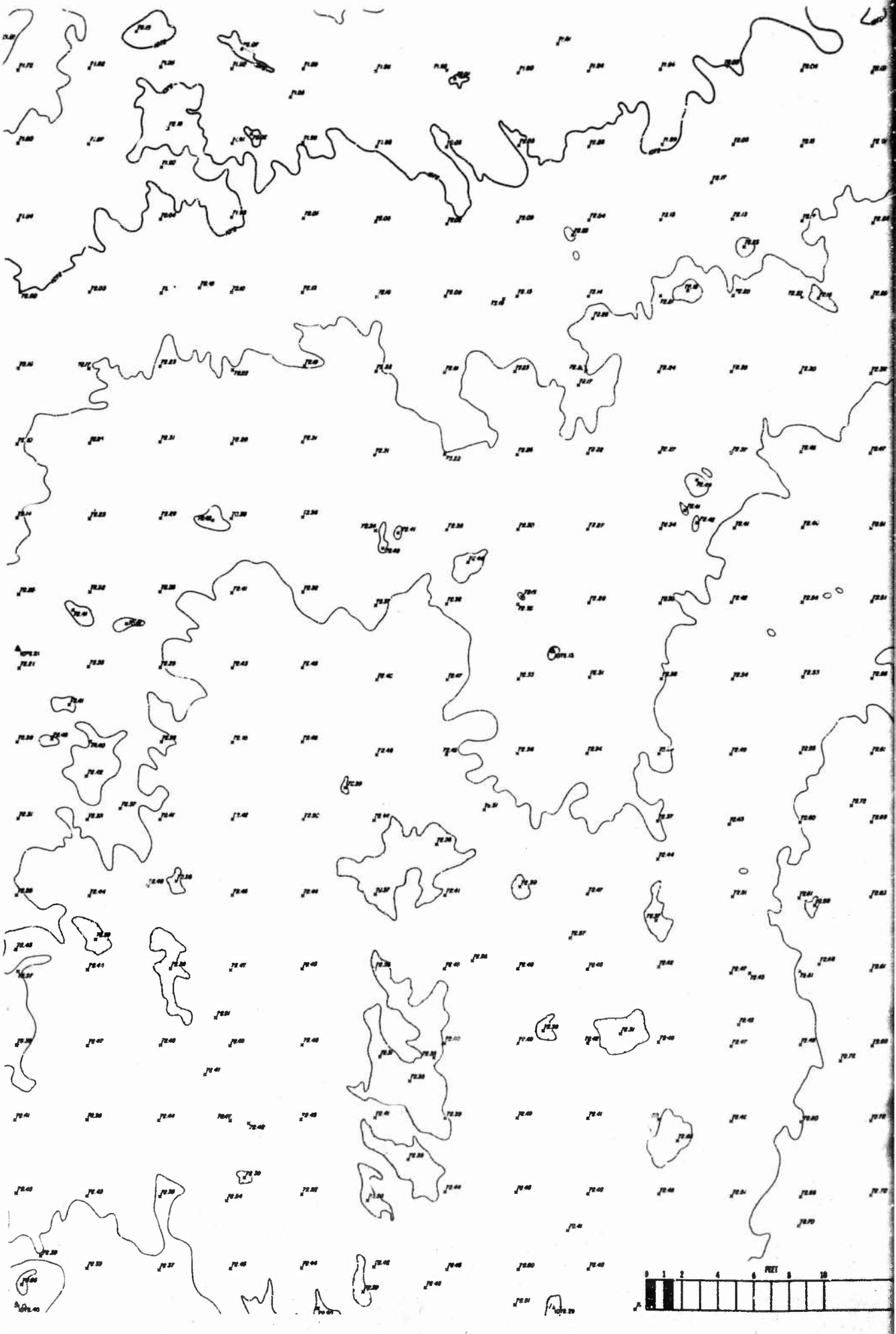
0 1 2 4 6 8 10
FEET

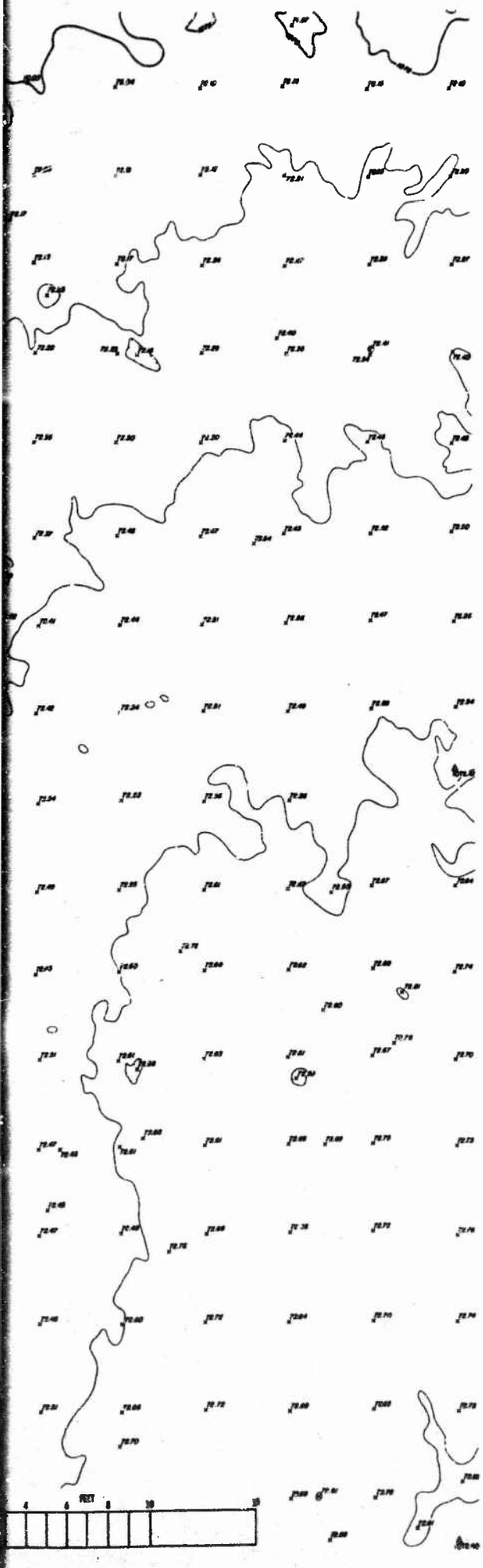

COMPILED BY
AMERICAN AERIAL SURVEYS, INC.
564 S. STEWART DR.
COVINA, CALIFORNIA

CONTOUR INTERVAL 0.2'

Figure I-49. Preshot Topographic Map of Shot ST1 Region.

COMPILED BY
AMERICAN AERIAL SURVEYS, INC.
564 S. STEWART DR.
COVINA, CALIFORNIA

CONTOUR INTERVAL 2'

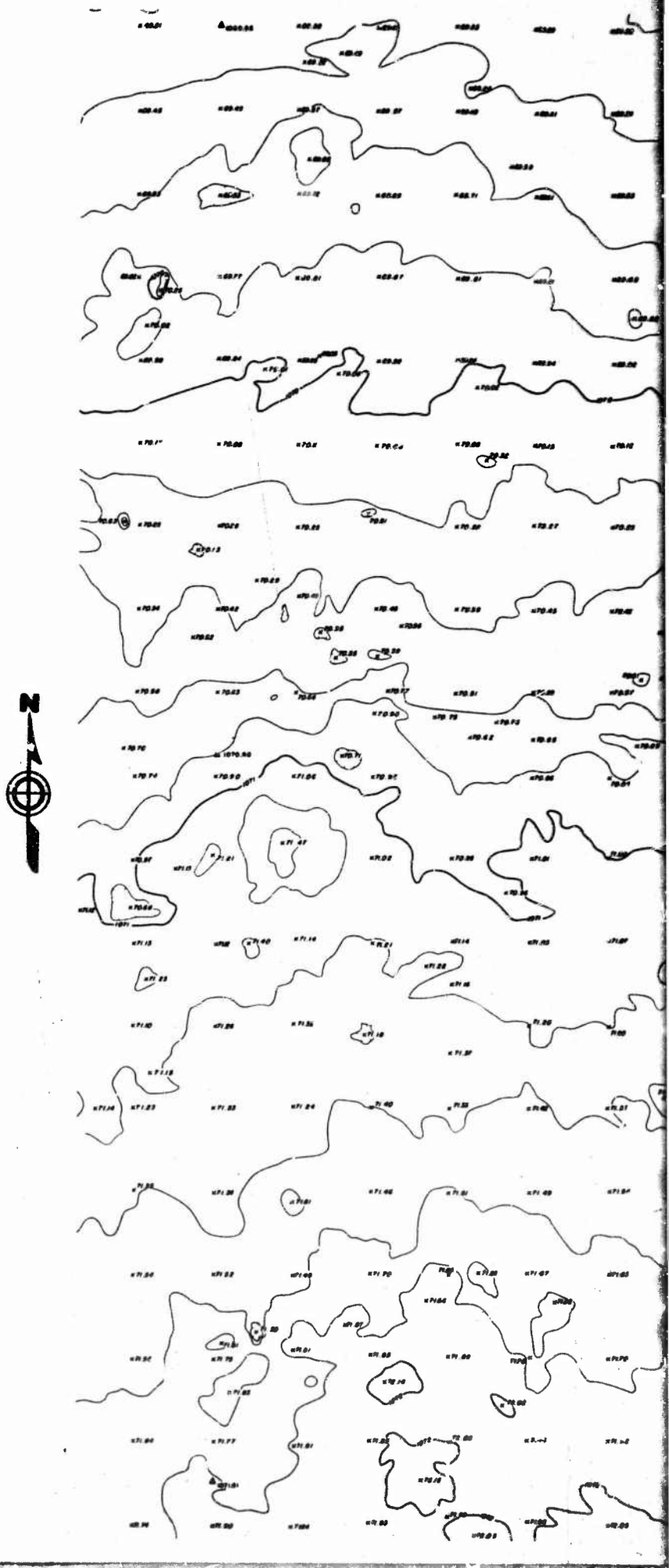

Figure I-50. Preshot Topographic Map of Shot ST2a Region.

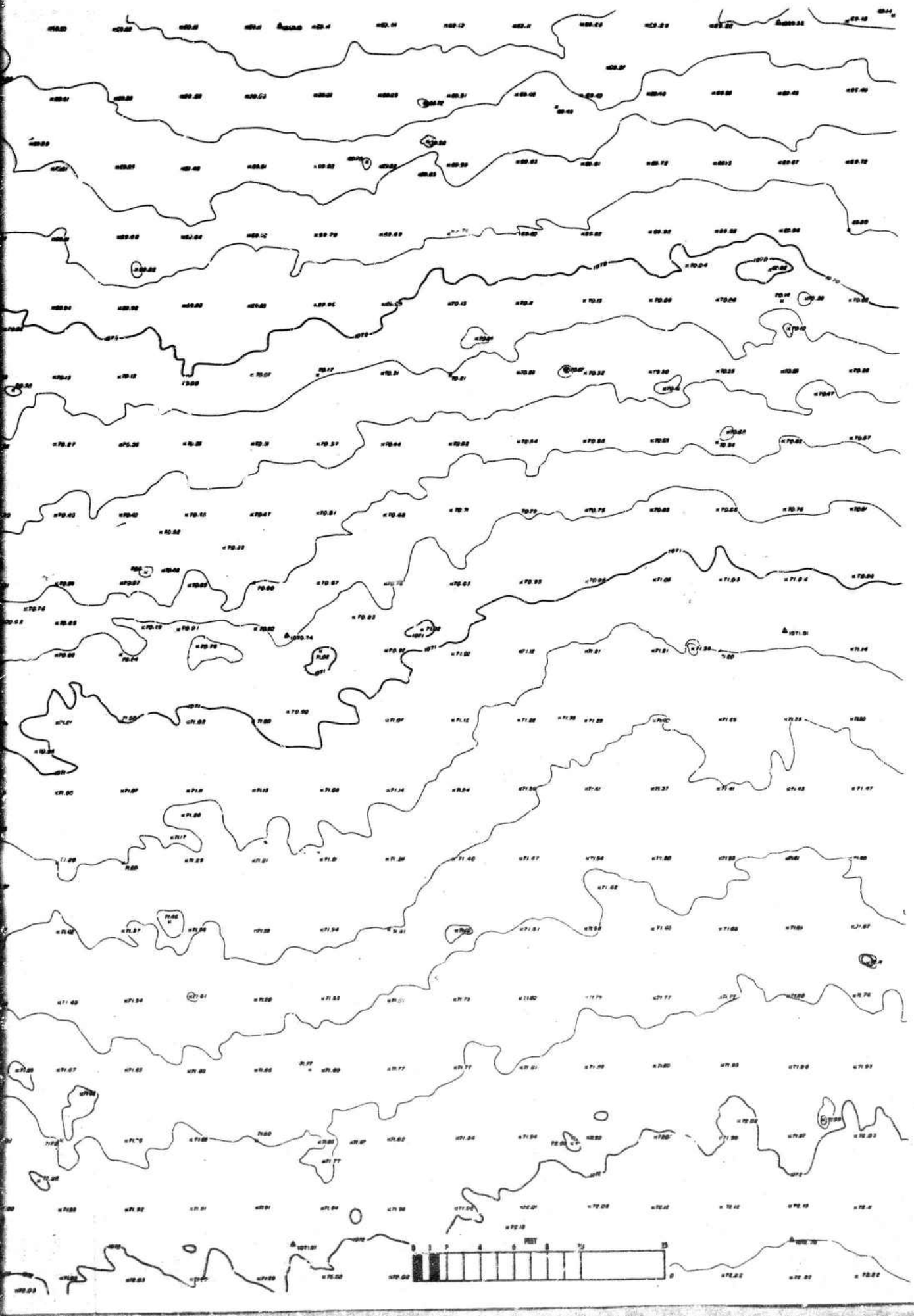

2

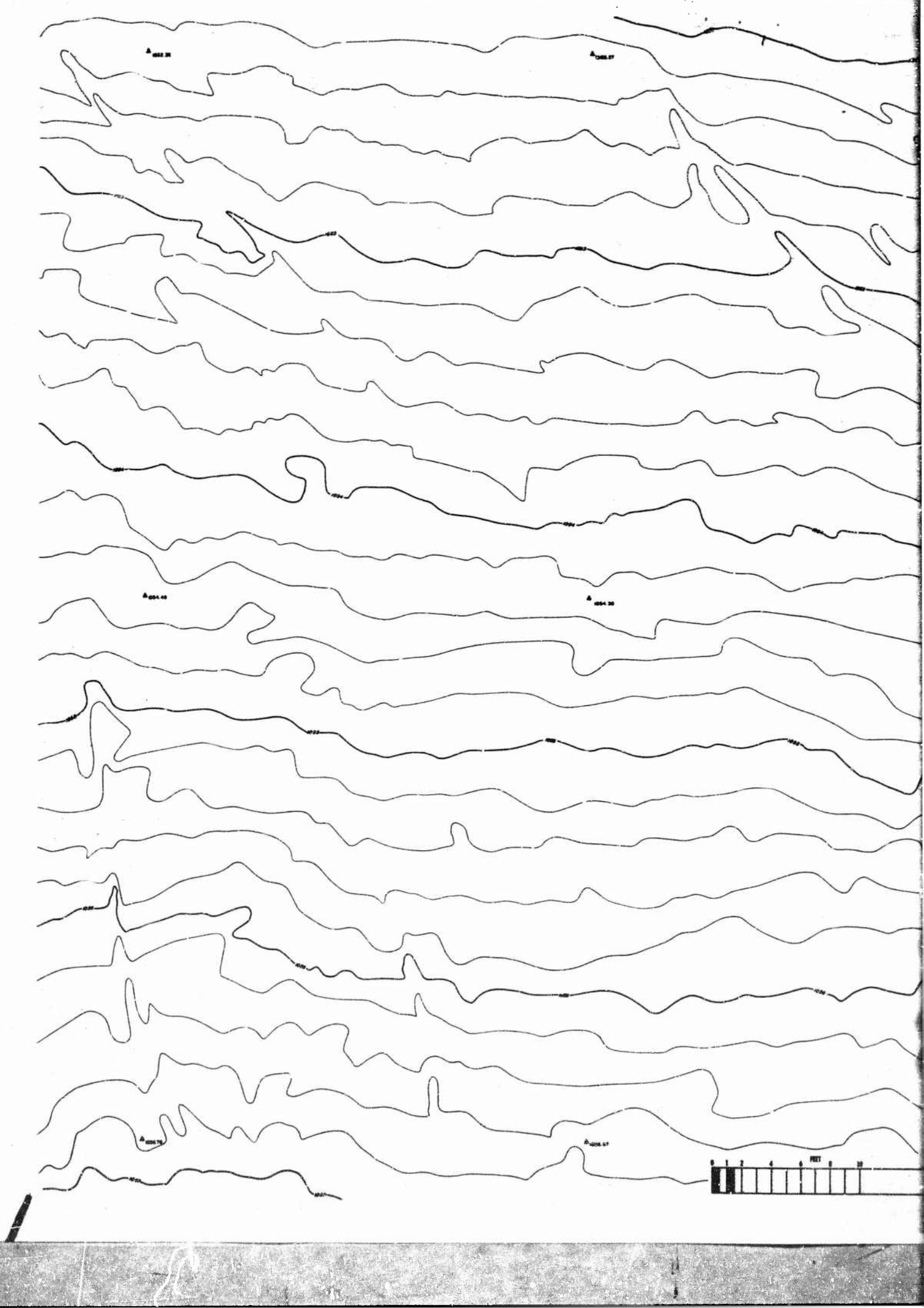
FEET

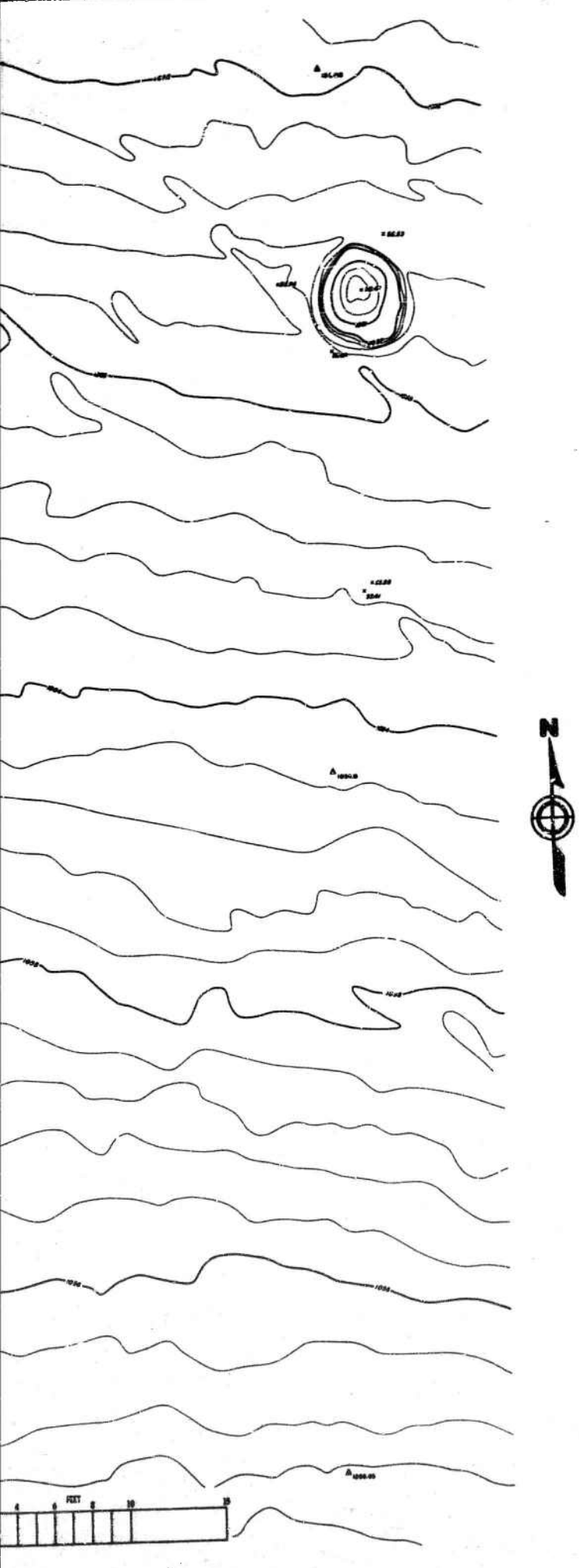

COMPILED BY
AMERICAN AERIAL SURVEYS, INC.
564 S. STEWART DR.
COVINA, CALIFORNIA

CONTOUR INTERVAL 0.2'

Figure I-51. Preshot Topographic Map of Shot ST3a(C3) Region.

2

COMPILED BY
AMERICAN AERIAL SURVEYS, INC.
564 S. STEWART DR.
COVINA, CALIFORNIA

CONTOUR INTERVAL 0.2'

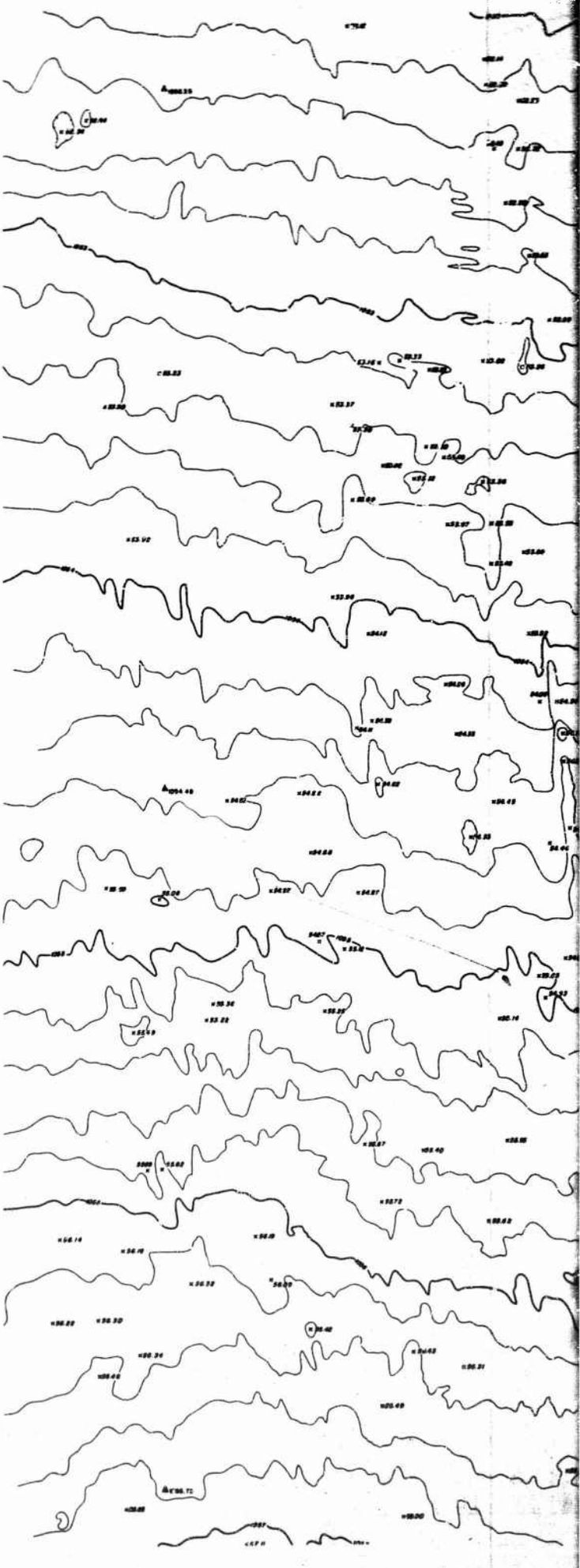

Figure I-52. Preshot Topcgraphic Map of Shot ST3b Region.

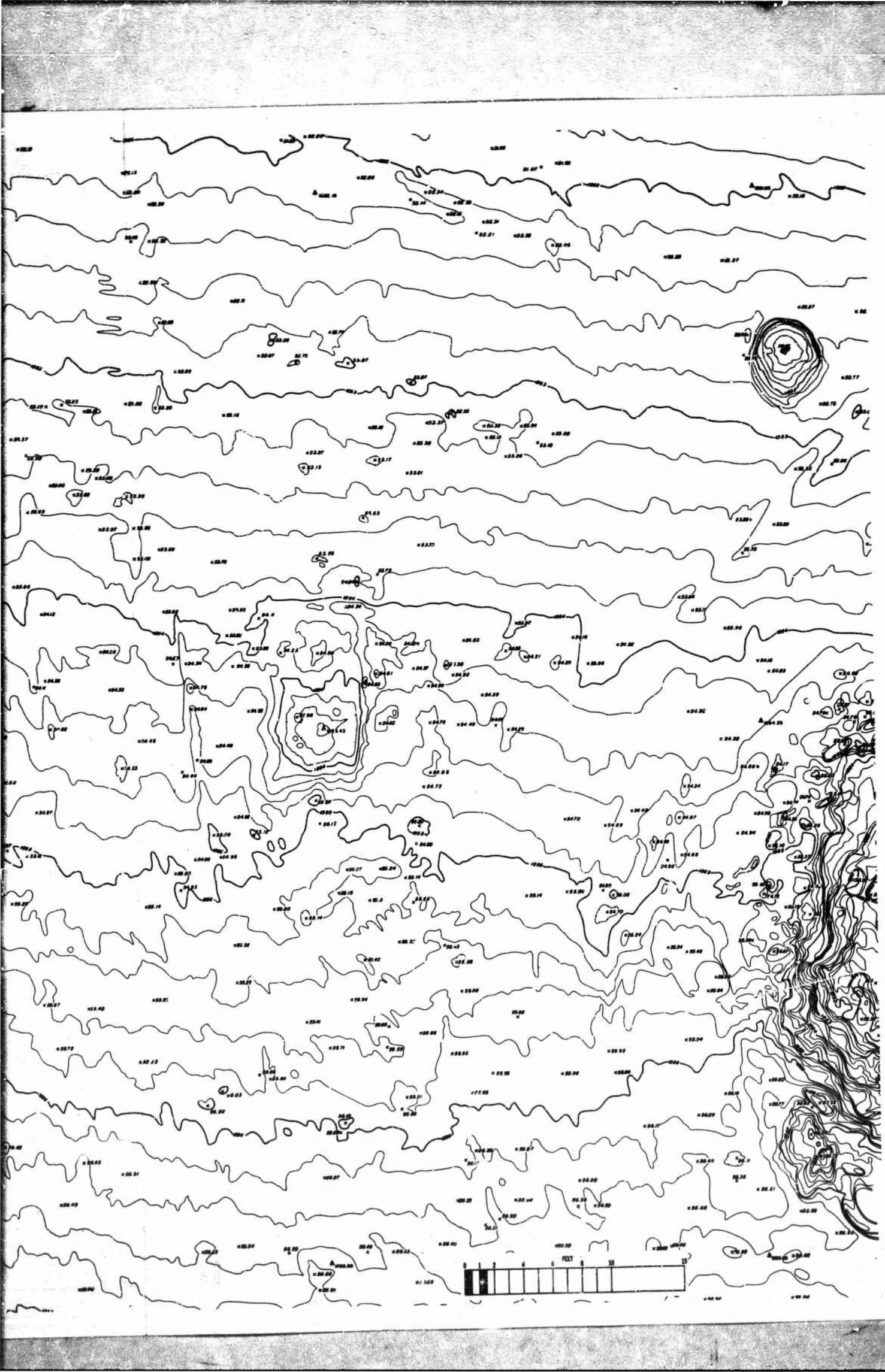

2

APPENDIX II

Raw Ejecta Thickness; Missile and Upthrust Data

Table II.1

PERMANENT VERTICAL DISPLACEMENT FOR MTCE CRATERS

All radial distances and vertical displacements are expressed in feet.

Shot	Radial	Distance from GZ	Vertical Displacement	Shot	Radial	Distance from GZ	Vertical Displacement	Shot	Radial	Distance from GZ	Vertical Displacement
S1(C1)	W	16.3	0.16	S2b	SE	33.0	0	S3b	NW	18.0	0.36
|	W	21.0	0.09	|	NW	16.25	0.3	|	NW	21.0	0.18
S1(C1)	NW	29.0	0.02	|	NW	18.0	0.18	|	NW	25.0	0.07
S2a	SE	17.0	0.05	|	NW	27.5	0.02	|	SW	21.0	0.07
|	SE	20.0	0.04	|	NW	38.0	0	S3b	SW	24.5	0.02
|	SE	24.0	0.02	|	SW	16.75	0.34	S3c	SE	18.3	0.36
|	SE	26.5	0.01	|	SW	21.75	0.08	|	SE	25.3	0.03
|	SE	33.0	0	|	SW	24.8	0.02	|	NW	18.0	0.47
|	NW	16.25	0.07	|	SW	31.5	0	|	NW	21.0	0.25
|	NW	18.0	0.08	|	NE	25.5	0.02	|	NW	25.0	0.09
|	NW	27.5	0	S2b	NE	27.0	0.02	|	SW	21.0	0.10
|	SW	14.5	0.26	S3a	SE	18.3	0.12	S3c	SW	24.5	0.02
|	SW	16.75	0.16	|	SE	21.6	0.02	S4a	SE	12.0	0.31
|	SW	21.75	0.04	|	SE	25.25	0	|	SE	15.3	0.12
|	SW	24.8	0.02	|	NW	18.0	0.24	|	SE	19.3	0.15
|	SW	31.5	0	|	NW	21.0	0.14	|	SE	24.5	0.05
|	NE	14.0	0.42	|	NW	25.0	0.05	|	NW	11.5	0.19
|	NE	25.5	0.02	|	SW	18.0	0.39	|	NW	14.5	0.12
S2a	NE	27.0	0.02	|	SW	21.0	0.02	|	NW	18.5	0.05
S2b	SE	17.0	0.15	S3a	SW	24.5	0	S4a	NW	23.5	0.02
|	SE	20.0	0.10	S3b	SE	18.3	0.31				
|	SE	24.0	0.04	S3b	SE	25.25	0.02				
S2b	SE	26.5	0.03								

Table II-1 (cont'd)

PERMANENT VERTICAL DISPLACEMENT FOR MTCE CRATERS

All radial distances and vertical displacements are expressed in feet.

Shot	Radial	Distance from GZ	Vertical Displacement	Shot	Radial	Distance from GZ	Vertical Displacement	Shot	Radial	Distance from GZ	Vertical Displacement
S4a	SW	12.0	0.20	S4b	NE	24.0	0.04	S4d	SW	14.75	0.30
|	SW	14.75	0.11	S4c	SE	12.0	0.94	|	SW	18.5	0.18
|	SW	18.5	0.06	|	SE	15.3	0.54	S4d	SW	22.0	0.14
|	SW	22.0	0.04	|	SE	19.3	0.66	LS	SE	25.0	0.24
|	NE	12.0	0.39	|	SE	24.5	0.10	|	SE	28.3	0.26
|	NE	15.0	0.10	|	NW	11.5	0.72	|	SE	31.5	0.18
|	NE	19.25	0.07	|	NW	14.5	0.28	|	SE	46.1	0.07
S4a	NE	24.0	0.04	|	NW	18.5	0.08	|	NW	24.5	0.71
S4b	SE	12.0	0.90	|	NW	23.5	0.04	|	NW	27.5	0.29
|	SE	15.3	0.52	|	SW	12.0	0.45	|	NW	31.5	0.14
|	SE	19.3	0.39	|	SW	14.75	0.26	|	SW	24.5	0.44
|	SE	24.5	0.10	|	SW	18.5	0.1[illegible]	|	SW	27.5	0.15
|	NW	11.5	0.44	|	SW	22.0	0.12	|	SW	32.0	0.08
|	NW	14.5	0.16	|	NE	12.0	0.69	|	SW	36.5	0.06
|	NW	18.5	0.08	|	NE	15.0	0.34	|	SW	46.1	0.05
|	NW	23.5	0.05	|	NE	19.25	0.14	|	NE	25.0	0.32
|	SW	12.0	0.44	S4c	NE	24.0	0.04	|	NE	28.0	0.16
|	SW	14.75	0.20	S4d	SE	12.0	1.09	|	NE	32.0	0.10
|	SW	18.5	0.13	|	SE	15.3	0.56	LS	NE	37.0	0.06
|	SW	22.0	0.09	|	SE	24.5	0.10				
|	NE	12.0	0.59	|	NW	14.5	0.28				
|	NE	15.0	0.18	|	NW	18.5	0.08				
S4b	NE	19.25	0.10	S4d	NW	23.5	0.04				

Table II-1 (cont'd)

PERMANENT VERTICAL DISPLACEMENT FOR MTCF CRATERS

All radial distances and vertical displacements are expressed in feet.

Shot	Radial	Distance from GZ	Vertical Displacement	Shot	Radial	Distance from GZ	Vertical Displacement	Shot	Radial	Distance from GZ	Vertical Displacement
H2	SE	26.1	0.30	H2	E	30.0	0.11	C2	NW	29.6	0.03
|	SE	34.9	0.10	|	W	23.3	0.38	|	SW	19.0	0.18
|	SE	46.1	0.03	|	W	26.4	0.14	|	SW	23.0	0.10
|	NW	34.5	0.16	H2	W	30.0	0.15	|	SW	26.0	0.06
|	NW	46.1	0.01	H1	SE	17.3	0.38	|	SW	30.6	0.03
|	SW	26.0	0.91	|	SE	25.0	0.02	|	NE	17.3	0.25
|	SW	36.1	0.14	|	NW	20.0	0.42	|	NE	20.25	0.12
|	SW	46.1	0.02	|	NW	27.0	0	|	NE	24.3	0.04
|	NE	20.1	0.98	|	SW	12.5	0.26	|	NE	29.0	0.03
|	NE	23.0	0.44	|	SW	14.0	0.08	C2	NE	33.5	0
|	NE	26.0	0.20	|	SW	19.25	0.02	ST2a	SE	13.0	0.41
|	NE	33.3	0.06	|	SW	21.25	0.02	|	SE	16.5	0.02
|	NE	46.1	0.01	|	SW	26.5	0	|	SE	21.0	0
|	S	20.4	0.62	|	NE	13.25	0.30	|	NW	5.5	0.08
|	S	23.3	0.45	H1	NE	22.5	0.04	|	NW	8.0	0.05
|	S	25.7	0.17	C2	SE	19.0	0.24	|	NW	10.5	0.03
|	S	35.0	0.07	|	SE	23.0	0.08	|	NW	15.25	0.01
|	N	23.8	0.32	|	SE	27.0	0.04	|	NW	19.0	0.04
|	N	26.5	0.15	|	SE	31.3	0.02	|	NW	22.5	0.02
|	N	35.0	0.04	|	NW	13.6	0.55	|	SW	10.0	0.09
|	E	20.2	0.36	|	NW	15.6	0.35	|	SW	14.25	0.17
|	E	23.2	0.23	|	NW	20.75	0.08	|	SW	19.0	0.02
H2	E	26.1	0.16	C2	NW	25.0	0.04	ST2a	SW	22.0	0.01

Table II-1 (cont'd)

PERMANENT VERTICAL DISPLACEMENT FOR MTCE CRATERS

All radial distances and vertical displacements are expressed in feet.

Shot	Radial	Distance from GZ	Vertical Displacement	Shot	Radial	Distance from GZ	Vertical Displacement	Shot	Radial	Distance from GZ	Vertical Displacement
ST2a	NE	14.25	0.07	ST3a(C3)	SW	13.25	0.03	ST3b	SW	20.0	0.03
|	NE	19.0	0.01	|	NE	7.5	0.10	ST3c	SE	15.6	0.09
ST2a	NE	22.5	0	|	NE	12.0	0.05	|	SE	18.0	0.08
ST2b	SE	16.5	0.06	ST3a(C3)	NE	16.0	0	|	SE	21.3	0.03
|	SE	21.0	0.02					|	SE	24.0	0
|	NW	15.25	0.17	ST3b	SE	12.0	0.42	|	NW	13.0	0.44
|	NW	19.0	0.09	|	SE	15.6	0.07	|	NW	16.0	0.12
|	NW	22.5	0.02	|	SE	18.0	0.05	|	NW	17.6	0.07
|	SW	10.0	0.56	|	SE	21.3	0.03	|	NW	22.0	0.02
|	SW	19.0	0.03	|	SE	24.0	0	|	NW	25.0	0.02
|	SW	22.0	0.01	|	NW	11.0	0.24	|	SW	13.25	0.45
|	NE	14.25	0.28	|	NW	13.0	0.26	|	SW	15.0	0.30
|	NE	19.0	0.04	|	NW	16.0	0.10	|	SW	18.5	0.32
|	NE	22.5	0.03	|	NW	17.6	0.06	|	SW	24.0	0.03
ST2b	NE	27.0	0	|	NW	22.0	0.02	|	NE	12.0	0.32
ST3a(C3)	SE	5.5	0.17	|	NW	25.0	0.02	|	NE	16.0	0.03
|	SE	7.5	0.19	|	SW	10.75	0.47	ST3c	NE	20.0	0.02
|	SE	12.0	0.03	|	SW	13.25	0.18				
|	SE	18.0	0.03	|	SW	15.0	0.20				
|	NW	7.0	0.15	|	SW	18.5	0.20				
|	NW	16.0	0.02	|	SW	24.0	0.03				
|	NW	17.6	0.02	|	NE	12.0	0.23				
ST3a(C3)	NW	22.0	0	ST3b	NE	16.0	0.08				

Table II-2

EJECTA THICKNESS DATA

All ejecta thickness data are expressed in feet.

Shot	NE Radial		NW Radial		SE Radial		SW Radial	
	Distance from GZ	Ejecta Thickness	Distance from GZ	Ejecta Thickness	Distance from GZ	Ejecta Thickness	Distance from GZ	Ejecta Thickness
S2a	10.7	0	7.8	0	14.0	0	11.5	0
	12.0	0.65	10.0	0.8	17.0	0.7	14.0	1.3
	17.0	0.01	15.0	0.6	22.0	0.05	19.0	0.35
	—	—	20.0	0.6	—	—	24.0	0.1
	—	—	25.0	0.2	—	—	29.0	0.25
	—	—	30.0	0.15	—	—	34.0	0.15
S2a	—	—	35.0	0.1	—	—	—	—
S2b	14.2	0	13.5	0	18.2	0	15.5	0
	15.0	1.3	16.0	0.75	22.0	1.1	16.0	1.3
	20.0	0.8	21.0	0.4	27.0	0.1	21.0	0.8
	25.0	0.2	26.0	0.45	—	—	26.0	1.1
	30.0	0.15	31.0	0.2	—	—	31.0	0.55
S2b	—	—	36.0	0.1	—	—	36.0	0.2
S3a	—	—	11.5	0	11.5	0	13.0	0
	—	—	15.5	0.95	12.5	1.5	22.2	0.7
	—	—	20.5	0.15	17.5	0.69	27.0	0.35
	—	—	25.5	0.31	22.5	0.15	32.0	0.4
	—	—	30.5	0.12	27.5	0.15	37.0	0.3
S3a	—	—	35.5	0.1	32.5	0.08	—	—
S3b	—	—	13.7	0	11.5	0	13.3	0
	—	—	18.0	0.2	21.2	0.7	18.0	0.8
	—	—	23.0	0.1	26.0	0.05	23.0	0.5
	—	—	—	—	31.0	0.1	28.0	0.5
	—	—	—	—	36.0	0.1	33.0	0.35
S3b	—	—	—	—	—	—	38.0	0.55

Table II-2 (cont'd)

EJECTA THICKNESS DATA

All ejecta thickness data are expressed in feet.

Shot	NE Radial		NW Radial		SE Radial		SW Radial	
	Distance from GZ	Ejecta Thickness	Distance from GZ	Ejecta Thickness	Distance from GZ	Ejecta Thickness	Distance from GZ	Ejecta Thickness
S3c	—	—	14.5	0	16.0	0	14.6	0
	—	—	20.5	0.85	19.5	1.45	23.5	0.9
	—	—	25.5	0.05	24.5	0.3	28.5	0.55
	—	—	30.5	0.5	—	—	33.5	0.55
	—	—	35.5	0.2	—	—	38.5	0.42
S3c	—	—	40.5	0.01	—	—	—	—
S4a	11.3	0	11.0	0	10.0	0	10.0	0
	14.0	1.5	13.0	0.65	28.0	1.75	11.6	0.65
	19.0	0.22	18.0	0.2	31.0	1.5	17.0	0.3
	24.0	0.31	23.0	0.1	36.0	1.0	22.0	0.15
S4a	29.0	0.25	23.0	0.05	41.0	0.9	—	—
S4b	13.7	0	13.6	0	12.8	0	13.2	0
	17.5	0.9	18.0	0.9	28.0	2.0	15.5	0.4
	22.5	0.3	23.0	0.3	33.0	0.8	20.5	0.3
	27.5	0.75	28.0	0.05	38.0	1.5	25.5	0.22
	33.5	0.15	33.0	0.05	42.0	0.85	—	—
S4b	38.5	0.35	—	—	—	—	—	—
S4c	13.0	0	13.8	0	14.0	0	13.5	0
	17.7	0.9	20.5	0.9	29.0	2.0	19.5	0.9
	23.0	0.55	25.5	0.51	34.0	1.2	24.5	0.25
	28.0	0.7	30.5	0.2	39.0	0.8	—	—
	33.0	0.25	35.5	0.2	44.0	1.21	—	—
S4c	38.0	0.3	40.5	0.12	—	—	—	—

Table II-2 (cont'd)

EJECTA THICKNESS DATA

All ejecta thickness data are expressed in feet.

Shot	NE Radial		NW Radial		SE Radial		SW Radial	
	Distance from GZ	Ejecta Thickness	Distance from GZ	Ejecta Thickness	Distance from GZ	Ejecta Thickness	Distance from GZ	Ejecta Thickness
S4d	13.5	0	16.0	0	14.0	0	15.5	0
	18.0	1.25	20.5	1.7	28.5	1.9	21.5	0.55
	23.0	0.6	26.0	0.4	33.5	1.25	—	—
	28.0	0.6	31.0	0.2	38.5	1.0	—	—
	33.0	0.3	36.0	0.15	43.5	0.78	—	—
S4d	—	—	41.0	0.15	—	—	—	—
LS	18.0	0	21.0	0	21.3	0	18.7	0
	20.05	2.5	23.7	0.6	22.0	1.95	20.1	1.45
	25.05	0.5	28.5	0.38	27.0	1.05	25.1	1.25
	30.05	0.01	33.5	0.12	33.0	0.1	30.1	0.2
LS	—	—	—	—	—	—	35.1	0.16
H2	14.0	0	19.5	0	17.0	0	16.5	0
	19.75	1.05	29.0	1.95	21.5	2.15	21.0	1.05
	25.0	0.2	34.0	0.8	26.5	1.5	26.0	0.2
	30.0	0.11	39.0	0.4	31.5	1.0	31.0	0.18
	35.0	0.1	43.0	0.3	36.5	1.0	36.0	0.06
H2	—	—	—	—	41.5	0.6	—	—
H1	10.2	0	—	—	12.5	0	8.0	0
	12.2	0.55	—	—	16.2	0.55	12.4	1.0
	17.0	0.4	—	—	21.0	0.1	17.0	0.1
	22.0	0.1	—	—	26.0	0.2	22.0	0.05
	27.0	0.05	—	—	31.0	0.01	—	—
H1	—	—	—	—	36.0	0.02	—	—

Table II-2 (cont'd)

EJECTA THICKNESS DATA

All ejecta thickness data are expressed in feet.

Shot	NE Radial		NW Radial		SE Radial		SW Radial	
	Distance from GZ	Ejecta Thickness	Distance from GZ	Ejecta Thickness	Distance from GZ	Ejecta Thickness	Distance from GZ	Ejecta Thickness
C2	12.5	0	14.8	0	13.5	0	14.7	0
	14.5	0.7	19.0	1.6	21.0	1.8	17.2	1.3
	19.5	0.1	24.0	0.3	26.0	1.05	23.0	0.75
	24.5	0.01	29.0	0.5	31.0	1.08	28.0	0.2
	—	—	34.0	0.1	36.0	0.8	33.0	0.1
	—	—	39.0	0.1	41.0	0.15	—	—
C2	—	—	44.0	0.18	—	—	—	—
ST2a	10.5	0	4.2	0	9.0	0	4.8	0
	18.0	1.7	8.5	0.2	10.0	0.1	7.5	1.1
	—	—	13.5	0.2	15.0	0.1	12.5	0.1
ST2a	—	—	18.5	0.12	20.0	0.01	—	—
ST2b	6.8	0	9.5	0	12.2	0	7.3	0
	7.5	0.5	13.0	1.5	17.0	0.75	8.5	0.4
	12.5	0	18.0	0.32	22.0	0.2	13.5	0.1
	17.5	0.3	23.0	0.32	27.0	0.1	18.5	0.25
	22.5	0.11	28.0	0.1	32.0	0.1	22.5	0.1
ST2b	—	—	33.0	0.05	37.0	0.05	—	—
ST3a(C3)	7.0	0	6.0	0	5.2	0	7.2	0
	—	—	—	—	12.5	0.05	7.5	0.1
	—	—	—	—	—	—	12.5	0.05
ST3a(C3)	—	—	—	—	—	—	17.5	0.05

Table II-2 (cont'd)

EJECTA THICKNESS DATA

All ejecta thickness data are expressed in feet.

Shot	NE Radial		NW Radial		SE Radial		SW Radial	
	Distance from GZ	Ejecta Thickness	Distance from GZ	Ejecta Thickness	Distance from GZ	Ejecta Thickness	Distance from GZ	Ejecta Thickness
ST3b	10.5	0	8.3	0	9.1	0	8.0	0
	—	—	9.0	0.3	11.0	0.95	13.2	1.55
	—	—	—	—	16.0	0.15	18.0	1.15
	—	—	—	—	21.0	0.1	23.0	1.0
ST3b	—	—	—	—	—	—	28.0	0.45
ST3c	12.3	0	10.0	0	12.0	0	11.8	0
	13.4	0.1	12.7	0.35	17.0	0.5	17.5	0.45
	—	—	18.0	0.07	22.0	0.2	22.5	0.15
	—	—	—	—	27.0	0.15	—	—
ST3c	—	—	—	—	32.0	0.1	—	—

Table II-3

EJECTA DATA RESULTING FROM AIR FORCE MISSILE SURVEY

Shot	Distance from GZ	Total Weight	No. of Missiles	Shot	Distance from GZ	Total Weight	No. of Missiles	Shot	Distance from GZ	Total Weight	No. of Missiles
—	(ft)	(lb)	—	—	(ft)	(lb)	—	—	(ft)	(lb)	—
S2a	80±5	1061	75	S4b	36-50	854	148	LS	50±5	2831	269
|	130±5	470	69	|	50-70	529	84	|	75±5	3001	314
|	180±5	216	38	|	70-110	1345	194	|	100-110	2185	267
|	230±5	73	33	|	110-150	478	70	|	110-130	2269	220
|	280±5	6	4	S4b	150-	1542	268	|	130-170	2994	318
|	300-400	98	39					|	170-210	1956	209
|	400-500	65	28	S4c	35-45	568	85	|	210-250	1649	213
|	500-600	64	36		45-65	773	80	|	250-290	1459	168
S2a	600-700	32	18		65-105	1366	155	|	290-340	1349	146
					105-145	633	76	LS	340-	3952	409
S4a	35-45	631	75	S4c	145-	1064	121				
|	45-65	845	86								
|	65-85	686	81	S4d	35-45	322	35				
|	85-125	921	119	|	45-60	252	33				
|	125-165	550	80	|	60-80	595	43				
|	165-205	580	60	|	80-100	589	54				
S4a	205-	1274	227	|	100-140	312	61				
				|	140-180	273	46				
				|	180-230	357	48				
				|	230-300	310	45				
				|	300-400	255	37				
				S4d	400-700	134	28				

Table II-3 (cont'd)

EJECTA DATA RESULTING FROM AIR FORCE MISSILE SURVEY

Shot	Distance from GZ (ft)	Total Weight (lb)	No. of Missiles	Shot	Distance from GZ (ft)	Total Weight (lb)	No. of Missiles	Shot	Distance from GZ (ft)	Total Weight (lb)	No. of Missiles
H2	35±5	2628	128	H1	380-430	173	36	ST1	25-40	58	11
	60±5	2961	163		430-530	164	46		40-60	14	6
	85±5	2293	136		530-680	144	64		60-80	17	13
	110±5	1490	113	H1	680-800	17	11		80-100	39	18
	135±5	1709	107						100-120	38	6
	160-200	1957	197	C2	75±5	5582	136		120-140	9	5
	200-240	2094	213		100±5	6488	160		140-160	9	3
	240-280	1176	149		125±5	3391	93		160-180	2	2
	280-320	848	111		150±5	2803	93		180-200	1	1
	320-360	965	126		175±5	6566	63		200-220	6	2
	360-400	369	57		200±5	1567	50		220-240	1	1
	400-440	512	82		205-230	376	49	ST1	240-260	3	2
	440-480	222	36		230-255	634	54				
	480-520	244	38		255-305	1347	72				
	520-560	425	63		305-355	535	46				
H2	560-	1162	136		355-405	1351	66				
					405-465	1222	51				
H1	80±5	595	44		465-505	74	21				
	130±5	150	25		505-580	1127	18				
	180±5	100	31	C2	600-900	1604	15				
	230±5	337	37								
	280-330	314	60								
H1	330-380	312	44								

Table II-3 (cont'd)

EJECTA DATA RESULTING FROM AIR FORCE MISSILE SURVEY

Shot	Distance from GZ	Total Weight	No. of Missiles	Shot	Distance from GZ	Total Weight	No. of Missiles	Shot	Maximum Missile Distance
—	(ft)	(lb)	—	—	(ft)	(lb)	—		R_z (ft)
ST3a(C3)	50-60	83	68	ST3c	40-60	555	124	S2a	840
	60-70	89	58		60-80	490	111	S4a	725
	70-80	46	41		80-100	257	70	S4b	610
	80-100	54	44		100-120	139	42	S4c	600
	100-120	30	18		120-140	73	35	S4d	700
	120-140	12	11		140-180	45	31	LS	3500
ST3a(C3)	140-210	8	8		180-220	107	33	H2	1475
					220-260	41	18	H1	800
ST3b	40-60	228	64		260-300	25	18	C2	3300
	60-85	707	111		300-350	67	27	ST1	260
	85-110	215	63		350-400	45	23	ST3a(C3)	205
	110-150	291	68		400-450	42	22	ST3b	900
	150-200	413	96		450-500	38	17	ST3c	1200
	200-320	127	35	ST3c	500-	28	26		
	320-375	2	2						
	375-475	26	19						
	475-600	34	19						
ST3b	600-	5	3						

REFERENCES

1. Carlson, R. H. and T. E. O'Brien, et al., Ejecta Distribution from Cratering Events in Soil and Rock, WL TR 64-111, Air Force Weapons Laboratory, Kirtland Air Force Base, New Mexico, February 1965.

2. Hansen, Spenst M., et al., Recommended Crater Nomenclature, UCRL-7750, March 16, 1964.

3. Vortman, L. J., Craters from Repeated Direct Hits at the Same Aiming Point, SC 4760(RR), Sandia Corporation, January 1963.

4. Bennett, B., Successive Cratering Shots Along the Same Vertical Axis, D2-90454, The Boeing Company, October 1963.

5. Strange, J. N. and A. D. Rooke, Jr., Craters Resulting from Repeated Explosions along a Common Vertical Axis, Technical Report No. 1-665, U. S. Army Engineers, Waterways Experiment Station, November 1964.

6. Fulmer, C. V., Private communication, The Boeing Company, Seattle, Washington, October 27, 1965.

7. Operation DISTANT PLAIN, United States Participation with Canada and Great Britain in a Nuclear Weapons Effects High Explosive Experimental Test Series, Headquarters DASA, July 1965.

8. Dietz, John P. and Dennis B. Hayes, Compilation of Crater Data, SC-RR-65-220, Sandia Corporation, Albuquerque, New Mexico, July 1965.

9. Vortman, L. J., et al., Project Buckboard, 20-Ton and 1/2-Ton High Explosive Cratering Experiments in Basalt Rock, SC-4675(RR), Sandia Corporation, August 1962.

10. Rooke, A. D. and L. K. Davis, Mass Distribution Measurements of Crater Ejecta and Dust, POR-1815, Project Danny Boy, U. S. Corps of Engineers Waterways Experiment Station, Vicksburg, Mississippi, 13 Feb 1964.

11. Carlson, R. H., (U) Evaluation and Interpretation of Ejecta Data from Cratering Explosions, WL-TDR 64-51, Air Force Weapons Laboratory, Kirtland Air Force Base, New Mexico, May 1964. (S-RD Report)

12. Davies, F. W. and J. R. Highlander, Strong Ground Shock from a Surface Burst on Basalt, D2-84084-1, The Boeing Company, Seattle, Washington, November 1965.

13. Carlson, R. H. and G. D. Jones, Ejecta Distribution Studies, Project Air Vent, Final Report, D2-90575, The Boeing Company, Seattle, Washington, November 1964.

14. Rooke, A. D., Jr. and L. K. Davis, Crater Measurements, Project Flat Top, POR 3008, U. S. Army Waterways Experiment Station, Vicksburg, Mississippi, 9 August 1966.

REFERENCES (cont'd)

15. Vortman, L. J., Dimensions of a Crater from a 500-Ton TNT Hemisphere Detonated on Rock, SC-RR-65-277, Sandia Corporation, Albuquerque, New Mexico, July 1965.

16. Carlson, R. H., High Explosive Ditching from Linear Charges, Final Report, Project Toboggan, SC-4483(RR), Sandia Corporation, Albuquerque, New Mexico, July 1961.

17. Rooke, A. D., Jr., Operation Flat Top, Preliminary Report, Project 1.9, Crater Measurements, Events II and III, U. S. Army Waterways Experiment Station, Vicksburg, Mississippi, April 1964.

18. Vortman, L. J., "Scaling of Craters from Surface Nuclear Explosions," Appendix I to The Boeing Company Report, Carlson, R. H., et al., Ejecta Distribution from Cratering Events in Soil and Rock, Air Force Weapons Laboratory, Report WL TR-64-111, Kirtland Air Force Base, New Mexico, February, 1965.

19. Rooke, A. D., Jr., Private communication regarding dimensions of Snowball crater, October 14, 1965.

UNCLASSIFIED
Security Classification

DOCUMENT CONTROL DATA - R&D

(Security classification of title, body of abstract and indexing annotation must be entered when the overall report is classified)

1. ORIGINATING ACTIVITY (Corporate author)
Air Force Weapons Laboratory
Kirtland Air Force Base, New Mexico 87117

2a. REPORT SECURITY CLASSIFICATION
UNCLASSIFIED

2b. GROUP

3. REPORT TITLE
MULTIPLE THREAT CRATERING EXPERIMENT
Volume 1. Successive Cratering in Hard Rock

4. DESCRIPTIVE NOTES (Type of report and inclusive dates)
January 1965 through December 1965

5. AUTHOR(S) (Last name, first name, initial)
O'Brien, Thomas E., Capt, USAF; Seknicka, John E., Lt., USAF; Carlson, R. H.
Jones, G. D.

6. REPORT DATE	7a. TOTAL NO. OF PAGES	7b. NO. OF REFS
May 1967	222	19

8a. CONTRACT OR GRANT NO. AF 29(601)-6787	9a. ORIGINATOR'S REPORT NUMBER(S)
b. PROJECT NO. 5710	AFWL-TR-67-8, Vol. I
c. Subtask No. 13.144	9b. OTHER REPORT NO(S) (Any other numbers that may be assigned this report)
d.	

10. AVAILABILITY/LIMITATION NOTICES This document is subject to special export controls and each transmittal to foreign governments or foreign nationals may be made only with prior approval of AFWL (WLDC), Kirtland AFB, NM, 87117. Distribution is limited because of the technology discussed in the report.

11. SUPPLEMENTARY NOTES	12. SPONSORING MILITARY ACTIVITY
	AFWL (WLDC) Kirtland AFB, NM 87117

13. ABSTRACT

A research program compares successive craters formed by high-explosive charges detonated in basalt along a common vertical axis with single explosions equivalent in yield to the sum of the successive burst. Studies include craters and ejecta distribution; energy coupling of cratering explosions at and near the ground surface; charge shape effect on craters and related phenomena; and distribution, size, and weight of discrete ejecta missiles. Results indicated that the excavated crater depth may be increased by a fourth half-buried successive shot. This increase is between zero and 25 percent, depending on the technique used. The data were not conclusive. The apparent crater formed by a hemispherical surface charge exhibits a radius about 90 percent and depth about 85 percent of the dimensions formed by a corresponding spherical, half-buried charge. Excavated craters formed by hemispherical charges are likewise smaller. Scaling relationships determined for apparent craters formed by half-buried spherical charges were $R_a = 1.30\ W^{0.27}$, $Da = 0.42\ W^{0.28}$; for apparent craters formed by hemispherical charges: $R_a = 0.48\ W^{0.37}$, $D_a = 0.06\ W^{0.47}$. Fifty percent of material ejected from the 4000-pound and 16,000-pound half-buried charge craters were deposited between the crater edge and 1.9 and 1.2 crater radii, respectively.

(Distribution limitation statement No. 2)

DD FORM 1 JAN 64 1473

UNCLASSIFIED
Security Classification

UNCLASSIFIED
Security Classification

14. KEY WORDS	LINK A		LINK B		LINK C	
	ROLE	WT	ROLE	WT	ROLE	WT
Cratering-successive Ejecta Missiles Coupling Charge Geometry Scaling Basalt Rock						

INSTRUCTIONS

1. ORIGINATING ACTIVITY: Enter the name and address of the contractor, subcontractor, grantee, Department of Defense activity or other organization *(corporate author)* issuing the report.

2a. REPORT SECURITY CLASSIFICATION: Enter the overall security classification of the report. Indicate whether "Restricted Data" is included. Marking is to be in accordance with appropriate security regulations.

2b. GROUP: Automatic downgrading is specified in DoD Directive 5200.10 and Armed Forces Industrial Manual. Enter the group number. Also, when applicable, show that optional markings have been used for Group 3 and Group 4 as authorized.

3. REPORT TITLE: Enter the complete report title in all capital letters. Titles in all cases should be unclassified. If a meaningful title cannot be selected without classification, show title classification in all capitals in parenthesis immediately following the title.

4. DESCRIPTIVE NOTES: If appropriate, enter the type of report, e.g., interim, progress, summary, annual, or final. Give the inclusive dates when a specific reporting period is covered.

5. AUTHOR(S): Enter the name(s) of author(s) shown on or in the report. Enter last name, first name, middle initial. If military, show rank and branch of service. The name of the principal author is an absolute minimum requirement.

6. REPORT DATE: Enter the date of the report as day, month, year; or month, year. If more than one date appears on the report, use date of publication.

7a. TOTAL NUMBER OF PAGES: The total page count should follow normal pagination procedures, i.e., enter the number of pages containing information.

7b. NUMBER OF REFERENCES: Enter the total number of references cited in the report.

8a. CONTRACT OR GRANT NUMBER: If appropriate, enter the applicable number of the contract or grant under which the report was written.

8b, 8c, & 8d. PROJECT NUMBER: Enter the appropriate military department identification, such as project number, subproject number, system numbers, task number, etc.

9a. ORIGINATOR'S REPORT NUMBER(S): Enter the official report number by which the document will be identified and controlled by the originating activity. This number must be unique to this report.

9b. OTHER REPORT NUMBER(S): If the report has been assigned any other report numbers *(either by the originator or by the sponsor)*, also enter this number(s).

10. AVAILABILITY/LIMITATION NOTICES: Enter any limitations on further dissemination of the report, other than those imposed by security classification, using standard statements such as:

(1) "Qualified requesters may obtain copies of this report from DDC."

(2) "Foreign announcement and dissemination of this report by DDC is not authorized."

(3) "U. S. Government agencies may obtain copies of this report directly from DDC. Other qualified DDC users shall request through _____."

(4) "U. S. military agencies may obtain copies of this report directly from DDC. Other qualified users shall request through _____."

(5) "All distribution of this report is controlled. Qualified DDC users shall request through _____."

If the report has been furnished to the Office of Technical Services, Department of Commerce, for sale to the public, indicate this fact and enter the price, if known.

11. SUPPLEMENTARY NOTES: Use for additional explanatory notes.

12. SPONSORING MILITARY ACTIVITY: Enter the name of the departmental project office or laboratory sponsoring *(paying for)* the research and development. Include address.

13. ABSTRACT: Enter an abstract giving a brief and factual summary of the document indicative of the report, even though it may also appear elsewhere in the body of the technical report. If additional space is required, a continuation sheet shall be attached.

It is highly desirable that the abstract of classified reports be unclassified. Each paragraph of the abstract shall end with an indication of the military security classification of the information in the paragraph, represented as *(TS), (S), (C), or (U)*.

There is no limitation on the length of the abstract. However, the suggested length is from 150 to 225 words.

14. KEY WORDS: Key words are technically meaningful terms or short phrases that characterize a report and may be used as index entries for cataloging the report. Key words must be selected so that no security classification is required. Identifiers, such as equipment model designation, trade name, military project code name, geographic location, may be used as key words but will be followed by an indication of technical context. The assignment of links, rules, and weights is optional.